**POLITECNICO DI MILANO**

SCHOOL OF CIVIL, ENVIRONMENTAL AND LAND PLANNING ENGINEERING

& SCHOOL OF INDUSTRIAL AND INFORMATION ENGINEERING

MASTER OF SCIENCE IN

ENVIRONMENTAL AND LAND PLANNING ENGINEERING

& ENERGY ENGINEERING

# INSIGHTS IN ANAEROBIC CO-DIGESTION VIA EXPERIMENTAL AND DYNAMIC MODELLING TOOLS

Supervisor:

Prof. Elena Ficara

Co-Supervisor:

Eng. Arianna Catenacci, PhD

Master Thesis of:

Angela Nunziata

Davide Soderino

Academic Year 2019-2020

# TABLE OF CONTENTS

# ABSTRACT

In the present thesis work, the results of experimentation on a pilot anaerobic digestion plant have been presented. The experiment, which lasted seven months, was carried out first on mono-digestion of the sludge produced by a wastewater treatment plant and subsequently on co-digestion with expired yogurt of well-known commercial brands. The reactor operated according to a Continuous Stirred Tank Reactor (CSTR) model and an operating volume of 60 L at a temperature of 38 ± 0.5 ° C. The pilot plant was fed daily in semi-continuous mode operating with an average HRT of 17 days. In the mono-digestion phase, the reactor was operating with an average OLR of 1.34 $kg_{VS}/m^3/d$. This average OLR, in the co-digestion phase, was increased by 20% to 1.61 $kg_{VS}/m^3/d$ by adding yogurt. The main purpose of this work was to develop and calibrate a co-digestion model based on ADM1 through the OpenModelica programming platform. The calibration was carried out through an iterative validation process with the analytical data, the results of the BMP tests and the biomass activity tests carried out. The proposed iteration method for the model calibration was found to be effective: the model adapts satisfactorily to the experimental data collected, as confirmed by the statistical indicators Theil's Inequality Coefficient (TIC) and Mean Absolute Relative Error (MARE). Among the various results obtained, the TIC and MARE indicators for simulating the concentration of VFAs in the digestate are 0.174 and 0.333, respectively (for both criteria, the closer the value to zero, the better the model performance, TIC < 0.3 represents a good simulation result). For the simulation of the ammonium concentration ($NH_4^+$), values of TIC = 0.081 and MARE = 0.167 are obtained. For the simulation of the BMP tests in co-digestion, values of TIC = 0.009 and MARE = 0.018 are obtained.

**Key words:** Anaerobic digestion, ADM1, co-digestion, pilot plant, substrate characterization, wastewater treatment plant.

# SOMMARIO

Nel presente lavoro di tesi sono stati presentati i risultati di una sperimentazione su un impianto pilota di digestione anaerobica. La sperimentazione, durata 7 mesi, è stata effettuata prima sulla mono-digestione del fango prodotto da un impianto di trattamento acque reflue e successivamente sulla co-digestione con dello yogurt scaduto di note marche commerciali. Il reattore ha operato secondo un modello CSTR (Continuous Stirred Tank Reactor) e un volume operativo di 60L a una temperatura di 38±0.5 °C. Il pilota è stato alimentato giornalmente in modalità semi-continua operando con un HRT medio di 17 giorni. Nella fase di mono-digestione il reattore è stato sottoposto ad un OLR medio di 1.34 $kg_{VS}/m^3/d$. Tale OLR medio, nella fase di co-digestione, è stato incrementato del 20% tramite l'aggiunta di yogurt passando a 1.61 $kg_{VS}/m^3/d$. Lo scopo principale del presente lavoro è stato quello di sviluppare e calibrare un modello di co-digestione su base ADM1 attraverso la piattaforma di programmazione OpenModelica. La calibrazione è stata effettuata attraverso un processo iterativo di validazione con i dati analitici, i risultati delle prove di BMP e delle prove di attività della biomassa svolte. Il metodo di iterazione proposto per la calibrazione del modello è risultato essere efficace: il modello si adatta in maniera soddisfacente ai dati sperimentali raccolti nel corso di 7 mesi di operatività dell'impianto pilota, come avvalorato tramite gli indicatori statistici Theil's Inequality Coefficient (TIC) e Mean Absolute Relative Error (MARE). Tra i vari risultati ottenuti, gli indicatori TIC e MARE per la simulazione della concentrazione dei VFA nel digestato sono rispettivamente 0.174 e 0.333 (per entrambi i criteri, più il valore si avvicina a zero, migliori sono le prestazioni del modello, TIC < 0.3 rappresenta un buon risultato di simulazione). Per la simulazione della concentrazione dell'ammonio ($NH_4^+$) si ottengono valori di TIC = 0.081 e MARE = 0.167. Per la simulazione dei test di BMP in co-digestione si ottengono valori di TIC = 0.009 e MARE = 0.018.

**Parole chiave:** digestione anaerobica, ADM1, co-digestione, impianto pilota, caratterizzazione dei substrati, impianto di trattamento acque reflue.

# LIST OF FIGURES

# LIST OF TABLES

# LIST OF ABBREVIATIONS

| | |
|---|---|
| AcoD | Anaerobic co-digestion |
| AD | Anaerobic digestion |
| ADM1 | Anaerobic digestion model No. 1 |
| BMP | Biochemical methane potential |
| BSA | Bovine serum albumin |
| COD | Chemical oxygen demand |
| CSTR | Continuous stirred tank reactor |
| HRT | Hydraulic retention time |
| IWA | International Water Association |
| LCFA | Long chain fatty acids |
| LHV | Lower Heating Value |
| OFMSW | Organic fraction of municipal solid waste |
| OLR | Organic loading rate |
| PLC | Programmable Logic Controller |
| SBR | Sulphate reducing bacteria |
| SGP | Specific Gas Production |
| SRT | Solid retention time |
| SS-OFMSW | Source selected organic fraction of municipal solid waste |
| TKN | Total Kjeldahl nitrogen |
| TS | Total solids |

| | |
|---|---|
| TSS | Total suspended solids |
| VFA | Volatile fatty acids |
| VS | Volatile solids |
| VSS | Volatile suspended solids |
| WAS | Waste activated sludge |
| WWTP | Wastewater treatment plant |

# ACKNOWLEDGMENTS

We would like to express our gratitude to our supervisor, Prof. Elena Ficara, for allowing us to work on a captivating and formative research project. We are grateful for the perseverance and dedication with which she followed us and for the important teachings she has provided us with.

Our gratitude also goes to our co-supervisor, Eng. Arianna Catenacci Ph.D., for having followed us throughout the experimentation by training, guiding and helping us. We are thankful as she shared with us her professional knowledge and for mentoring us with kind-heartedness.

We also thank all the members of the PerFORM WATER 2030 research group in San Giuliano Ovest WWTP. In particular, our gratitude goes to Eng. Mirko Trionfini and Dr. Anna Santus, for their collaboration and help, and for creating a dynamic and enjoyable work environment.

We also thank Dr. Matteo Grana for always assisting us in the collection of sludge in Sesto San Giovanni WWTP and for his stimulating companionship.

Thank you all for allowing us to grow and train as students, engineers, and people through this astonishing experience.

# Chapter 1: INTRODUCTION

## *1.1. Background*

The production of bioenergy from anaerobic digestion (AD) is a promising alternative to climate change reduction and it is considered a viable treatment technology for waste management. This technology has a positive net energy production rate and the methane gas produced from the process could replace fossil fuels (Anukam et al., 2019).

Nowadays, renewable and efficient energy recovery in wastewater facilities is of great interest because they are notoriously large energy consumers in the municipal infrastructures.

In the context of wastewater treatment plants, anaerobic digestion is a technology widely used to treat sewage sludge. Most municipal wastewater treatment plants have reported an excess digestion capacity of 15 to 30 percent. In those plants, the AD process is conducted with a low OLR, therefore they may be capable to process with their current digester capacity an ample range of organic materials. This process of digesting more than one substrate is called co-digestion (Metcalf & Eddy I AECOM, 2014).

Currently, the digestion of sewage sludge is generally characterized by a low yield in methane production (100-300 $NL_{CH4}$ per kg of volatile solid fed or 0.3-9 $Nm^3_{CH4}$ per ton of sludge). If there is excess capacity in municipal facility anaerobic digesters, co-digestion with other wastes can be an interesting means for increasing the energy production.

A major benefit of co-digestion is the ability to turn a waste product into a source of energy, while at the same time curtailing the carbon dioxide release from the waste decomposition in landfills (Rosso and Stenstrom, 2008). Therefore, AcoD can be an attractive alternative for the treatment of source selected organic fraction of municipal solid waste or various food by-products.

The use of mathematical models such as ADM1 could be extremely helpful in order to maximize the methane production from AcoD, monitoring the parameters of the process and performing scenario analysis (Siddique & Wahid, 2018).

## 1.2. *Goals*

The central purpose of this work was to develop and calibrate a co-digestion model based on ADM1. This aim was achieved by running and monitoring an anaerobic digestion pilot plant and by carrying out batch tests. Figure 1.1 shows the scheme of the iterative calibration process used to achieve such an objective.

This work is part of the European research project PerFORM WATER 2030. Partners involved: GruppoCAP Holding, Politecnico di Milano, SEAM Engineering Srl. The experimentation took place at the wastewater treatment plant of San Giuliano Milanese Ovest (GruppoCAP, Amiacque) using the sewage sludge produced by the wastewater treatment plant of Sesto San Giovanni (GruppoCAP, Amiacque) and the expired yogurt supplied by GruppoCAP. The start-up of the pilot plant was carried out in July 2020 while the monitoring lasted from October 2020 to today, for a total duration of seven months.

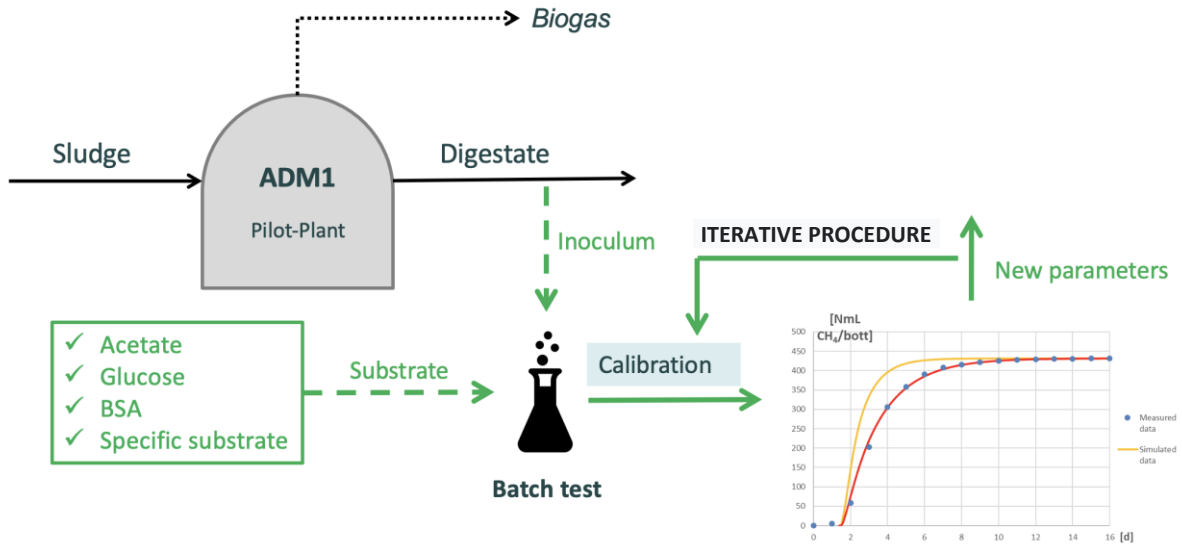


Figure 1.1 - Schematic representation of the iterative process for the calibration of the ADM1 model.

## 1.3. *Thesis outline*

This thesis is organized in five chapters preceded by an abstract, available both in Italian and English language.

The first chapter provides an overview of the subject and summaries the goals of the current research, highlighting the importance of dealing with energy recovery through co-digestion of waste materials and mathematical modeling of the process.

In the second chapter a general literature review about anaerobic digestion, batch test and mathematical modeling is reported.

Following, the third chapter gives an accurate description of materials and methods employed. Hence, this chapter describes all the analytical and statistical methods adopted to perform a complete characterisation of the samples, together with the BMP and biomass activity tests and the apparatus used. It is also described the methods of implementation and calibration of ADM1 model.

All the results of the experimental procedures are reported and discussed in the fourth chapter.

Finally, in the fifth and last chapter the main achievements and future developments are reported.

# Chapter 2: LITERATURE REVIEW

## *2.1. Basic principles of anaerobic digestion*

Anaerobic digestion is among the oldest processes used for the stabilization of sludge. The process involves the decomposition of organic matter and reduction of inorganic matter (principally sulfate) in the absence of free and chemically bound oxygen, such as nitrates or sulfates. Anaerobic conditions are necessary so that the organic matter itself serves as an electron acceptor (Metcalf & Eddy I AECOM, 2014).

Anaerobic digestion consists in the efficient conversion of organic matter into an energy-rich product known as biogas, with methane ($CH_4$) and carbon dioxide ($CO_2$) as their main constituents. The process depends on the mutual and synergistic interaction of a consortium of microorganisms to break down the complex organic matter into soluble monomers such as amino acids, fatty acids, simple sugars, and glycerols. The AD process takes place in four key stages: hydrolysis, acidogenesis, acetogenesis, and methanogenesis. In each stage, the degradation of feedstock in the absence of oxygen is facilitated by a combination of specific microorganisms, leading to the formation of digestate and biogas. (Anukam et al., 2019).

### *2.1.1. Process stages of anaerobic digestion*

The AD process is characterized by a series of biochemical reactions where the intermediate products are used as a substrate for the following stages. The four steps can occur simultaneously and, while the first one (hydrolysis) is an extra-cellular process, acidogenesis, acetogenesis, and methanogenesis are intra-cellular processes. During those stages of AD, a substantial portion of the chemical oxygen demand (COD) is converted to methane gas.

The first stage is hydrolysis which degrades particulate organic material and high molecular weight compounds such as lipids, polysaccharides, proteins, and nucleic acids, into soluble organic substances (e.g. amino acids and fatty acids) (Dewil et al., 2008).

From a chemical perspective, hydrolysis refers to the break of chemical bonds by the addition of water. Cations and anions react with water molecules, altering pH in the process to create a splitting of H–O bonds. It is a relatively slow step limiting the overall digestion process rate, mainly when solid waste substrates are used (Anukam et al., 2019).

The growth of biomass is usually described by a first-order kinetics, concerning the biomass's concentration, and by Monod equation with respect to the substrate. Inhibition terms may be present, generally of a non-competitive type (i.e. determining a reduction in the maximum reaction speed) and less frequently of a competitive kind (i.e. determining an increase in the semi-saturation constant). For hydrolysis, the dependence on hydrolyzing biomass concentration is neglected. As displayed in formula 2.1, Hydrolysis First-order kinetics are adopted concerning particulate matter concentration (distinguished between carbohydrates, proteins and fats) (Bonomo, 2014).

$$-\frac{dx_{p,i}}{dt} = k_{p,i} \cdot x_{p,i} \qquad (2.1)$$

Where:

- $x_{p,i}$ is the concentration of particulate matter: carbs, lipids, and proteins $\left[\frac{g}{m^3}\right]$;
- $k_{p,i}$ is the hydrolysis constant for the specific substrates $\left[\frac{1}{d}\right]$.

The components produced through hydrolysis are further split during acidogenesis. This second step of the process is the fermentation stage, where soluble compounds formed in the hydrolysis stage are degraded and converted into $CO_2$ and $H_2$ through the bacteria known as acidogenic bacteria (fermentative microorganisms). Moreover, Volatile Fatty Acids (VFA) are produced by acidogenic bacteria along with ammonia ($NH_3$), $CO_2$, $H_2S$ and other by-products. The most important acid in this stage is the acetic acid ($CH_3COOH$), which is the most significant organic acid used as a substrate by $CH_4$-forming microorganisms. During acidogenesis, propionic ($CH_3CH_2COOH$), butyric ($CH_3CH_2CH_2COOH$), valeric ($CH_3CH_2CH_2CH_2COOH$), formic ($HCOOH$), and lactic ($C_3H_6O_3$) acids are also generally produced (Anukam et al., 2019).

The third stage in AD is acetogenesis, which refers to the further fermentation of higher organic acids and alcohols produced by acidogenesis to acetic acid, $CO_2$ and $H_2$. Thus, the ultimate fermentation products are acetate, hydrogen, and $CO_2$, which are the precursors of methane production. This transformation is controlled to a considerable extent by the partial pressure of $H_2$ in the mixture. Indeed, the free energy change associated with the conversion of propionate and butyrate to acetate and hydrogen requires that hydrogen is at low concentrations; otherwise, the reaction will not proceed spontaneously. If $H_2$ is maintained low by the methanogenic bacteria, acetate would be the primary output, and the process will not be inhibited (Metcalf & Eddy I AECOM, 2014).

For both stages, acidogenesis and acetogenesis, reference is made to the kinetics of Monod, with a limitation on the concentration of the corresponding organic substrate. The growth and decay kinetics are of first order with respect to the biomass concentration. The kinetics is described through formula 2.2. It is possible to consider also a limitation on the concentration of inorganic nitrogen, which is needed for bacterial growth. Inhibition terms could also be introduced for pH and molecular hydrogen (Bonomo, 2014).

$$\frac{dx_B}{dt} = \mu_{max} \cdot \frac{S}{K_S + S} \cdot x_B - k_d \cdot x_B \tag{2.2}$$

Where:

- $\mu_{max}$ is the maximum specific growth rate of microorganisms $\left[\frac{1}{d}\right]$;
- $x_B$ is the concentration of fermentative microorganisms $\left[\frac{g}{m^3}\right]$;
- $S$ is the concentration of soluble substrate $\left[\frac{g}{m^3}\right]$;
- $k_d$ is the specific decay rate of fermentative microorganisms $\left[\frac{1}{d}\right]$;
- $K_S$ is the half-saturation constant $\left[\frac{g}{m^3}\right]$.

Nonmethanogenic microorganisms responsible for hydrolysis and fermentation include various facultative and obligate anaerobic bacteria such as: *Clostridium spp., Peptococcus anaerobus, Bifi- dobacterium spp., Desulphovibrio spp., Corynebacterium spp., Lactobacillus, Actinomy-ces, Staphylococcus, and Escherichia coli*. Other physiological groups present include those producing proteolytic, lipolytic, ureolytic, or cellulytic enzymes (Metcalf & Eddy I AECOM, 2014).

Methanogenesis constitutes the fourth and final stage of the AD process where methane is produced. The microorganisms responsible for methane production, classified as archaea, are strict obligate anaerobes (Metcalf & Eddy I AECOM, 2014). In this stage, two groups of methanogenic archaea produce methane. Methanogens can be classified into two groups, namely acetophilic and hydrogenophilic. Acetophilic produces $CH_4$ by decarboxylation of $CH_3COOH$. Hydrogenophilic produces methane by anaerobic oxidation of molecular hydrogen and contextual reduction of carbon dioxide (Anukam et al., 2019). These two major pathways are described in the following reaction equations:

$$CH_3COOH \rightarrow CH_4 + CO_2 \quad (2.3)$$

$$CO_2 + 4\,H_2 \rightarrow CH_4 + 2\,H_2O \quad (2.4)$$

The hydrogenotrophic methanogens can be found within four Archaea orders: Methanobacteriales, Methanococcales, Methanomicrobiales, and Methanopyrales. They gain their energy from the oxidation of hydrogen and use $CO_2$ as their carbon sources. The archaea that produce methane from acetate are in the order Methanosarcinales. Solely two genera within the order Methanosarcinales can use acetate to generate methane and carbon dioxide: Methanosarcina and Methanoseta. The Methanosarcina is characterized by a high maximum specific growth rate and a high half-saturation coefficient. Simultaneously, the Methanosaeta have a low maximum specific growth rate and moderate semi-saturation coefficient values. The Methanosaeta are dominant in anaerobic digesters due to the long SRT and low acetate concentration. Nevertheless, Methanosarcina manages increases in acetate more efficiently and hence favors more stable digestion (Metcalf & Eddy I AECOM, 2014).

Generally, about 72% of the methane produced in anaerobic digestion is from acetate formation. However, hydrogenotrophilic *Archaea* are crucial for adjusting the level of hydrogen. Indeed, methanogens, acidogens and acetogens have a mutually beneficial syntrophic relationship in which the first produce methane and carbon dioxide from fermentation end products. Hydrogenotrophilic Archaea are responsible for maintaining an extremely low partial pressure of $H_2$. Consequently, the equilibrium of the fermentation reactions is shifted toward the formation of more oxidized end products. If these microorganisms do not use the hydrogen fast enough, there would be a slowdown of propionate and butyrate fermentation, resulting in the accumulation of VFA in the reactor and a possible reduction in pH (Metcalf & Eddy I AECOM, 2014).

Methanogenesis has first-order kinetics concerning biomass concentration. For acetoclastic methanogenesis, Monod terms referring to the concentrations of acetate and inorganic nitrogen are used. An inhibition function from pH and a non-competitive inhibition from ammonia can be considered. For hydrogenotrophic methanogenesis, Monod terms referring to molecular hydrogen and inorganic nitrogen and a pH inhibition function are included (Bonomo, 2014).

### *2.1.2. Parameters and performance indicator of anaerobic digestion*

AD processes are highly susceptible to various environmental factors. Indeed, some parameters have a particularly relevant effect on the metabolism of the process and on the individual phases of the anaerobic trophic chain, which, as already pointed out, are strongly interdependent. It is sufficient to inhibit a single stage of AD to risk bringing the whole process to failure. Moreover, the methanogens which are the slowest growing microorganisms are also particularly sensitive to environmental modifications. From this point of view, parameters such as: pH and alkalinity, VFA concentration, the relationship between VFA and Alkalinity, temperature, mixing, availability of nutrients, and the presence of toxic or inhibiting substances take on particular importance (Cecchi et al., 2005).

#### *pH and ALkalinity*

The pH provides an indicator of the reaction medium's stability, as its variation is associated both with the buffering capacity of the system by the reaction medium and with variations in the balance between the species participating in the trophic chain of the microorganisms involved in the process. Consequently, the pH is determined by the contribution of acidifying fermentation, by the alkalizing methanogenesis and by the buffering effect of chemical balances (Cecchi et al., 2005).

Each group of microorganisms has a distinct optimum pH range. Methanogenic *Archaea* are the most sensitive to pH variations and have an optimum within 6.5 and 7.2. The fermentative microorganisms are slightly less sensitive and can function in a broader range of pH between 4.0 and 8.5. At a low pH, the main products are acetic and butyric acid, while at a pH of 8.0, mainly acetic and propionic acid are produced (Dewil et al., 2008).

The pH value in a digester is essentially determined by the presence of $CO_2$ in the liquid medium, and therefore by its partial pressure in the biogas, and by the concentration values of VFAs and ammonia. It is essential to highlight how this parameter can indicate the equilibrium conditions of the system, but its changes are limited by the medium's buffering capacity. Indeed, the pH variation appears evident only when alkalinity has been remarkably depleted. (Cecchi et al., 2005).

Acidogenesis is the fastest conversion step. For that reason, anaerobic reactors are subjected to sudden pH drops, especially when reactors are overloaded or in the presence of toxic compounds. Once the produced acids consume alkalinity, the pH starts to drop, resulting in a higher concentration of non-dissociated VFAs, leading to more severe methanogens inhibition.

The latter leads to an even quicker accumulation of VFAs and consequent pH drop. The fact that acidifiers are active even at low pH means the reactor souring to pH 4 to 5 can and will occur when the system's methanogenic capacity is trespassed (McCarty & Smith, 1986).

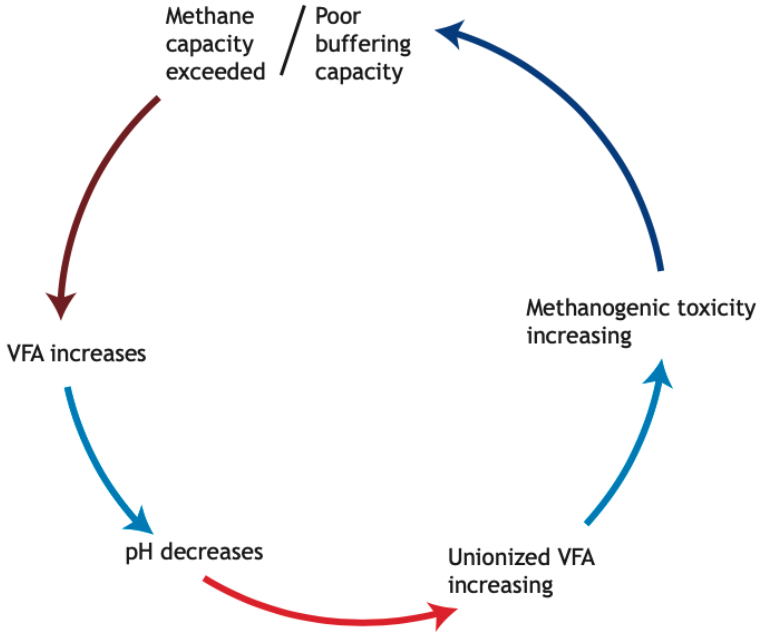


Figure 2.1 - Reactor pH drops as a result of methanogenic overloading and accumulating VFAs.

Therefore, it is crucial to have a buffer capacity provided by alkalinity, neutralizing the pH lowering. Alkalinity values of the order of 3000-5000 mg$CaCO_3$/L are typical for anaerobic digesters operating under stable conditions. Alkalinity is, therefore, a parameter of fundamental importance in anaerobic processes. Indeed, as already pointed out, the growth rates of methane biomass are extremely low. Consequently, on the occasion of an increase in the organic load, the increased hydrolytic and acidifying capacities of the system determine an imbalance of the bacterial population in favor of the acidogenic component. Therefore, there will be a transitory phase in which an increase in VFA concentration will be observed. In these cases, the system's buffering capacity is fundamental because it must be able to neutralize the lowering of the pH caused by the accumulation of VFAs. The alkalinity of an anaerobic digester tends to be determined by a buffer system due to the coexistence of ammonia, originating from the degradation of proteins, and bicarbonate, resulting from the dissolution of carbon dioxide in the medium. Generally, $NH_4HCO_3$ is formed:

$$CO_2 + H_2 \leftrightarrows HCO_3^- + H^+ \quad (2.5)$$

$$HCO_3^- + NH_4^+ \leftrightarrows NH_4HCO_3 \quad (2.6)$$

The presence of this salt dissolved in solution leads to the medium's high alkalinity with consequent control of the process, even in the case of VFAs accumulation (Cecchi et al., 2005).

*Volatile fatty acids*

Volatile fatty acids are the most important intermediates in the AD process. VFA can be toxic to microorganisms, especially methanogens. VFA increase results from accumulation due to process imbalances that could be caused by an alteration in temperature, organic overloading, toxic compounds, etc. In such cases, the methanogens cannot remove the hydrogen and VFAs quickly enough. As a result, the acids accumulate, and the pH decreases to such a low value that could inhibit hydrolysis and acetogenesis. The toxicity is due to an increase in the undissociated form of the VFA. VFA can heighten the inhibitory effect of pH on methane production and VFA degradation in anaerobic digesters (Dewil et al., 2008).

The concentration of volatile fatty acids and alkalinity are the two parameters that show a more rapid variation when the system tends to move away from stable conditions. Indeed, in the event of problems, the concentration of fatty acids tends to increase, while alkalinity tends to decrease. A valid parameter to consider identifying a threat to the process is the ratio between these two quantities. Fatty acids in the numerator are generally expressed in terms of acetic acid, while alkalinity is expressed in calcium carbonate concentration. Values of the ratio around 0.3 indicate a stable operation of the digester, while higher values may indicate the onset of stability problems (Cecchi et al., 2005).

*Long-chain fatty acids*

Long-chain fatty acids (LCFA) are produced during the degradation of fat and lipids and are further reduced to acetate and hydrogen. LCFAs are known to be inhibitory at low concentrations. The LCFAs toxicity mechanism is caused by adsorption onto the cell membrane, interfering with the cell's transport and protection functions. Furthermore, the sorption of a layer of LCFA to biomass leads to the flotation of sludge and sludge washout. Typically, Acetoclastic methanogenic archaea are more affected by the LCFA than the hydrogenotrophic methanogens. Also, thermophilic microorganisms appear to be more

susceptible to LCFA toxicity compared to mesophilic ones. This behavior could be related to the different compositions of cell membranes for the two species (Dewil et al., 2008).

*Temperature*

The temperature has an essential effect on the physicochemical properties of the components found in the digestion substrate. It also influences the growth rate and metabolism of micro-organisms and the population dynamics involved in the process (Dewil et al., 2008).

Indeed, temperature influences the speed and completeness of the reactions involved; in this regard, three different operating intervals are distinguished:

• psychrophilic range: 4-15 °C;

• mesophilic range: 20-40 ° C, with optimal value at 35 °C;

• thermophilic range: 45-70 ° C, with optimal value at 55 °C.

In each field, specific bacterial populations are adapted to the corresponding temperature range and cannot operate effectively outside it. Within each interval, an increase in process kinetics is observed with a trend that reflects the Vant's Hoff-Arrhenius relationship, with a subsequent slowdown near the optimal value, followed by a rapid decrease (Bonomo, 2014). In figure 2.3 it is possible to appreciate the effect of temperature on the kinetics of anaerobic degradation.

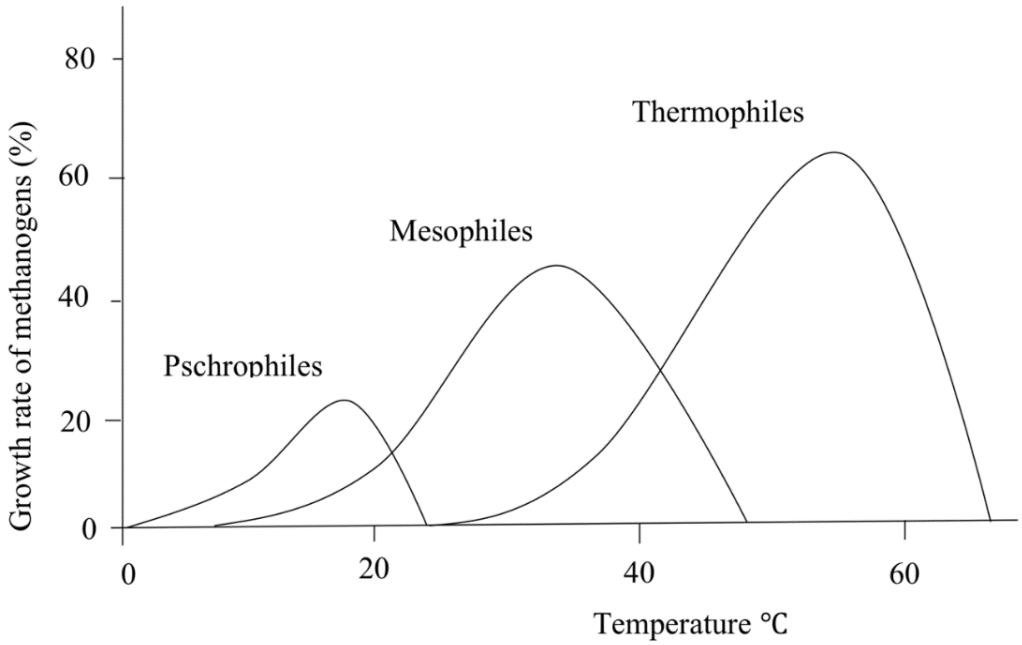


Figure 2.2 - growth rate of different methanogens with varying temperatures.

The bacteria available for the digestion process are sensitive to temperature fluctuation; therefore, it is necessary to maintain a constant temperature. Thermophilic bacteria are more efficient in terms of process kinetics leading to reduced retention time and increased loading rate, and gas yield. Still, they require higher heat input and are also more sensitive to temperature variations and environmental variables than mesophilic ones (Deepanraj et al., 2014).

Comparing the three fields, from psychrophilic to thermophilic it is possible to observe an increase in the process kinetics. In the mesophilic range, the process is more stable, i.e., less sensitive to variations in operating conditions. In the thermophilic field, high temperatures also exert a sanitizing effect against pathogenic microorganisms (Bonomo, 2014). Summing up, thermophilic digestion is faster, could increase solids reduction, and destroy pathogenic organisms. On the other hand, thermophilic digestion has a higher energy requirement, a lower quality of the supernatant with large quantities of dissolved solids, higher odour emission potential, and much lower process stability (Filer et al., 2019).

### *Mixing*

Proper mixing during AD is crucial for providing optimum performance. Mixing provides:

- Intimate contact among the substrate and active biomass.
- Yielding uniformity of temperature, substrate concentration, other chemicals, physical and biological aspects throughout the digester.
- Preventing both the formation of surface scum layers and the deposition of sludge on the digester's bottom.

Due to the rise of gas bubbles and possible thermal convection currents, there is always some degree of spontaneous mixing in the digestion tank. However, this is not sufficient for optimum performance; therefore, additional mixing is needed. Methods of possible auxiliary mixing could be external pumped recirculation, internal mechanical mixing, and internal gas mixing (Dewil et al., 2008).

### *Organic Loading Rate*

The Organic loading rate (OLR) is an important parameter that affects biogas production in anaerobic digestion. OLR is a measure of the biological conversion capacity of the AD system. It is expressed as the amount of raw material (kg of volatile solids) fed to the digester per unit volume per day, as expressed in formula (Deepanraj et al., 2014).

$$OLR = \frac{C}{HRT} \left[\frac{kg_{SV}}{m^3 \cdot d}\right] \quad (2.7)$$

Where:

- $C$ expresses the concentration of the substrate in the feed as VS $\left[\frac{kg_{SV}}{m^3}\right]$;
- $HRT$ expresses the hydraulic retention time $[d]$.

OLR is a fundamental parameter to control the AD process both because it quantifies the specific mass feeding rate: higher values lead to higher the specific biogas production, lower conversion efficiencies and higher risks for instability.

Overloading a digester may provoke a quick hydrolyzation and acidification in the substrate, thus leading to an over-accumulation of VFAs, which has the potential of inhibiting methanogenesis, thus causing the anaerobic digestion process failure (Meegoda et al., 2018).

On the other hand, as long as the digestor can handled it, higher OLR results in higher biogas production because more organics components are available to be degraded. At the same time, if the OLR is too low, it results in an underfed digester, thus an unexploited biogas production. Consequently, it is crucial to find an optimum OLR that guarantees an elevated production while avoiding the AD process failure.

The optimum loading rate depends on the degradability of the feed. When treating waste sludge, it is within 0.5 kg and 2 kg of total VS per $m^3$ of the digester per day, which can be chosen based on the type of raw material, retention time, and the process temperature (Deepanraj et al., 2014).

*Solid and hydraulic retention time*

The average hydraulic retention time (HRT) is defined as the ratio between the reactor volume and the volumetric feeding rate of the reactor:

$$HRT = \frac{V}{Q} \ [d] \quad (2.8)$$

Where:

- $V$ is the volume of the reactor $[m^3]$;
- $Q$ is the flow rate withdrawn $\left[\frac{m^3}{d}\right]$.

It represents the average residence time of various fluid elements in the reactor.

The solids retention time (SRT) is the average time the solids spend in the digester. The average residence time of the sludge inside the reactor is given by the ratio between the biomass present in the reactor and the flow rate biomass extracted from the reactors:

$$SRT = \frac{X \cdot V}{X \cdot Q} = \frac{V}{Q} \quad [d] \tag{2.9}$$

Where:

- $X$ is the biomass concentration $\left[\frac{g}{m^3}\right]$;
- $V$ is the volume of the reactor $[m^3]$;
- $Q$ is the flow rate withdrawn $\left[\frac{m^3}{d}\right]$.

As shown in formula 2.8 if the reactor is mixed and without recirculation, the biomass concentration will be the same inside the reactor and in the flow withdrawn.

Each time sludge is withdrawn, a fraction of the bacterial population is removed, implying that the cell growth must compensate for the cell removal to ensure a steady-state condition and avoid process failure (Dewil et al., 2008).

The slow growth kinetics of the methanogens affects the reactors sizing due to the need to avoid their washout from the digester. Therefore, adequate SRT must be maintained. The digester volume can also be defined based on the solids retention time since the digestion process is a function of the time required by the microorganisms to digest the organic material and to reproduce (Dewil et al., 2008). Therefore, there is a minimum value of SRT to be guaranteed to ensure the adequate advancement of the process, which is strictly related to the growth kinetics of microorganisms. At the same time, an increase in SRT can result in a higher removal efficiency of the organic matter, hence a more efficient biogas production. For instance, under the hypothesis of hydrolysis as the limiting kinetics of the AD process, removal efficiency can be expressed as shown in the following formula:

$$\eta = 1 - \frac{1}{1 + k \cdot SRT} \tag{2.10}$$

Where:

- $\eta$ is the removal efficiency of the of the hydrolysable organic matter
- $k$ is the hydrolysis kinetic constant $\left[\frac{1}{d}\right]$
- $SRT$ is the solids retention time $[d]$

### *Nutrients demand*

Microbial metabolic activity during a biological process is highly dependent on the presence of nutrients. This can be divided between macronutrients, such as C, H, N, O, and S, and micronutrients, also known as trace elements. Specifically, microorganisms use carbon for cell structure, nitrogen for protein biosynthesis, and Sulphur during the methanogenesis phase. It appears that AD, $CH_4$, and $CO_2$ are mainly derived from the conversion of C, H, and O. On the other hand, N and S are normally converted to ammonia and $H_2S$. As already pointed out, ammonia is fundamental for process buffering. An excessive amount of N in the digester may result in methanogens inhibition. On the contrary, too little may result in process failure due to the growth limitation. Regarding micronutrients, they may be used to improve the process performance. Commonly used trace elements include zinc, iron, cobalt, tungsten, and molybdenum. The addition of trace elements has been found to optimize the growth of methanogenic bacteria, on the other hand, an excess of their availability in a digester may lead to inhibition (Sibiya et al., 2015).

### *Inhibitory compounds*

The AD process can be negatively affected by inhibiting elements such as heavy metals, salts, ammoniacal nitrogen, pesticide residues, pharmaceutical products, detergents, disinfectants, etc. (Cecchi et al., 2005).

Therefore, inhibiting compounds are either already present in the feedstock or are generated during the process itself.

One of the most significant inhibitory compounds for AD is Ammonia, which is generated during the degradation of nitrogenous matter, mainly proteins, and urea. Inorganic nitrogen is mainly present in the form of Ammonium ($NH_4^+$) and free ammonia ($NH_3$). The latter has been indicated to be the toxic form because it can permeate the cell membrane, generating proton imbalance and potassium deficiency. Free ammonia concentration is mainly influenced by temperature, pH, and total ammonia concentration. An increase in temperature leads to a shift of the equilibrium reaction towards a higher concentration of free ammonia. As a result, it is found that thermophilic digestion is more easily inhibited than mesophilic digestion. In the same way, an increase in pH results in a higher concentration of free ammonia and therefore in greater toxicity. The resulting instability of the process may drive to an increment in the amount of VFAs, which again directs to a reduction in pH and a lower free ammonia concentration. Therefore, the process remains stable, but the methane yield is reduced. As

already pointed out, nitrogen is an essential nutrient for microorganisms, then ammonia concentrations beneath 200 mg/L are advantageous to AD. It is also relevant to point out that methanogenic archaea can be acclimated to ammonia inhibition as a result of a shift in the methanogenic population (Dewil et al., 2008).

Another relevant inhibition is associated with the presence of Sulphate, which is ordinarily found in wastewaters and consequently in WAS. Under anaerobic conditions, sulphate could be used as an electron acceptor and consequently reduced to sulphide by sulphate reducing bacteria (SRB). Hence, inhibition could be provoked by the competition for substrate between SBR and methanogens. Also, inhibition could be caused by the toxicity of sulphides for the different groups of microorganisms (Dewil et al., 2008).

Heavy metals also can inhibit the anaerobic digestion process. Industrial discharges are the primary source of heavy metals in urban wastewater and are responsible for up to 50% of the total metal content in sewage sludge. Industrial contaminants include zinc, copper, chromium, nickel, cadmium, and lead. On the other side, domestic sources are essentially connected with leaching from plumbing materials carrying Cu and Pb, use of detergents containing Cd, Cu, and Zn, and use of personal care products containing Zn (Dewil et al., 2008).

In general, the reason for the toxicity of metal ions is due to the fact that they inactivate a large number of enzymes by interacting with their sulfhydryl groups (Cecchi et al., 2005).

### *Biogas production*

The main product of AD is biogas which contains methane (55 - 65%) and carbon dioxide (30 - 40%) as major components with traces of water vapour, hydrogen sulfide, and hydrogen (Deepanraj et al., 2014). The composition of $H_2S$ in the biogas range from 0 - 3% and depends on the concentration of sulfur in the substrate. Nevertheless, the range of percentage composition of the gases generated from AD processes is dependent upon several factors including the digestibility of organic matter, kinetics, HRT, and temperature (Anukam et al., 2019).

The presence of methane, whose lower heating value (LHV) is 35,846 kJ/$m_n^3$ gives biogas considerable interest in energy recovery, with LHW values depending on the percentage of methane contained in it, between 18,800 kJ/$m_n^3$ and 25,000 kJ/$m_n^3$. All values refer to gas volumes in normal conditions (temperature = 0 ° C, pressure = 1 atm). Other components which are usually present, in much lower percentages, are not relevant in terms of energy however they can influence the process kinetics and biogas valorization (Bonomo, 2014).

Monitoring the quantity and composition (at least in terms of methane and carbon dioxide) of the biogas is of fundamental importance for the control of the stability of the anaerobic digestion process. If the reactor is operating under stable conditions, the production and composition of the biogas are constant. A decrease in the overall production of biogas and an increase in the percentage of $CO_2$ may indicate process potential inhibition and instability. It follows that the analysis of the production and the percentage composition of biogas should always be associated with the control of parameters such as the concentration of volatile fatty acids and the alkalinity of the medium. It can be observed that in the presence of overloads the percentage of $CO_2$ tends to increase and the volatile fatty acids as well (Cecchi et al., 2005).

According to Bonomo (2014), the maximum theoretical production of biogas and its composition (in the simplified hypothesis of a binary mixture limited to $CH_4$ and $CO_2$) can be predicted based on the elemental composition of the organic matrix subjected to anaerobic degradation, $C_aH_bO_cN_d$. Neglecting the growth of the biomass, the degradation products can be quantified as follows:

$$C_aH_bO_cN_d + \left(a - \frac{b}{4} - \frac{c}{2} + \frac{3d}{4}\right) \cdot H_2O \rightarrow \left(\frac{4a+b-2c-3d}{8}\right) \cdot CH_4 + \left(\frac{4a-b+2c+3d}{8}\right) \cdot CO_2 + d \cdot NH_3 \qquad (2.11)$$

The hypothesis assumed implicates the gasification of all the carbon present at the origin. Recalling that, under normal conditions, a mole of any gas corresponds to a volume of 22.415 $L_n$, taking into account the atomic weight of the elements considered, the volume of biogas produced per unit of degraded volatile solids is:

$$G_{th} = \frac{\left[\left(\frac{4a+b-2c-3d}{8}\right)+\left(\frac{4a-b+2c+3d}{8}\right)\right] \cdot 22.415}{12a+b+16c+14d} = \frac{a \cdot 22.415}{12a+b+16c+14d} \left[\frac{m_n^3}{kg_{VS}}\right] \qquad (2.12)$$

The volume of biogas produced per unit of degraded volatile solids can be calculated as:

$$G_{CH_4,th} = \frac{\frac{4a+b-2c-3d}{8} \cdot 22.415}{12a+b+16c+14d} \left[\frac{m_n^3}{kg_{VS}}\right] \qquad (2.13)$$

Consequently, the methane mole fraction, equivalent to its volume percentage, results equal to:

$$f_{CH_4} = \%_{v,CH_4} = \frac{G_{CH_4,th}}{G_{th}} = \frac{4a+b-2c-2d}{8a} \qquad (2.14)$$

According to formula 2.13, the methane volume percentage increases with the H/C ratio in volatile solids and decreases with increasing O/C and N/C ratios.

To set the mass balances, it may be useful to refer the biogas production calculated above to the degraded COD unit. The conversion between volatile solids and COD is obtained by

evaluating the stoichiometric quantity of oxygen necessary for the complete oxidation of the substrate.

The production of only methane in terms of COD can be directly obtained acknowledging that the COD content of the degraded organic substance is entirely transferred to methane, since carbon dioxide, unable to be further oxidized, has a null COD. Moreover, the COD corresponding to methane can be determined by considering its oxidation reaction:

$$CH_4 + 2O_2 \rightarrow CO_2 + 2H_2O \qquad (2.15)$$

It can be deduced that in 1 mole of $CH_4$ are involved $2 \cdot 32\ g_{O_2}$, equal to 64 $g_{COD}$, therefore for every $g_{COD}$ of methane (and therefore for every $g_{COD}$ removed) corresponds 1/64 of a mole. Therefore, for each $g_{COD}$ removed is expected a volume production of methane equal to 22.4/64 = 0.35 Ln.

### *2.1.3. Principles and perspective of co-digestion*

Anaerobic digestion has been implemented traditionally as a single substrate. Most municipal wastewater treatment plants have reported an excess digestion capacity of 15 to 30 percent. In those plants, the AD process is conducted with a low OLR, therefore they may be capable to co-process other organic materials. This process of digesting more than one substrate is called co-digestion. Anaerobic co-digestion (AcoD) or "co-fermentation" is the contemporary digestion of a mix of two or more organic substrates, generally an initial substrate such as waste sludge summed up with lower amounts of one or more secondary substrates. When combining organic substrates, the potential results could be synergistic, antagonistic, or neutral based upon methane production variations within the various scenarios. AD seems to become more stable when various substrates are co-digested provoking an improvement in the overall performance (Metcalf & Eddy I AECOM, 2014).

Therefore, AcoD with other biodegradable organic substrates among which OFMSW leads to increasing biogas production and digestate quality (Cabbai et al., 2016).

As shown in Figure 2.3 AcoD can improve biological activity and therefore biogas production.

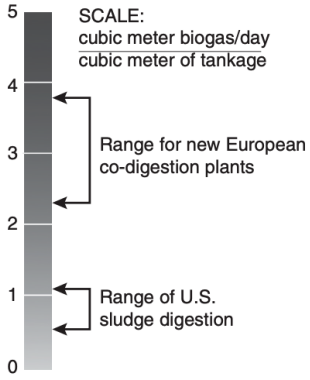


Figure 2.3 - Biogas production efficiency comparison (Metcalf & Eddy I AECOM, 2014).

As already pointed out, the optimum performance of AD depends on various parameters. Also, for the optimization of a co-digestion system, different parameters must be taken into account such as the chemical properties of wastewater and of the co-substate, their biodegradability, functioning parameters (temperature, pH, Particle sizes, C/N ratio, OLR, and HRT etc). Furthermore, in order to maximize the methane production from AcoD, in conjunction with the maintaining of stable conditions, the use of mathematical models such as ADM1 could be extremely helpful (Siddique & Wahid, 2018).

The suitability of a substrate in an AcoD process depends on its own composition in terms of proteins, carbohydrates, lipids, and inerts. For instance, food waste could cause a decrease in pH during the process due to its abundance of sugars that could be easily degraded into VFAs. However, food waste is generally considered a charming option for AcoD because of its high biogas potential. Another case of attractive substrates for AcoD in terms of biogas production improvement is animal manure or slaughterhouse wastewater. Those are rich in proteins and could release ammoniacal nitrogen during the digestion process which provides buffering capacity but at the same time free ammonia form could inhibit the microbial activity (S. Xie et al., 2017).

In recent times, to compensate for the oversizing of the many anaerobic digesters in WWTPs and at the same time solve the problem of the high production of organic waste, more and more research has been carried out on co-digestion with the most diverse substrates. For instance, Cabbai et al. (2016) has performed ACoD of source selected organic fraction of municipal solid waste (SS-OFMSW) and sewage sludge. Tests were conducted on a 3.4 $m^3$ pilot pant of CSTR reactor at mesophilic temperature. As SS-OFMSW substrate a mix of fruit and vegetable waste was used. The test was conducted in different phases at various OLR, which was increased from 0.80 $kg_{VS}/m^3$ d in the first phase up to 3.20 $kg_{VS}/m^3$ d in the last phase. The goal was to

test the maximum loading condition for the design of a full-scale AcoD plant. At maximum OLR was registered a VS abatement of 67.3%. This indicated the good adaptability of the biomass to treat more concentrated loads. Regarding the biogas, its composition during mono-digestion was about 63% methane, while it ranged between 64% and 71% during the following AcoD phases. As expected, the maximum biogas production was observed in the last phase of ACod with maximum OLR. In this last phase was registered an increment in biogas production of 192% in respect of the first phase. In conclusion, co-digestion of sludge and SS-OFMSW produced many advantages in AD process performance. The increase in biodegradable content and the low inert concentration in the secondary substrate allowed to reach high performances and high biogas production. The results achieved in this study was comparable with other experiences reported in literature, the biogas production of ACoD increase with increasing proportions of OFMSW.

Another significant study was conducted by Bolzonella, D. (2006) on two full-scale applications of the ACoD process of WAS with OFMSW. The experiences were carried out at Viareggio and Treviso WWTP in Italy. The first plant treats the wastewaters coming from the municipality of Viareggio for 100,000 PE with a working sludge digester of 3,000 m3. During the experiment, 3 tons per day of SS-OFMSW were co-digested with WAS, with an increase of the OLR from 1.0 to 1.2 $kg_{TVS}/m^3d$. Both substrates ha appropriate characteristics for co-digestion process in terms of total solids (TS) and total volatile solids (TVS) content. Also, the nutrients content resulted to be well balanced for the digestion process. The Specific Gas Production (SGP) increased from 0.21 to 0.26 $m^3/kg_{TVS}$ with only a 20% increase in the organic loading rate (OLR). In the second plant, the sludge treatment line considers a single-stage anaerobic digestion mesophilic reactor. Even in this case, the implementation of the OFMSW in AD allowed for a significant improvement of the digester yields. In terms of SGP, it increased from 0.22 to 0.43 $m^3/kg_{TVS}d$ thanks to the improved biodegradability of the fed mixture. This increase could completely change the energetic balance of the AD section in a WWTP. During the experiments were also monitored the parameters of AD. VFAs were constantly below a concentration of 100 $mg_{COD}/L$ and pH remained in the adequate range.

Although co-digestion can be considered an established technology, there are still several substrates on which it is possible to experiment. In addition to the SS-OFMSW, the waste from the agro-food industry could be used for ACoD. This application could bring significant benefits both in economic and environmental terms. With this in mind, Lab-scale experiments,

pilot plant experiments, and modeling can be useful to evaluate the expected performance of AcoD in order to identify the synergistic effects between the co-digested substates.

## *2.2. Biochemical methane potential (BMP) tests*

The evaluation of the anaerobic biodegradability and the maximum production of biogas obtainable from a specific substrate can be measured in the laboratory through batch tests. These tests are called Biochemical Methane Potential (BMP). A BMP test consists of a batch test in which lab-scale reactors are filled with a substrate and an anaerobic inoculum, typically retrieved from an active digester. The reactors are then kept at a constant temperature, generally between 35 ° C and 55 ° C, and continuously mixed for a period of about 30 days (Filer et al., 2019).

During the test, the anaerobic degradation of the organic content in the substrate will result in the generation of methane and carbon dioxide. Methane production is constantly measured, and its steady state value defines the methane production potential of the component. The substrate's methane potential can be expressed by the mass of volatile solids entered or by COD added, which is calculated by subtracting the methane volume from a blank (Filer et al., 2019).

The main result of the BMP tests that can be obtained is the measure of substrate biodegradability. It can be calculated by dividing the cumulative methane volume by the theoretical cumulative methane volume, which can be calculated from the stoichiometric ratio of 1 g COD = 0.35 mL CH4 at standard temperature and pressure conditions (Filer et al., 2019).

The executability of these batch tests requires a lower investment in terms of equipment, labor and time compared to experimentation in continuous reactors.

The idea of a BMP test was first described by Owen et al. (1979) with the aim of developing a test to calculate the biodegradability of a material subjected to anaerobic treatment. The original approach was then further developed and refined afterward. There are currently several companies selling complete automated BMP test equipment resulting in a large-scale deployment of the BMP test in AD research (Koch et al., 2020).

Nowadays, BMP tests are widely used to characterize a large variety of substrates. They have become a useful tool to assess the amount of methane that can be produced from organic materials in order to design different components of a full scale AD plant (Holliger et al., 2017).

Therefore, they provide an essential tool for the economic and technical optimization of AD plants and calibrating and validating mathematical models such as ADM1.

On the other hand, there tests still lack standardization, which impact on the comparability and validity of the BMP results. Nonetheless, the methods continue to evolve with the goal of eliminating systematic errors (Filer et al., 2019).

One of the most popular method is the one provided by the Association of German Engineers standard procedure VDI 4630. According to VDI the minimum test duration should be 25 days. The criterion for terminating the test is when the daily biogas rate on three consecutive days is below 0.5 % of the total volume of biogas produced up to that time. All parallel tests are terminated simultaneously, and the criterion is regarded as met when all batches have met it. If after more than 25 days of test duration, the result of mathematically subtracting the inoculum's gas production shows a negative rise in the test substrate's cumulative frequency curve for the gas, the test should also be terminated. During the course of the test, care should be taken that the fermentation material is sufficiently mixed. Continuous mixing (i.e. with a magnetic stirrer) should be preferable. In the case of substrates that do not form scum layers, periodic mixing (such as daily shaking) is mostly sufficient for completely resuspending the sediments. The biogas or the methane quantity should be read off as frequently as is necessary to make the dynamics of gas formation fully recognizable. This calls for daily readings at the beginning of the measurements. Once the daily gas production falls, readings can be made every two or three days. At the end of the test the pH value of the material in the fermentation test vessel should be determined and recorded (organischer Stoffe Substratcharakterisierung, 2016).

In general, to validate BMP test results the duration of the test should not be decided in advance and the test should only terminate when daily methane production during three consecutive days is < 1% of the accumulated volume of methane (Holliger et al., 2016).

In Italy, there is a standard called Uni 1601755/2018, which provides a method to perform BMP tests.

### *2.2.1. BMP tests preparation*

In order to obtain valid results from batch tests, the AD process must reach the highest possible degree of degradation. For this purpose, it is necessary to provide the optimal conditions for the AD process that occurs in the BMP tests (Koch et al., 2020).

The ideal BMP tests volume depends on the substrate homogeneity. Smaller volumes (125 - 500 mL) can be used in case of homogenous substrates, while heterogeneous substates require larger volumes (500 - 2000 mL). In any case, smaller bottles may not guarantee realistic operation conditions due to the smaller and non-representative microbial consortia. (Pearse et al., 2018).

BMP tests require a blank, filled with the inoculum, water and nutrients, but no substrate to provide the methane generation from the organic material in the inoculum. Generally, besides blank and substrate, a control test it is also performed. The control bottles are filled with inoculum, the control substrate, water and nutrients. Blank, control and substrate tests should be performed in triplicates or duplicates to check for reproducibility of the results and statistical analysis (Filer et al., 2019).

The inoculum supplies the microorganism to the anaerobic digestion process. It can be sampled from many different sources such as WWTP digesters, agricultural biogas plants, or OFMSW digestion plants. Different inocula can lead to different substrate biodegradability and different methane potential production due to different bacteria populations in the inoculum (Morendo-Andrade, 2004).

It is commonly recommended to select an inoculum from a source already adapted to the substrate. Part of the standardization process of inoculum involves quality control to designate whether the operational parameters of the digester are of good quality. Another common recommendation is to pre-incubate the inoculum for 1 to 5 days at 35 °C for degasing. In this way it is possible to reduce its residual methane production.

Table 2.1 - Recommended inoculum conditions for BMP tests (Filer et al., 2019)

| *Parameter* | *Recommended range* | *Units* | *Reference* |
|---|---|---|---|
| *Origin Source* | Active digester treating municipal wastewater sludge | - | (Holliger et al., 2016), (Pearse et al., 2018), (Elbeshbishy et al., 2012) |
| *pH* | $7 \leq x \leq 8.5$ | - | (Holliger et al., 2016) |
| *VFA* | < 1 | g $CH_3COOH$/L | (Holliger et al., 2016) |
| *$NH_4$* | < 2.5 | g $NH_4$/L | (Holliger et al., 2016) |
| *Alkalinity* | > 1.5 | g $CaCO_3$/L | (Holliger et al., 2016) |
| *Concentration* | 15 to 20 | g VS/L | (Holliger et al., 2016) |
| *Storage* | 1 to 5 days at 25 °C | - | (Elbeshbishy et al., 2012) |
| *Methane Yield* | ~ 50 | NL $CH_4$/g VS | (Holliger et al., 2016) |

Inoculum quality can also be analyzed and described through biomass activity tests using different standard substrates such as glucose and acetate (Holliger et al., 2016).

Regarding the substrate, there are fewer requirements, which are reported in table 2.2. Specifically, the samples should have a particle size smaller than 10 mm in any dimension. Before starting the BMP tests, substrate should be characterized in terms of total solid (TS), volatile solid (VS), volatile fatty acid (VFA), total Kjeldahl nitrogen (TKN), ammonium and alkalinity concentrations with the purpose to avoid potential inhibition problems (Wang et al., 2015). Besides, the German standard recommended that substrate concentration should be approximately 10 g VS/L, when inoculum concentration are between 1.5 - 2 % to obtain a inoculum to substrate ratio of 2 $g_{VS}/g_{VS}$ (organischer Stoffe Substratcharakterisierung, 2016).

The measured methane yield might depend on substrate concentration. High concentrations substrate could overload the digester, leading to inhibition caused by the built-up of intermediate products. On the other hand, if the substrate concentration is too low,

microorganism's metabolic activity may be low leading to low methane yield (Wang et al., 2015).

Table 2.2 - Recommended substrate conditions for BMP tests.

| ***Factors*** | **Recommendation** | **Reference** |
|---|---|---|
| *Particle size* | < 10 mm | (Angelidaki et al., 2009) |
| *Concentration* | 10 g VS/L | (Rozzi & Remigi, 2004) |
| *Compulsory parameters* | TS, VS, pH, VFA, TKN, NH4, ALK, COD | (Holliger et al., 2016) |

In the BMP tests, lack of nutrients can lead to growth limitation. Generally, it is not evident if inoculum and substrate contain enough nutrients to support microbial growth, therefore BMP nutrients solutions can be used.

During the test, it is mandatory to maintain consistent environmental conditions for the microbiology and biochemistry for anaerobic digestion to achieve optimal performance. Therefore, the test has to be done with a sufficient incubation time, in a temperature-controlled environment, with proper mixing. Temperature is a parameter that influences the growth rate and metabolism of micro-organisms and the population dynamics in the anaerobic reactor but also affects factors such as gas transfer rates and chemical equilibria. The chosen temperature influences the AD process that could be either mesophilic (30 – 38 °C) or thermophilic (50 – 58 °C). It is good practice that the temperature of the BMP bottles corresponds to the digester's temperature at which the inoculum is adapted. (Filer et al., 2019). The maximum temperature variation should be on the order of ± 2 °C (Holliger et al., 2016).

Mixing influences the distribution of microorganisms, substrate, alkalinity, and nutrients. It prevents the sedimentation of particulate material, causes the release of gas bubbles, and guarantees an equal distribution of the digester's temperature. The complete absence of mixing can cause inhibition due to the accumulation of toxic metabolic byproducts. So far, it is hard to define an optimal mixing pattern for BMP tests (Filer et al., 2019).

### *2.2.2. BMP fitting models*

Generally, the BMP test results are provided as final values of the methane yields of substrates. Nevertheless, methane production curves provide other useful information regarding substrate degradation kinetics (Brulé et al., 2014).

Therefore, the patterns these curves follow depend on substrate degradation pathways and kinetics. The kinetics of the different stages of the AD process and the shape of the methane production curves are affected by the biodegradability characteristics of the substrate, inhibition process, and the methanogenic bacterial populations performance in the inoculum (Ware & Power, 2017).

Using a model that describes methane production curves should allow an interpretation of substrate degradation kinetic and estimate the ultimate methane yield (Brulé et al., 2014).

Models describing the kinetics of batch anaerobic digestion generally derived from Monod kinetics that assumes that the growth rate of bacterial culture is affected by a growth-limiting nutrient. However, under certain conditions, it is possible to neglect saturation effects. In this case, the Monod equation can be simplified to become first-order kinetics (Brulé et al., 2014).

The first-order model assumes that the substrate's rate of degradation is proportional to the amount of substrate available.

$$r = k \cdot S_t \tag{2.16}$$

Where:

- r is the rate of substrate degradation;
- k is the first-order kinetics constant;
- $S_t$ is the amount of available substrate, undegraded at time t.

It is possible to obtain within an integration an exponential equation describing the remaining substrate at time t:

$$S_t = S \cdot e^{-kt} \tag{2.17}$$

Where:

- S is the total amount of degradable substrate;
- k is the first-order kinetics constant;
- t is the time after the experiment start-up.

The cumulated methane generated (Mt) can be calculated as follow, applying the kinetics of product formation to batch anaerobic digestion.

$$M_t = BMP \cdot (1 - e^{-kt}) \quad (2.18)$$

From an experimental point of view, the most significant value is BMP, which is the ultimate methane yield, that is the cumulated methane yield at t = +∞. Models to estimate methane production kinetics in batch BMP could be: two-step, dual-pool first-order, and dual-pool two-step (Brulé et al., 2014). There are also a considerable number of sigmoidal models in the literature, such as the models of Gompertz, and the modified Gompertz (Ware & Power, 2017).

Therefore, it is important to assess the quality of a model and choose the better model for parameter evaluation and methane production kinetics estimation.

The first-order kinetics model is usually the most broadly used, likely because it is simple and known to provide realistic estimates of the ultimate methane yields (Brulé et al., 2014).

### *2.2.3. Co-Digestion BMP tests*

To obtain a stable AcoD process and optimum biogas production, BMP tests are an essential tool. Indeed, the information provided by BMP tests is helpful to characterize and assess the optimal design and performance of the AcoD process. Besides, BMP tests could reveal the potential mechanisms of synergy among the co-digestion mixtures. (Siddique & Wahid, 2018).

A study on AcoD was conducted in batch through conventional BMP tests by T. Xie et al. (2017). In this study the specific methane yields of sludge and food waste were calculated both in mono and co-digestion. A significant improvement in terms of biodegradability values in co-digestion was noted. During the tests, synergistic effects in co-digestion of these two feedstocks have been identified, which were associated with the improved kinetics of acidification and methanogenesis stages.

## *2.3. Biomass activity tests*

The biomass activity tests are experimental procedures that can be used to determine either the specific microbial activity, expressed by a sole parameter (e.g., maximum specific activity) or the kinetics of substrate consumption. These tests can be applied to characterize the biomass present in a specific inoculum. Activity tests indeed provide an experimental method that

allows determining the microbial activity in the different steps of the degradation process. A typical application is process start-up. The start-up is one of the most critical phases and could be very helpful to determine the microbial activity to select an adequate inoculum (Soto et al., 1993).

Activity indicates the intrinsic ability to degrade a substrate of a microbial population. Activity can commonly be calculated as the specific consumption rate of a substrate referred to as the total biomass (i.e. VSS) or to the targeted microbial population. For instance, if the substrate concentration is the monitored variable, then the activity would be the slope of the curve of the substrate utilization (mass of substrate removed per unit biomass per unit time). It is also relevant to highlight how commonly the experimental work has used biogas measurements to assess activity and inhibition (Rozzi & Remigi, 2004).

It is important to make a fundamental distinction between specific methanogenic activity tests (SMA) and non-methanogenic activity tests.

SMA tests generally involve adding a known amount of soluble substrate (usually acetic acid or a mixture of acetic, propionic, and butyric acids) to a sample of biomass confined within a sealed vessel (Cho et al., 2005).

Specific methanogenic activity determines the methane-producing capability of the inoculum for a specific substrate. SMA can be utilized to outline the operating conditions for anaerobic digesters and a parameter to assess the system performance and its stability. During start-up, the SMA is of great importance in assessing the proper initial organic loading rate (Hussain & Dubey, 2017).

Consequently, while a methanogenic activity test allows the selection of an adapted sludge to be used as inoculum and an optimal OLR, an individual activity determination allows the apprehension of the potential unbalanced situation among different bacterial species and the determination of the relative significance of the different steps of the process (Soto et al., 1993).

Another interesting application of this kind of test is to determine the toxic effect that a specific substance exerts on an anaerobic sludge. Indeed, a change in SMA indicates an inhibition or an accumulation of slow degradable or even non-biodegradable organic matter from the influents (Hussain & Dubey, 2017).

As pointed out by Sørensen & Ahring (1993), the need for a standard activity test has repeatedly been proposed in the literature. The activity of the biomass is measured by the addition of specific substrates to batches of the biomass followed by measurements of the gas production.

Therefore, activity can be estimated by supplying sufficient substrate (acetate, propionate, butyrate, $H_2$, etc.) to saturate the catabolic systems of the various physiological groups, in order to determine the specific methane production rate. Activity can be defined as the substrate-dependent methane production rate per unit mass of volatile solids biomass. To check if any significant changes had occurred, pH must be measured in the vials at the beginning and at the end of the experiment. The Specific methanogenic activity can be calculated as the initial, linear methane accumulation rate divided by the biomass VS content in each test. The activity test requires generally 10- 25 days. As the maximum slope of the cumulative methane production curve can be used for activity calculations, the SMA is the highest value obtained after adaptation and growth of the microbial population. Thus, during the use of an activity test the initial rate of the methane accumulation should be linear to indicate that adaptation, significant growth of the biomass, or substrate depletion has not occurred. Activity tests as described in this study should be run under test conditions (i.e. pH, temperature, and mixing) that closely imitate the environment of a given system. It was also highlighted how in order to compare SMA values from different biomasses on specific substrates, methane accumulation in the control reactor (without specific substrate addition) must be subtracted from the accumulation in the reactor with substrate added. Thus, if there is a degradation of the substrate tested even in the control reactor, this will be subtracted from the degradation in the test reactor.

## *2.4. Anaerobic digestion model (ADM1)*

The Anaerobic Digestion Model No. 1 (ADM1) is to date the most extensive and broadly used model for AD processes and reports its main biochemical reactions and physicochemical processes (Poggio et al., 2016).

The ADM1 has been proposed by a task group of the International Water Association (IWA) to build a standard platform to simulate different scenarios of AD processes. ADM1 considers 7 groups of bacteria and archaea, catalyzing 19 biochemical kinetic processes, coupled to 3 gas–liquid mass transfer equations and 8 algebraic variables. It takes into consideration the biological conversions which happen during AD, from the first step (disintegration and hydrolysis) to the formation of methane (Kleerebezem & van Loosdrecht, 2006).

With the increasing popularity and spread of anaerobic digestion plants a generalized model of AD such as ADM1 can produce numerous advantages. It could be used to calculate the reactor volumes requirement in a full-scale plant, to predict biogas production, and digestate

composition. It could be helpful to optimize and control the AD process in existing full-scale plants. It might also be useful to assist the technology transfer from research to industry (Batstone et al., 2002).

Therefore, the ADM1 is a structured model which takes into account disintegration and hydrolysis, acidogenesis, acetogenesis, and methanogenesis steps, as shown in Figure 2.4. The Extracellular solubilization steps are divided into disintegration and hydrolysis. The first one is responsible for the conversion of composite particulate substrate into particulate protein lipids and carbohydrate and into inerts. Disintegration is a non-biological process. Both disintegration and hydrolysis are represented by first-order kinetics. As already widely stated, the reaction system in an anaerobic digester is complicated with several sequential and parallel steps. These reactions can be classified into two main classes:

- Biochemical reactions, which are usually catalyzed by enzymes (intra- or extracellular) and act on the biologically available organic material. As already mentioned, disintegration of composites, and their subsequent enzymatic hydrolysis extracellular processes. On the other hand, the digestion of soluble substances mediated by organisms is intracellular and this process leads to biomass growth and decay.
- Physicochemical reactions, which are not biologically mediated and include ion association/dissociation, and gas-liquid transfer. Also, in this group of reactions, there is precipitation that is not included in the ADM1 (Batstone et al., 2002).

COD ($kg_{COD}/m^3$) is the base unit used in ADM1 due to its use in wastewater measures. An important aspect to take into consideration is the distinction between the available degradable (usually termed as "substrate") and total input COD. In terms of units of measure, Molar basis ($kmole/m^3 \equiv M$) is applied for components with no COD such as inorganic carbon ($CO_2$ and $HCO_3^-$) and inorganic nitrogen ($NH_4^+$ and $NH_3$). The core of ADM1 is constituted by biochemical equations. Nevertheless, the physicochemical state (e.g. pH and gas concentration) and physicochemical conversions are also significant due to their effect on biochemical reactions (Batstone et al., 2002).

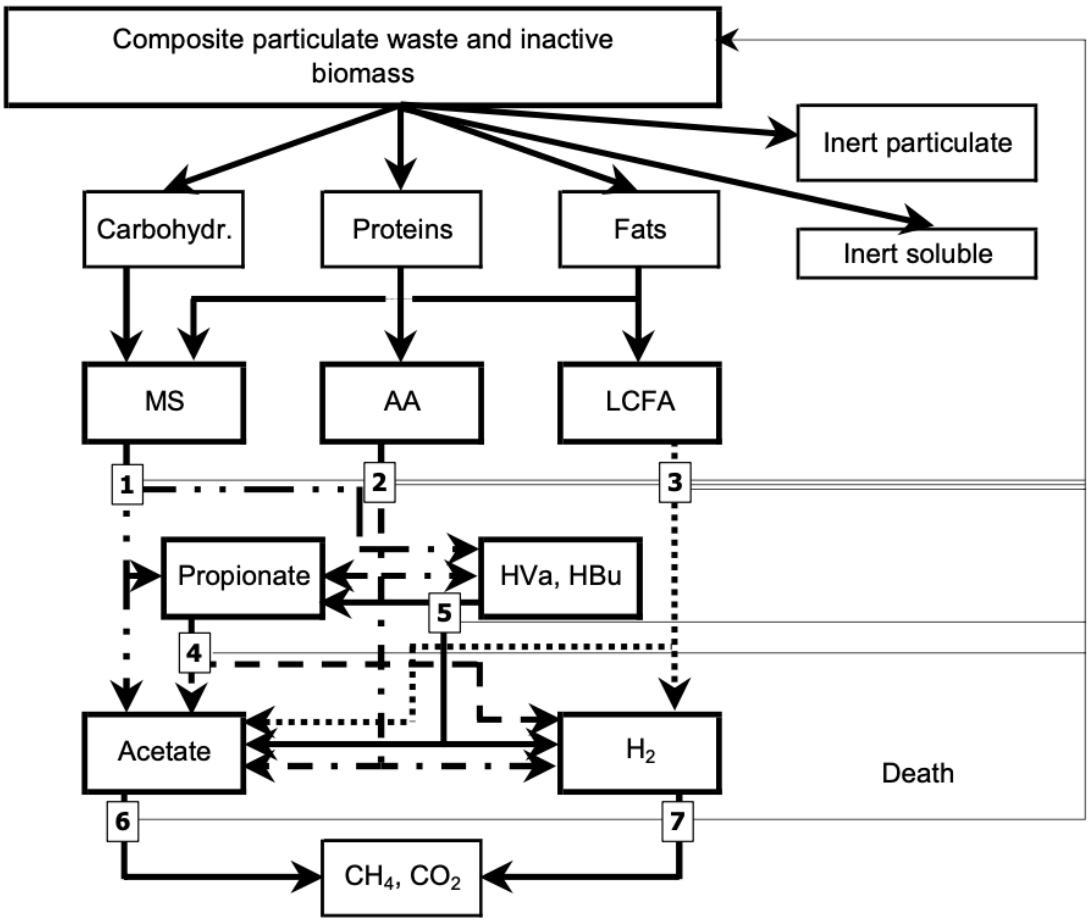


Figure 2.4 - ADM1 including biochemical processes (1) acidogenesis from sugars: (2) acidogenesis from amino acids; (3) acetogenesis from LCFA; (4) acetogenesis from propionate; (5) acetogenesis from butyrate and valerate; (6) aceticlastic methanogenesis; and (7) hydrogenotrophic methanogenesis *(Batstone et al., 2002)*.

A Petersen matrix is used to describe all the biochemical rate coefficients and kinetic rate equations for soluble and particulates components (APPENDIX A).

As already pointed out, ADM1 was developed for general modeling of AD leaving the opportunity to implement the model for specific applications.

For instance, Rosen & Jeppsson (2006) made some changes and additions to ensure that the model was as suitable as possible for wastewater treatment sludge digestion.

Directly after the introduction of the standardized ADM1, several publications showed that the model's requirement of a detailed influent characterization can hardly be fulfilled. The main weakness of the model application was addressed in the reliable and practical identification of the model's input state variables for particulate and soluble carbohydrates, proteins, and lipids, as well as for the inerts. Several authors derived biomass characterization methods, most of them dedicated to a particular substrate, while some of them were of general nature. Lübken et

al. (2015) provide an overview of existing approaches that improve substrate influent characterization to be used for state-of-the-art anaerobic digestion models, trying to develop a practical standard protocol.

### *2.4.1. Applications*

Since its development, AMD1 has been used to simulate the AD process of sludge but also of various other substrates and for various plant configurations. For instance, it has been used to simulate agricultural wastes (Antonopoulou et al., 2012), microalgae (Mairet et al., 2011), and other solid wastes like animal manure (Astals et al., 2015). Most of these simulation results show that ADM1 can well simulate the AD processes by making some modifications to the structure or the kinetic parameters of the original ADM1 model.

As expected ADM1 has also provided a useful tool to simulate the AcoD processes of sludge with other feedstocks. For instance, ADM1 was applied by Derbal et al. (2009) to simulate a full-scale AcoD process for the treatment of the OFMSW along with WAS from a municipal wastewater treatment plant. In this study, the simulation results were then compared with experimental values. During the tests it was found that the kinetic parameters of disintegration and hydrolysis, evaluated considering batch test and the modeling of experimental data, were similar to typical values reported in the literature. The simulated results showed a good fit for pH, biogas composition, biogas volume, COD, total VFAs, inorganic nitrogen, and inorganic carbon. On the other hand at the start of the experiment, where a transient state prevails, the simulated results did not show a good fit. It was also assessed that inorganic carbon or bicarbonate alkalinity is a very sensitive parameter to VFAs accumulation and hence it can be used as a monitoring parameter for this phenomenon.

Another interesting ADM1 application study was carried out by Montecchio et al. (2019). In this case, the application of the ADM1 model to the co-digestion of food waste and WAS was studied to explore the acidification problem affecting food waste in mono-digestion. The results of this study show that through modeling and experimental results it is possible to demonstrate that acidification could be due to the methanogenic activity decline. Another important result is that ADM1 was only adequate for digestions with a high activity level for both bacteria and methanogens and, under these conditions, the model was able to correctly predict the relative abundance of microbial populations.

G. Esposito et al. (2011) used the ADM1 model to optimize the anaerobic co-digestion of sewage sludge and OFMSW, assessing the effect of the OLR and OFMSW particle size on the reactor performances. In particular, the methane production has been evaluated to assess the model capability to estimate the potential energy production under different process conditions; then a sensitivity analysis on OLR and OFMSW particle size has been carried out. The latter shows the model suitability to assess the combined effect of such parameters on the digester performances, predicting the process failure occurrence. It resulted from the study that the mathematical model used was capable to assess the effect of the OFMSW particle size on the methane production rate and its cumulative formation. Also, the mathematical model can be used to assess the maximum OLR increase due to OFMSW co-digestion that an anaerobic digester can tolerate. Model simulations show that if this maximum OLR value is exceeded it will result in a pH drop and thus a digester failure. Furthermore, the study shows how the model calibration is an essential step in order to use the proposed mathematical model to predict the performances of a full-scale digester fed with a specific OFMSW.

### *2.4.2. Substrate characterization*

As already pointed out, since the development of the current state-of-the-art model for describing anaerobic digestion processes (Anaerobic Digestion Model No. 1 - Batstone et al., 2002), researchers have dealt with two key constrains for model application: (i) the lack of generally accepted guidelines for influent substrate characterization according to model input variables, and (ii) the wide range of variability of a large number of kinetic parameters, requiring the estimation of the most sensitive ones (Girault et al., 2012).

A reliable analytical determination of all model input components, as well as the full identification of all individual parameters are not straightforward nor practical (Kleerebezem and Van Loosdrecht, 2006). Default values are available from literature (Batstone et al., 2002, Lübken et al., 2015; Rosen and Jeppsson, 2006) and are recommended for the digestion of municipal wastewater sludge but may not be appropriate for a wide range of organic wastes or for co-digestion applications (Razaviarani and Buchanan, 2015).

Several methods have been proposed to determine ADM1 input state variables with minimal analytical efforts. The most common way is to estimate substrate fractionation from direct analysis of the biochemical fractions: carbohydrates, proteins and lipids (Astals et al., 2013; Girault et al., 2012, Koch et al., 2010; Wichern et al., 2009). An alternative approach relies on

the determination of the elemental mass fractions of carbon, hydrogen, oxygen, nitrogen, and phosphorus starting from practical chemical measurements (Kleerebezem and Van Loosdrecht, 2006; Zaher et al., 2007; Zaher et al., 2009) or directly from the elemental analysis (Poggio et al., 2006); fractions for proteins, carbohydrates, lipids and VFAs are then calculated using the elemental substrate composition and an ideal molecular formula for each component. Further, anaerobic respirometry has been proved to be essential for the three main purposes: (i) to identify the kinetic parameters associated with degradation/hydrolysis; (ii) to quantify the degradability extent ($f_d$) or the inert influent COD fractions ($X_i$, $S_i$); (iii) to distinguish between soluble and particulate fractions by interpreting methane production rate (MPR) curves obtained from batch experiments (Astals et al., 2013; Batstone et al., 2009; Girault et al., 2012; Poggio et al., 2016; Razaviarani and Buchanan, 2015).

Regarding this matter, Poggio et al. (2016) assessed a rigorous substrate characterization methodology to be used for ADM1 simulation based on a combined biochemical and kinetic fractionation approach. The study shows that the prediction of methane production from complex substrates such as green waste and food waste can be improved by incorporating different particulate fractions with different degradation kinetics. Further, they showed that the quality of fit between experimental and simulated outputs increases with the number of fractions that are used to represent the particulate and soluble organic matter. Nevertheless, depending on the data set used to estimate the fractionation and kinetic parameters, the associated parameter uncertainty may be too great to justify the more complex substrate description.

Solon et al. (2015) investigated the effects of influent fractionation, kinetics, stoichiometry, and mass transfer on $CH_4$, $H_2$, and $CO_2$ production for modeling of anaerobic digesters. It was observed that in AD units operating with long SRTs, influent fractionation is determined to be the most influential parameter with respect to $CH_4$ and $CO_2$ production, while for shorter SRTs at mesophilic conditions also the role of acetate degraders becomes important. Knowledge of these highly influential parameters is useful for understanding the AD process including situations of a process failure and for model calibration and validation exercises.

# Chapter 3: MATERIALS AND METHOD

## *3.1. Pilot plant and procedures*

The experimental apparatus used for this study consists of five main parts: pre-storage tank, anaerobic digester, hydraulic seals, gas meter and control panel.

The plant as a whole was designed and built by the company Seam Engineering aimed at carrying out the research and development project called "PerFORM WATER 2030".

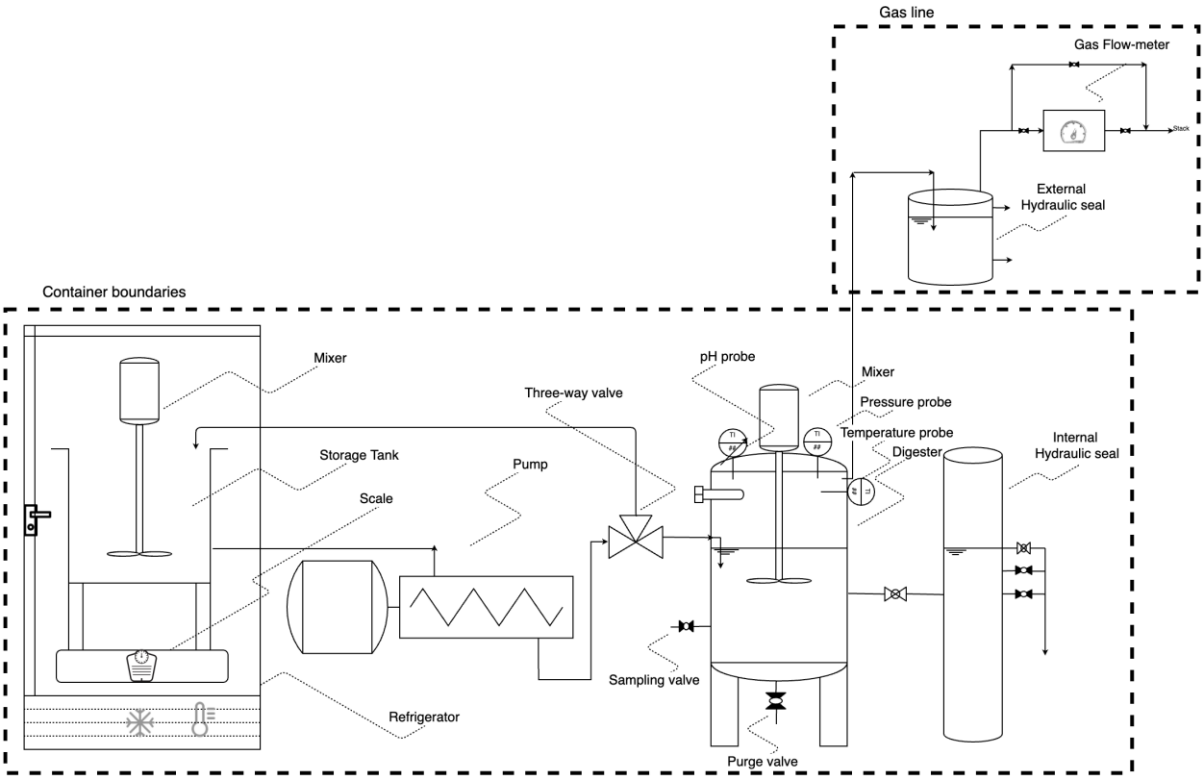


Figure 3.1 - Scheme of the pilot plant.

Figure 3.1 shows a scheme of the pilot plant. The pre-storage tank, with a useful volume of 25 L, is located on a balance, inside a refrigerator capable of maintaining the temperature below 4 °C. Inside the tank there is a mixer (ARGO LAB AM40-D) to avoid sludge settling. The mixer can work in a speed range of 50-2200 rpm. It has generally been set to work at 250 rpm. The storage tank is connected via a pump to the pilot digester (NETZSCH CY15/15). The pump can operate with a flow rate range of 5-20 L/h. A three-way valve defines if the sludge is fed to the digester or recirculated back to the tank. The digester is characterized by an overall volume of 77 L. The liquid volume is regulated by two hydraulic seals. The experimentation

was carried out with a liquid volume of 60 L and a headspace of 17 L. The digester is equipped with a mechanical mixer operating at 104 rpm. It is also equipped with a heating system to maintain the temperature at 38±0.5 °C and a set of sensors capable of measuring pH, temperature, pressure, and RedOx potential. Finally, the digester is equipped with a bottom purge valve and a side valve for digestate sampling. There is also a system for measuring the gas produced by the digester which is described in paragraph 3.3.4. Finally, a programmable logic controller (PLC) is available for signals storage and operation of the main equipment. This can also be managed remotely and has the purpose of allowing the user to check the operating conditions of the system, as well as to feed up the digester (by opening the three-way valve) and check that there are no malfunctions.


Figure 3.2 - photographs of the anaerobic digester, the pump, the internal and external hydraulic seals and the external structure before the start-up.

### *3.1.1. Pilot Plant Procedures*

A pilot plant check has always been carried out on a weekly basis. Every week, the pre-storage tank was refilled with enough feedstock to feed the digester for the following week. Before carrying out this operation, it was generally necessary to clean the mixer inside the tank on which sludge accumulations sometimes formed.

Also, the digestate was taken every week through the appropriate sampling valve. During these operations, the biogas outlet valve directed to the external hydraulic seal and the connection valve to the internal hydraulic seal have always been closed. This precaution was applied to prevent the water from the external hydraulic seal or the digestate contained in the internal hydraulic seal from entering the digester. These two valves were therefore reopened only after the pressure inside the digester had re-established at 35 mbar, generally following the feeding of the sludge.

The external water guard was reloaded weekly. In addition, the digester and hydraulic seals bolts were sometimes tightened to prevent loosening and leaks.

Finally, weekly, a biogas sample was taken so that its composition could then be studied using a gas chromatograph.

## *3.2. Feed*

The feed was composed of different organic matrices dosed at different times. There was the first phase of mono-digestion in which only the sludge was used. This phase was necessary for the start-up of the digester and the achievement of steady-state conditions. Subsequently, in a second phase, co-digestion was started by dosing yogurt as a secondary co-substrate together with the sludge. The feeding was carried out semi-continuously, feeding all the daily food in a specific hour.

### *3.2.1. Sludge*

The initial substrate was a mixed sludge, composed of about 90% of primary sludge and 10% of waste-activated sludge. The sludge was collected from the WWTP of Sesto San Giovanni (Gruppo CAP - Amiacque) generally every week. Then it was stored in a fridge below 4 °C for 1 day. Subsequently, it was manually thickened and fed to the storage tank at the pilot plant, always below 4 °C. For each sludge sampling carried out the following analyses were performed to evaluate its characteristics:

- Volatile (VS) and total solids (TS)
- pH and alkalinity
- $NH_4^+$
- VFA

About once every 2 weeks a comprehensive monitoring plan was carried out including the following additional analyzes:

- Soluble and total COD
- Soluble and total TKN
- Soluble and total carbohydrates
- Soluble and total proteins
- soluble and particulate lipids
- VS and TS of the soluble and particulate sludge fraction
- BMP tests

BMP tests were performed approximately every 3 weeks. Overall, 4 BMP tests were performed during the first phase of mono-digestion and 3 BMP tests during the second phase of co-digestion with yogurt.

### *3.2.2. Yogurt*

The yogurt used during the experimentation as a second substrate for co-digestion was also supplied by Gruppo Cap and collected from the WWTP of Sesto San Giovanni. These were packaged yogurts of popular commercial brands whose composition in terms of carbohydrates, proteins, and lipids was already known as it was shown on the labelling. The yogurt was stored in a refrigerator at a temperature below 4 ° C. From the moment the co-digestion was started, yogurt was dosed together with the sludge in the pre-storage tank where they were then mixed.

The yogurt load was 20% of the OLR of the sludge. The following analyzes were performed on the yogurt:

- Volatile (VS) and total solids (TS)
- pH
- carbohydrates
- proteins
- BMP tests

## *3.3. Analytical Methods*

### *3.3.1. pH / Alkalinity*

The pH was directly measured in liquid samples by means of a portable multi-probe meter (Hach-Lange, HQ40d).

The alkalinity was determined by two methods:

1. In the laboratory of San Giuliano Ovest, sulfuric acid ($H_2SO_4$) was used to manually titrate the sample to pH 4.3. Sulfuric acid was added slowly to 100 ml of continuously mixed sample, while measuring the pH with the portable multi-probe meter (Hach-Lange, HQ40D). Once the pH reached stably the value of 4.3, the volume of sulfuric acid used was quantified and the alkalinity value of the sample was calculated.
2. In the A. Rozzi laboratory in Cremona, total alkalinity (corresponding to TAC in German) was measured by means of the FOS/TAC instrument (Hach Lange BIOGAS Tritation Manager). Samples were always diluted 1:10 with deionized water. Then, titration was performed with Sulfuric acid ($H_2SO_4$) to pH 8.3 first, pH 4.3 then.

In both cases total alkalinity was calculated as the product of the volume of acid used to reach the pH end point, the normality of the acid and the conversion coefficient of Calcium carbonate ($CaCO_3$) to equivalent (50 mg$CaCO_3$/eq), divided by the volume of the sample.

### *3.3.2. Ammoniacal nitrogen*

The ammoniacal nitrogen determination ($NH3+NH_4^+$) was carried out on a filtered sample at 0.45 µm and analysed using the HACH-Lange colorimetric kit.

### *3.3.3. COD*

The determinations of the total COD $\left(\frac{g_{COD}}{g_{TQ}}\right)$ were performed at the A. Rozzi laboratory according to Standard Methods 5220 (APHA 2005). Determinations of dissolved COD were performed using HACH-Lange colorimetric kits on the soluble fraction.

### *3.3.4. Biogas*

The biogas was sampled, through a gas sapling bag, directly from the pilot's gas line every week to study its composition. This analysis was carried out using the tool Inficon Micro GC fusion. The composition of the biogas was obtained in terms of methane, carbon dioxide, hydrogen, and hydrogen sulfide.

The pilot plant was also equipped with a biogas flow meter. Specifically, BPC® µFlow, which is a compact standalone volumetric gas flow meter. The µFlow is a flow meter for ultralow gas flow detection. It provides a large detection range, with high linearity from 4 to 850 mL/h with a 2 mL flow cell. This makes it highly suitable for most lab- and small pilot-scale applications. The µFlow automatically normalizes gas flow and volume measurements with real-time temperature and pressure compensation. The volumes are normalized to 0 °C and 1 atm.

In the month of December, due to the winter frost, this apparatus was no longer able to work effectively.

### *3.3.5. Lipids*

The lipid analyzes were conducted at the environmental engineering laboratory of Politecnico di Milano. Particulate and soluble lipids were measured. The samples were prepared by centrifugation for 15-30 minutes at 5000 rpm to separate the solid fraction from the liquid fraction. Samples were stored in the refrigerator at 4-6 °C after being acidified to pH 2 by concentrated $H_2SO_4$.

#### *Particulate lipids*

The analysis of the particulate lipids was carried out using the Soxhlet solvent extractor of Velp SER 148 shown in Figure 3.3. The SER 148 can be used to separate a substance or a group of elements from solid and semi-solid samples according to the Randall technique (consisting of

immersion, washing, and solvent recovery). The fast solubilization made by hot solvent permits a considerable reduction of the extraction time (approx. 90 minutes). The extraction is made by immersion of the sample in the boiling solvent, followed by a rinsing phase with cold solvent. The sample must be dried before it can be analyzed. This procedure was carried out using anhydrous sodium sulfate ($Na_2SO_4$). Specifically, about 20-25 g of anhydrous sodium sulfate is dosed on a sample of about 3-5 g. After the addition of $Na_2SO_4$ the sample has been stirred to a smooth paste and spread on sides of the beaker to facilitate subsequent sample removal. It has been stand until solidified (15 to 30 min). Then the solids were removed and grinded in a porcelain mortar into a powder. The powder was then added to a paper extraction thimble. In addition, the beaker and mortar were wiped with small pieces of filter paper moistened with n-hexane and added to the thimble. Then the thimble was covered with cotton wool. For each thimble, a SER 148 specific Velp beaker was filled with 60 mL of n-hexane (used as a solvent) and small glass beads. At the end of the procedure, oil and grease extracted are transferred to a 25 mL vial using n-hexane for precise measurement of their weight. Before being weighed, they must be kept in an oven at 45 ° C for about 2 hours. A blank test is also carried out in which the paper extraction thimble is filled with small pieces of filter paper moistened with n-hexane and covered with cotton wool. The blank results are then subtracted from the tests.


Figure 3.3 - Soxhlet solvent extractor VELP SER 148.

*Soluble lipids*

Soluble lipids are extracted from water by intimate contact with an extracting solvent. In this case, the first apparatus used is a separatory funnel of 2 L. 200 mL of acidified sample are transferred using a liquid funnel to the separatory funnel. The sample bottle is then carefully rinsed with 30 mL of n-hexane (used as extracting solvent) and then the solvent is added to the separatory funnel. It is then shaken for two minutes. After that 10-15 min are waited to let the layers separate. After that, the aqueous layer is drained in the original sample container while the solvent is drained through a funnel containing a filter paper and 10-15 g $Na_2SO_4$ into a distilling flask. During the analysis, an emulsion very difficult to break is formed. The emulsion is drained into a centrifuge tube and centrifuge for 5 min at 2400 rpm. The centrifuged material is then collected into the distilling flask after draining through the funnel containing the filter paper and $Na_2SO_4$. The remaining emulsion and the aqueous part are then recombined with the aqueous layer into the original sample container. Then the same procedure is repeated three times. The second apparatus used for this analysis is the laboratory rotary evaporator "Heidolph VV 2000". The rotary evaporator is an equipment used to remove solvents from a solution of a compound of interest, by evaporation at low pressure. It consists of five main elements which are an evaporating flask containing the solution to be evaporated, a thermostatic bath, in which the evaporating flask is immersed to maintain the solution at the appropriate temperature, a motorized mechanism capable of rotating the flask of evaporation, a vertical or inclined condenser that removes the bulk of the vapors developed and a collection flask for condensed solvents. The flasks, the condenser, and the connecting elements between them are made of glass, and the whole assembled system guarantee a perfect vacuum seal. A pump is used to maintain the vacuum. Then, the evaporating flask containing the oil and greases extracted is connected to the rotary evaporator and waits for about half an hour until all the hexane is separated. Therefore, as seen previously in the last phase of particulate lipids, using the hexane, oils and greases are transferred into a 25 mL vial to carry out a more precise weighing. At this point measurement of soluble lipids and hydrocarbons present in the analyzed sample are obtained, consequently, it is necessary to proceed with the extraction of the hydrocarbons.

Figure 3.4 - On the left the laboratory rotary evaporator "Heidolph VV 2000" while on the right the separatory funnel of 2 L.

*Hydrocarbons extraction*

As seen, both procedures for the analysis of particulate and liquid lipids, in addition to the lipids, the hydrocarbons are also extracted. Consequently, these hydrocarbons must be isolated and quantified to obtain the exact measurement of the lipids. This is done using syringes containing florisil. If the solution of hydrocarbons and fatty materials in a non-polar solvent passes through florisil, the fatty acids are removed selectively from the solution. The not eliminated material are designated as hydrocarbons. In this way, it is possible to calculate the quantity of lipids contained in the sample without any difference.

### *3.3.6. TKN*

TKN (Total Kjeldahl Nitrogen) is defined by the sum of ammonia nitrogen and organic nitrogen present in a sludge $\left(\frac{mg_N}{g_{TQ}}\right)$. Its determination was carried out in the A. Rozzi laboratory according to ISO 5663-1984 Method.

### *3.3.7. VFA*

The VFAs (Volatile Fatty Acids) were determined by quantifying each single volatile fatty acid (acetic, propionic, isobutyric, butyric, isovaleric and valeric) by gas chromatography, according to Standard Method n. 5560 (APHA, 2005). Specifically, a gas chromatograph

(DANI Master GC) was used coupled to a flame ionization detector (FID Nukol fused silica). Organic compounds burning in the flame produce ions and electrons which can conduct electricity through the flame. A large electrical potential is applied at the burner tip, and a collector electrode is located above the flame. The current resulting from the pyrolysis of any organic compounds is measured and converted into mass of the corresponding VFA.

In particular, 25 mL of fresh sample were stabilized with 1 mL of 3N NaOH solution and subsequently centrifuged and filtered at 0.45 μm in San Giuliano Ovest laboratory. Then about 3-5 ml of stabilized sample was stored in the refrigerator below 6°C and analyzed at the A. Rozzi laboratory in Cremona.

### *3.3.8. Pretreatment of samples for the determination of the total content of carbohydrates and proteins*

In order to determine the total content of carbohydrates ($CH_{tot}$) and proteins ($PT_{tot}$), the following pre-treatment procedure of the sludge sample was adopted, previously developed and selected at the A. Rozzi laboratory in Cremona. This procedure involves the following steps:

- freezing of about 30 mL of sample as it is;

- defrosting;

- sonication for 1h;

- dilution with deionized water (variable according to the type of analysis - proteins or carbohydrates -, in order to fall within the range of concentrations defined by the calibration line, and the type of sample).

This is followed by the analysis of carbohydrates and proteins using Dubois and BCA methods directly on the diluted sample ‘as received’.

### *3.3.9. Protein Content Analysis*

The BCA (Bicinchoninic Acid) method was selected to determine the protein content. Concentrations are expressed in mg of Bovine Serum Albumin (BSA) equivalent per liter of solution and the kit provided by Thermo Fisher Scientific was used. The method involves the

dosage of 2 ml of BCA reagent and 0.1 ml of sample. The samples to be analyzed for proteins were incubated at 37 ° C for 30 minutes, following the "standard" procedure. After cooling to room temperature, the absorbance at 562 nm was measured using a UV-VIS spectrophotometer. For the determination of the calibration curve, bovine serum albumin (BSA) was used as a standard. The range of validity is $20 - 2000\ \frac{mg_{BSA}}{L}$.

### *3.3.10. Carbohydrates Content Analysis*

Carbohydrate content analysis were conducted using the Dubois colorimetric method using a 5% w/v solution of phenol and pure sulfuric acid (≥ 97%). The results are expressed in mg of glucose equivalent per liter of sample $\left(\frac{mg_{Glu}}{L}\right)$. Specifically, 1 mL of phenol solution is added to 1 mL of sample. Then 5 mL of $H_2SO_4$ are added and wait 10 minutes. At this point the sample can be mixed and a further 30 minutes are waited in order to allow the sample to cool down to room temperature. The absorbance reading at 490 nm is then carried out using a spectrophotometer. Glucose was used as a standard for the determination of the calibration curve. The validity range for the calibration curve is $0 - 200\ \frac{mg_{Glu}}{L}$.

### *3.3.11. Total and volatile solids*

Total and volatile solids were determined in duplicate according to Standard Methods 2540 (APHA, 2005).

### *3.3.12. BMP Tests*

The following tests were carried out in duplicate:

- blank BMP test containing the inoculum (degassed digestate), water and nutrients.

- Sludge BMP test containing inoculum, sludge, water and nutrients

- Particulate BMP test containing the inoculum, the separated sludge solid, water and nutrients

- Yogurt BMP test containing the inoculum, yogurt, water and nutrients (only during the co-digestion phase)

- Co-digestion BMP test containing inoculum, sludge, yogurt, water and nutrients (only during the co-digestion phase)

- Residual BMP test containing fresh digestate as inoculum, water and nutrients.

The apparatus used to perform these BMP tests is the Nautilus Anaerotech model by Anaero technologies which is shown in Figure 3.5. Through a gearbox this equipment uses one motor to mix 15 batch reactors through stainless/silicone paddles, assuring equal mixing intensity. By immersion in a water bath with a tight water lid, the temperature is maintained constant at 38 °C for all reactors, and evaporation is minimized. The reactor features a high volume of 1 L. As already said, all 15 reactors are mixed at the same speed driven by a gearbox. Gas generation is measured using the liquid displacement method. The gas flow meter is a single Perspex block with 15 cells of 0.2 L and Perspex tumbling buckets of around 7 ml gas volume. A spare cell is used for the automatic monitoring of temperature. The liquid in all cells is interconnected to keep equal head pressure in all reactors. The liquid used is NaOH 3M to remove $CO_2$ from the gas. Each cell has a tumbling bucket with an active volume of around 7ml (easily calibrated). The smaller measuring volume allows for better recording of the kinetics of the test. The data are constantly monitored through an Arduino-based system which consists of an Arduino 2560 Mega microcontroller which acts as the main controller for the data logger. All tumbler events are written to a log file on the microSD card including the channel number, the time at which the event occurred, the air pressure at that time, and the temperature as recorded by the thermocouple.

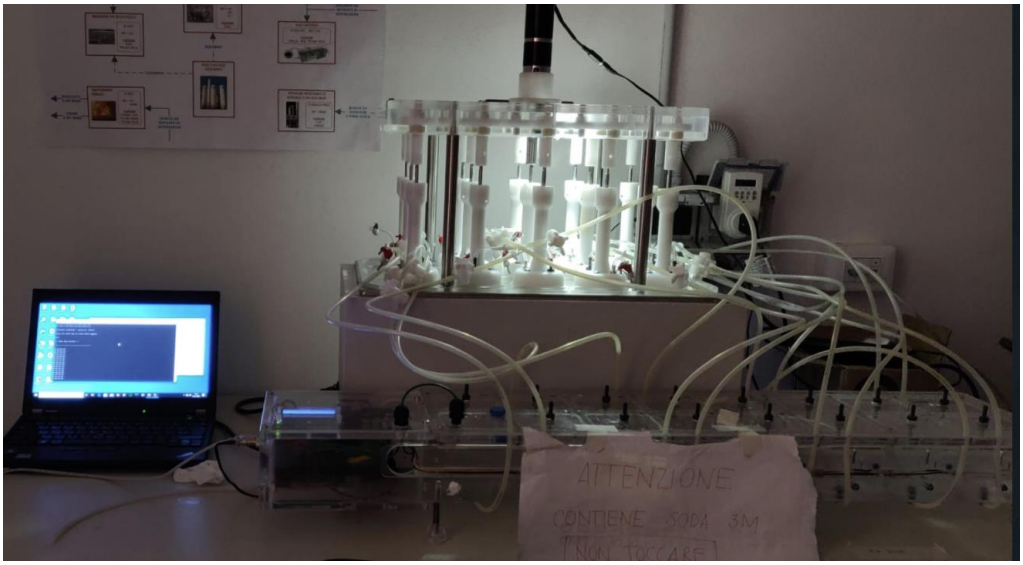


Figure 3.5 - Nautilus Anaerotech model by Anaero technologies.

The BMP tests were prepared by dosing inoculum and the substrate, together with water and nutrients inside the 1 L anaerotech reactors. These were dosed to have a working volume of 800 mL. This way a ratio between the working volume and the total volume of 80% is obtained. Regarding the BMP tests of sludge, sludge particulate matter, yogurt, and co-digestion (sludge plus yogurt), they were established on the assumption of an Inoculum / Substrate (I / S) ratio based on VS. Table 3.1 shows the BMP tests performed and the relevant test conditions.

Table 3.1 - Summary of BMP test conditions.

| BMP test | Number of tests | Date | Inoculum dosed [g] | I/S ratio [$g_{VS,I}/g_{VS,S}$] | Yogurt VS fraction [$g_{VS,yogurt}/g_{VStot,s}$] |
|---|---|---|---|---|---|
| Blank | 7 | 22/10/20<br>05/11/20<br>19/11/20<br>30/12/20 | 500 | - | - |
| | | 04/02/21<br>25/02/21 | 550 | | |
| Sludge | 7 | 22/10/20<br>05/11/20<br>19/11/20<br>30/12/20 | 500 | 2 | - |
| | | 04/02/21<br>25/02/21 | 550 | | |
| Particulate sludge | 7 | 22/10/20<br>05/11/20<br>19/11/20<br>30/12/20 | 500 | 2 | - |
| | | 04/02/21<br>25/02/21 | 550 | | |
| Yogurt | 3 | 30/12/20 | 500 | 3.5 | - |
| | | 04/02/21<br>25/02/21 | 550 | | |
| Co-digestion | 3 | 30/12/20 | 500 | 2.5 | 0.45 |
| | | 04/02/21 | 550 | | 0.5 |
| | | 25/02/21 | 550 | | 0.65 |

In each BMP test, three nutrient solutions were added for a total volume of 88 mL. The composition of these nutrient solutions was reported in APPENDIX G. Finally, once the quantity of inoculum and substrate to be dosed in the test was established, the dilution water was calculated as the difference between a working volume of 0.8 L and the sum of the

substrate, inoculum, and nutrients volumes. The blank test was conducted by dosing the same amount of inoculum as the BMPs it is to be compared with. Also in this case, nutrients and a volume of water were added to bring the working volume to 0.8 mL. During the BMP setting, it was verified that the concentration of inoculum and substrate as VS was in the range 1-5 $g_{VS}$/L. Further verification of the BMP setting was carried out on the total solids in the batch, verifying that the concentration of ST was in the range 10-50 $g_{TS}$/L.

As for the Residual BMPs, 600 g of fresh digestate were used. Even for Residual BMPs, 88 mL of nutrients were dosed and enough water to reach a working volume of 800 mL.

For each test, volatile and total solids of inocula and substrates were measured. Furthermore, the pH was measured at the start of the test. If the pH was lower than 7.2 it was adjusted by dosing NaHCO3 to add buffering capacity. BMP tests were only discontinued when the methane production increased by less than 1% of the cumulated volume for three straight days. Following this criterion, the tests generally lasted 21 days.

At the end of the BMP tests, further analyzes were carried out on the contents of each bottle. Specifically, the following analyzes were carried out:

- pH;
- Analysis of proteins, carbohydrates, soluble lipids, and particulate lipids;
- Total TKN;
- Ammonium ($NH_4^+$);
- VS and TS;
- VS and TS of the soluble fraction;
- VS and TS of the particulate fraction.

These analyzes were not conducted only in the case of residual BMPs for which only the pH was measured at the end of the test.

### *3.3.13. Activity Tests*

Activity tests were performed with the Nautilus Anaerotech, the same instrument used for the BMP tests and described in the previous paragraph. Three types of activity tests were performed using different substrates: acetate, glucose, and BSA (bovine serum albumin). In all tests, fresh digestate from the pilot plant was used as an inoculum, dosed to ensure a concentration of 10 $g_{VS}$/L in each bottle. The tests were always carried out in duplicate. The

tests were designed to last between 5 and 14 days, according to the same 1% term-criterion of BMP tests.

As regards the activity tests with acetate, a sodium acetate solution (100 $g_{COD}$/L) was used. It was dosed to have a concentration in the test bottle of 3 $g_{COD}$/L.

In the case of the activity tests with glucose, a glucose (100 $g_{COD}$/L) was used as substrate, that was dosed to have different concentrations of COD. Specifically, the tested concentrations were: 2.5, 3.0, 3.5, 4 and 5 $g_{COD}$/L.

The activity tests with BSA were carried out using a BSA solution (25 or 30 $g_{COD}$/L), dosed to have 3.0, 3.5, or 4.5 $g_{COD}$/L in the test bottle.

Table 3.2 displays a summary of the biomass activity tests performed and the substrate concentrations as COD for each test.

Table 3.2 - Summary of biomass activity test conditions.

| *Biomass activity tests* | *Number of tests* | *Date* | *Substrate concentration [$g_{COD}$/L]* |
|---|---|---|---|
| *Acetate* | 6 | 22/10/20, 26/11/20, 10/12/20, 17/12/20, 14/01/21, 04/02/21 | 3.0 |
| *Glucose* | 7 | 22/10/20 | 5.0 |
| | | 19/11/20, 26/11/20 | 4.0 |
| | | 03/12/20 | 2.5 |
| | | 10/12/20 | 3.0 |
| | | 17/12/20, 10/02/21 | 3.5 |
| *BSA* | 6 | 05/11/20, 26/11/20, 10/12/20 | 3.0 |
| | | 17/12/20 | 3.5 |
| | | 29/12/20, 17/02/20 | 4.5 |

## *3.4. Calculation*

### *3.4.1. Feed and Digestate characterization*

Substrate and digestate characterization are one of the main issues when applying the ADM1 model. The characterization aims at assigning the correct value to all relevant state variables in the influent or, more in general, to associate a single or a combination of state variables with experimental data from laboratory analysis.

In accordance with the model requirements, all the variables were expressed as $g_{COD}$/L, but carbon, nitrogen and ionic compounds that were expressed as molar concentration (kmol/$m^3$ or M). Many assumptions were done because some data could not be directly measured. Indeed, they were either derived or assumed from the literature.

The concentration of hydrogen ions ($S_{h_{ion}}$) was derived by the measured pH value. Consequently, the concentration of hydroxide ions ($S_{oh_{ion}}$).

$$S_{h_{ion}} = 10^{-pH} \tag{3.1}$$

$$S_{oh_{ion}} = \frac{K_w}{S_{h_{ion}}} \tag{3.2}$$

The concentration of total inorganic nitrogen ($S_{IN}$) was derived from the ammoniacal nitrogen content of the samples.

$$S_{IN} = \frac{(NH_4^+ + NH_3)_{measured}\left[\frac{mg_N}{L}\right]}{14\left[\frac{kg}{kmol}\right]\cdot 1000} \tag{3.3}$$

The concentrations of ammonium ($S_{nh4_{ion}}$), free ammonia ($S_{nh3}$) and the dissociate fractions of each VFAs ($S_{ac_{ion}}$, $S_{pro_{ion}}$, $S_{bu_{ion}}$, $S_{va_{ion}}$) were calculated according to the acid-base equilibrium equations reported in ADM1.

$$S_{nh4_{ion}} - \frac{S_{h_{ion}} S_{IN}}{K_{a,nh4} + S_{h_{ion}}} = 0 \tag{3.4}$$

$$S_{IN} - S_{nh3} - S_{nh4_{ion}} = 0 \tag{3.5}$$

$$S_{ac_{ion}} - \frac{K_{a,ac} S_{ac}}{K_{a,ac} + S_{h_{ion}}} = 0 \tag{3.6}$$

$$S_{pro_{ion}} - \frac{K_{a,pro} S_{pro}}{K_{a,pro} + S_{h_{ion}}} = 0 \tag{3.7}$$

$$S_{bu_{ion}} - \frac{K_{a,bu} S_{bu}}{K_{a,bu} + S_{h_{ion}}} = 0 \tag{3.8}$$

$$S_{va_{ion}} - \frac{K_{a,va} S_{va}}{K_{a,va} + S_{h_{ion}}} = 0 \tag{3.9}$$

The concentration of bicarbonate ($S_{hco3_{ion}}$) was calculated from alkalinity and VFA ionic forms:

$$S_{hco3_{ion}} \left[\frac{mol}{L}\right] = Alk \left[\frac{mol_{CaCO_3,EQ}}{L}\right] - \left(S_{ac_{ion}} + S_{pro_{ion}} + S_{bu_{ion}} + S_{va_{ion}}\right)\left[\frac{mol}{L}\right] \quad (3.10)$$

Bicarbonate concentration was used to derive the concentration of inorganic carbon ($S_{IC}$) and carbon dioxide ($S_{co2}$) by the acid-base equilibrium:

$$S_{IC} = S_{hco3_{ion}} \cdot \frac{K_{a,co2} + S_{h_{ion}}}{K_{a,co2}} \quad (3.11)$$

$$S_{co2} = S_{IC} - S_{hco3_{ion}} \quad (3.12)$$

The value of the net charge of all other ions ($S_{delta_{ions}}$) was calculated from the charge balance:

$$S_{delta_{ions}} = S_{hco3_{ion}} + \frac{S_{ac_{ion}}}{64} + \frac{S_{pro_{ion}}}{112} + \frac{S_{bu_{ion}}}{160} + \frac{S_{va_{ion}}}{208} + S_{oh_{ion}} - S_{nh4_{ion}} - S_{h_{ion}} \quad (3.13)$$

Total COD was calculated as the sum of the contribution of total carbohydrates, proteins, lipids and all the VFA species. The conversion factors to calculate the COD associated to each fraction of carbohydrates, proteins and lipids are shown in Table *3.3*

Table 3.3 - COD conversion factors for carbohydrates, proteins and lipids.

| **COD/Glucose** | **1.07** | **gCOD/gGlu** | **Conversion from glucose to COD** |
|---|---|---|---|
| **COD/BSA** | 1.58 | gCOD/gBSA | Conversion from BSA to COD |
| **COD/VS_lip** | 2.90 | gCOD/gVS(lip) | Conversion from mass of lipids (VS) to COD |

The COD associated to the particulate fraction of the substrate ($X_c$) was calculated as the difference between the total COD and the COD of soluble components including VFA.

$$X_c = COD_p = COD_{tot} - COD_{s+VFA} \quad (3.14)$$

The concentration of particulate inerts ($X_i$) was calculated starting from the results of the BMP tests on the particulate fraction. In fact, $X_i$ can be considered as the non-degradable fraction of the substrate.

$$X_i = \%COD_{undegradable,sub} * COD_P \quad (3.15)$$

(Note: for simplicity only $X_i$ is reported but the result of the previous equation actually refers to $X_i$+ X_i_xc + S_i_Xc. As can be deduced from Figure 3.6)

The percentage of non-degradable material ($\%COD_{undegradable,sub}$) is calculated as the part of the substrate that is not degraded in BMP tests. The degradable material ($1 - \%COD_{undegradable,sub}$) fractions is calculated from the methane produced in BMP tests plus the COD converted in new biomass during the test (organischer Stoffe Substratcharakterisierung, 2016). The COD converted in new biomass ($\%COD_{new\ bio}$) was considered to be 8% of total COD by hypothesis.

$$X_i + S_i = \%COD_{undegradable,sub} * COD_{tot} \quad (3.16)$$

$$\%COD_{undegradable,sub} = 1 - \%COD_{CH4} - \%COD_{new\ bio} \quad (3.17)$$

With:

$$\%COD_{CH4} = \frac{BMP_{PART}\left[\frac{NmLCH4}{gCODp}\right]}{350} \quad (3.18)$$

The concentration of soluble inert substances (S_i) was calculated as the difference between the total inerts concentration (X_i + S_i) determined from the BMP tests on the sludge sample and the particulate inerts concentration (X_i) evaluated from the BMP tests on the particulate fraction of the sludge. To better clarify this concept, a scheme of COD fractionation entering the digester is proposed in Figure 3.6, with a focus on the inert fractions that can be evaluated by the proper BMP test.

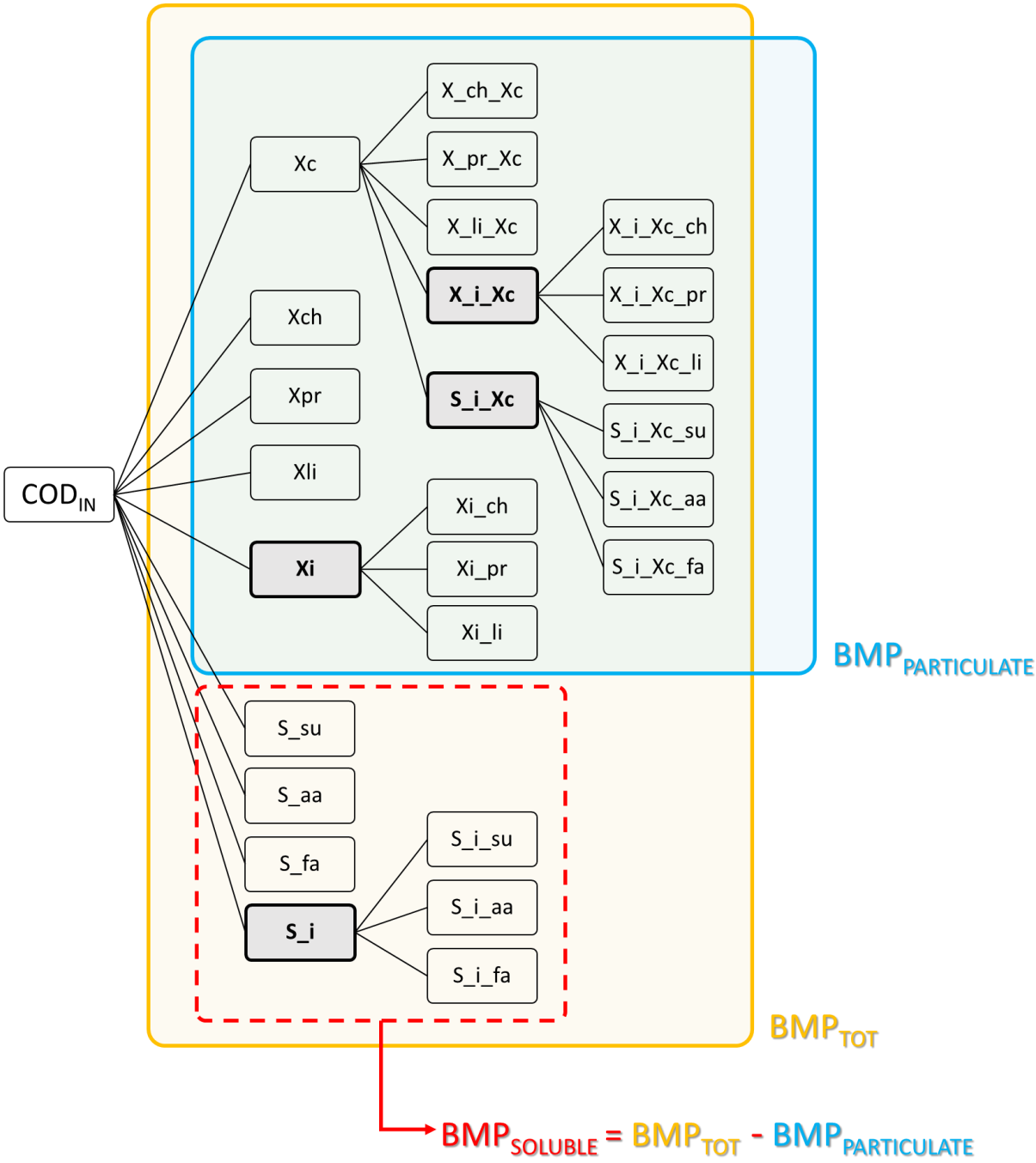


Figure 3.6 - Input COD fractionation scheme

Once the inert fractions of the substrate are known, the concentrations of carbohydrates, proteins and lipids ($C_{ch}$, $C_{pr}$, $C_{li}$) are associated to the degradable particulate COD.

$$COD_{P,deg} = COD_P - X_i - S_i \tag{3.19}$$

$$X_{fr} = COD_{P,deg} \cdot \frac{C_{fr}}{COD_P} \tag{3.20}$$

with $fr = ch, pr, li$

The disintegration fractions of the composite (f_Xch_Xc, f_Xpr_Xc, f_Xli_Xc, f_Xi_Xc, f_Si_Xc) were derived from the breakdown of the particulate COD as follow:

$$f_{X_{fr},Xc} = \frac{X_{fr}}{COD_P} \quad (3.21)$$

with $fr = ch, pr, li, i$

$$f_{S_i,Xc} = \frac{S_i}{COD_P} \quad (3.22)$$

The determination of soluble sugars ($S_{Su}$), soluble amino acids ($S_{aa}$) and soluble fatty acids ($S_{fa}$) were computed using respectively the experimental data of soluble carbohydrates, soluble proteins, soluble lipids and converting them using the same COD ratios reported in .

The sludge fed to the pilot plant is be a mixture of primary sludge and secondary sludge. The two types were defined differently. The primary sludge was assumed to enter the digester already disintegrated into $X_{ch}$, $X_{pr}$, $X_{li}$, $X_i$, $S_i$; so that the composite material ($X_c$) was assumed to be negligible. Instead, the secondary sludge was assumed to be composed only of composite particulate organics ($X_c$ only).

The same approach applies to the characterization of the digestate, with the main difference that the inert fraction is calculated starting from the residual BMP test.

## *3.5. ADM1 model*

### *3.5.1. Implementation of the ADM1*

The ADM1 was implemented according to Batstone et al. (2002) and used for modelling both the continuous reactor and the batch experiments. The OpenModelica platform was used as a simulation software tool, selecting DASSL (Differential/Algebraic System Solver) code for the numerical solution of the systems of differential/algebraic equations. Starting values of stoichiometric and kinetic parameters were taken from Rosen and Jeppsson (2006).

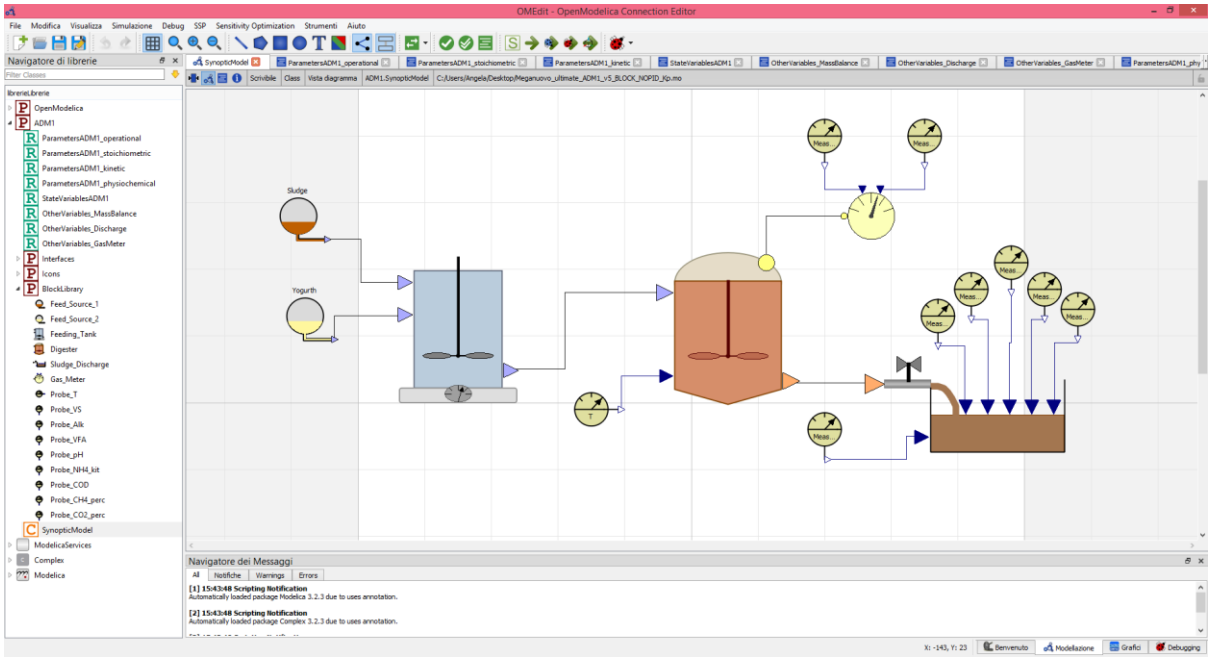


Figure 3.7 - User interface of the OpenModelica platform

Figure 3.7 shows the user interface of OpenModelica. In the 'Record' panels (R) all the variables and parameters were defined; while in the 'Package' panels (P) all the equations describing the system were reported as described in Rosen et al. (Rosen & Jeppsson, 2006). Since the system had numerical instability, the alternative way of calculating the gas flow rate given in Batstone et al. (2002) was chosen, where the gas flow rate is described by the following expression:

$$Q_{gas} = k_p * (P_{gas} - P_{atm}) \quad (3.23)$$

Where $k_p$ is a parameter related to the friction in the gas outlet.

In addition, the pilot plant response to overpressure variations due to variable head-losses in the hydraulic guard was implemented. Indeed, the in reactor liquid level changes as the pressure varies, so that the digester is not working at a constant volume (the higher the pressure in the headspace, the lower the liquid volume in the digester). Therefore, the real volume of the digester was recalculated as:

$$V_{real} = V_{fixed} + V_{variable} \quad (3.24)$$

$$V_{variable} = h_{variable} \cdot \text{Sectional area of digester}$$

$$h_{variable} = h_{max} - \frac{\Delta p}{\rho * g} \quad (3.25)$$

In the modelling, the system was in fact simulated as a constant volume reactor feed with a variable flow rate and the latter was computed so that the HRT of the real and simulated reators were the same. After computing the real HRT from the actual reactor volume, an artificial flow rate for modelling purposes was computed as follows:

$$Q_{artificial} = \frac{V_{digester} * \rho}{HRT_{real}} \quad (3.26)$$

$$HRT_{real} = \frac{V_{real}}{Q_{real}} \quad (3.27)$$

The overall system was modelled in OpenModelica as similar as possible to the pilot plant described in the current work. As described in Figure 3.7, the system includes a storage tank, where sludge and yogurt inflow are mixed, a digester and a storage tank for the digestate. Meters are used to retrieve simulated values of relevant variables. Three meters for temperature, pressure and gas flow were applied to the main digester and six meters were applied in the digestate storage tank to retrieve volatile solids, alkalinity, VFA, pH, ammonium, COD, percentage of methane and percentage of carbon dioxide in the biogas. Meter values were compared to the real experimental data.

The system in OpenModelica was arranged to simulate the batch tests, too. The units of the AMPTS II system were simulated as if they were small digesters, without outgoing digestate. The digestate extrapolated from the plant simulation pilot was then degassed using the model for the batch tests simulation and used as an inoculum for the BMP tests.

### *3.5.2. Calibration*

To exploit the synergy between the results obtained from batch experiments and those collected from the pilot-scale reactor, kinetic parameters were calibrated according to an iterative procedure in view of a simultaneous optimization of batch and continuous tests. Specifically, the parameters on which the calibration is based are:

- $k_{dis}$: the first order constant of complex particulate disintegration;
- $k_{H,Ch}$: the first order constant of the carbohydrate hydrolysis;
- $k_{H,pr}$: the first order constant of the protein hydrolysis;
- $k_{H,li}$: the first order constant of the lipids hydrolysis;
- $k_{m,su}$: the maximum uptake rate for monosaccharide degrading organisms;
- $k_{m,aa}$: the maximum uptake rate amino acid degrading organisms;

- $k_{m,ac}$: the maximum uptake rate for acetate degrading organisms;
- $K_{s,su}$: the half saturation constant for monosaccharide degradation;
- $K_{s,aa}$: the for amino acid degradation;
- $K_{s,ac}$: the half saturation constant for acetate degrading organisms;
- $K_{s,pro}$: the half saturation constant for propionate degrading organisms.

The iterative process consists in using the characteristics of the digestate from the pilot plant, as simulated by the pilot-plant model, to compute the initial conditions of the batch tests. In the case of the biomass activity tests, the digestate is used as it is, while in the case of the simulation of the BMP tests the degassed digestate is used. Through a comparison between the simulated methane production in these batch tests and the experimental one, the parameters indicated above are identified so that the difference between the curves is minimised. These new set of parameters are transferred to the model of the pilot plant and a new simulation is performed. New simulated data are compared with the experimental data. Then, again, the simulated digestate characteristics are used for batch tests simulation. This procedure is reiterated until no major changes are further required. Figure 3.8 shows a conceptual scheme of the iterative calibration process just described.

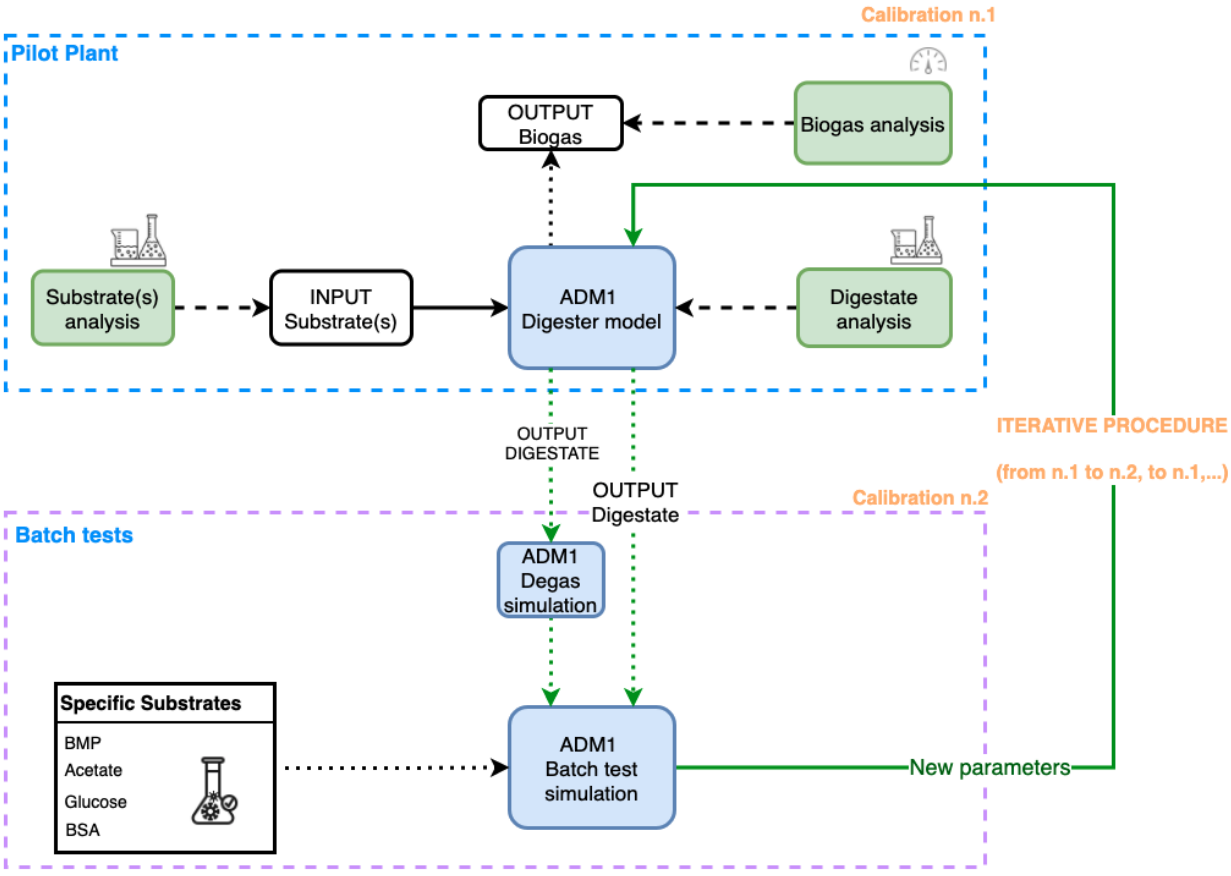

Figure 3.8 - Schematic representation of the iterative process for the calibration of the ADM1 model.

### *3.5.3. Sensitivity analysis*

Sensitivity analysis is a core tool in dynamical models. This becomes critical for nonlinear models with many parameters subject to large uncertainties. In such contexts too often, numerical simulations are required due to the lack of the analytical derivatives of state variables with respect to parameters.

In this work, the OMSens tool was used, an open platform to assess the sensitivity of Modelica models tailored to work with OpenModelica. OMSens was effective to pinpoint a nonintuitive subset of parameters that, when perturbed within small ranges, yield strong changes on key state variables.

There are two broad approaches to numerical-based sensitivity analysis: individual and simultaneous. The individual approach studies perturbations of one parameter at a time over a set of parameters of interest, typically testing the extreme values of the uncertainty interval $p_i \pm \Delta p_i$. The simultaneous approach can also take into account several combinations of values of $p_i$ lying within that interval which can produce strong changes in state variables $x_i$. (Danós et al., 2017)

In the current work, both an individual approach and a simultaneous approach of sensitivity analysis were tested.

The individual sensitivity analysis was a very useful tool for the calibration of the model and especially for the identification of which laboratory analyzes were essential for the influent characterization. In particular, it was applied in two different ways, depending on the parameters analyzed:

- In most cases, it was possible to use the OpenModelica tool itself. After choosing the perturbation percentage level to apply to the parameter, OpenModelica returns a sensitivity index $s_{rel}$ relying on comparisons of perturbed ($x_{per}$) and unperturbed runs (x):

$$s_{rel}(tk) = \frac{\sigma(t_k)}{x(t_k)} \tag{3.28}$$

  With:

$$\sigma = x_{per} - x \tag{3.29}$$

$s_{rel}$ can be used to rank the parameters affecting a variable the most.

- In some cases, a manual approach was used instead. The parameter of interest was perturbed manually, and the simulation was performed. At the end of the simulation the variables value was compared to the value obtained with the simulation with the original parameter value.

The simultaneous sensitivity analysis performed in this work is very helpful in the model calibration process, particularly in understanding whether the kinetic parameters were over or underestimated.

In particular, after defining the parameters of interest and their intervals of perturbation ($\pm \Delta p_i$), an algorithm tries to find the vector of smallest perturbation values that produces the largest impact on the state variables. The OpenModelica output not only reports a simple numerical result but also presents the effect of the perturbation plotted over time.

## *3.6. Model performance*

Model prediction performances were evaluated through the modified Theil's Inequality Coefficient, TIC, (Decostere at al. 2016) and the modified Mean Absolute Relative Error, MARE, (Hauduc et al. 2015) as reported in Eq. 3.30 and 3.31:

$$TIC = \frac{\sqrt{\sum_i \left(sat_\sigma(y_{s,i}, y_{m,i})\right)^2}}{\sqrt{\sum_i y_{s,i}^2} + \sqrt{\sum_i y_{m,i}^2}} \tag{3.30}$$

$$MARE = \frac{1}{n} \cdot \sum_{i=1}^{n} \frac{|sat_\sigma(y_{m,i}, y_{s,i})|}{y_{m,i} + \varphi} \tag{3.31}$$

Where $y_{s,i}$ represents the value of the variable measured experimentally; and $y_{m,i}$ the value estimated by the model. The function $sat_\sigma(y_{s,i}, y_{m,i})$ is zero when both $y_{m,i}$ and $y_{s,i}$ are lower than the associated measurement standard deviation (accepted as perfect fit situation), and otherwise: $sat_\sigma(y_{s,i}, y_{m,i}) = y_{s,i} - y_{m,i}$. The small correction factor φ (0.1) is applied to avoid division by zero.

Both criteria quantify the difference between model predictions and experimental values and normalize them according to the magnitude of the considered variable. TIC <0.3 represents a

good simulation result. In general, for both criteria, the closer the value to zero, the better the model performance.

# Chapter 4: RESULTS & DISCUSSION

## *4.1. Sludge characterization*

### *4.1.1. Analytical characterizations*

Table 4.1 shows the results of the laboratory analyses performed on the sludge samples as total fraction, particulate fraction (solid separated by centrifugation) and soluble fraction (liquid separated by centrifugation).

Table 4.1 - Analyses results for sludge characterization

| ***PARAMETER*** | ***UNIT*** | *Average of 10 samples* | *Standard deviation* |
|---|---|---|---|
| ***TOTAL FRACTION*** | | | |
| *pH* | - | 6.08 | 0.35 |
| *Alkalinity* | $mgCaCO_3/L$ | 1665 | 316 |
| *TS* | gTS/kgFM | 28.9 | 4.6 |
| *VS* | gVS/kgFM | 22.7 | 3.7 |
| *Total COD* | gCOD/kg | 33.6 | 5.7 |
| *Total TKN* | gN/kg | 1.53 | 0.51 |
| *Total Carbohydrates* | gGlu/L | 8.98 | 2.27 |
| *Total Proteins* | gBSA/L | 8.55 | 1.88 |
| *BMP Total* | NmLCH4/gVS | 388 | 27 |
| ***PARTICULATE FRACTION*** | | | |
| *BMP Particulate* | NmLCH4/gVS,p | 385 | 22 |
| *Particulate Lipids* | g/kgVS,p | 132 | 13 |
| *Particulate Lipids* | g/kgVS | 127 | 13 |
| *TS - particulate fraction* | gTS,p/kgFM,p | 113 | 4 |
| *VS - particulate fraction* | gVS,p/kgFM,p | 89 | 3 |
| ***SOLUBLE FRACTION*** | | | |
| *VFA: acetic acid* | mg/L | 748 | 196 |
| *VFA: propionic acid* | mg/L | 249 | 79 |
| *VFA: iso-butyric acid* | mg/L | 37 | 12 |
| *VFA: butyric acid* | mg/L | 101 | 41 |
| *VFA: iso-valeric acid* | mg/L | 26 | 13 |
| *VFA: valeric acid* | mg/L | 27 | 18 |
| *TS - soluble fraction* | gTS,s/kgFM,s | 2.2 | 0.5 |
| *VS - soluble fraction* | gVS,s/kgFM,s | 1.2 | 0.4 |
| *Soluble Carbohydrates* | mgGlu/L | 102 | 63 |
| *Soluble Proteins* | mgBSA/L | 367 | 248 |
| *Soluble Lipids* | g/kgVS,s | 48 | 7 |
| *Soluble Lipids* | g/kgVS | 1.82 | 0.35 |
| *Soluble TKN* | mgN/L | 166 | 46 |
| *Soluble COD* | gCOD/L | 2.44 | 0.96 |
| *Ammoniacal Nitrogen* | mgN/L | 79 | 37 |

The table shows only the averages and standard deviations of all the sludges analyzed. A complete table of all individual values is given in APPENDIX C.

The trends of VFAs, pH, alkalinity and ammonium ion in the sludge are also shown in Figure 4.1, Figure 4.2 and Figure 4.3 respectively.

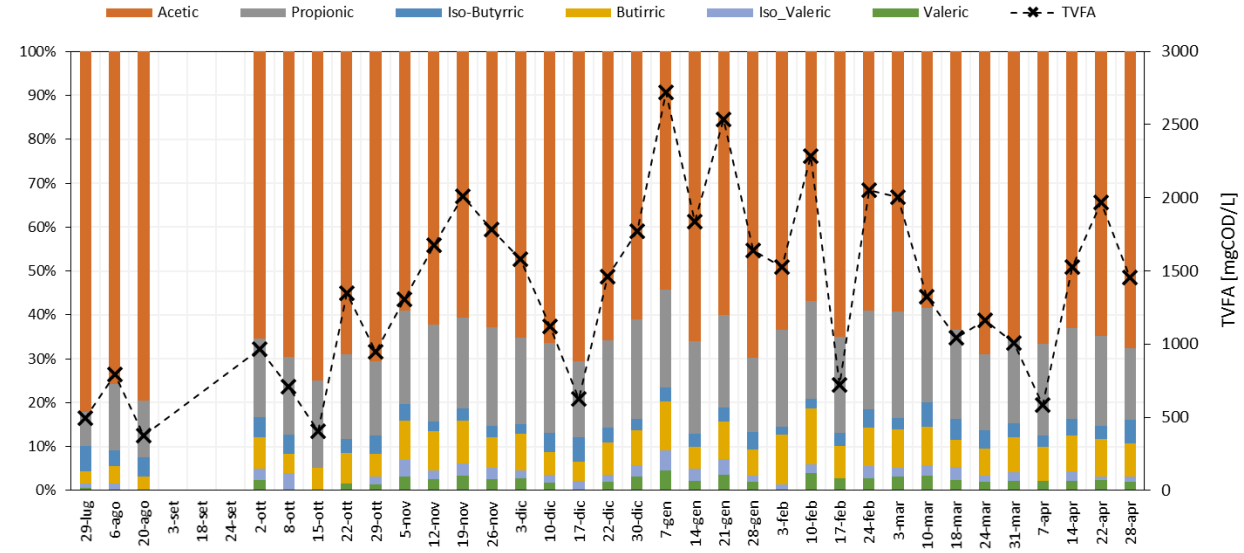


Figure 4.1 - TVFA trend and VFA speciation of sludge samples

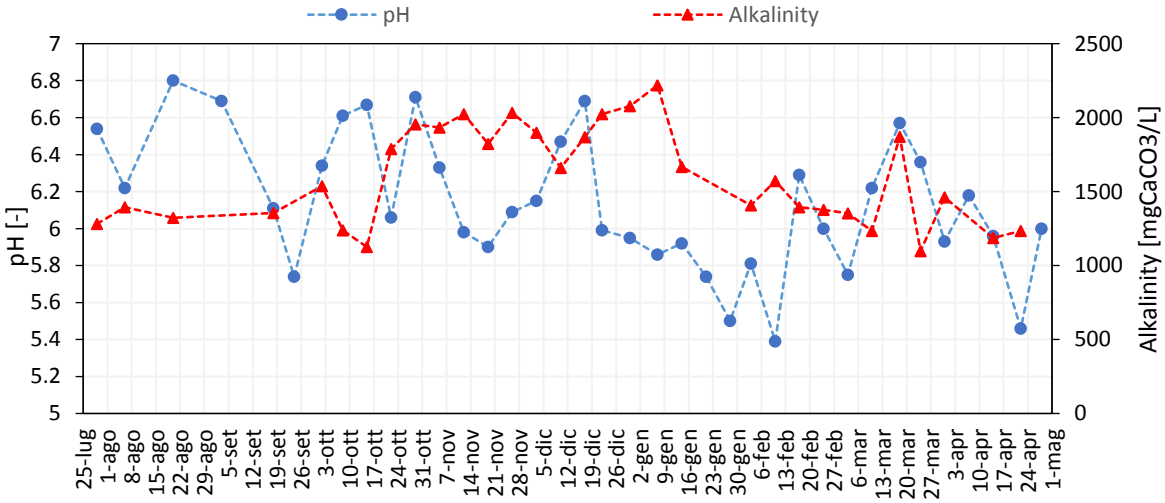


Figure 4.2 - pH and alkalinity trend of sludge samples

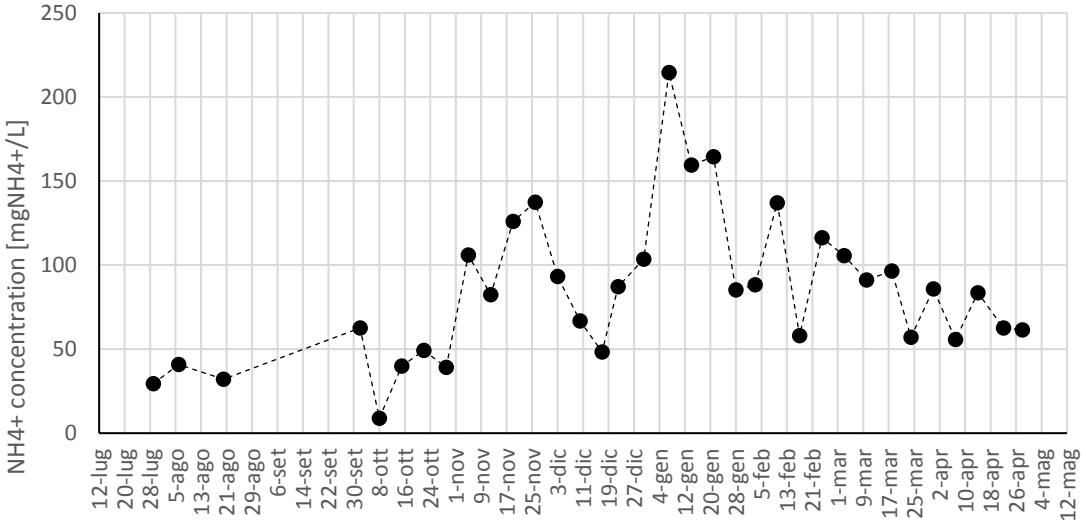


Figure 4.3 - Ammonium concentration trend of sludge samples

In Table 4.2 a data analysis on sludge analytical measurements is reported. A total of five more variables were derived as ratio between two variables (VS/TS, N/COD, VFA/ CODsol, CODsol/COD).

Table 4.2 - Data analysis of sludge analytical measurements

| ***PARAMETER*** | ***UNIT*** | *Average of 10 samples* | *Standard deviation* |
|---|---|---|---|
| *Total Carbohydrates* | gCOD/L | 9.61 | 2.43 |
| *Total Proteins* | gCOD/L | 13.4 | 3.0 |
| *Total Lipids* | gCOD/L | 8.55 | 1.90 |
| *Carbohydrates/CODtot* | - | 29% | 5% |
| *Proteins/CODtot* | - | 40% | 4% |
| *Lipids/CODtot* | - | 26% | 2% |
| *VS/TS* | gVS/gTS | 0.78 | 0.01 |
| *TVFA* | **gCOD/L** | 1.50 | 0.43 |
| *COD total as pr,ch,li,VFA* | gCOD/L | 33.2 | 6.4 |
| *COD/VS* | gCOD/gVS | 1.48 | 0.09 |
| *N/COD* | gN/gCOD | 0.0023 | 0.0011 |
| *CODsol/COD* | - | 0.07 | 0.03 |
| *VFA/CODsol* | - | 0.66 | 0.22 |

Figure 4.4 shows the boxplots of the concentration of lipids, carbohydrates and proteins in the sludge which provide an indication of how the values in the data are spread out.

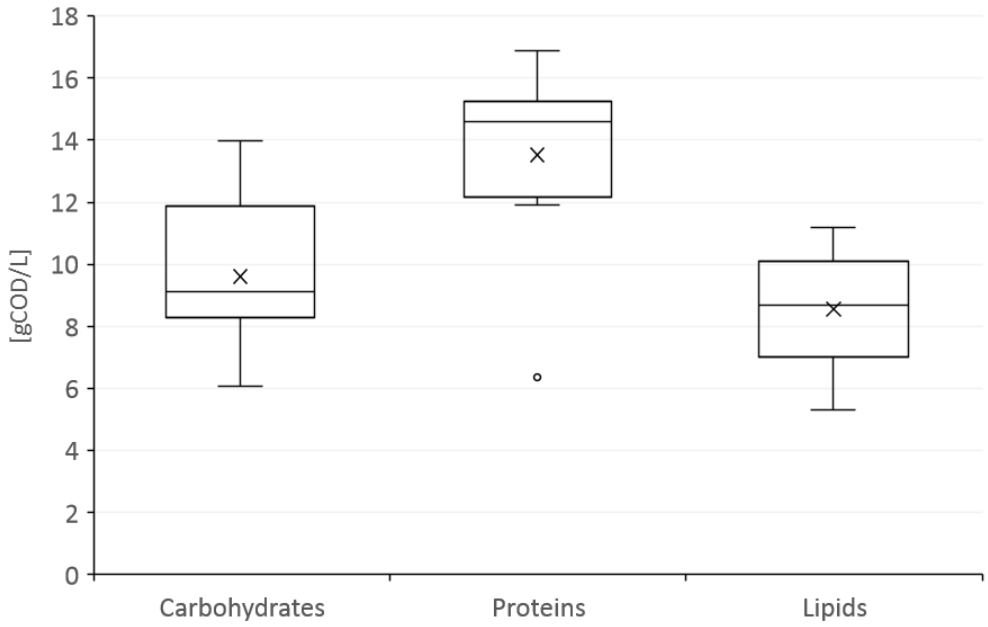


Figure 4.4 - Boxplot of carbohydrates, proteins and lipids content in the sludge samples.

Table 4.3 reports literature data about sludge characteristics. These data were used to make a comparison with the results of the analyses carried out. For most of the measurements, values comparable to the literature are obtained. Specifically, the analyses on VS, TS, VFA, COD, CODsol, and TKN seem to be comparable results; carbohydrates, proteins and lipids have the same order of magnitude; lipids and carbohydrates have values slightly higher than those reported in the literature; Ammoniacal nitrogen analysis is the one that shows the highest deviation from literature data.

Table 4.3 – Sludge characterizations comparison

| ***Sludge type*** | ***Carb.*** | ***Proteins*** | ***Lipids*** | ***VS/ TS*** | ***VFA/ CODsol*** | ***CODsol/ COD*** | ***N*** | ***TKN*** | ***TS*** | ***VS*** | ***CODsol*** | ***COD*** | ***VFA*** | ***Bibliographic reference*** |
|---|---|---|---|---|---|---|---|---|---|---|---|---|---|---|
| | gCOD/L | gCOD/L | gCOD/L | - | - | - | mgN/L | gN/kg | gTS/kgFM | gVS/kgFM | gCOD/L | gCOD/kg | gCOD/L | |
| *Primary sludge* | 0.59 | 2.16 | 1.41 | 0.70 | 0.52 | 0.05 | 1519 | 1.37 | 32.1 | 22.6 | 1.83 | 34.7 | 1.03 | Catenacci et al., 2019 |
| *Primary sludge* | N.A. | N.A. | N.A. | N.A. | N.A. | N.A. | 121 | N.A. | N.A. | N.A. | 8.56 | 68.3 | 3.41 | Zhou et al., 2021 |
| *Primary sludge* | N.A. | N.A. | N.A. | N.A. | N.A. | N.A. | 111 | N.A. | N.A. | N.A. | N.A. | 22.8 | 1.20 | Serna-García et al., 2020 |
| *Activated Sludge* | N.A. | N.A. | N.A. | 1.49 | N.A. | 0.07 | N.A. | 2.30 | 35.3 | 52.5 | 3.43 | 46.4 | N.A. | Wett et al. 2009 |
| *Activated Sludge* | 2.13 | 13.5 | 3.19 | 0.65 | N.A. | N.A. | 130 | N.A. | 26.7 | 17.3 | 0.35 | 24.8 | 0.61 | Chen et al., 2020 |
| *Mixed sludge* | 9.72 | 17.6 | 12.47 | 0.76 | 0.57 | 0.08 | 194 | 2.02 | 35.8 | 27.1 | 3.51 | 47.5 | 1.99 | Astals et al. 2013 |
| *Experimental values* | 9.61 | 13.4 | 8.55 | 0.78 | 0.66 | 0.07 | 79 | 1.53 | 28.9 | 22.7 | 2.44 | 33.6 | 1.50 | |

### *4.1.2. ADM1 characterization*

As explained in paragraph 3.4.1, the results of the analyses carried out on the sludge samples have been processed to obtain the characterization of the sludge as required by the ADM1 model. The results are shown in Table 4.4.

Table 4.4 - ADM1 sludge characterization

| ***PARAMETER*** | **UNIT** | **Average of 10 samples** | **Standard deviation** |
|---|---|---|---|
| $S_{su}$ | gCOD/L | 0.11 | 0.07 |
| $S_{aa}$ | gCOD/L | 0.60 | 0.43 |
| $S_{fa}$ | gCOD/L | 0.11 | 0.02 |
| $S_{va}$ | gCOD/L | 0.11 | 0.06 |
| $S_{bu}$ | gCOD/L | 0.25 | 0.09 |
| $S_{pro}$ | gCOD/L | 0.38 | 0.12 |
| $S_{ac}$ | gCOD/L | 0.80 | 0.21 |
| $S_{h2}$ | gCOD/L | 1.00E-08 | 0.00 |
| $S_{ch4}$ | gCOD/L | 1.00E-05 | 0.00 |
| $S_{ic}$ | M | 0.04 | 0.02 |
| $S_{in}$ | M | 0.01 | 0.003 |
| $S_i$ | gCOD/L | 1.76 | 1.90 |
| $S_{cat}$ | M | 0.05 | 0.01 |
| $S_{an}$ | M | 0.02 | 0.00 |
| $X_c$ | gCOD/L | 3.19 | 0.39 |
| $X_{ch}$ | gCOD/L | 6.90 | 1.65 |
| $X_{pr}$ | gCOD/L | 9.83 | 2.23 |
| $X_{li}$ | gCOD/L | 5.63 | 2.06 |
| $X_{su}$ | gCOD/L | 0.01 | 0.00 |
| $X_{aa}$ | gCOD/L | 0.01 | 0.00 |
| $X_{fa}$ | gCOD/L | 0.01 | 0.00 |
| $X_{c4}$ | gCOD/L | 0.01 | 0.00 |
| $X_{pro}$ | gCOD/L | 0.01 | 0.00 |
| $X_{ac}$ | gCOD/L | 0.01 | 0.00 |
| $X_{h2}$ | gCOD/L | 0.01 | 0.00 |
| $X_i$ | gCOD/L | 4.54 | 3.20 |

The table shows only the averages and standard deviations of all the characterizations. A complete table of all individual values is given in APPENDIX C.

In accordance with the model requirements, all the variables were expressed as $g_{COD}/L$, but carbon, nitrogen and ionic compounds that were expressed as molar concentration ($k_{mol}/m^3$ or M). Many assumptions were done because some data could not be directly measured. Indeed,

they were either derived or assumed from the literature. In particular $S_{h2}$, $S_{ch4,}$ $X_{su}$, $X_{aa}$, $X_{fa}$, $X_{c4}$, $X_{pro}$, $X_{ac}$ and $X_{h2}$ were assumed from Rosen et al. (Rosen & Jeppsson, 2006).

## *4.2. Yogurt characterization*

### *4.2.1. Analytical characterizations*

Table 4.5 shows the results of the laboratory analyses carried out on the yogurt samples. All data were measured directly apart from lipids which were read from the nutritional table on the label. Since yogurt could not be separated by centrifuge, yogurt measurements are referred to the particulate fraction.

Table 4.5 - Analyses results for yogurt characterization

| ***PARAMETER*** | **UNIT** | **Average of 10 samples** | **Standard deviation** |
|---|---|---|---|
| ***VS - particulate fraction*** | $g_{VS,p}/kg_{FM,p}$ | 141 | 7 |
| ***TS - particulate fraction*** | $g_{TS,p}/kg_{FM,p}$ | 159 | 12 |
| ***Lipids from label*** | g/L | 19.3 | 8.1 |
| ***Carbohydrates measured*** | g/L | 151 | 13 |
| ***Proteins measured*** | g/L | 46.5 | 5.9 |
| ***BMP $_{part}$*** | $NmL_{CH4}/gVSp$ | 762 | 44 |

The contribution of VFA was added considering an average value of 2800 ppm as concentration of acetate, a value resulting from previous analysis made on yogurt samples of similar quality.

The table shows only the averages and standard deviations of all the characterizations. A complete table of all individual values is given in APPENDIX C.

Table 4.6 reports the data analysis on yogurt measurements. The VS/TS and COD/VS ratios are higher than those observed in the sludge samples.

Table 4.6 - Data analysis of yogurt analytical measurements

| *PARAMETER* | *UNIT* | *Average of 3 samples* | *Standard deviation* |
|---|---|---|---|
| *VS/TS* | gVS/gTS | 0.88 | 0.03 |
| *Total Carbohydrates* | gCOD/L | 161 | 14 |
| *Total Proteins* | gCOD/L | 73.5 | 9.3 |
| *Total Lipids* | gCOD/L | 56 | 24 |
| *CODtot as pr,ch,li,VFA* | gCOD/L | 294 | 36 |
| *Carbohydrates/CODtot* | - | 0.55 | 0.03 |
| *Proteins/CODtot* | - | 0.25 | 0.03 |
| *Lipids/CODtot* | - | 0.19 | 0.06 |
| *COD/VS* | gCOD/gVS | 2.08 | 0.15 |

The protein and carbohydrate analyses were compared with the values displayed on the yogurt label. The average error between the measures is reported in Table 4.7.

Table 4.7 - Comparison of analyses results with measures reported on the yogurt label

| *MEASURE* | **Average error of 3 samples** | **Standard deviation** |
|---|---|---|
| *Carbohydrates* | 23.5% | 3.2% |
| *Proteins* | 4.6% | 4.9% |

It is noted that the measured proteins and those reported on the label are very similar, while carbohydrates are always overestimated by about 23.5%. This could be due to the carbohydrate measurement method which involves a very high dilution of the sample. However, the error is always very similar (standard deviation 3.2%), consequently the measurement of carbohydrates could be verified by better calibrating the measurement method.

Therefore, in order to reduce the number of analyses to be carried out on the influent, it is possible to avoid the measurement of proteins and carbohydrates of the yogurt, and use the values displayed on the label instead.

### *4.2.2. ADM1 characterization*

For the characterization of yogurt, it was assumed that carbohydrates and lipids enter the process as insoluble carbohydrates ($X_{ch}$) and insoluble lipids ($X_{li}$) respectively. While proteins were introduced as amino acids ($S_{aa}$).

The choice of considering proteins entering the system as a soluble material derives from the model calibration: according to simulations during the co-digestion phase the proteins in the yogurt were hydrolyzed at a much higher rate than predicted according to the hydrolysis constant previously calibrated on sludge mono-digestion. Consequently, two hydrolysis processes with different values for the hydrolysis constant ($k_{hyd,pr}$) would have been needed in order to fully interpret this observation, requiring a modification in the model structure. As this is an important modification to the model, it was decided to simplify the modeling process, by introducing the yogurt proteins as an already hydrolyzed material. This will be properly explained in paragraph 4.8.1, where the calibration process conducted through the modeling of BMP tests is shown.

Table 4.8 - ADM1 yogurt characterization

| PARAMETER | UNIT | Average of 3 samples | Standard deviation |
|---|---|---|---|
| $S_{su}$ | gCOD/L | 0.00 | 0.00 |
| $S_{aa}$ | gCOD/L | 73.47 | 9.34 |
| $S_{fa}$ | gCOD/L | 0.00 | 0.00 |
| $S_{va}$ | gCOD/L | 0.00 | 0.00 |
| $S_{bu}$ | gCOD/L | 0.00 | 0.00 |
| $S_{pro}$ | gCOD/L | 0.00 | 0.00 |
| $S_{ac}$ | gCOD/L | 0.00 | 0.00 |
| $S_{h2}$ | gCOD/L | 0.00 | 0.00 |
| $S_{ch4}$ | gCOD/L | 0.00 | 0.00 |
| $S_{ic}$ | M | 0.00 | 0.00 |
| $S_{in}$ | M | 0.00 | 0.00 |
| $S_i$ | gCOD/L | 0.00 | 0.00 |
| $S_{cat}$ | M | 0.02 | 0.00 |
| $S_{an}$ | M | 0.02 | 0.00 |
| $X_c$ | gCOD/L | 0.00 | 0.00 |
| $X_{ch}$ | gCOD/L | 161.10 | 14.42 |
| $X_{pr}$ | gCOD/L | 0.00 | 0.00 |
| $X_{li}$ | gCOD/L | 56.04 | 23.52 |
| $X_{su}$ | gCOD/L | 0.00 | 0.00 |
| $X_{aa}$ | gCOD/L | 0.00 | 0.00 |
| $X_{fa}$ | gCOD/L | 0.00 | 0.00 |
| $X_{c4}$ | gCOD/L | 0.00 | 0.00 |
| $X_{pro}$ | gCOD/L | 0.00 | 0.00 |
| $X_{ac}$ | gCOD/L | 0.00 | 0.00 |
| $X_{h2}$ | gCOD/L | 0.00 | 0.00 |
| $X_i$ | gCOD/L | 0.0 | 0.00 |

## 4.3. Digestate characterization

### 4.3.1. Analytical characterizations

Table 4.9 shows the results of the laboratory analyses carried out on the digestate samples as total fraction, particulate fraction (solid separated by centrifugation) and soluble fraction (liquid separated by centrifugation). The table shows only the averages and standard deviations of all the digestates analyzed. A complete table of all individual values is given in APPENDIX C.

Table 4.9 - Analyses results for digestate characterization.

| *PARAMETER* | UNIT | Average of 10 samples | Standard deviation |
|---|---|---|---|
| ***TOTAL FRACTION*** | | | |
| *pH* | - | 7.31 | 0.19 |
| *Alkalinity* | $mgCaCO_3/L$ | 4484 | 819 |
| *TS* | gTS/kgFM | 21.1 | 2.1 |
| *VS* | gVS/kgFM | 13.6 | 1.4 |
| *Total COD* | gCOD/kg | 13.6 | 3.7 |
| *Total TKN* | gN/kg | 1.30 | 0.23 |
| *Total Carbohydrates* | mgGlu/L | 3.12 | 0.68 |
| *Total Proteins* | mgBSA/L | 8.89 | 2.20 |
| *Residual BMP* | NmLCH4/gVS | 0.40 | 0.19 |
| ***PARTICULATE FRACTION*** | | | |
| *Particulate lipids* | g/kgVS,p | 33.7 | 15.0 |
| *Particulate lipids* | g/kgVS | 29.7 | 12.5 |
| *TS - particulate fraction* | gTS,p/kgFM,p | 92.4 | 6.6 |
| *VS - particulate fraction* | gVS,p/kgFM,p | 60.3 | 3.0 |
| ***SOLUBLE FRACTION*** | | | |
| *VFA: acetic acid* | mg/L | 58.4 | 24.2 |
| *VFA: propionic acid* | mg/L | 0.00 | 0.00 |
| *VFA: iso-butyric acid* | mg/L | 2.20 | 4.65 |
| *VFA: butyric acid* | mg/L | 0.00 | 0.00 |
| *VFA: iso-valeric acid* | mg/L | 0.00 | 0.00 |
| *VFA: valeric acid* | mg/L | 0.00 | 0.00 |
| *TS - soluble fraction* | gTS,s/kgFM,s | 3.44 | 0.68 |
| *VS - soluble fraction* | gVS,s/kgFM,s | 1.91 | 0.47 |
| *Soluble Carbohydrates* | mgGlu/L | 209 | 59 |
| *Soluble Proteins* | mgBSA/L | 1152 | 431 |
| *Soluble TKN* | mgN/L | 719 | 163 |
| *Soluble COD* | mgCOD/L | 2.89 | 0.71 |
| *Ammonium* | mgN/L | 691 | 216 |

Table 4.10 reports the data analysis on digestate measurements. It is observed that the analytically measured COD and the COD calculated as the sum of proteins, carbohydrates, lipids and VFAs as COD do not coincide. It could highlight possible errors in the COD measurements, which show a high standard deviation (Table 4.9). For this reason, the derived variables were computed from the total COD calculated as the sum of proteins, carbohydrates, lipids and VFAs contributions.

Table 4.10 - Data analysis of digestate analytical measurements

| ***PARAMETER*** | ***UNIT*** | *Average of 10 samples* | *Standard deviation* |
|---|---|---|---|
| *Total Carbohydrates* | gCOD/L | 3.34 | 0.73 |
| *Total Proteins* | gCOD/L | 14.1 | 3.5 |
| *Total Lipids* | gCOD/L | 1.17 | 0.55 |
| *Carbohydrates/CODtot* | - | 18% | 2% |
| *Proteins/CODtot* | - | 75% | 4% |
| *Lipids/CODtot* | - | 7% | 3% |
| *VS/TS* | gVS/gTS | 0.65 | 0.03 |
| *TVFA* | **mgCOD/L** | 66.3 | 31.0 |
| *COD total as pr,ch,li,VFA* | gCOD/L | 18.3 | 5.3 |
| *COD/VS* | gCOD/gVS | 0.99 | 0.24 |
| *COD calculated/VS* | gCOD/gVS | 1.36 | 0.38 |
| *N/COD* | gN/gCOD | 0.03 | 0.01 |
| *CODsol/COD* | - | 0.15 | 0.04 |
| *VFA/CODsol* | - | 0.03 | 0.02 |

## *4.4. Degassed digestate characterization*

### *4.4.1. Analysis results*

Table 4.11 shows the results of the laboratory analyzes carried out on the degassed digestate samples as total fraction, particulate fraction (solid separated by centrifugation) and soluble fraction (liquid separated by centrifugation). The table shows only the averages and standard deviations of all the digestates analyzed. A complete table of all individual values is given in APPENDIX C.

Table 4.11 - Analyses results for degassed digestate.

| *PARAMETER* | UNIT | Average of 10 samples | Standard deviation | Comparison with fresh digestate |
|---|---|---|---|---|
| ***TOTAL FRACTION*** | | | | |
| *pH* | - | 7.76 | 0.31 | 5% |
| *TS* | gTS/kgFM | 19.8 | 2.3 | -6% |
| *VS* | gVS/kgFM | 12.1 | 1.6 | -12% |
| *Total Carbohydrates* | gGlu/L | 2.10 | 0.67 | -49% |
| *Total Proteins* | gBSA/L | 6.79 | 3.00 | -31% |
| *Total Lipids* | g/L | 0.36 | 0.15 | -12% |
| ***PARTICULATE FRACTION*** | | | | |
| *Particulate lipids* | g/kgVS,p | 34 | 9 | 2% |
| *Particulate lipids* | g/kgVS | 31 | 12 | 18% |
| *TS - particulate fraction* | gTS,p/kgFM,p | 87 | 6 | -6% |
| *VS - particulate fraction* | gVS,p/kgFM,p | 54 | 3 | -12% |
| ***SOLUBLE FRACTION*** | | | | |
| *TS - soluble fraction* | gTS,s/kgFM,s | 1.95 | 0.68 | 5% |
| *VS - soluble fraction* | gVS,s/kgFM,s | 0.99 | 0.45 | -9% |
| *Ammonium* | mgN/L | 593 | 136 | -35% |

Soluble lipids were analysed only on one sample resulting in 3.2 g/kgVS. This measure turned out to be of little significance, not only in numerical terms, but also for modelling purposes. In fact, the soluble lipid parameter (as fatty acids concentration, $S_{fa}$) has a negligible effect on the AD process variables, as will be demonstrated in chapter 4.9 through the sensitivity analysis carried out on the model.

Table 4.11 also shows the measurements variation between fresh and degassed digestate. This comparison was made on average values. From this comparison, it emerges that there are generally small variations except for proteins, carbohydrates and ammonium concentrations. For degassed digestate, a VS/TS ratio of 0.61 $g_{TS}/g_{VS}$ is obtained, therefore lower than the value of fresh digestate (Table 4.9)

## *4.5. Pilot plant performance*

### *4.5.1. OLR & HRT*

Figure 4.5 shows the hydraulic retention time at which the pilot plant operated over time. Some variations are observed concerning the average target HRT, equal to 17 d. A first variation is observed between 9 and 17 November in which there was a pump malfunction that prevented

sludge feeding causing an HRT increase. A further deviation from the average value is observed between 27 December and 4 January. On that date, a lowering of the temperature had caused some pipes to freeze, preventing sludge feeding.

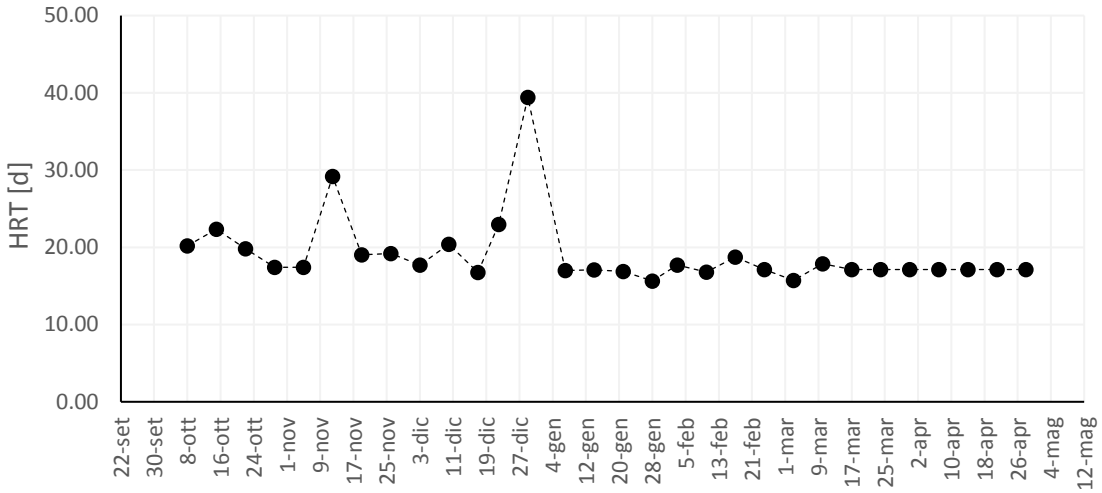


Figure 4.5 - Pilot plant hydraulic retention time.

Figure 4.6 shows the trend over time of the pilot plant's organic loading rate. In the mono-digestion phase, the reactor was operating with an average OLR of 1.34 $kg_{VS}/m^3/d$. During the co-digestion phase, the average OLR, was increased by 20% to 1.61 $kg_{VS}/m^3/d$ by adding yogurt. Also in this case, there are deviations from the average values linked to the problems described above, in addition to the variation in the sludge characteristics.

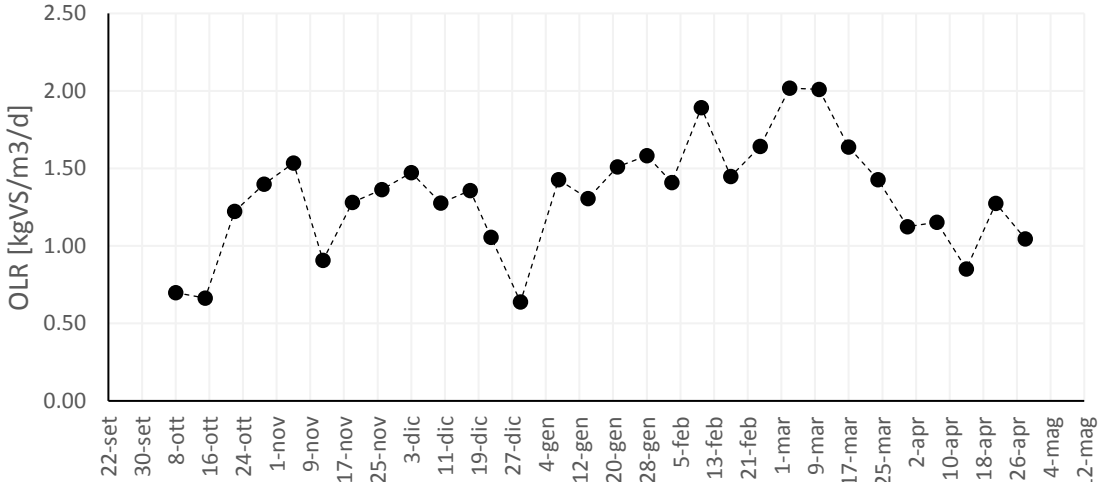


Figure 4.6 - Pilot plant organic loading rate.

### *4.5.2. Volatile solids reduction*

Figure 4.7 shows the cumulative trend of the VS entering the digester (in sludge and yogurt inflow) in comparison to the VS coming out from the digester (in digestate).

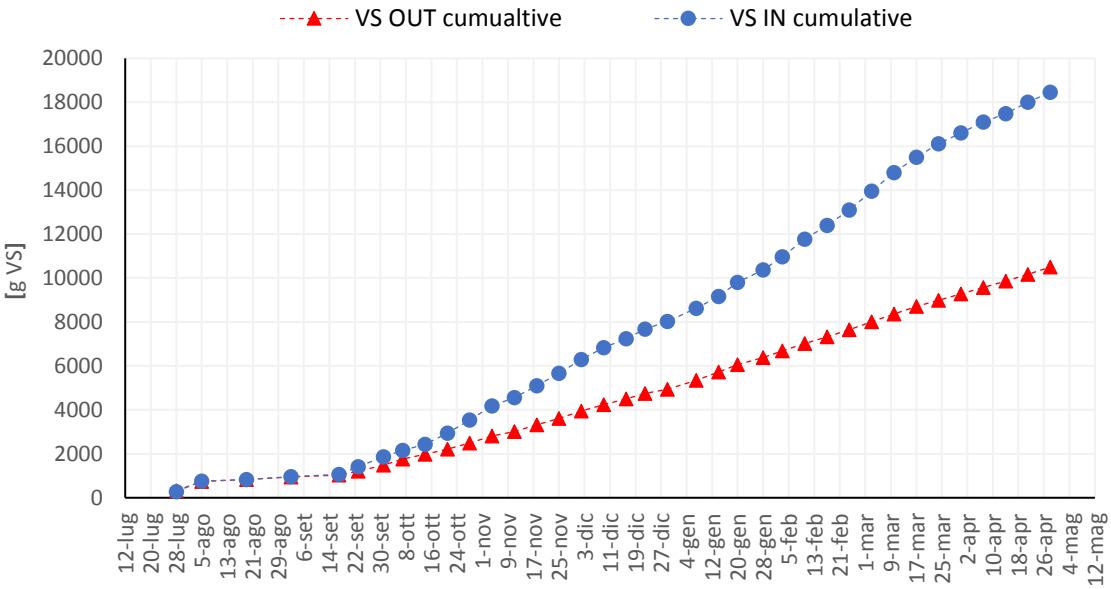


Figure 4.7 - Comparison between influent and effluent cumulated VS

It is evident that in the mono-digestion period (October-December) and in the co-digestion period (January-March) the deviation between the two curves changes. By comparing the slope of the curves in the two periods, it is possible to obtain the average reduction efficiency of the total VS as the ratio of the angular coefficient of the lines that best interpolates the experimental points in those periods. According to this calculation an average VS reduction efficiency in the mono-digestion period is 43.7%; while in the co-digestion period the average efficiency is 54.4%. While considering the entire monitoring period, an average efficiency of total VS reduction 46.7% is obtained.

The same concept can be visualized on the same curve through the graph represented in Figure 4.8

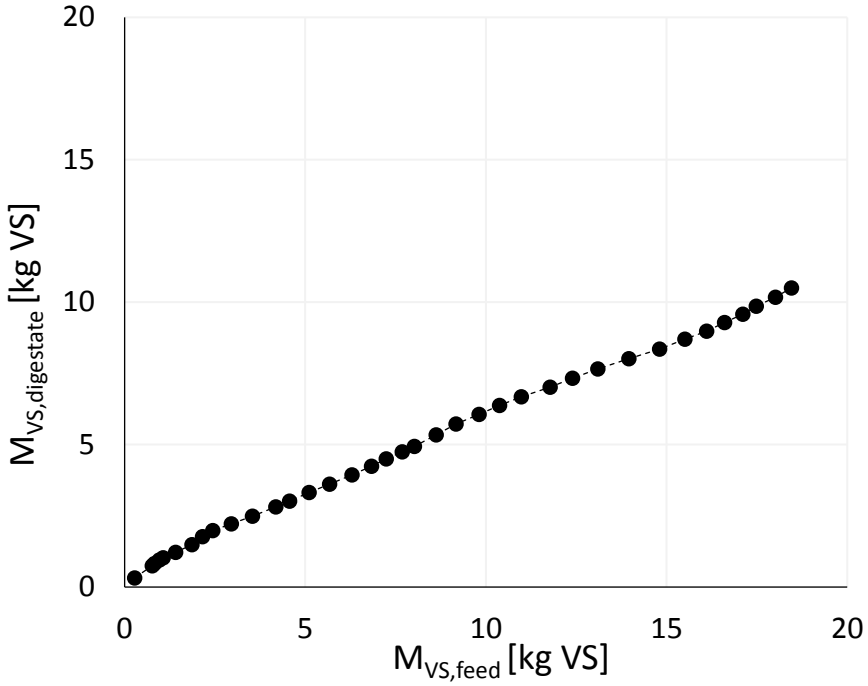


Figure 4.8 - Pilot plant VS reduction.

### *4.5.3. pH and alkalinity*

Figure 4.9 shows the trend of pH and alkalinity. These parameters remained sufficiently constant during the experimentation. For both, there was an increase following the co-digestion phase.

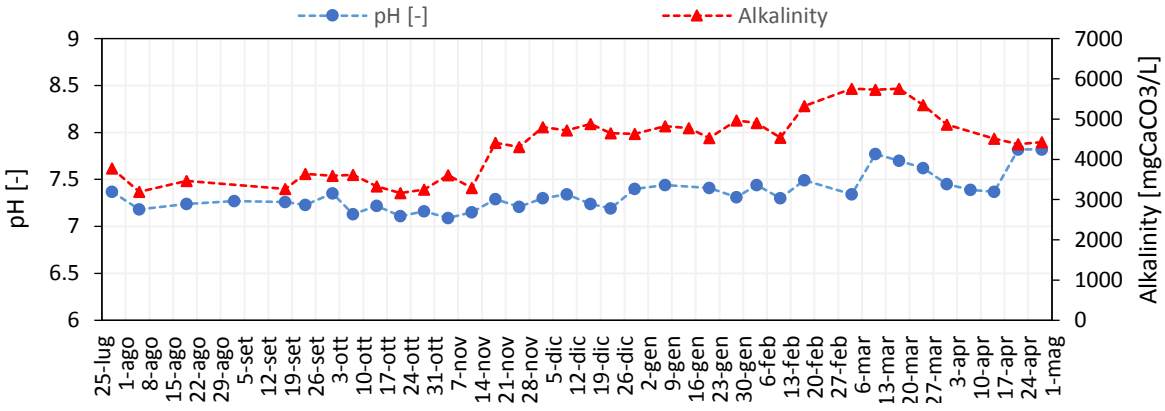


Figure 4.9 - Measurements of pH and alkalinity for the digestate.

### *4.5.4. Ammonium concentration*

The trend of ammonium ion concentration in the digestate is shown below in Figure 4.10. It should be noted that during the co-digestion period (21/01/2021-31/03/2021) ammonium concentration increased in the digestate thanks to the contribution of yogurt.

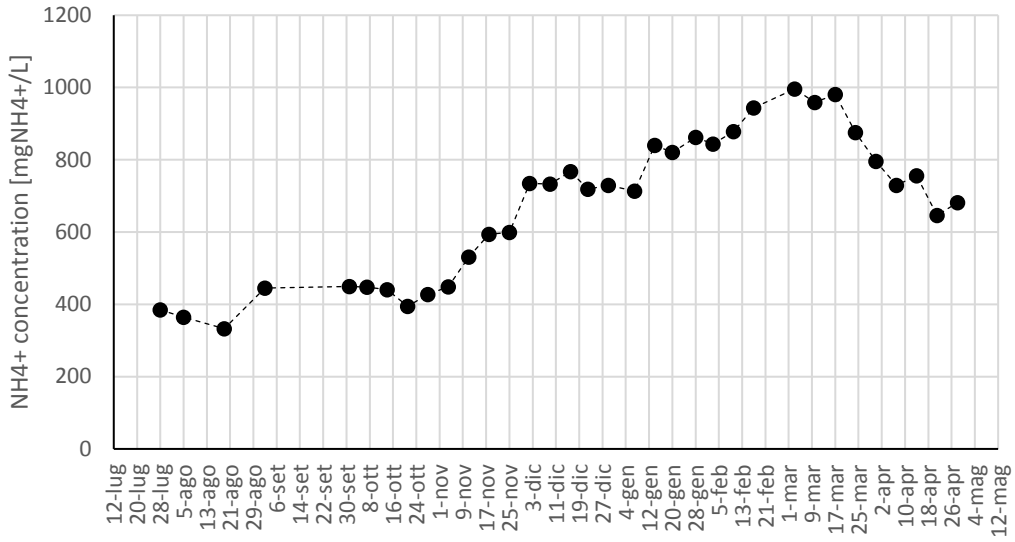


Figure 4.10 - Measurements of the ammonium concentration in the digestate.

### *4.5.5. Volatile fatty acids*

Figure 4.11 shows the various volatile fatty acids trend in the digestate. The effects of winter frost are observed with an increase in VFA in the digestate. Despite all the problems encountered, the pilot plant showed a proper systems response capacity to perturbations. The effluent VFAs went from an average value of 67 $mg_{COD}/L$ in mono-digestion to 35 $mg_{COD}/L$ in co-digestion.

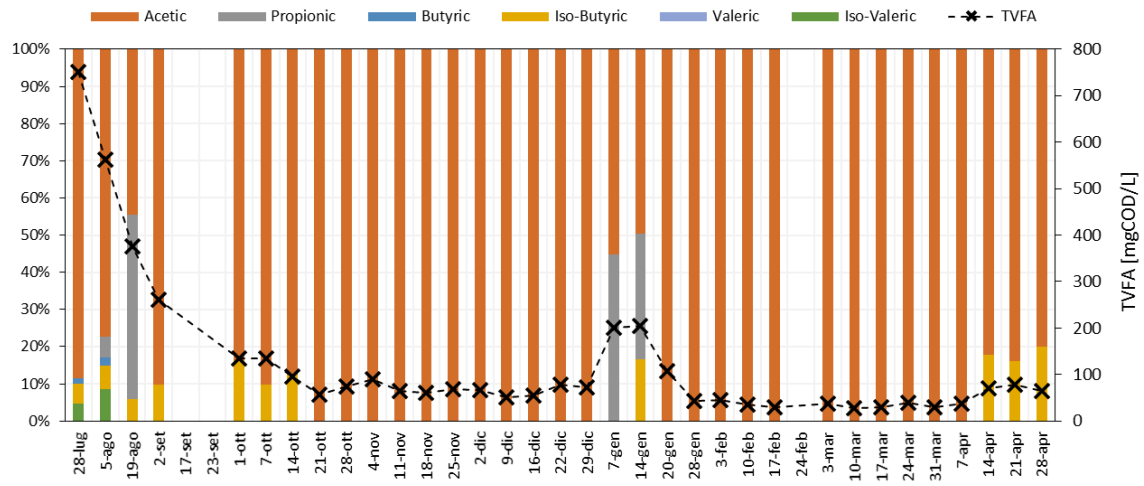


Figure 4.11 - Digestate volatile fatty acids reduction.

## *4.5.6. Biogas*

### *Biogas production*

Figure 4.12 shows the pilot plant specific average methane production expressed as $NmL_{CH4}$ per $g_{VS}$ fed to the digester. A slightly increasing trend is observed. As reported in paragraph 3.3.4, the biogas production data are available only until the second half of December. During the experimentation, problems were encountered with the biogas measurement, which was expected to be underestimated. For this reason, a comparison was made with the maximum specific production obtained by the BMPs. Therefore, starting from the BMP results, the expected production from a CSTR reactor was estimated through equation 4.1.

$$G_t\left[\frac{NmL_{CH_4}}{g_{VS}}\right] = BMP\left[\frac{NmL_{CH_4}}{g_{VS}}\right] =\cdot \left(1 - \frac{1}{k_H[\frac{1}{d}]\cdot HRT[d]}\right) \quad (4.1)$$

Where:

- $G_t$ is the cumulated specific methane production expected in the reactor,
- BMP is the cumulated methane yield at t = +∞.
- $k_H$ kinetic constant of the First-order kinetic model.

Based on these values, reported in Figure 4.12, the expected curve of methane production was reconstructed by rescaling it by a factor of 2.6. As can be seen in Figure 4.40, the biogas values corrected through this processing seem to coincide with the values simulated by the ADM1 model.

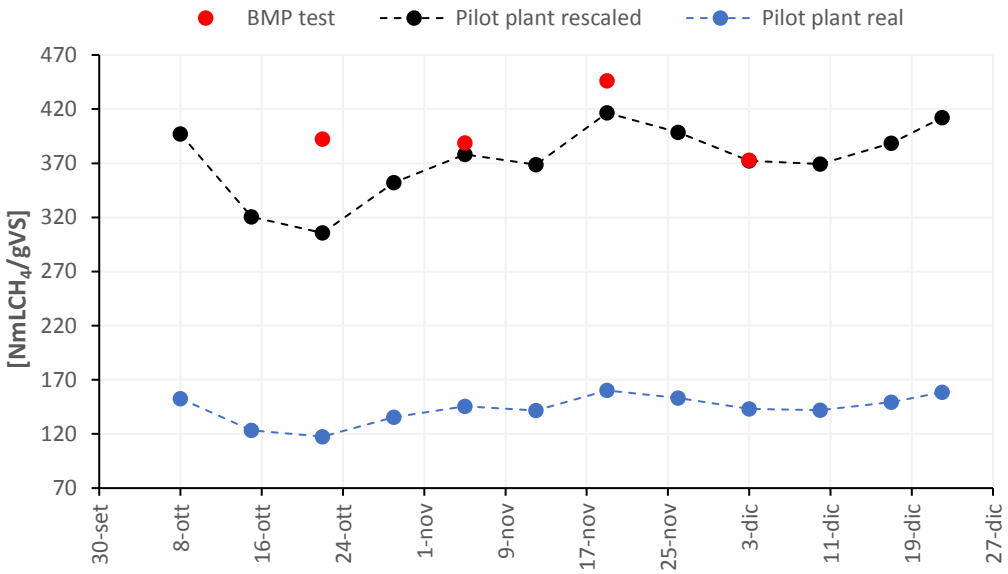


Figure 4.12 - Pilot plant average specific methane production.

Figure 4.13 shows the pilot plant's average methane production rate. An increase in production is observed over time.

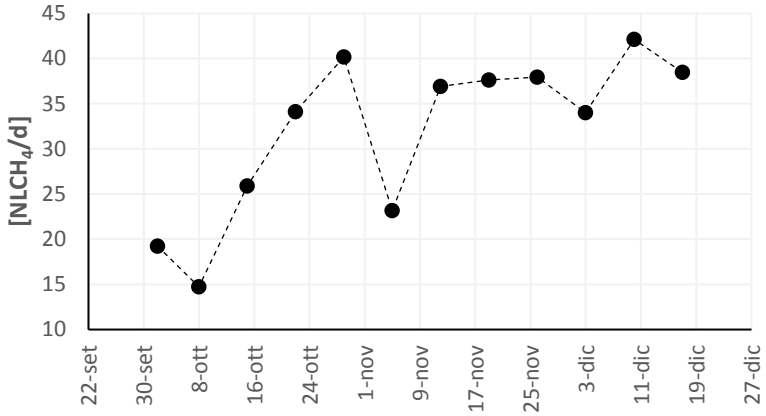


Figure 4.13 - Pilot plant average methane production rate.

*Biogas composition*

Figure 4.14 shows the trend of the dry biogas composition during the experimentation. An average percentage of methane equal to 64.5% and a standard deviation of 2.85% was measured. All measurements appear to be within the typical biogas composition range.

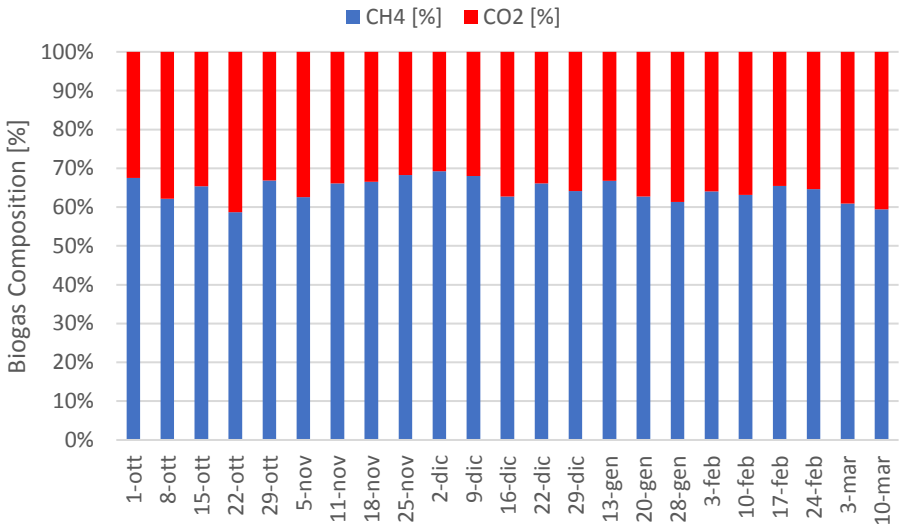


Figure 4.14 - Dry biogas composition.

Table 4.12 reports the mean and standard deviation of the percentage of methane in the dry biogas. There is an average decrease in the methane percentage passing from mono-digestion to co-digestion.

Table 4.12 - Methane percentage in dry biogas.

| | **Total [%]** | **Mono-digestion [%]** | **Co-digestion [%]** |
|---|---|---|---|
| *Average* | 64.5 | 65.4 | 62.7 |
| *Standard deviation* | 2.85 | 2.83 | 2.05 |

## *4.6. BMP tests*

This paragraph shows the results of the BMP tests. The net cumulative methane production per gram of volatile solid of the dosed substrate is reported for each test. For blank and residual BMP test cumulative methane production per gram of volatile solid of inoculum is reported. Since the tests were carried out in duplicate, the graphs shown represent the average between the duplicates and their standard deviation.

### *4.6.1. Blank BMP tests*

Figure 4.15 shows the comparison between the methane production obtained for the various blank BMP tests carried out. As anticipated, this was carried out on the inoculum alone, without substrate addition. The result of this test shows how much methane can be produced per gram of volatile solids present in the degassed digestate used as inoculum.

The graphs show some variability, which could be explained both by variations in the digestate leaving the pilot plant and by the variability of the degassing process.

The peculiar initial trend could relate to the lower accuracy of the instrument due to the low methane production in this test.

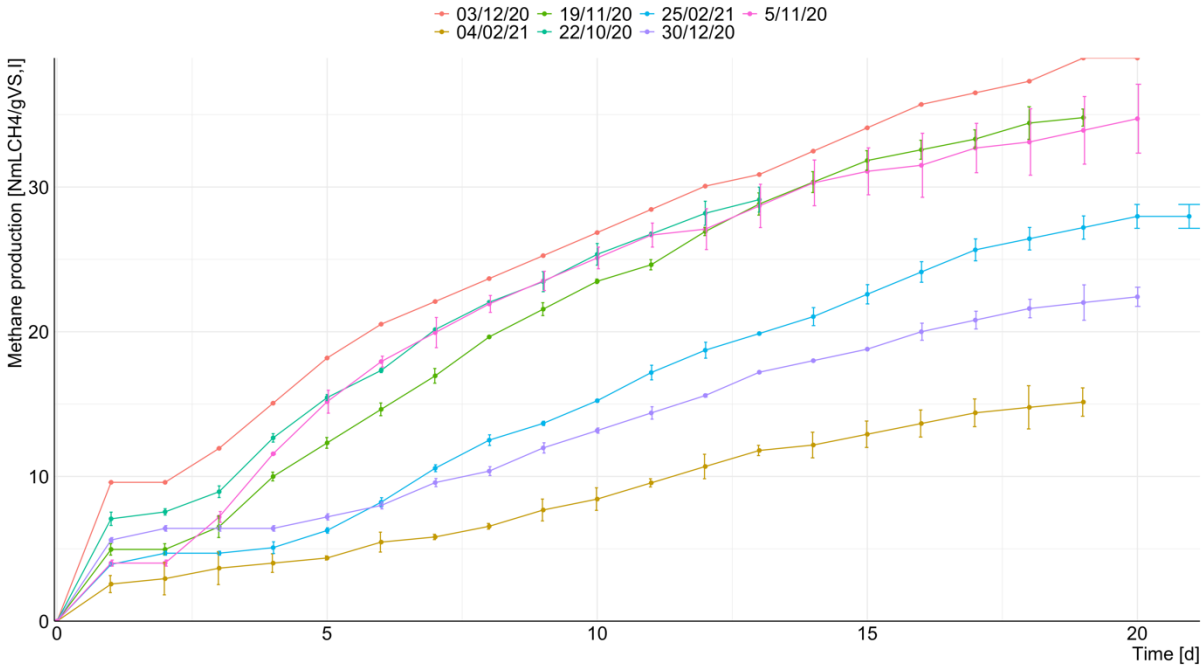


Figure 4.15 - Methane production comparison between blank BMP tests carried out.

### *4.6.2. Sludge BMP tests*

Figure 4.16 shows the comparison between the methane production obtained for the sludge BMP tests carried out. A typical BMP curve is observed, including a first phase of rapid production associated with fast degradation of the substrate until reaching a plateau. As time goes by, the amount of solids left to digest decreases as well as the bio-methanation rate. The higher the biodegradability of the substrate, the higher the bio-methanation rate is, keeping equal all operational conditions. The curves do not show high variability. They all seem to follow first-order kinetics. There are no significant variations following the different quantities of inoculum dosed (see paragraph 3.3.12).

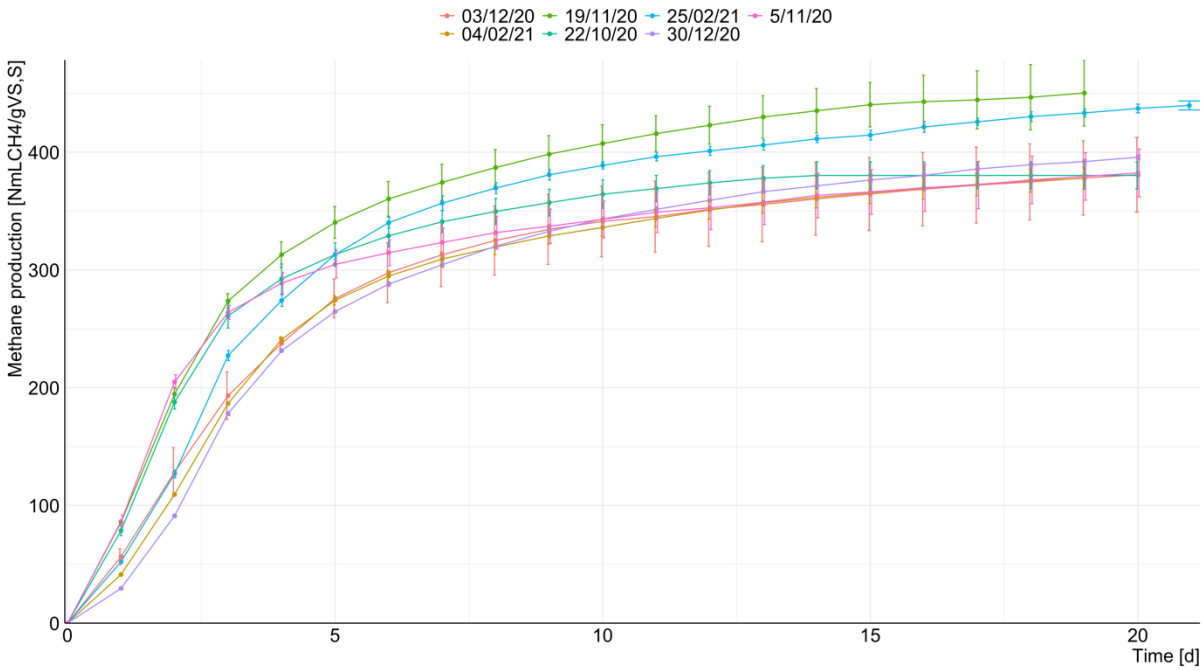


Figure 4.16 - Methane production comparison between sludge BMP tests carried out.

### *4.6.3. Particulate sludge BMP tests*

Figure 4.17 shows a comparison between all the results of the sludge particulate BMP tests performed. The curves show similar kinetics to that seen for the BMP test sludge in figure 4.17.

The curves do not show high variability. However, the tests carried out on 04/02/21, 25/02/21, and 30/12/20 have slightly slower kinetics and slightly lower production.

Particulate sludge BMP tests have been used, among other things, to calculate the percentage of particulate COD in the anaerobically degradable sludge. Known the COD associated with the particulate fraction and its non-degradable percentage, it was possible to calculate the inert particulate fraction $X_i$.

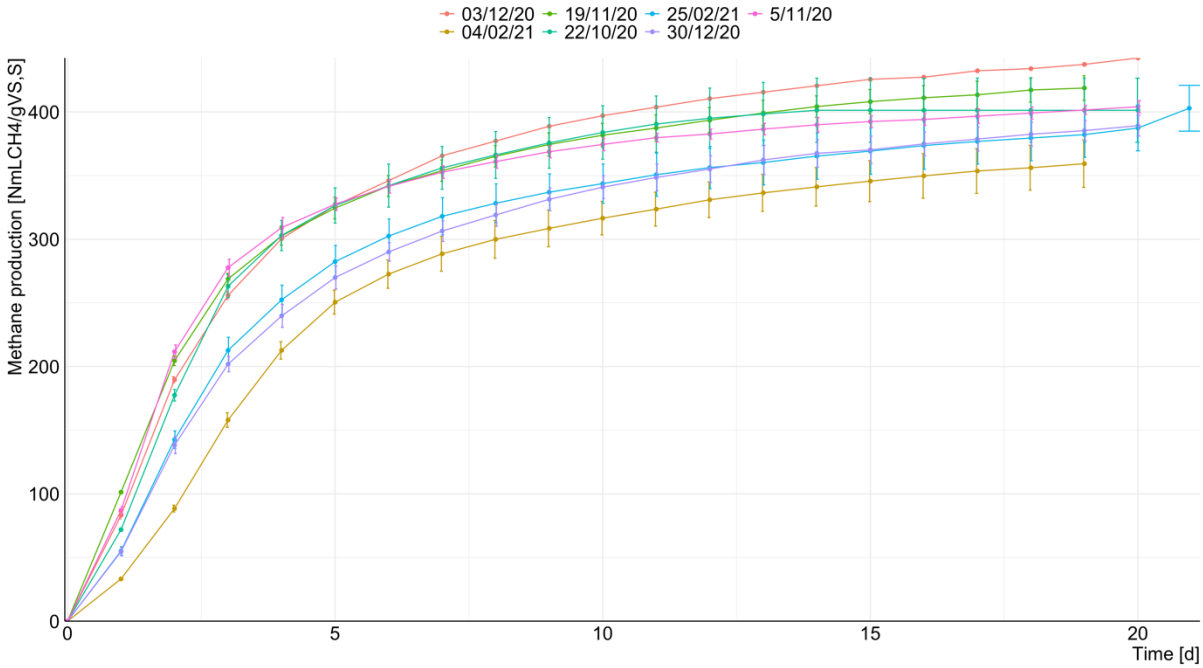


Figure 4.17 - Methane production comparison between particulate sludge BMP tests carried out.

### *4.6.4. Yogurt BMP tests*

Figure 4.18 shows the comparison between the methane production obtained for the yogurt BMP tests performed. All the tests show a high standard deviation. The curves show very high variability.

The test carried out on 04/02/21 shows a very different trend. Specifically, in this test, a total change in slope is observed after the first stretch. This test was performed with 2.26 $g_{VS,s}$/ bottle compared to 1.58 $g_{VS,s}$/bottle in the test of 30/12/20 and 1.55 $g_{VS,s}$/bottle in the test of 25/02/21. The greater presence of yogurt could have led to a possible phenomenon of pH inhibition which could justify the different trend.

The test of 25/02/20 shows a higher production and kinetics than the test of 30/12/20. On 12/30/20 the pilot plant was still operating in mono-digestion, consequently, the biomass had not yet adapted to the digestion of yogurt. This could be the motivation for their differences.

The trend of the test of 25/02/20 shows a steeper first slope than those seen for the sludge and the particulate sludge. This behavior highlights a higher initial production of methane and consequently a faster degradation.

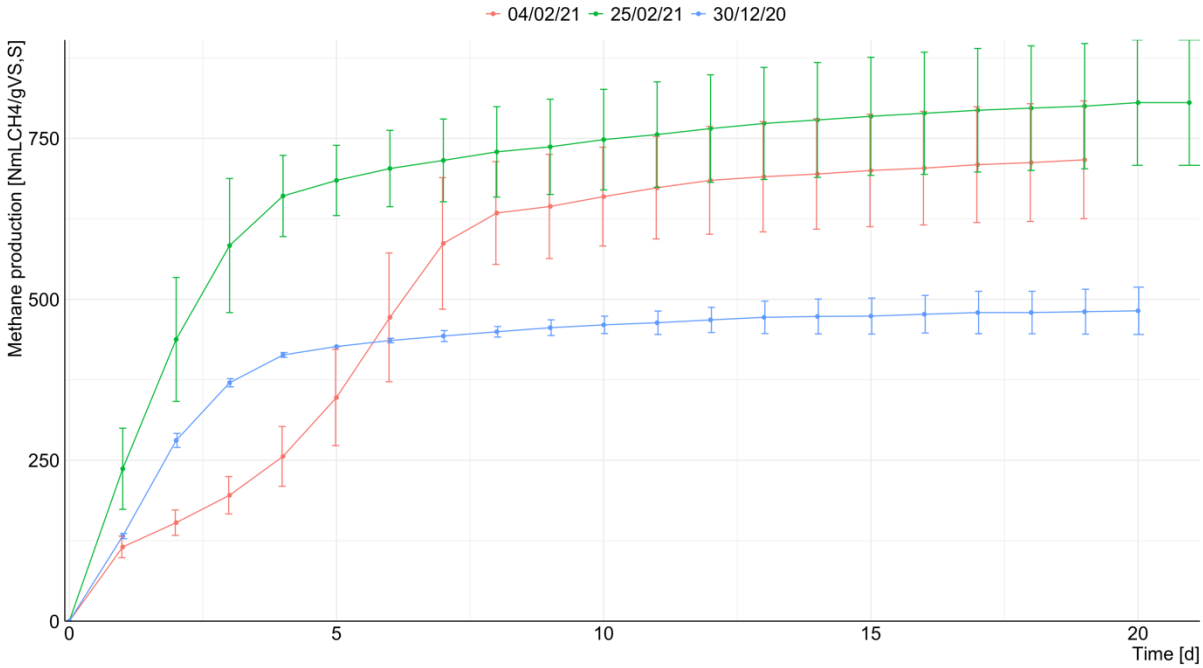


Figure 4.18 - Methane production comparison between yogurt BMP tests performed.

### *4.6.5. Co-digestion BMP tests*

Figure 4.19 shows the comparison between the methane production obtained for the BMP tests carried out in co-digestion. Table 3.1 shows the percentages of yogurt as volatile solids dosed in the test. Increasing the percentage of yogurt dosed also increases the kinetics and methane production. On 30/12/20, biomass had not yet adapted to co-digestion, operating the pilot in mono-digestion on that date. It could justify the lower methane production found in this test.

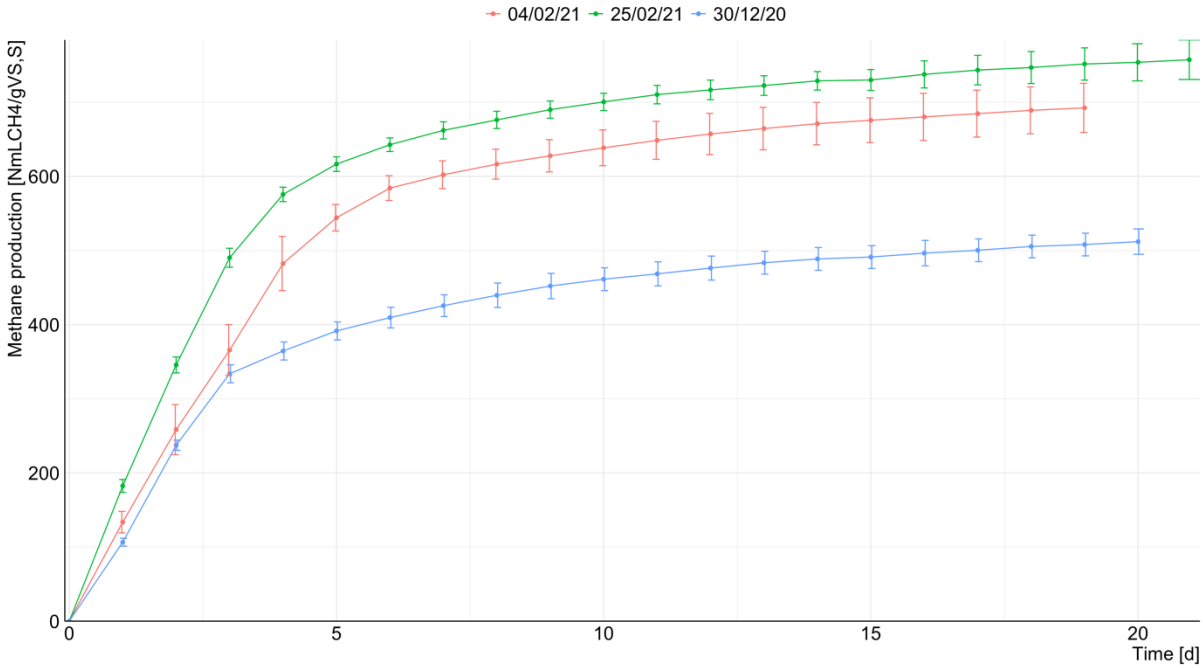


Figure 4.19 - Methane production comparison between yogurt BMP tests carried out.

Table 4.14 shows the increase in BMP co-digestion over expected production by cumulating the BMP yogurt and BMP sludge tests. In co-digestion BMP tests, there is an increase in methane production due to possible synergistic effects. The expected methane production in the co-digestion BMP test was calculated using equation $BMP_{co-dig,expected}\left[\frac{NmL_{CH_4}}{g_{VS,co-substrates}}\right] = BMP_{sludge}\left[\frac{NmL_{CH_4}}{g_{VS,sludge}}\right] \cdot VS_{sludge,co-dig.\ BMP}\left[g_{VS,sludge,co-dig.}\right] + BMP_{yogurt}\left[\frac{NmL_{CH_4}}{g_{VS,yogurt}}\right] \cdot VS_{yogurt,co-dig.BMP}\left[g_{VS,yogurt,co-dig.}\right]$ (4.2.

$$BMP_{co-dig,expected}\left[\frac{NmL_{CH_4}}{g_{VS,co-substrates}}\right] = BMP_{sludge}\left[\frac{NmL_{CH_4}}{g_{VS,sludge}}\right] \cdot VS_{sludge,co-dig.\ BMP}\left[g_{VS,sludge,co-dig.}\right] + BMP_{yogurt}\left[\frac{NmL_{CH_4}}{g_{VS,yogurt}}\right] \cdot VS_{yogurt,co-dig.BMP}\left[g_{VS,yogurt,co-dig.}\right] \quad (4.2)$$

This increase improves with the volatile solids fraction increase of the yogurt dosed in the test.

Table 4.13 - BMP increase in co-digestion.

| ***Co-digestion BMP test*** | **Yogurt VS fraction [$g_{VS,yogurt}/g_{VStot,s}$]** | **BMP increase [%]** |
|---|---|---|
| *30/12/20* | 0.45 | 17% |
| *04/02/21* | 0.5 | 23% |
| *25/02/21* | 0.65 | 27% |

### *4.6.6. Residual BMP tests*

Figure 4.20 shows the comparison of the specific methane production per gram of volatile solid of inoculum of the residual BMP tests performed. A very moderate slope and a slow kinetics is observed for this test. As mentioned, the inoculum used for the residual BMPs is the fresh digestate. The residual BMP tests can be used to calculate the net production of the biomass activity tests having the same inoculum.

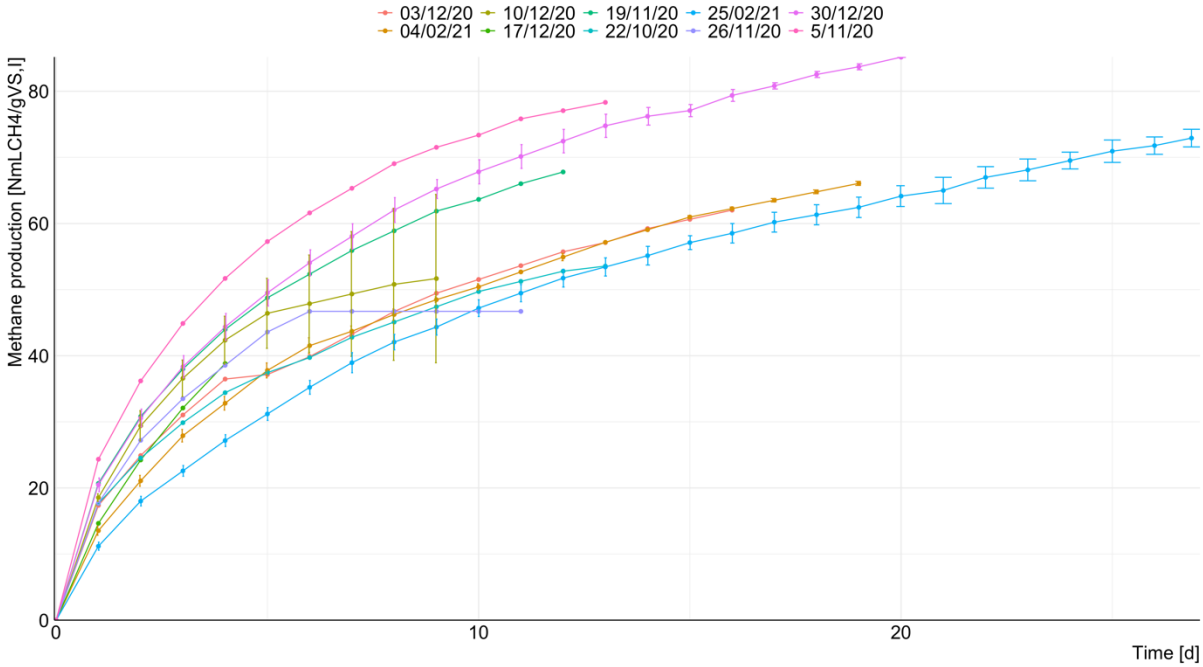


Figure 4.20 - Methane production comparison between residual BMP tests performed.

## *4.7. Biomass activity tests*

The results of the biomass activity tests are reported in this paragraph. For each type of test, the results of a single representative test are reported and discussed. All the other results can be consulted in APPENDIX E.

Since the tests were carried out in duplicate, the graphs shown below represent the average between the duplicates and their standard deviation. These graphs represent the cumulative methane production per gram of COD dosed as a specific substrate.

### *4.7.1. Acetate activity test*

Figure 4.21 shows results of tests conducted using acetate at a COD of 3.0 $g_{COD}$/L. A slight and almost undetectable increase in the methane production rate is exhibited during the first hours of the test, thereafter the rate remains constant until the substrate is exhausted. In the first phase highlighted by the vertical dashed red lines, it can be seen that there is a linear slope, associated with the degradation of the acetate. The slope of the final part of the curve instead shows methane production due to the degradation of the residual organic substance present in the fresh digestate used as inoculum. These curves are used to estimate the model parameters $k_{m,ac}$ and $K_{s,ac}$ through an iterative process.

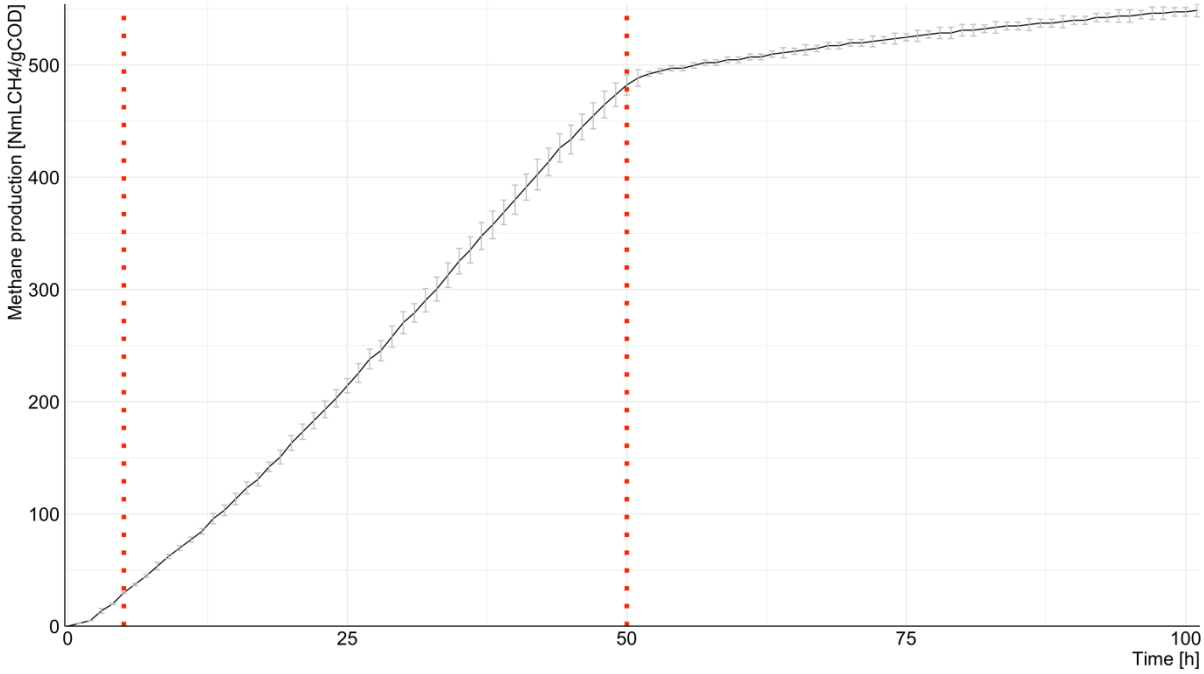


Figure 4.21 - Methane production of acetate activity test (10/12/2020).

### *4.7.2. Glucose activity test*

Figure 4.22 shows the result of the glucose activity test carried out on 19/11/2020. In the portion of the graph delimited by the dashed red lines, there is a double change in slope. There is a first slope, followed by a more vertical slope which indicates a fast production associated with rapid degradation of the substrate. Then there is a new change in slope which becomes almost parallel to the first one. The glucose dosage leads to an initial pH lowering which may explain the above-mentioned phenomenon. This lowering is not capable of causing inhibition

but could be responsible for the initial slowdown. As soon as the methanogens begin to degrade the VFA, the pH rises, and a fast biogas production is observed.

The test shown in Figure 4.22 was carried out by injecting the glucose to obtain a concentration of COD dosed in the test equal to 4 $g_{COD}$/L. As anticipated in the previous chapter, the tests with glucose were carried out at different concentrations of COD. This choice was made to check whether the almost vertical slope section was attenuated. However, this slope continued to repeat itself in each test carried out. Figure 4.23 shows a glucose test performed on 03/12/20. This test has the lowest concentration of glucose as COD tested, equal to 2.5 gCOD/L, and the same trend previously described is observed.

These tests are used in the ADM1 calibration phase to identify the parameters of $k_{m,su}$ and $K_{s,su}$.

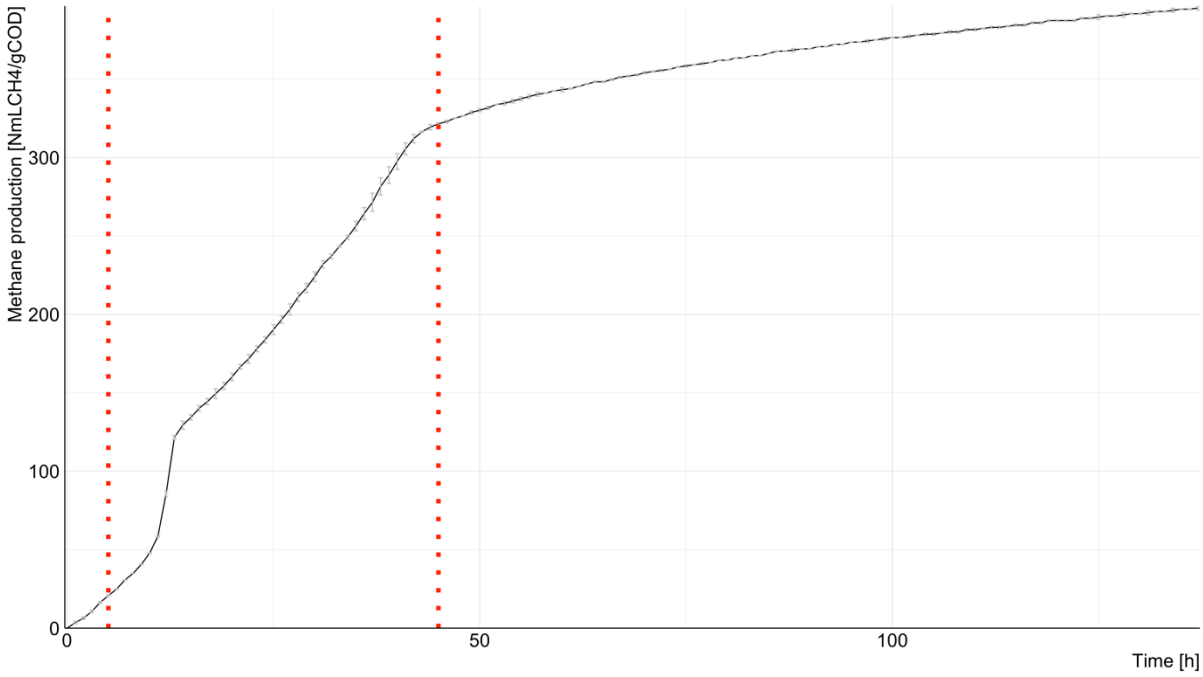


Figure 4.22 - Methane production of glucose activity test carried out with a concentration of 4 $g_{COD,glu}$ / L (19/11/2020).

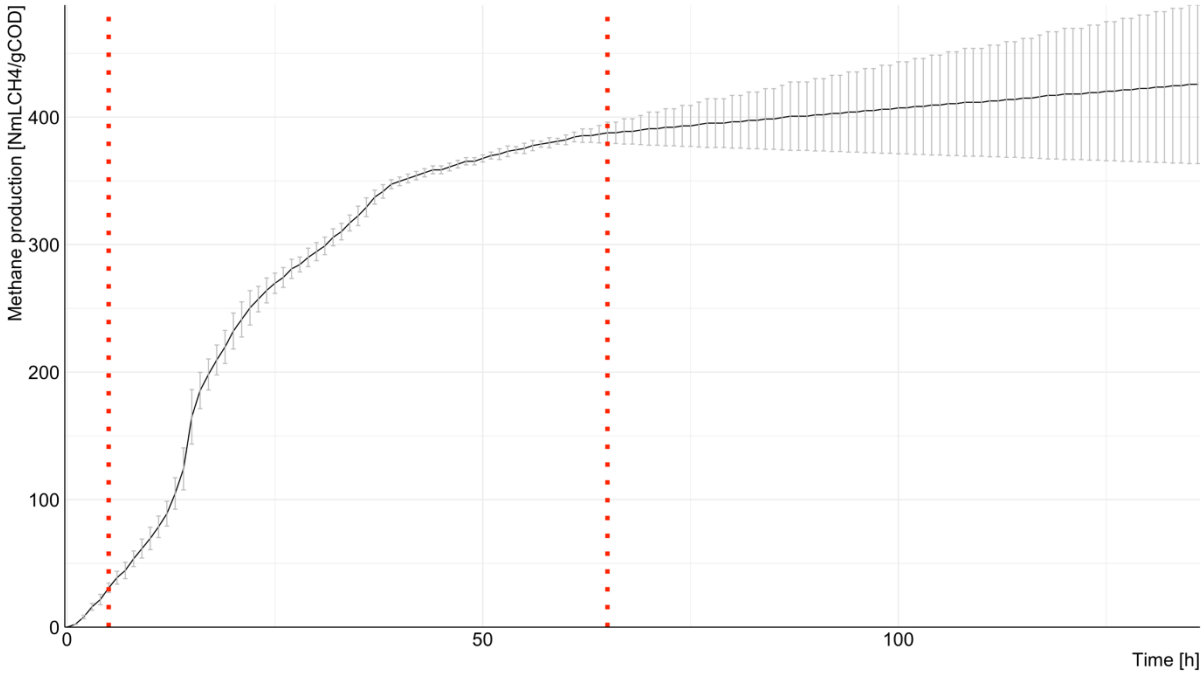


Figure 4.23 - Methane production of glucose activity test carried out with a concentration of 2.5 $g_{COD,glu}$ / L (03/12/2020).

### *4.7.3. BSA activity test*

The BSA test is used for the calibration of $k_{m,aa}$ and $K_{s,aa}$. This paragraph reports the results of two tests carried out during the experimentation. The test represented in Figure 4.24 was carried out with a concentration of COD as BSA of 4.5 $g_{COD}$/L. In the curve interval contained between the red dotted lines, a double slope is highlighted due to the degradation of this substrate in which there is a first faster part followed by a slowdown. The utilization of substrate starts almost instantaneously and, when the substrate is exhausted, the activity drops sharply. The test in Figure 4.25 instead shows a test carried out with a lower concentration of BSA as COD equal to 3 $g_{COD}$/L. It is observed that at a lower concentration of BSA as COD the trend remain similar.

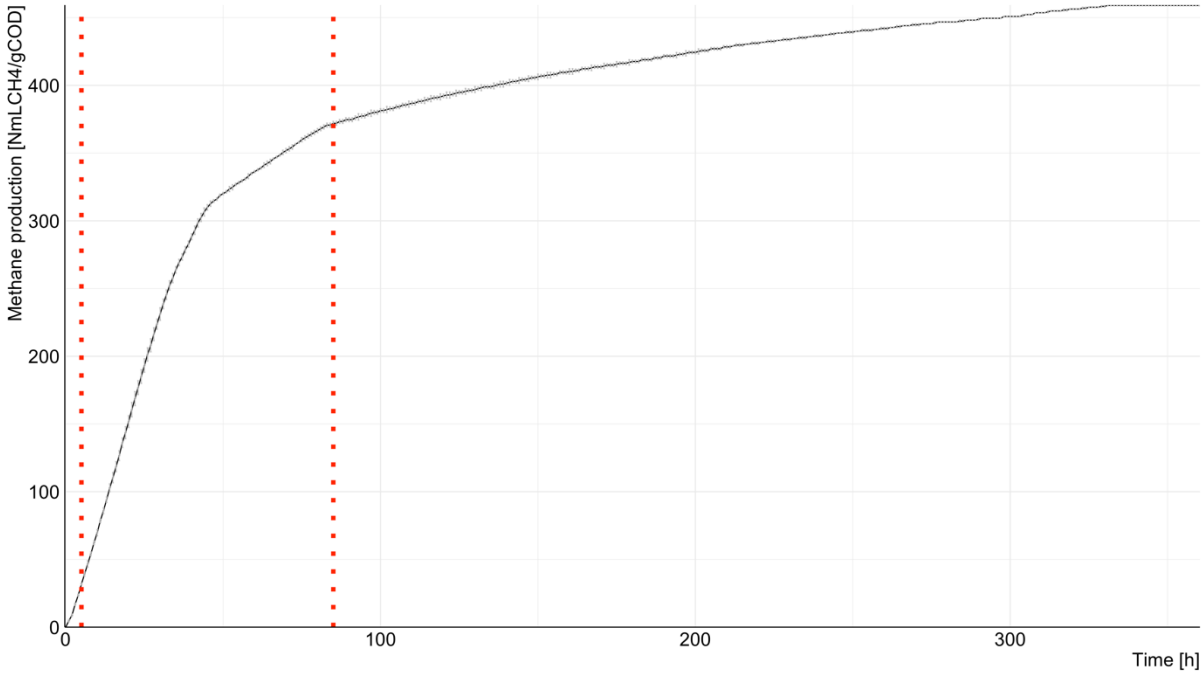


Figure 4.24 - Methane production of BSA activity test carried out with a concentration of 4.5 $g_{COD,BSA}$ / L (29/12/2020).

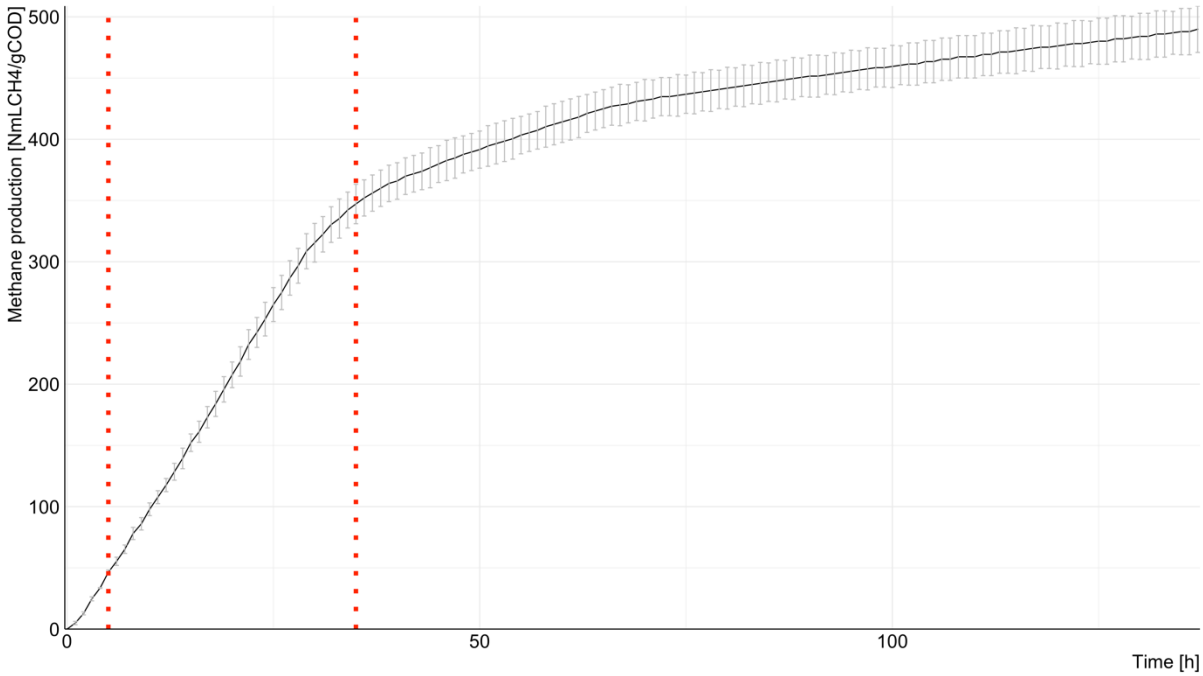


Figure 4.25 - Methane production of BSA activity test carried out with a concentration of 3 $g_{COD,BSA}$ / L. (26/11/2020).

## *4.8. ADM1 dynamic simulations*

### *4.8.1. Calibration*

Table 4.14 summarizes the results of the iterative calibration process and the parameter values estimated during the various iterations. The actual iterative process stopped at the fifth iteration. At this point, both the simulation of the pilot plant and the simulation of the batch tests gave satisfactory results, as supported by the values of the TIC and MARE indicators. However, using these parameters, a deviation was observed between some experimental and simulated values of the pilot plant model starting from co-digestion onwards (see paragraph 4.8.3). The model with the parameters estimated at the fifth iteration works better for mono-digestion than for co-digestion as supported by the model fitting criteria reported in Table 4.22. This behavior led to the evaluation of two hypotheses:

1. Hydrolysis constants are depending on the phase in which the biomass is working due to synergistic effects during co-digestion. If that is the case, as the microbial population adapts to the new working conditions different hydrolysis constants should be considered for co-digestion.
2. There are different hydrolytic constants for sludge and yogurt which depend on the type of substrate and not only on the biomass.

To identify which hypothesis is correct, a sixth iterative step was carried out in which the value of the hydrolysis constant of the proteins was modified. By increasing the protein hydrolysis rate by varying the $k_{hyd,pr}$ from 0.3 $d^{-1}$ to 0.5 $d^{-1}$, there has been a significant improvement in the simulation of the yogurt BMPs (Figure 4.28 and Table 4.17 shows how the first iteration is more reliable than the fifth to simulate this BMP yogurt test. In the sixth iteration, the hydrolysis kinetics constant of proteins has been increased. This further modification highlights a significant improvement compared to the fifth iteration, supported by the model prediction performance analysis reported in Table 4.17. The TIC also shows minimal improvement between the sixth and first iteration.

Table 4.17). Even in the co-digestion BMP tests, there was such an improvement (Figure 4.29 and Table 4.18).

However, the same modification of the hydrolysis kinetic constant ($k_{hyd,pr}$) on the sludge BMP test resulted in a worsening of the simulation. This evidence indicates that the hydrolytic constants of proteins also depend on the type of substrate and not only on the biomass.

The improvement found in the co-digestion BMP tests could be justified by the high percentage of yogurt proteins present in the test, equal to 67%.

Table 4.14 - ADM1 kinetics parameters estimated during each iterative step of the calibration process.

| ***Parameters*** | **UM** | **Initial** | **1st iteration** | **2nd iteration** | **3rd iteration** | **4th iteration** | **5th iteration** | **6th iteration (yogurt)** |
|---|---|---|---|---|---|---|---|---|
| $k_{dis}$ | $d^{-1}$ | 0.4 | 1.2 | 2 | 1.5 | 1.5 | 1.5 | 1.5 |
| $k_{H,Ch}$ | $d^{-1}$ | 0.25 | 0.75 | 0.75 | 0.3 | 0.3 | 0.3 | 0.3 |
| $k_{H,Pr}$ | $d^{-1}$ | 0.2 | 0.6 | 0.6 | 0.2 | 0.2 | 0.2 | 0.5 |
| $k_{H,Li}$ | $d^{-1}$ | 0.1 | 0.3 | 0.8 | 0.45 | 0.5 | 0.5 | 0.5 |
| $k_{m,su}$ | $d^{-1}$ | 30 | 30 | 38 | 38 | 8 | 8 | 8 |
| $k_{m,aa}$ | $d^{-1}$ | 50 | 50 | 8 | 8 | 8 | 8 | 8 |
| $k_{m,ac}$ | $d^{-1}$ | 8 | 8 | 6 | 6 | 8 | 8 | 8 |
| $K_{s,su}$ | $g_{COD}/L$ | 0.5 | 0.5 | 0.4 | 0.3 | 0.3 | 0.3 | 0.3 |
| $K_{s,aa}$ | $g_{COD}/L$ | 0.3 | 0.3 | 0.2 | 0.2 | 0.2 | 0.2 | 0.2 |
| $K_{s,ac}$ | $g_{COD}/L$ | 0.15 | 0.15 | 0.3 | 0.01 | 0.01 | 0.01 | 0.01 |
| $K_{s,pro}$ | $g_{COD}/L$ | 0.3 | 0.3 | 0.3 | 0.3 | 0.3 | 0.2 | 0.2 |

### *4.8.2. Batch tests simulations*

#### *Blank BMP tests simulation*

Figure 4.26 shows the simulation of the blank BMP test of 12/30/20. In the initial phase, the test has a peculiar behavior, distinguished by different slopes. This behavior is difficult to predict by the ADM1 model. The final part, on the other hand, can be estimated better. As mentioned in chapter 3.3.12, the fresh digestate was sampled weekly and left to degas.

Consequently, the inoculum used for the BMP tests during the experimentation has high variability. As already anticipated, the simulations of the BMP tests were carried out using the output digestate from the pilot-plant model and characterized according to the pilot-plant ADM simulation; a degassing step was also considered by simulating an extra batch digestion phase. However, the degassing phase, was carried out without mixing, while it was simulated by assuming complete mixing conditions. These have entailed additional uncertainties in modeling the BMP tests.

A further explanation of the difficulty of simulating Blank BMP tests could relate to the lower accuracy of the instrument due to the low methane production in this test.

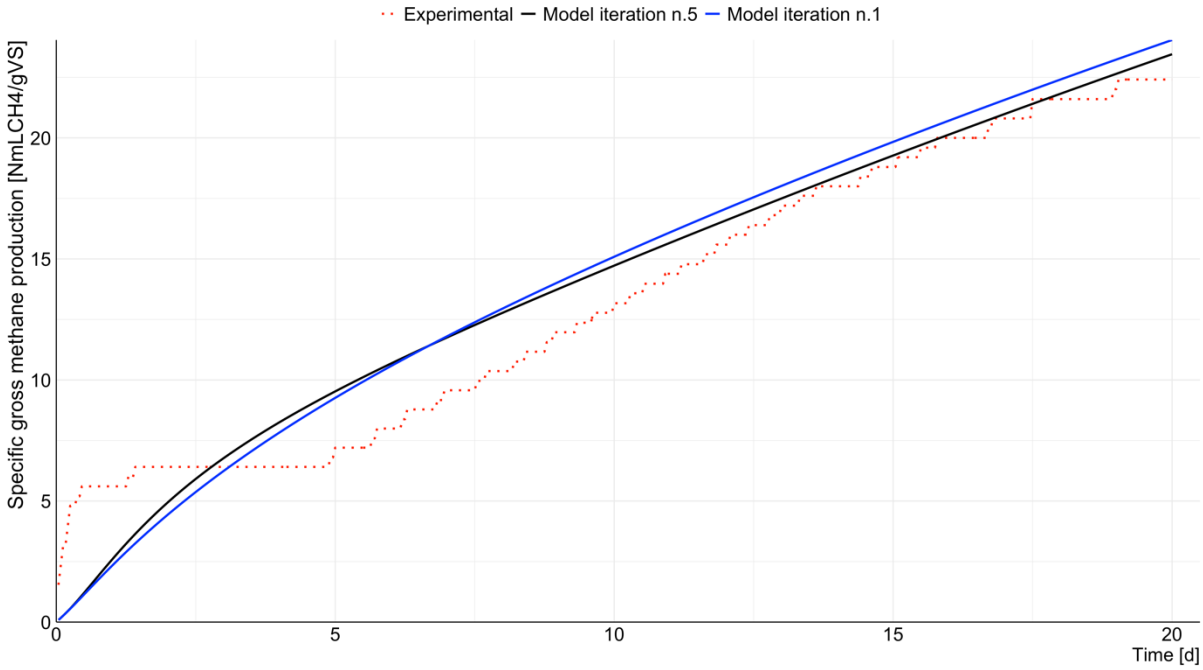


Figure 4.26 - Blank BMP test simulation (30/12/2020).

Table 4.15 shows the model fitting criteria, which show that an improvement is obtained between the first and fifth iteration.

Table 4.15 - Model prediction performances for blank BMP test simulation (19/11/2020).

| ***Model Fitting Criteria*** | **1st iteration** | **5th iteration** |
|---|---|---|
| *TIC* | 0.064 | 0.056 |
| *MARE* | 0.35 | 0.199 |

*Sludge BMP tests simulation*

Figure 4.27 shows the comparison between the simulation of a Sludge BMP test (carried out on 19/11/20) at the first and fifth iteration with the experimental result. The graph refers to the gross production of methane expressed as $NmL_{CH4}$ per gram of volatile solid of the substrate.

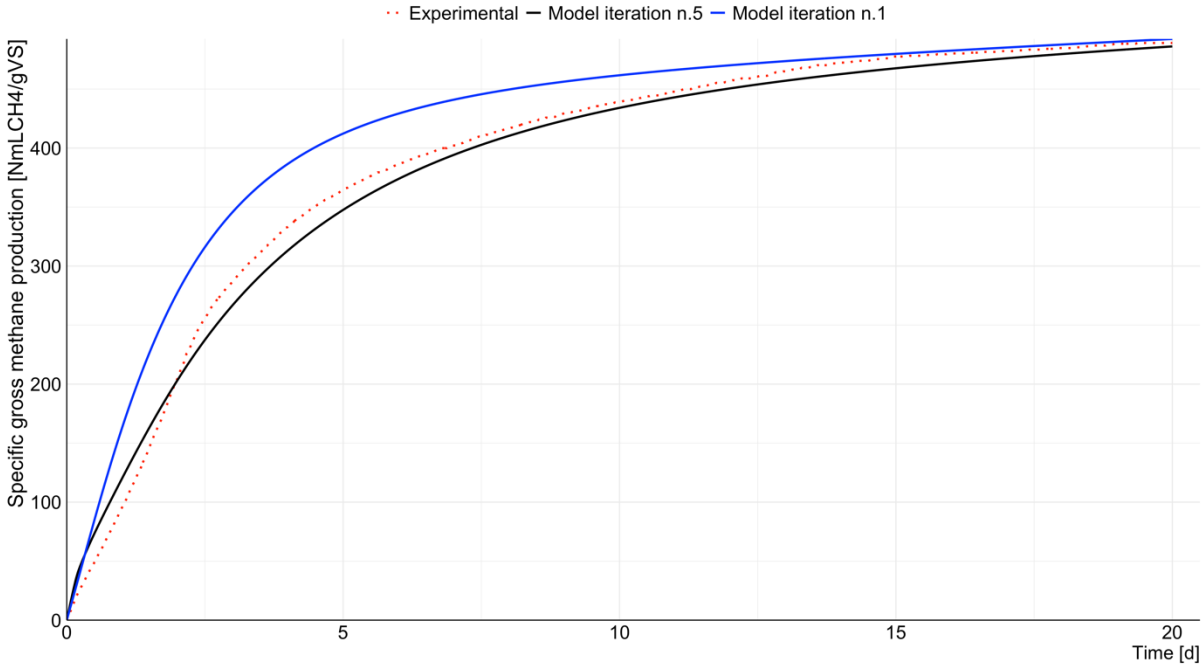


Figure 4.27 - Sludge BMP test simulation (19/11/2020).

Calibration proved to be very effective in this case, fifth iteration parameters seem to be much more reliable, as also shown by the TIC and MARE indicators reported in Table 4.16 which are closer to zero in the case of the fifth iteration.

Table 4.16 - Model prediction performances for sludge BMP test simulation (19/11/2020).

| ***Model Fitting Criteria*** | **1st iteration** | **5th iteration** |
|---|---|---|
| *TIC* | 0.0421 | 0.0145 |
| *MARE* | 0.09 | 0.04 |

*Yogurt BMP tests simulation*

Figure 4.28 shows the comparison between the first, fifth and sixth iteration for the BMP yogurt test (carried out on 25/02/2021). The first and the sixth iterations seem to fit the experimental curve well, while the fifth iteration provides a less reliable result. This behavior is probably

linked to the constant hydrolysis kinetics of proteins which in the first and sixth iteration is higher than in the fifth.

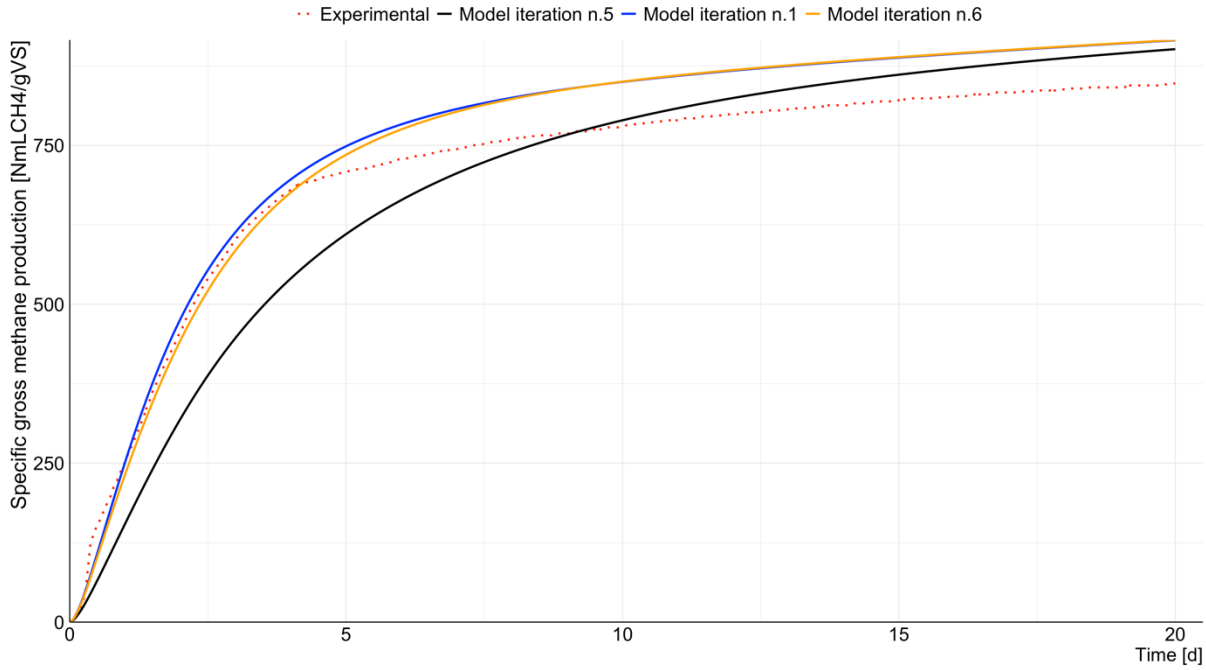


Figure 4.28 - Yogurt BMP test simulation (25/02/2021).

Table 4.17 shows how the first iteration is more reliable than the fifth to simulate this BMP yogurt test. In the sixth iteration, the hydrolysis kinetics constant of proteins has been increased. This further modification highlights a significant improvement compared to the fifth iteration, supported by the model prediction performance analysis reported in Table 4.17. The TIC also shows minimal improvement between the sixth and first iteration.

Table 4.17 - Model prediction performances for yogurt BMP test simulation (25/02/2021).

| ***Model Fitting Criteria*** | **1st iteration** | **5th iteration** | **6th iteration** |
|---|---|---|---|
| *TIC* | 0.038 | 0.049 | 0.037 |
| *MARE* | 0.07 | 0.14 | 0.07 |

### *Co-digestion BMP tests simulation*

The same considerations made for the BMP of yogurt are also valid for the BMP of co-digestion. Figure 4.29 shows a significant improvement due to the implementation of the constant hydrolysis kinetics of proteins. As already mentioned, this improvement could be

justified by the percentage of yogurt proteins in this test (carried out on 30/12/2020) compared to the total proteins is equal to 67% and, therefore, having a high impact on the simulation.

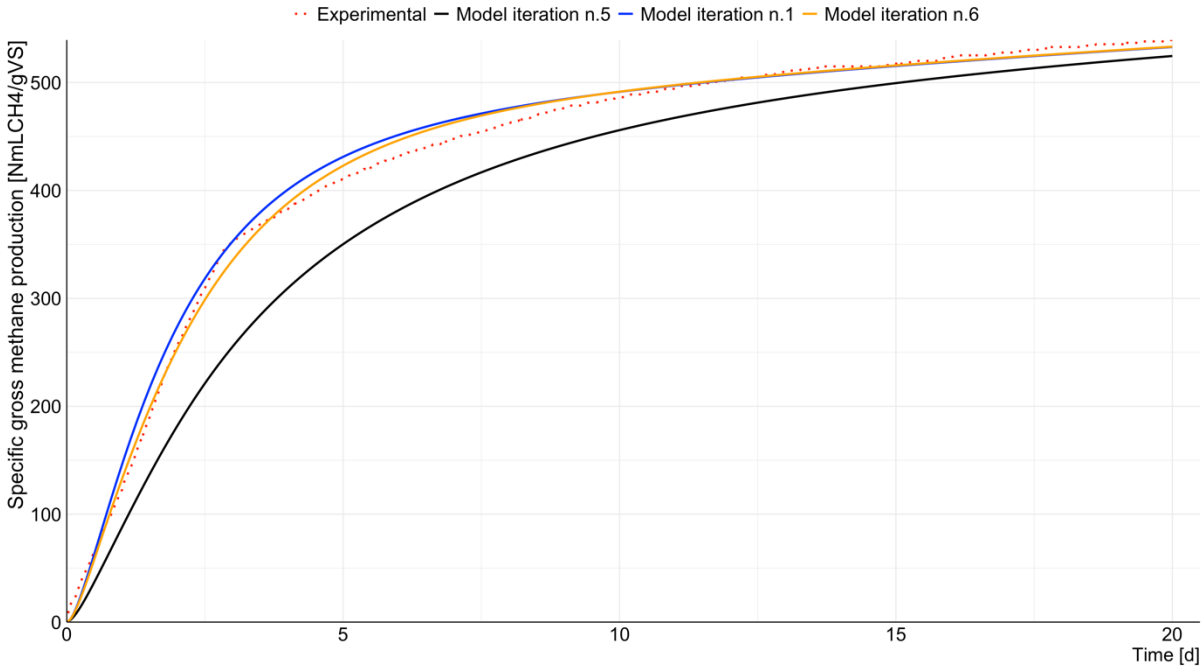


Figure 4.29 - Co-digestion BMP test simulation (30/12/2020).

The comparison of the three simulations, performed using the TIC and MARE criteria (Table 4.18), gives results consistent with what previously stated, confirming the sixth iteration as the most effective.

Table 4.18 - Model prediction performances for co-digestion BMP test simulation (30/12/2020).

| ***Model Fitting Criteria*** | **1st iteration** | **5th iteration** | **6th iteration** |
|---|---|---|---|
| *TIC* | 0.0127 | 0.049 | 0.009 |
| *MARE* | 0.026 | 0.13 | 0.018 |

### *Acetate activity tests simulation*

Figure 4.30 shows the result of the simulation of an Acetate activity test started on 14/01/2021. Through the simulation, it was possible to replicate the initial phase of acetate degradation very

well. It is observed how the simulation improves passing from the first to the fifth iteration. This improvement is confirmed by the TIC and MARE indicators reported in Table 4.19.

A comparison was also performed between the acetate fraction as COD converted into methane by the model and in the experimental test. In the experimental test, subtracting the residue, it was estimated that 94% of the acetate as COD is converted into methane. Instead, the model simulates a conversion rate of 97.7%.

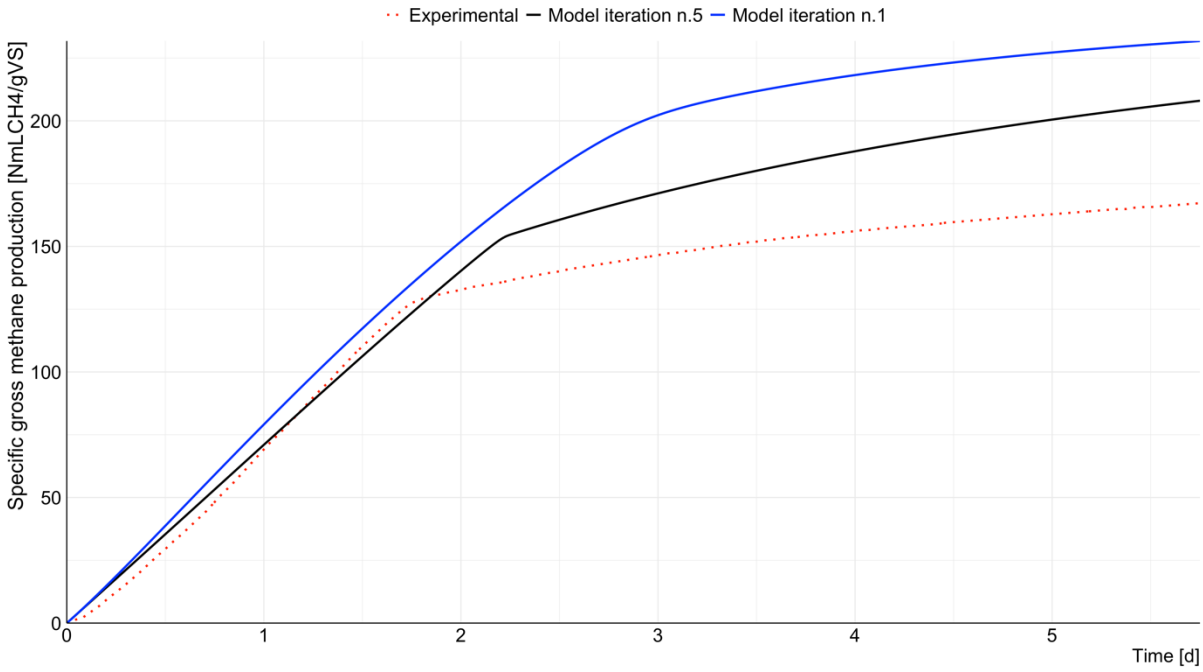


Figure 4.30 - Acetate activity test simulation (14/01/2021).

Table 4.19 - Model prediction performances for Acetate activity test simulation (14/01/2021).

| ***Model Fitting Criteria*** | **1st iteration** | **5th iteration** |
|---|---|---|
| *TIC* | 0.151 | 0.087 |
| *MARE* | 0.236 | 0.146 |

### *Glucose activity tests simulation*

Figure 4.31 shows the simulation of a biomass activity test with glucose performed on 17/12/2020. Simulating the initial course of the test is very complicated. As anticipated, the

cause of the very first slope could be an inhibition phenomenon that involves the initial slowdown and subsequent rapid production of methane (i.e., the inhibition from volatile fatty acids that ADM does not foresee). Therefore, it is complicated to simulate the real trend without calibrating the parameters of the inhibition kinetics. In any case, between the first and fifth iteration, there was a notable improvement in the simulation as also found numerically through the TIC and MARE parameters reported in Table 4.20.

In this experimental test, 86.5% of the glucose as COD was converted to methane. According to the model, 96.7% is converted. This deviation between experimental and model could be related to the inhibition phenomena, already mentioned, which the model does not take into account at present.

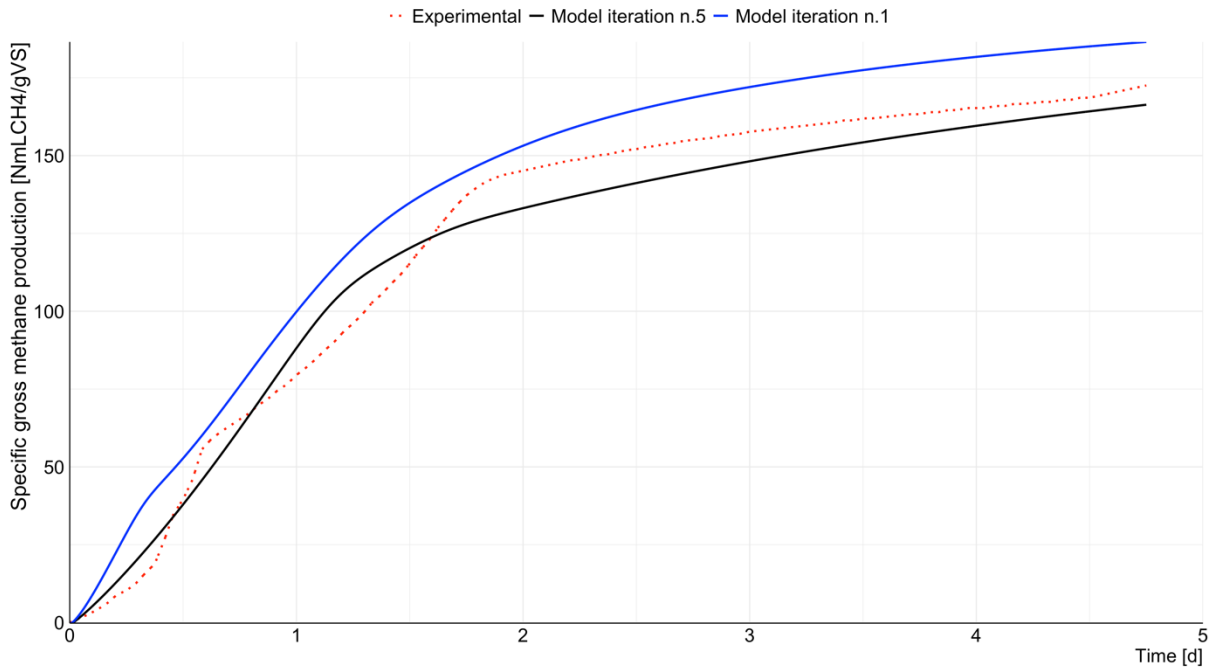


Figure 4.31 - Glucose activity test simulation (17/12/2020).

Table 4.20 - Model prediction performances for Glucose activity test simulation (17/12/2020).

| ***Model Fitting Criteria*** | **1st iteration** | **5th iteration** |
|---|---|---|
| *TIC* | 0.054 | 0.031 |
| *MARE* | 0.14 | 0.04 |

*BSA activity tests simulation*

Figure 4.32 shows the result of a simulation of a biomass activity test with BSA (started on 17/02/2021). In this case, the simulation seems to have degradative kinetics faster than those found in reality. The simulation of this test takes into account not only the uptake of BSA but also the uptake of the resulting by-products. Therefore, the degradation kinetics of the various VFAs should also be taken into account in the calibration process to improve the simulation. Nonetheless, the iterative process also proved successful as can be seen from the results in Table 4.21.

In the experimental test, 66.8% of the BSA as COD converted into methane. According to the model (fifth iteration), this conversion percentage is equal to 71.6%. These low values could be due to a too short test duration. According to the model, using the first iteration parameters, 82.3% of BSA as COD is converted into methane. The maximum uptake rate of amino acid degrading organisms ($k_{m,aa}$) from the first to the fifth iteration goes from 50 $d^{-1}$ to 8$d^{-1}$. It can explain the higher conversion ratio. This phenomenon also justifies the high deviation between the model curve at the first iteration and the experimental curve.

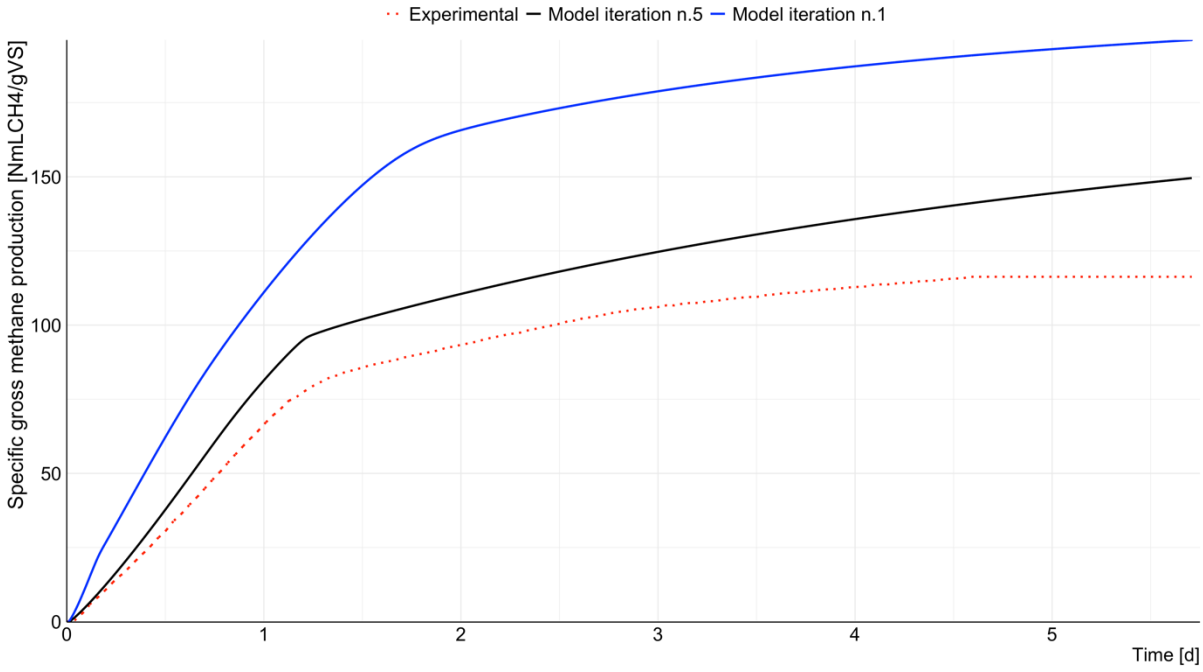


Figure 4.32 - BSA activity test simulation (17/02/2021).

Table 4.21 - Model prediction performances for BSA activity test simulation (17/02/2021).

| ***Model Fitting Criteria*** | **1st iteration** | **5th iteration** |
|---|---|---|
| *TIC* | 0.302 | 0.096 |
| *MARE* | 0.45 | 0.13 |

### *4.8.3. Pilot plant simulations*

The results obtained from the batch test simulations were used to model the operation of the pilot-scale digester. This was achieved through the iterative calibration method illustrated previously in chapter 4.8.1.

The simulation of the pilot plant was performed for 203 days as in reality, thus reflecting the time frame between 8/10/2020 and 28/4/2021 in which the monitoring of the pilot plant was carried out. The time distribution between simulation in mono-digestion (08/10/2020-20/1/2021 and 01/04/2021-2/10/2021) and simulation in co-digestion (21/1/2021 -31/03/2021) also describe the real pilot plant behavior.

The feeding was simulated in semi-continuous mode as it happened in reality. In the co-digestion period, the yogurt feeding was added to increase the digester OLR by 20%, as done on the real pilot plant.

The graphs from Figure 4.33 to Figure 4.42 illustrate the simulation results obtained in the last iteration of the calibration process. In order to highlight how effective, the calibration of the model is, the trends of the variables simulated by the model at the first iteration and at the fifth iteration are represented, compared with the experimental data. On each graph, the trend of the simulated variable at the fifth iteration is shown in black; the simulations obtained at the first iteration are shown with a gray line, while the experimental data are shown in red. The period in which the co-digestion with yogurt was carried out is highlighted by a yellow box.

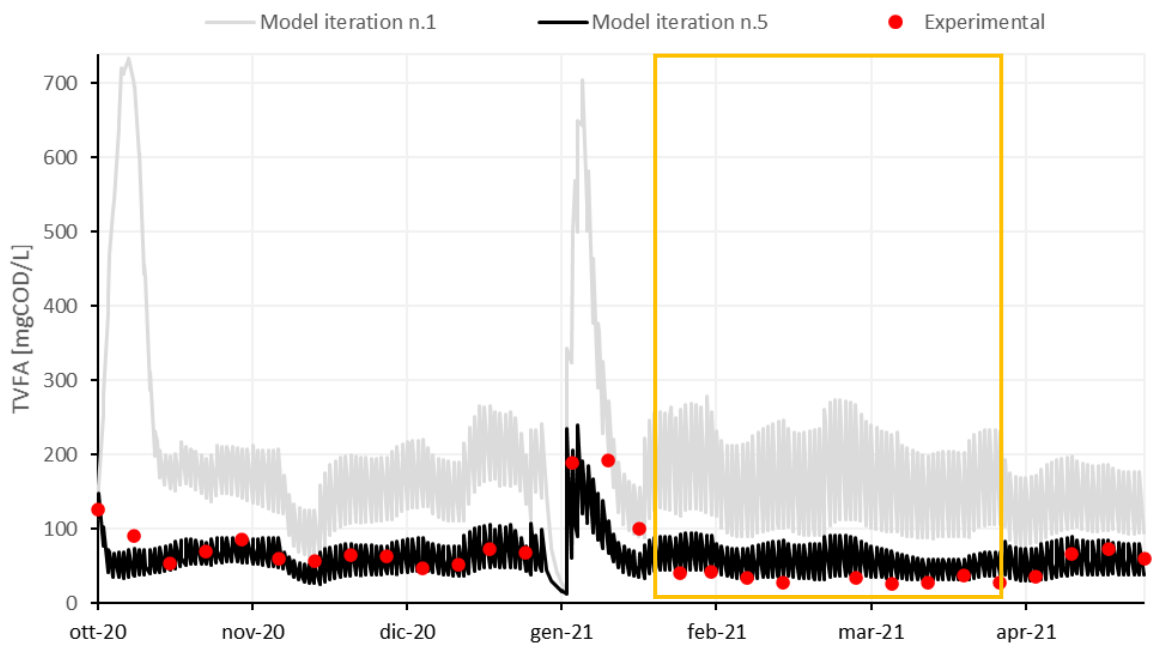


Figure 4.33 – Digestate VFA simulation.

The simulation curve of the VFAs, represented in Figure 4.33, has a noticeable improvement from the first to the fifth iteration of the calibration process: in fact, the model at the fifth iteration clearly simulates the experimental data much better compared to the first iteration. However, it is evident that in the period of co-digestion, the modelling is not very accurate.

As can be seen from Table 4.22, the TIC has a noticeable improvement: from 0.529 in the first iteration to 0.174 in the fifth iteration. The MARE index also went from 0.614 to 0.333 indicating that the calibration was very effective. The comparison between mono-digestion and co-digestion was also evaluated numerically through TIC and MARE, which are evidently lower in mono-digestion than in co-digestion, as can be read from the values shown in Table 4.22.

The simulation of the ammoniacal nitrogen, shown in the Figure 4.34, has an excellent fit with the experimental data, as it is also demonstrated by the TIC and MARE statistical indices in Table 4.22.

As already noted in the VFA simulation, there is a notable improvement between the first and fifth iteration, especially in the mono-digestion period, as numerically supported by the TIC and MARE values.

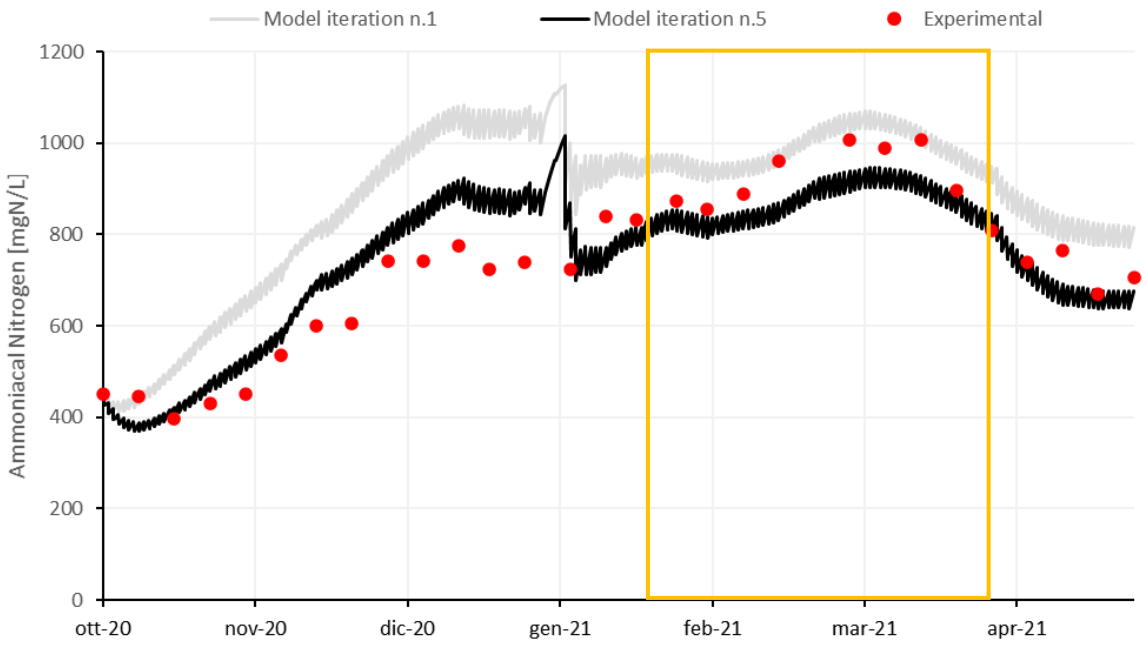


Figure 4.34 – Ammoniacal nitrogen simulation.

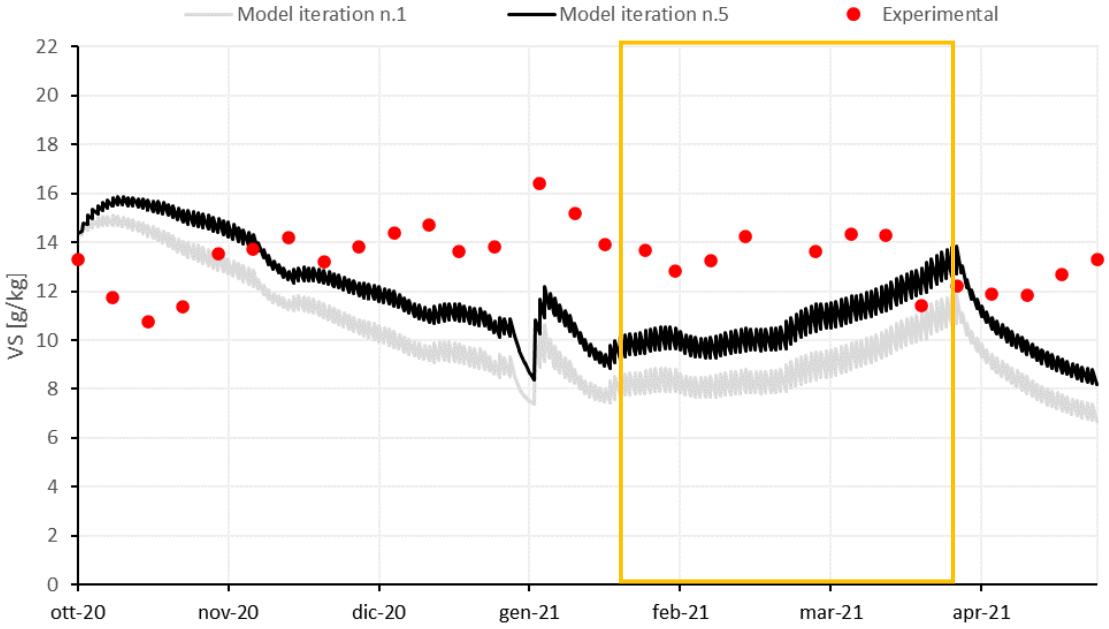


Figure 4.35 – Digestate VS simulation.

Given the excellent results obtained for the various simulated experimental parameters, the volatile solids of the outgoing digestate are those that show the greatest deviation. This is certainly due to the fact that the calculation of volatile solids is very complex as it contains several aggregate measures and COD conversion coefficients which are mere hypotheses. However, even if the VS trend is not perfectly simulated by the model, it is nevertheless

possible to estimate its order of magnitude. In addition, the TIC index of VS simulation shown in Table 4.22 is 0.128, a value much lower than 0.3 which is the maximum threshold for having a model that represents an acceptable fitting. Therefore, it is to be considered a reliable simulation.

Since the probable cause of the poor simulation quality is to be attributed to the hypothesized value of COD/VS, an analysis comparing the COD/VS ratio values estimated by the model to those actually measured is presented. The COD/VS values are calculated in two ways:

- using a COD calculated as the sum of proteins, carbohydrates, lipids and VFAs contributions;
- using the experimentally measured COD.

As can be seen from the graph in Figure 4.36, both the COD/VS data series do not fit well the curve simulated by the model: the experimental data is always lower than the model curve; while the COD calculated curve seems to have more acceptable results.

Therefore, in order to have a better modelling of the VS, it is advisable to find a better system for measuring and calculating the COD/VS ratio.

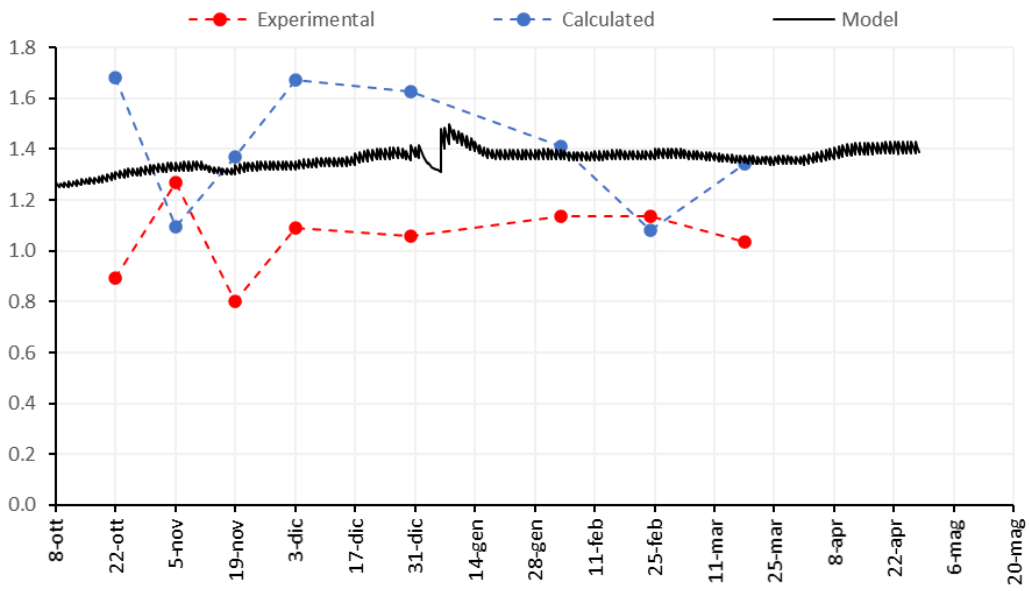


Figure 4.36 – COD/VS ratio simulation results.

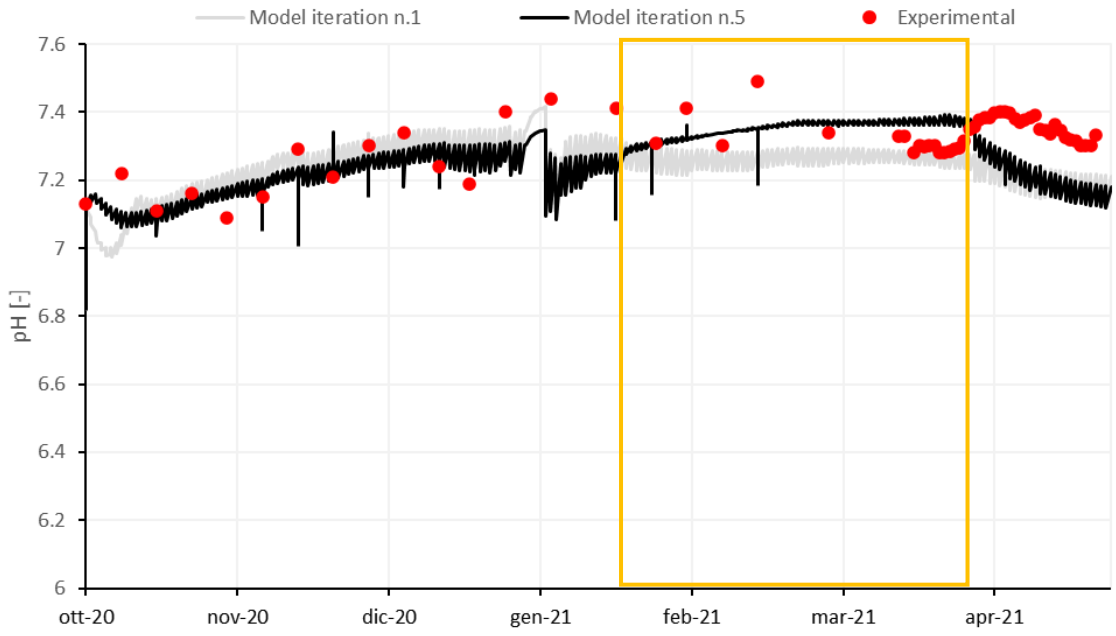


Figure 4.37 – pH simulation.

The pH simulation in Figure 4.37 fits well with the experimental data, as demonstrated also by the TIC and MARE statistical indices in Table 4.22. In the last phase of the experimentation, it was possible to use the online data collected by the pH-probe of the pilot-plant. The on-line data are in fact to be preferred since they are not affected by process sampling and manipulation. Online data seem to follow the trend of the model well.

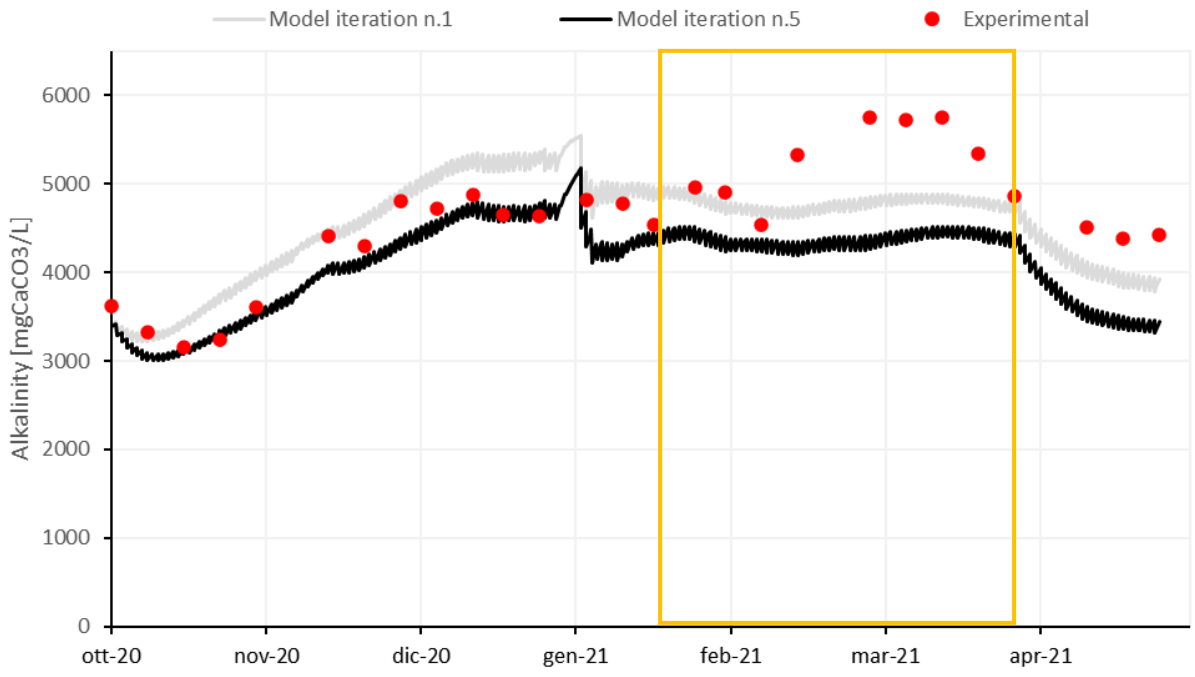


Figure 4.38 – Digestate alkalinity simulation.

As regards the simulation of alkalinity, represented in Figure 4.38, the contrast between the excellent fit in the mono-digestion phase and the poor fit in the co-digestion phase is evident.

This is probably due to a lack of alkalinity contribution associated with the yogurt dosage, which was not measured analytically. To verify this hypothesis, a fictitious simulation was performed, where the alkaline content of the yogurt was increased by the addition of ionic species which could be for example ammonium, organic acids or phosphate salts. In particular, the inorganic cations concentration ($S_{cat}$) in the yogurt characterization was fictitiously increased by 0.5 mol/L.

The fictitious simulation is represented in Figure 4.39. If the hypothesis formulated were confirmed, it is evident that the simulation would be able to predict the alkalinity very precisely.

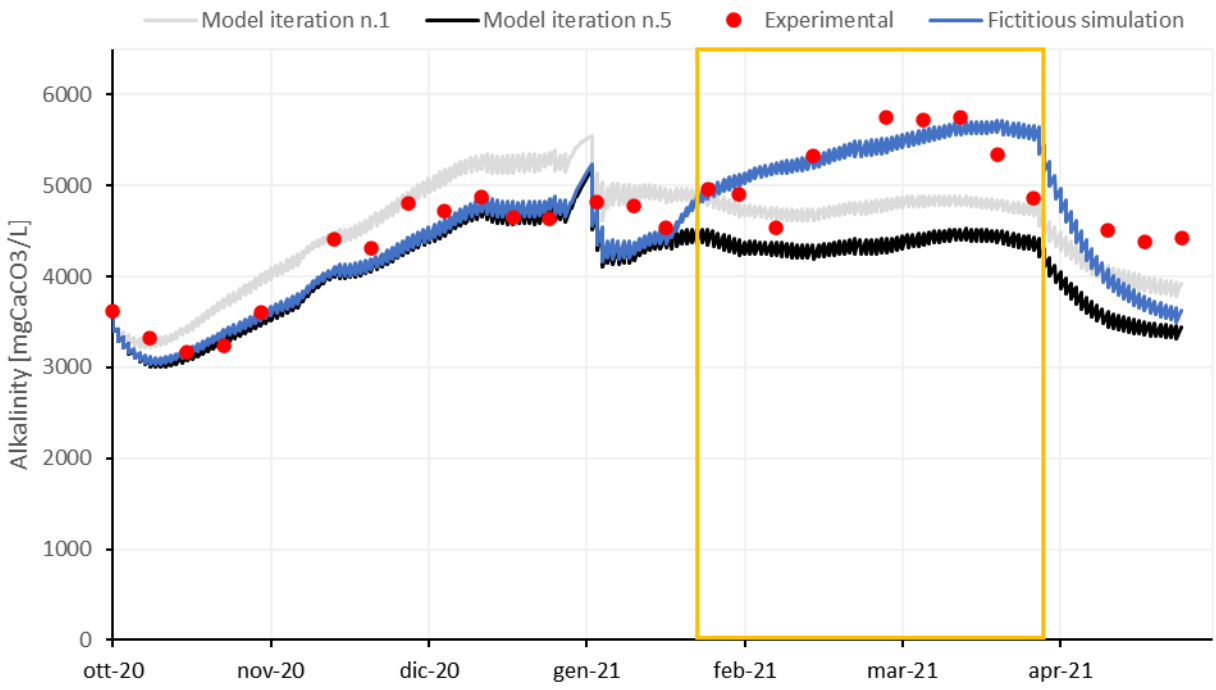


Figure 4.39 – Fictitious digestate alkalinity simulation.

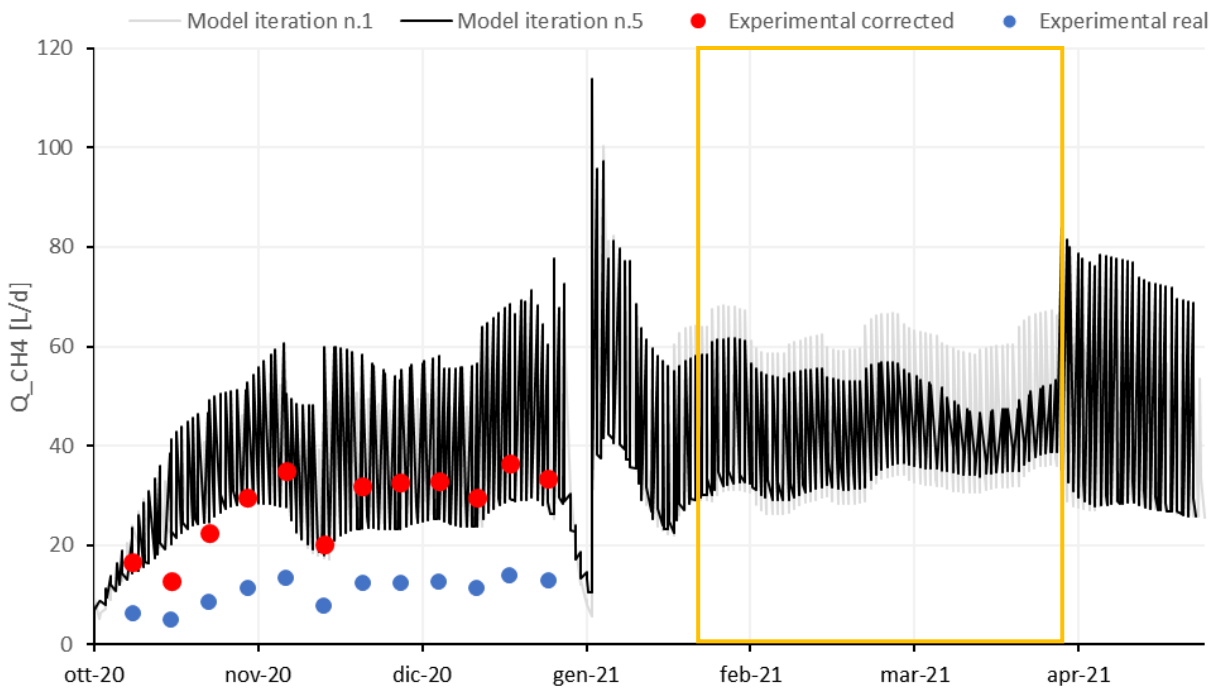


Figure 4.40 - Methane production simulation.

Regarding the simulation of gas production, as shown in Figure 4.40, the model predicts the trend of the experimental data very well, even in sudden production changes. The order of magnitude of gas production is also well simulated, albeit slightly overestimated. Consider that, as explained in chapter 4.5.6, the magnitude of the experimental data is not the one actually measured, but a derived measure based on comparison with BMP tests. However, the trend of the data is the one actually recorded by the instrument, since the manipulation of the data consists only in a rescaling. The graph also shows the original data recorded by the instrument in blue colour.

In any case, the simulation appears to have a good fit with the real data as also demonstrated by the TIC and MARE indices in Table 4.22.

Due to the operational difficulties encountered during the experimentation, reported in the plant maintenance diary in APPENDIX H, the experimental data of gas production after December are not available. However, it can be observed that the model presents a higher production of gas in the co-digestion period, as would be expected: in particular, according to the model, there would be an increase in gas production of about 22% compared to the mono-digestion period.

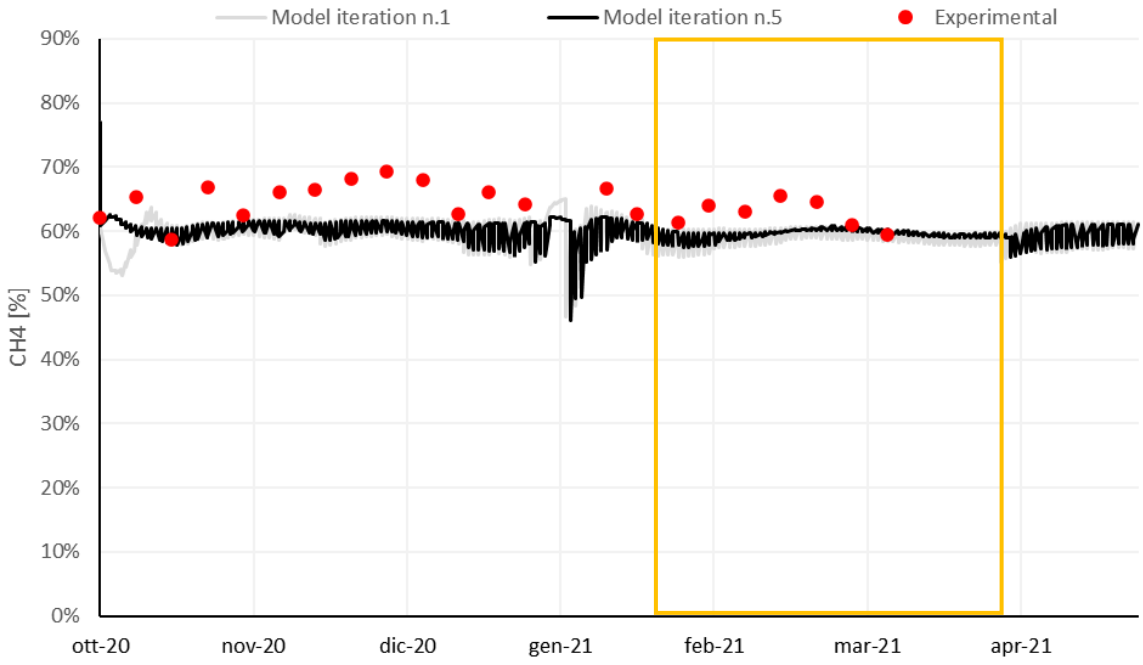


Figure 4.41 – Biogas methane content simulation.

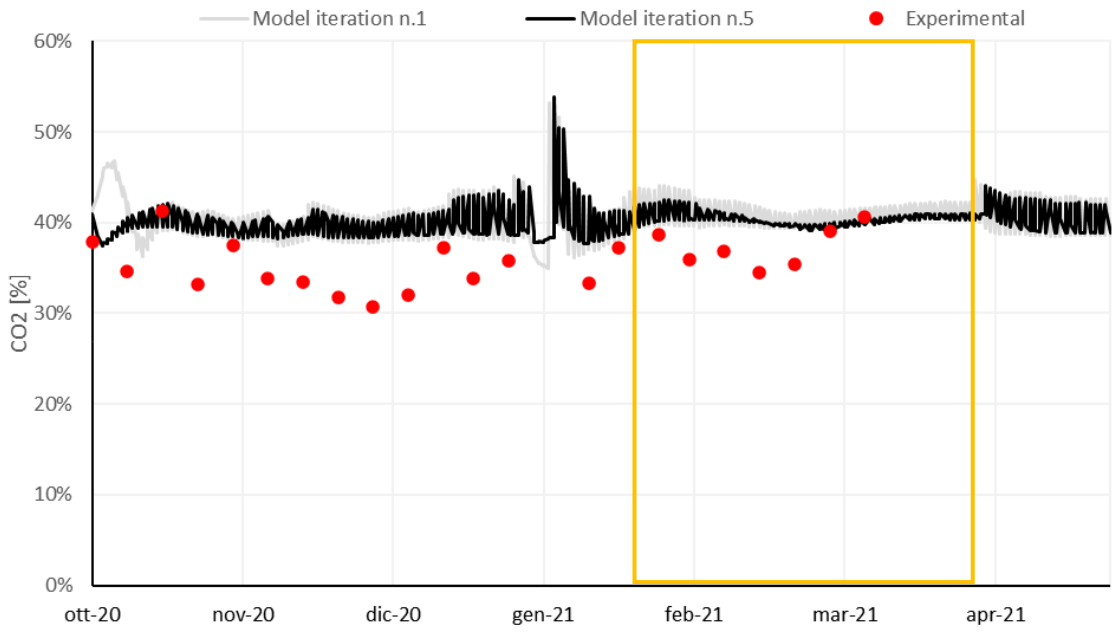


Figure 4.42 - Biogas carbon dioxide content simulation.

Regarding the composition of the biogas, in Figure 4.41 and Figure 4.42, the prediction does not seem to fit very well with the experimental points. This could be due to a measurement error of the experimental data or an inadequate gas sampling and storage method.

However, the simulation reports very low TIC and MARE values (as reported in Table 4.22), which therefore indicate that the simulation has a good fit with the experimental data.

Table 4.22 - TIC and MARE results for pilot plant simulation in the total monitoring period, in the mono-digestion period and in the co-digestion period

| | | ***1st iteration*** | | | ***5th iteration*** | | |
|---|---|---|---|---|---|---|---|
| | *Model Fitting Criteria* | *Total* | *Mono-digestion* | *Co-digestion* | *Total* | *Mono-digestion* | *Co-digestion* |
| *VFA* | TIC | 0.529 | 0.529 | 0.583 | 0.174 | 0.148 | 0.260 |
| | MARE | 0.614 | 0.536 | 0.711 | 0.333 | 0.245 | 0.428 |
| *VS* | TIC | 0.185 | 0.157 | 0.213 | 0.128 | 0.119 | 0.134 |
| | MARE | 0.453 | 0.337 | 0.516 | 0.263 | 0.221 | 0.292 |
| *Ammoniacal nitrogen* | TIC | 0.116 | 0.148 | 0.041 | 0.081 | 0.071 | 0.036 |
| | MARE | 0.221 | 0.225 | 0.070 | 0.167 | 0.119 | 0.065 |
| *pH* | TIC | 0.008 | 0.008 | 0.007 | 0.006 | 0.006 | 0.007 |
| | MARE | 0.014 | 0.013 | 0.011 | 0.010 | 0.010 | 0.012 |
| *Alk* | TIC | 0.050 | 0.040 | 0.058 | 0.075 | 0.030 | 0.093 |
| | MARE | 0.086 | 0.064 | 0.100 | 0.122 | 0.050 | 0.177 |
| $Q_{ch4}$ | TIC | 0.109 | 0.109 | N.A. | 0.085 | 0.085 | N.A. |
| | MARE | 0.297 | 0.297 | N.A. | 0.263 | 0.263 | N.A. |
| $x_{ch4}$ | TIC | 0.042 | 0.047 | 0.030 | 0.039 | 0.043 | 0.029 |
| | MARE | 0.066 | 0.078 | 0.045 | 0.060 | 0.069 | 0.044 |

## *4.9. Sensitivity Analysis*

In the current work sensitivity analysis was a useful tool to support the calibration process and to understand which laboratory analyzes were not so relevant for modeling purposes.

Both, individual and simultaneous approaches of sensitivity analysis, were tested on different model parameters. The focus was on the characterization parameters of the influent and the kinetic constants of disintegration, hydrolysis, and the half-saturation constant of acetate and propionate.

The sensitivity analyzes were performed starting from the hypothesis that the incoming influent was for 90% entering the digester already disintegrated into $X_{ch}$, $X_{pr}$, $X_{li}$, $X_i$, $S_i$; and the remaining 10% of sludge entering the digester in the aggregated form, $X_c$. The fractionation of $X_c$ consists of the following disintegration factors:

- $f_{Si}$ = 10% for disintegration of $X_c$ in $S_i$
- $f_{Xi}$ = 20% for disintegration of $X_c$ in $X_i$
- $f_{ch}$ = 20% for disintegration of $X_c$ in $X_{ch}$
- $f_{pr}$ = 20% for disintegration of $X_c$ in $X_{pr}$
- $f_{li}$ = 30% for disintegration of $X_c$ in $X_{li}$

The sensitivity analysis performed on the percentages of disintegration started from different hypotheses: the fractionation is equally divided into the five fractions (all at 20%) and the parameters $S_i$, $X_i$, $X_{pr}$, $X_{ch}$, $X_{li}$ of the influent entering the system were set to zero.

### *4.9.1. Individual Sensitivity Analysis*

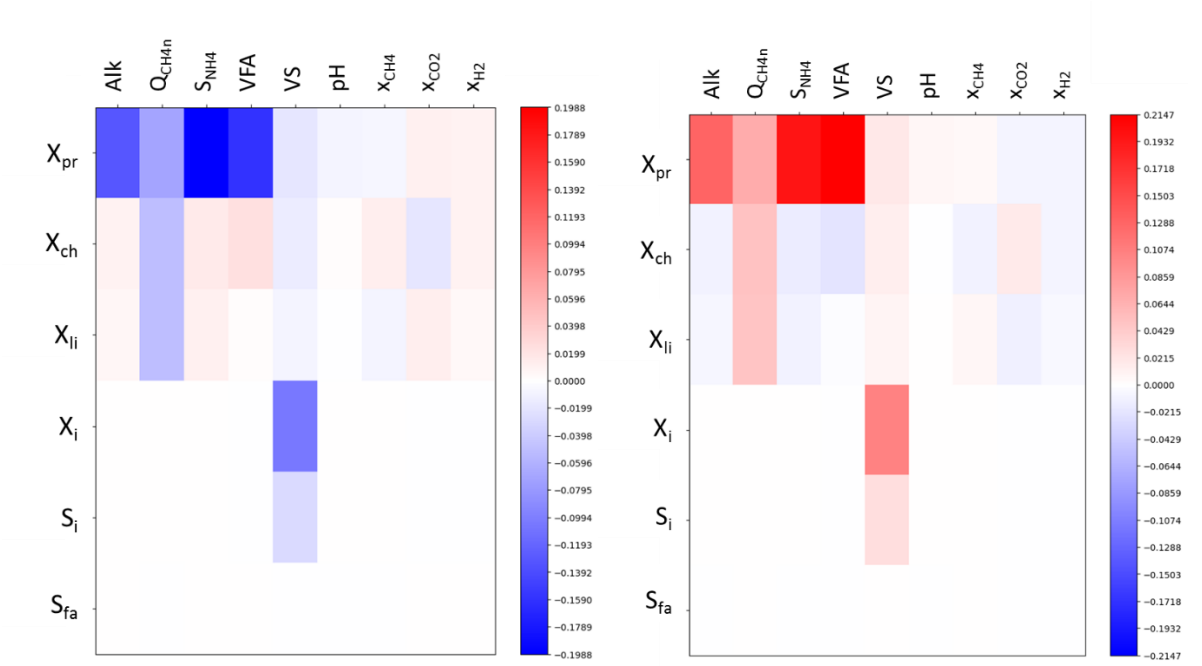


(a) (b)

Figure 4.43 - Results of individual sensitivity analysis with -20% perturbation (a) and +20% perturbation (b) of the parameters

A first sensitivity analysis was performed on parameters which were of interest for the characterization of the influent and therefore on the organization of the analytical plan. So, the parameters $X_{pr}$, $X_{ch}$, $X_{li}$, $X_i$, $S_i$ and $S_{fa}$ were selected to be perturbed by 20%. The variables on which the effect of the perturbation has been ascertained are the typical indicators of the AD process quality: alkalinity, methane production, ammoniacal nitrogen concentration, VFA, VS, pH, and the percentages of gas species $CH_4$, $CO_2$ and $H_2$ in the biogas.

In this case, OpenModelica tool itself was used and the resulting $s_{rel}$ index (index comparing the perturbed and unperturbed runs) for each couple *parameter* - *variable* is shown through a color code, scaled according to the strength of the effect of the perturbation on each variable. In general, the red color on the heat map indicates an increase in the variable while the blue color a decrease. The legend on the right side quantifies the strength of the variation of the perturbed variable.

The results are reported in descending order from top to bottom in Figure 4.43, and the most significant correlations that can be deduced from the heat map include:

- Insoluble proteins ($X_{pr}$) are the parameter that most of all influences the process variables. A 20% variation of insoluble proteins in the influent would cause an equal

change in ammonia nitrogen and VFA; an important effect on alkalinity (about 15%); a milder effect on methane production; and an almost negligible effect on VS, $x_{CO2}$ and $x_{H2}$. The pH and the percentage of methane in the biogas would not be affected at all.

- Long-chain fatty acids concentration ($S_{fa}$) is a parameter that negligibly influences the variables of the process.

Other non-negligible effects are those of the carbohydrate and lipid content on methane production. In addition, the variation in the carbohydrate content has a non-negligible adverse effect on the VFA content: if the carbohydrates increase by 20%, the VFAs decrease by 5%.

Subsequently, the effect of the variation of the disintegration factors was analyzed; in particular, the disintegration factors of proteins, carbohydrates and lipids have been doubled with respect to the base case. The variation of the percentages of each fraction was performed by making the other fractions also vary proportionally with respect to the base case, only the inert fractions were kept unchanged. A scheme of the applied variations is shown in Figure 4.44

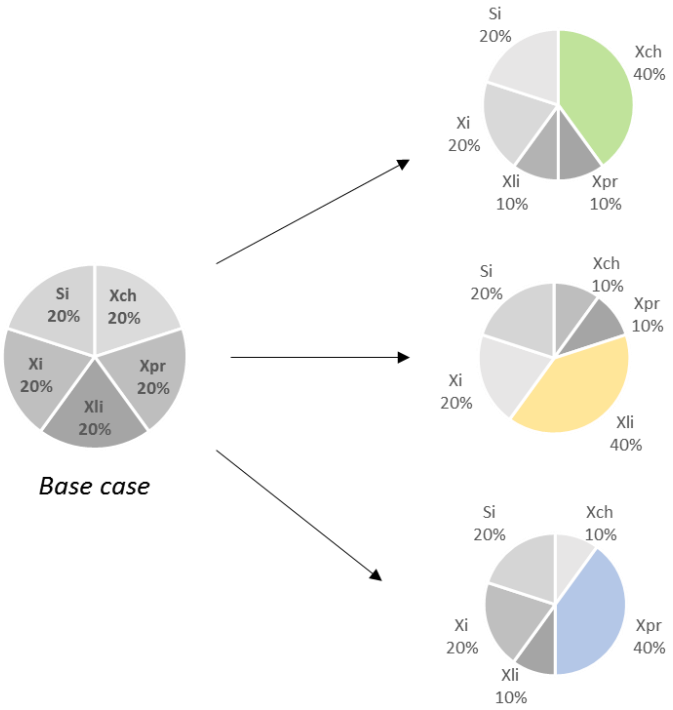


Figure 4.44 - Scheme of disintegration percentage variation for sensitivity analysis

In this case, a manual approach was used: the parameters $f_{pr}$, $f_{ch}$ and $f_{li}$ were perturbed manually, and the simulation was performed. At the end of the simulation the variables value was

compared to the value obtained with the non-perturbed simulation. The results are shown in Figure 4.45.

The most evident result concerns the ammonium concentration in the digestate, which increases as the proteins increase and decreases as the other fractions increase (as the protein fraction decreases). Alkalinity also has similar behavior, as expected. An increase in the biogas methane percentage would occur by increasing the fractionation of carbohydrates or proteins. At the same time, the methane production would be penalized by the increase in lipids and carbohydrates.

It should be considered that the effect of the fractionation of $X_c$ in the specific case of this study does not greatly influence the process as the influent used is 90% primary sludge, therefore entering the digester already disintegrated.

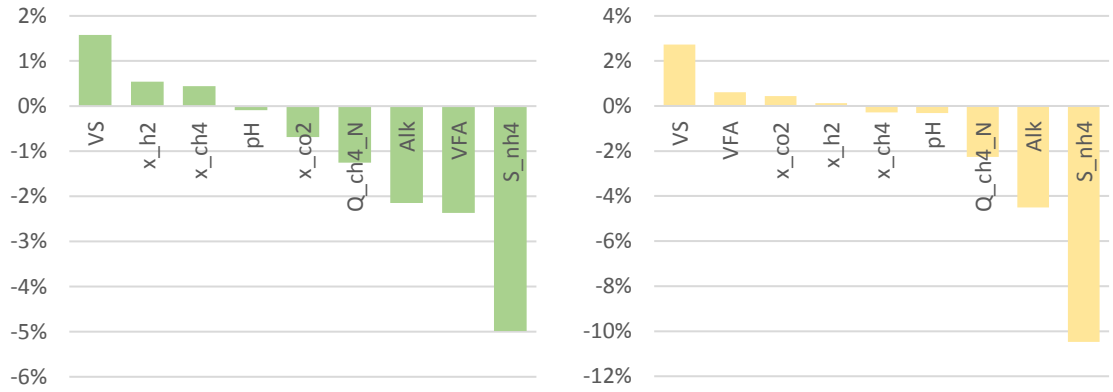


(a)




(b)

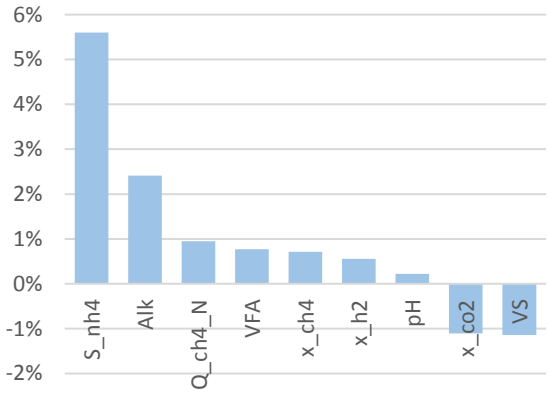


(c)

Figure 4.45 - Sensitivity analysis perturbing f_ch (a), f_li (b), f_pr (c): effect on process variables

The effect on biomass was also studied, as shown in Figure 4.46. The increase in protein fractionation would lead to an increase in all the biomasses analyzed. This is probably due to

the biomass assimilating ammonium in their growth process. The behaviors of biomass that consume amino acids, sugars and fatty acids are predictably linked to the fractionation of proteins, carbohydrates and lipids respectively.

In general, the hydrogenotrophic methanogens are never penalized, while the acetoclastic methanogens are penalized by the increase in the carbohydrate fraction.

Acetogenic bacteria, are penalized by the increase in the lipid fraction; in the case of an increase in the carbohydrate fraction, on the other hand, the bacteria that consume propionate would be favored, while those that consume butyrate and valerate would be disadvantaged.

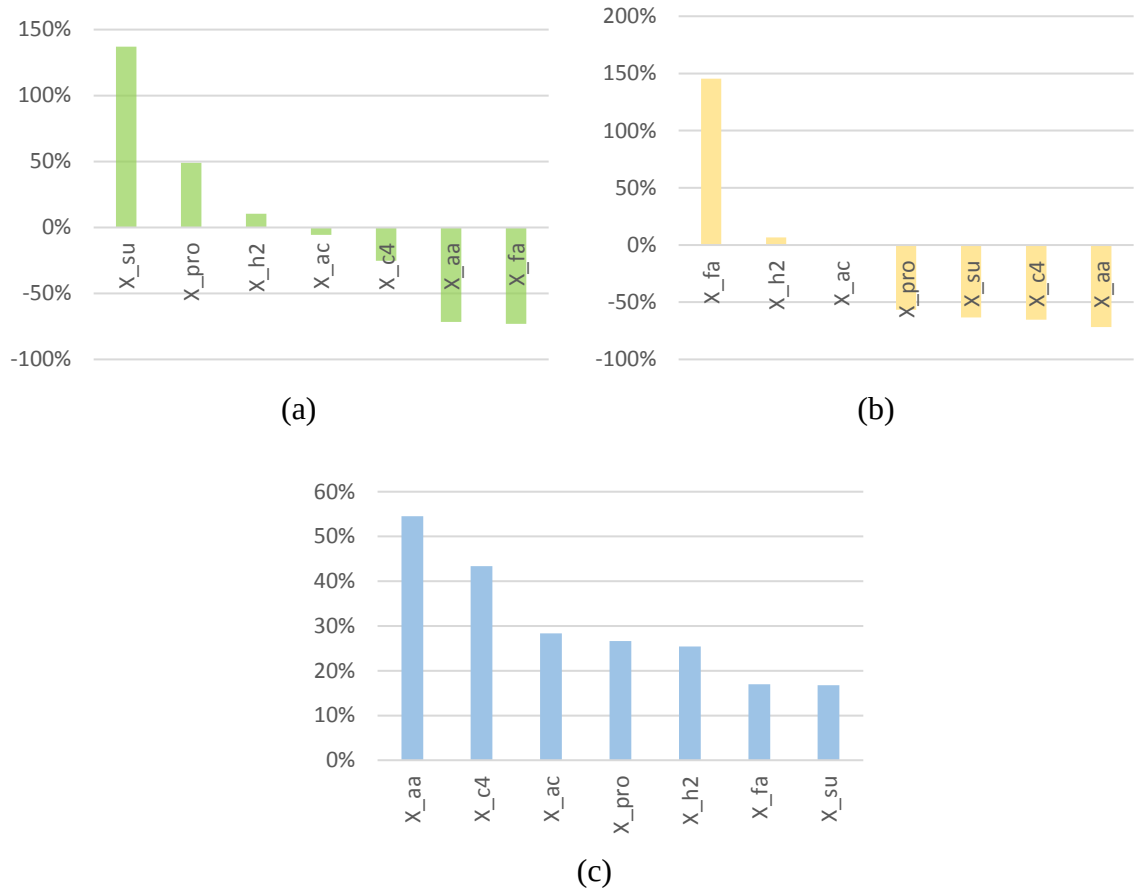


Figure 4.46 - Sensitivity analysis perturbing f_ch (a), f_li (b), f_pr (c): effect on biomass

The effect of the disintegration kinetic constant was also studied through sensitivity analysis. The results are presented in Figure 4.47 and Figure 4.48, showing that the greatest advantage in terms of biomethane production would come from increasing the disintegration constant, at the expense of an increase in digestate VS.

It should be considered that the effect of disintegration kinetics in the specific case of this study does not greatly influence the process as the influent used is 90% primary sludge, therefore entering the digester already disintegrated.

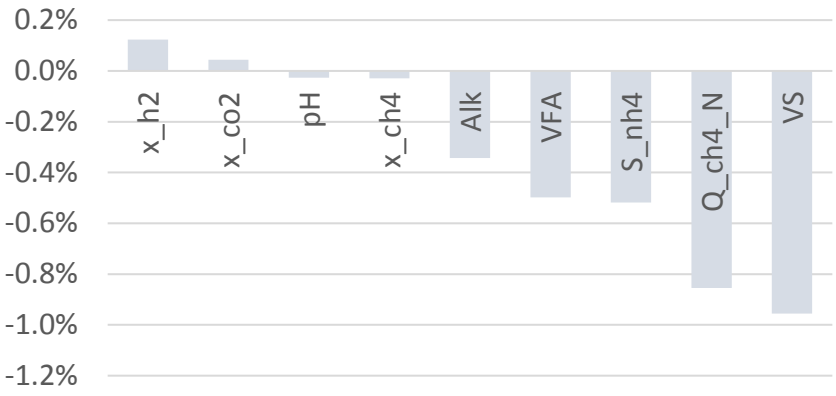


Figure 4.47 – Sensitivity analysis perturbing k_dis by -50%

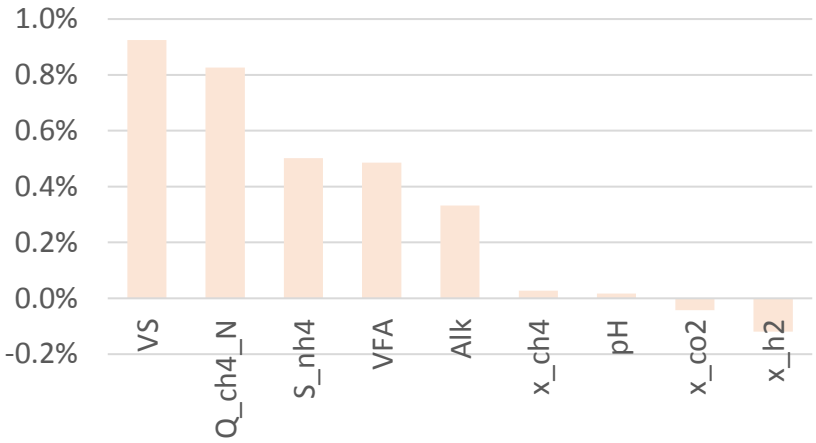


Figure 4.48 - Sensitivity analysis perturbing k_dis by +500%

Another sensitivity analysis was performed on the kinetic constants of proteins, lipids and carbohydrates hydrolysis ($k_{H,pr}$, $k_{H,li}$, $k_{H,ch}$). All the hydrolytic constants were varied in a range of 0.1-10 [1/d], starting from the initial condition of 10 [1/d].

The results presented in Figure 4.49 show that methane production would be improved for faster hydrolysis of all fractions but especially of proteins.

The biogas methane percentage would increase as the hydrolysis of proteins and especially carbohydrates increase, while an increase in the hydrolyzation of lipids would lead to its decrease.

Protein hydrolysis has a great effect on ammonia concentration, alkalinity and VFAs as expected.

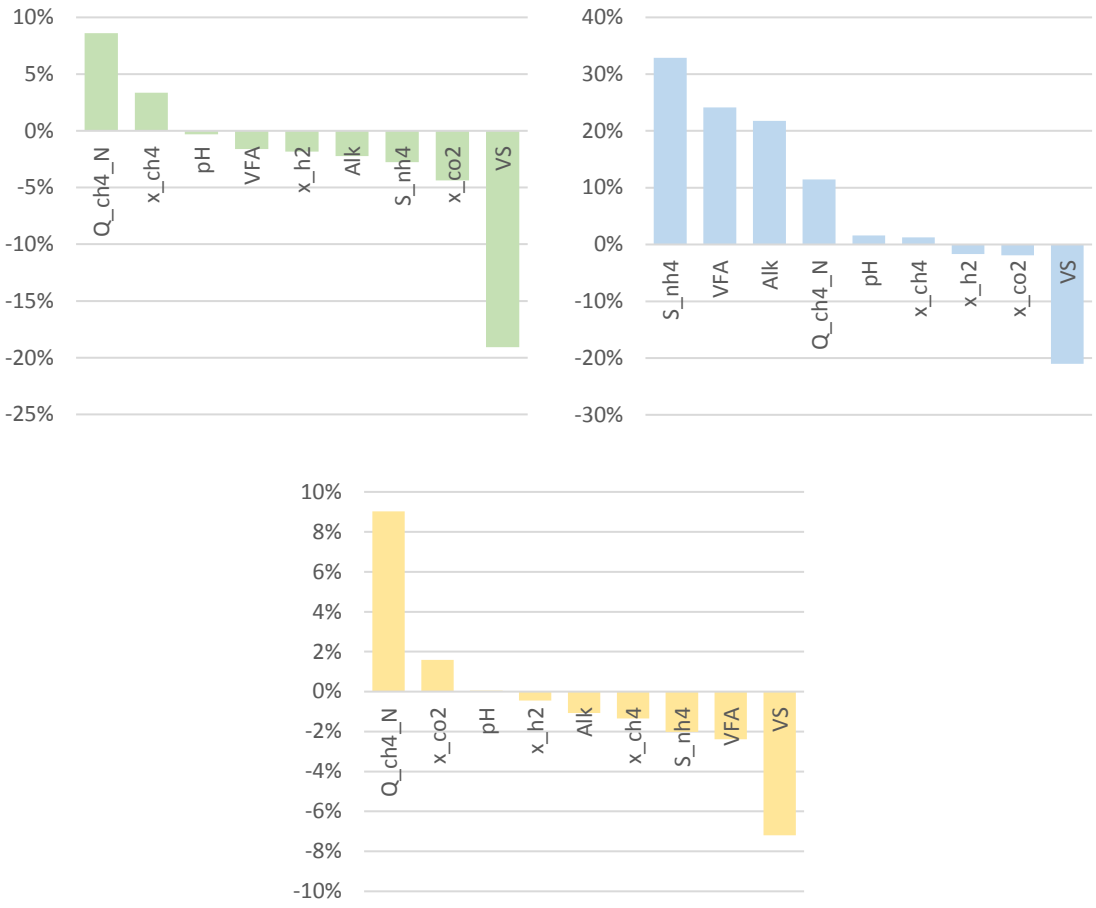


Figure 4.49 - Sensitivity analysis perturbing k_hyd_ch (a), k_hyd_li (b), k_hyd_pr (c)

### *4.9.2. Simultaneous Sensitivity Analysis*

The simultaneous sensitivity analysis performed in this work was used in the model calibration process, particularly in understanding whether the half saturation constants of acetate and propionate were over or underestimated. The analysis was based on the shape of the simulated VFA curve after the winter period. In fact, during the frost period (December 30-January 2) the simulated curve had undergone a sharp change, just like the real data. But after returning to a stable state, the simulated curve no longer reported the same precision in predicting real data.

The goal was to understand how the parameters $K_{s,ac}$ and $K_{s,pro}$ affected the shape of the VFA curve and how to improve the simulation.

The output of OpenModelica is presented in Figure 4.50 where the dynamic trend of the parameter is represented. In particular, the comparison of the base case with the curves that would be obtained by perturbing the parameters simultaneously is shown. Thus, obtaining a

number of curves equal to $3^{NP}$ (where NP is the number of perturbed parameters), because each parameter is perturbed by [-$\Delta p_i$ %, + 0%, + $\Delta p_i$ %]. A perturbation of $\Delta p_i$ = 30% to both $K_{s,ac}$ and $K_{s,pro}$ was applied. The simultaneous sensitivity analysis was very useful in identifying $K_{s,pro}$ as a determining parameter. In particular, it turned out that by lowering the $K_{s,pro}$ by 30%, the model can simulate more reliably.

Analyzing the data, it was discovered that, in that period, there was an anomalous accumulation of propionate (Figure 4.11) and consequently it is understandable that the decrease in the propionate half saturation constant led to a significant improvement of the simulation. The iterative passage from iteration 4 to iteration 5 was carried out thanks to this sensitivity analysis leading to the reduction of $K_{s,pro}$ from 0.3 to 0.2 $kg_{COD,S}/m^3$.

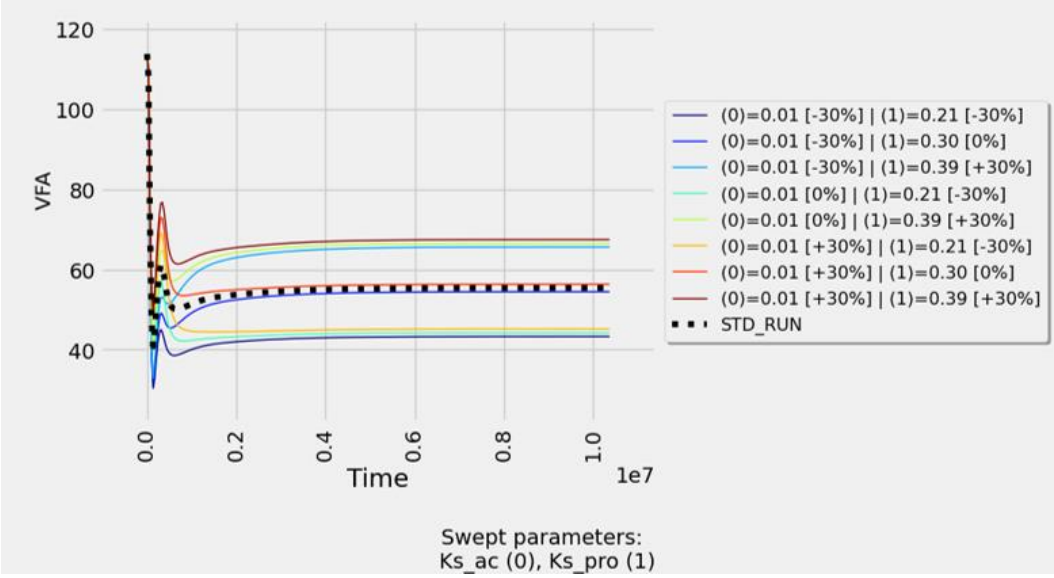


Figure 4.50 - Simultaneous sensitivity analysis results for K_s_ac and K_s_pro

# Chapter 5: CONCLUSIONS

The experimentation was carried out first on mono-digestion of sludge and then on co-digestion of sludge and yogurt. The main goal of this work was to develop and calibrate a co-digestion model based on ADM1 through the OpenModelica programming platform. The calibration was carried out through an iterative validation process using the analytical data from the pilot plant and the results of the BMP tests and the biomass activity tests carried out. The proposed model calibration iterative process was found to be effective opening up to the possibility of various applications and future developments.

## *5.1. Main achievements*

The pilot plant responded very well to all transient phase (e.g. start-up and transition from mono to co-digestion). Furthermore, various problems were encountered during the experimentation as winter frost, clogging of the gas line, interruption of the operation of the pump, etc. Despite this, the pilot plant showed a proper resilience to perturbations (good buffering capacity: the effluent VFAs increased slightly, but pH and alkalinity did not vary significantly).

The effects of co-digestion on the pilot plant were positive. VS reduction efficiency increased from 43.7% in mono-digestion to 54.4% in co-digestion. The effluent VFAs went from an average value of 67 $mg_{COD}$/L in mono-digestion to 35 $mg_{COD}$/L in co-digestion.

The co-digestion BMP tests showed an increase in methane production justified by possible synergistic effects between yogurt and sludge.

The proposed model calibration iterative process was found to be effective: the model satisfactorily adapts to the experimental data collected, as confirmed by the model fitting criteria. Furthermore, sensitivity analysis was a useful tool to support the calibration.

The success of the simulation is also linked to an adequate method of characterization of the substrates carried out starting from the analytical plan. Therefore, not only the choice of the analyzes carried out and the methods of analysis proved to be valid, but also the processing of such data to associate experimental data to the ADM1 state variables.

Through the simulation, it was also discovered that the hydrolytic kinetics during co-digestion does not depend only on the biomass but also on the characteristics of the substrate. Indeed, yogurt has faster protein hydrolysis constant than sludge.

The model offers potential application in the study of co-digestion scenarios.

## *5.2. Further developments*

The following list reports both proposals for possible improvements and future applications:

- Having observed that the hydrolytic kinetics during co-digestion also depend on the intrinsic characteristics of the substrate, the simulation could be improved by separating the hydrolysis process for the two substrates in the model with different values for the constant hydrolysis kinetics.

- To improve the characterization of substrates and specifically the portioning between what enters as particulate and as soluble, the analytical plan of the BMP tests could be reviewed. In the experimentation, the BMP was performed on the sludge and its particulate component. A more precise characterization could be obtained by carrying out BMP tests on the soluble component too.

- It is possible to reduce the monitoring plan by carrying out less analysis. Specifically, through the sensitivity analysis, it was observed that the soluble lipid concentration in the sludge is a parameter that does not have a particular influence on the process variables. Even numerically the soluble lipid concentration is negligible compared to the solid lipid concentration. Furthermore, in order to reduce the number of analyses to be carried out on the influent, it is possible to avoid the measurement of proteins and carbohydrates of the yogurt, and use the values displayed on the label instead.

- To improve the simulation as a whole, activity tests with propionate and butyrate could be carried out to obtain the following kinetic constants through the calibration process, i.e.: $k_{m,pro}$, $k_{m,bu}$, $K_{s,pro}$ and $K_{s,bu}$. A more accurate estimate of VFAs degradation kinetics could have a positive impact on the simulation of glucose and BSA activity tests.

- To improve the glucose activity test simulation, tests with very low glucose concentration as COD could be carried out. In this way, inhibition phenomena due to the initial lowering of the pH should be avoided. Therefore, in the absence of inhibition phenomena, it should be possible to estimate the kinetic parameters of the degradation of sugars ($k_{m,su}$, $K_{s,su}$) more correctly.

Once these parameters are known, the test can be repeated at high glucose concentrations as COD so as to be able to estimate the parameters of the inhibition process.

- A further modification to the experimental plan aimed at improving the simulation of the BMP tests is the degassing phase. The sampled digestate could be stored at room temperature and only degassed one week before the test. In this way a more uniform inoculum could be obtained for all tests.

- The model used in this work does not foresee the VFA inhibition kinetics on methanogenic biomass. Consequently, a future development could be to integrate this process to simulate the failure of the pilot-plant following yogurt over-loading.

- Alkalinity simulations highlighted a lack of alkalinity contribution associated with the yogurt dosage, which however was not measured analytically. Therefore, it is possible to further improve the yogurt analytical plan by measuring other ionic components which could be ammonium, organic acids or phosphate salts

- Testing higher yogurt loads (i.e. to achieve an increase of + 40% in terms of SV fed compared to mono-digestion) could provide a further validation of the model.

- During the experimentation, unreliable data were obtained on biogas composition. To overcome this issue, more suitable gas sampling bags have to be used and analyzes have to be carried out immediately after sampling.

- It is possible to further improve the predictive capabilities of the model by implementing an automated iterative procedure for parametric identification.

# BIBLIOGRAPHY

Angelidaki, I., Alves, M., Bolzonella, D., Borzacconi, L., Campos, J. L., Guwy, A. J., Kalyuzhnyi, S., Jenicek, P., & Van Lier, J. B. (2009). Defining the biomethane potential (BMP) of solid organic wastes and energy crops: A proposed protocol for batch assays. *Water Science and Technology*, *59*(5), 927–934. https://doi.org/10.2166/wst.2009.040

Antonopoulou, G., Gavala, H. N., Skiadas, I. V., & Lyberatos, G. (2012). ADM1-based modeling of methane production from acidified sweet sorghum extract in a two stage process. *Bioresource Technology*, *106*(1), 10–19. https://doi.org/10.1016/j.biortech.2011.11.088

Anukam, A., Mohammadi, A., Naqvi, M., & Granström, K. (2019). A review of the chemistry of anaerobic digestion: Methods of accelerating and optimizing process efficiency. *Processes*, *7*(8), 1–19. https://doi.org/10.3390/PR7080504

Astals, S., Musenze, R. S., Bai, X., Tannock, S., Tait, S., Pratt, S., & Jensen, P. D. (2015). Anaerobic co-digestion of pig manure and algae: Impact of intracellular algal products recovery on co-digestion performance. *Bioresource Technology*, *181*, 97–104. https://doi.org/10.1016/j.biortech.2015.01.039

Batstone, D. J., Keller, J., Angelidaki, I., Kalyuzhnyi, S. V., Pavlostathis, S. G., Rozzi, A., Sanders, W. T., Siegrist, H., & Vavilin, V. A. (2002). The IWA Anaerobic Digestion Model No 1 (ADM1). *Water Science and Technology : A Journal of the International Association on Water Pollution Research*, *45*(10), 65–73. https://doi.org/10.2166/wst.2002.0292

Bolzonella, D. (Department of science and technology, University of Verona, Strada Le Grazie 15, 37134 Verona, I., Battistoni, P. (Institute of Hydraulics and Transportation Infrastructures, Politechnical University of Marche - via Breccie Bianche, 60131 Ancona, I., Susini, C. (Sea Acque S.p.a. di Viareggio, Via degli Aceri 20, 55049 Viareggio, I., & Cecchi, F. (Department of science and technology, University of Verona, Strada Le Grazie 15, 37134 Verona, I. (2006). bolzonella 2006.pdf. *Water Science & Technology Vol 53 No 8 Pp 203-211 IWA Publishing 2006*.

Bonomo, L. (2014). *Trattamenti delle acque reflue*. McGraw-Hill Companies, S.r.l.

Brulé, M., Oechsner, H., & Jungbluth, T. (2014). Exponential model describing methane production kinetics in batch anaerobic digestion: A tool for evaluation of biochemical methane potential assays. *Bioprocess and Biosystems Engineering*, *37*(9), 1759–1770. https://doi.org/10.1007/s00449-014-1150-4

Cabbai, V., De Bortoli, N., & Goi, D. (2016). Pilot plant experience on anaerobic codigestion of source selected OFMSW and sewage sludge. *Waste Management*, *49*, 47–54. https://doi.org/10.1016/j.wasman.2015.12.014

Catenacci, A., Azzellino, A., & Malpei, F. (2019). Development of statistical predictive models for estimating the methane yield of Italian municipal sludges from chemical composition: A preliminary study. *Water Science and Technology*, *79*(3), 435–447. https://doi.org/10.2166/wst.2019.063

Cecchi, F., Battistoni, P., Pavan, P., Bolzonella, D., & Innocenti, L. (2005). *APAT - Digestione anaerobica della frazione organica dei rifiuti solidi*.

Chen, H., Yi, H., Li, H., Guo, X., & Xiao, B. (2020). Effects of thermal and thermal-alkaline pretreatments on continuous anaerobic sludge digestion: Performance, energy balance and, enhancement mechanism. *Renewable Energy*, *147*, 2409–2416. https://doi.org/10.1016/j.renene.2019.10.051

Cho, Y. T., Young, J. C., Jordan, J. A., & Moon, H. M. (2005). Factors affecting measurement of specific methanogenic activity. *Water Science and Technology*, *52*(1–

2), 435–440. https://doi.org/10.2166/wst.2005.0550
Danós, A., Pop, A., Braun, W., Scolnik, H., Fritzson, P., & Castro, R. (2017). Towards an OpenModelica-based sensitivity analysis platform including optimization-driven strategies. *ACM International Conference Proceeding Series*, *December*, 87–93. https://doi.org/10.1145/3158191.3158206
Deepanraj, B., Sivasubramanian, V., & Jayaraj, S. (2014). Biogas generation through anaerobic digestion process-an overview. *Research Journal of Chemistry and Environment*, *18*(5), 80–94.
Derbal, K., Bencheikh-lehocine, M., Cecchi, F., Meniai, A. H., & Pavan, P. (2009). Application of the IWA ADM1 model to simulate anaerobic co-digestion of organic waste with waste activated sludge in mesophilic condition. *Bioresource Technology*, *100*(4), 1539–1543. https://doi.org/10.1016/j.biortech.2008.07.064
Dewil, R., Appels, L., Baeyens, J., & Degre, J. (2008). *Principles and potential of the anaerobic digestion of waste-activated sludge*. *34*, 755–781. https://doi.org/10.1016/j.pecs.2008.06.002
Esposito, G., Frunzo, L., Panico, A., & Pirozzi, F. (2011). Modelling the effect of the OLR and OFMSW particle size on the performances of an anaerobic co-digestion reactor. *Process Biochemistry*, *46*(2), 557–565. https://doi.org/10.1016/j.procbio.2010.10.010
Filer, J., Ding, H. H., & Chang, S. (2019). for Anaerobic Digestion Research. *Water*, *11*(921). https://doi.org/10.3390/w11050921
Holliger, C., Alves, M., Andrade, D., Angelidaki, I., Astals, S., Baier, U., Bougrier, C., Buffière, P., Carballa, M., De Wilde, V., Ebertseder, F., Fernández, B., Ficara, E., Fotidis, I., Frigon, J. C., De Laclos, H. F., Ghasimi, D. S. M., Hack, G., Hartel, M., … Wierinck, I. (2016). Towards a standardization of biomethane potential tests. *Water Science and Technology*, *74*(11), 2515–2522. https://doi.org/10.2166/wst.2016.336
Holliger, C., de Laclos, H. F., & Hack, G. (2017). Methane production of full-scale anaerobic digestion plants calculated from substrate's biomethane potentials compares well with the one measured on-site. *Frontiers in Energy Research*, *5*(JUN), 1–9. https://doi.org/10.3389/fenrg.2017.00012
Hussain, A., & Dubey, S. K. (2017). Specific methanogenic activity test for anaerobic degradation of influents. *Applied Water Science*, *7*(2), 535–542. https://doi.org/10.1007/s13201-015-0305-z
Kleerebezem, R., & van Loosdrecht, M. C. M. (2006). Critical analysis of some concepts proposed in ADM1. *Water Science and Technology*, *54*(4), 51–57. https://doi.org/10.2166/wst.2006.525
Koch, K., Hafner, S. D., Weinrich, S., Astals, S., & Holliger, C. (2020). Power and Limitations of Biochemical Methane Potential (BMP) Tests. *Frontiers in Energy Research*, *8*(April), 1–4. https://doi.org/10.3389/fenrg.2020.00063
Lübken, M., Guebitz, G. M., Bauer, A., Bochmann, G., Gronauer, A., & Weiss, S. (2015). Biogas Science and Technology. In *Biogas Science and Technology* (Issue September). https://doi.org/10.1007/978-3-319-21993-6
Mairet, F., Bernard, O., Ras, M., Lardon, L., & Steyer, J. P. (2011). Modeling anaerobic digestion of microalgae using ADM1. *Bioresource Technology*, *102*(13), 6823–6829. https://doi.org/10.1016/j.biortech.2011.04.015
McCarty, P. L., & Smith, D. P. (1986). Anaerobic wastewater treatment. In *Environmental Science and Technology* (Vol. 20, Issue 12). https://doi.org/10.1021/es00154a002
Meegoda, J. N., Li, B., Patel, K., & Wang, L. B. (2018). A review of the processes, parameters, and optimization of anaerobic digestion. *International Journal of Environmental Research and Public Health*, *15*(10). https://doi.org/10.3390/ijerph15102224

Metcalf & Eddy I AECOM. (2014). *Wastewater Engineering: Treatment and Resource Recovery, Fifth Edition* (McGraw-Hill Education (ed.); 5th ed.). McGraw-Hill Education.

Montecchio, D., Astals, S., Di Castro, V., Gallipoli, A., Gianico, A., Pagliaccia, P., Piemonte, V., Rossetti, S., Tonanzi, B., & Braguglia, C. M. (2019). Anaerobic co-digestion of food waste and waste activated sludge: ADM1 modelling and microbial analysis to gain insights into the two substrates' synergistic effects. *Waste Management*, *97*, 27–37. https://doi.org/10.1016/j.wasman.2019.07.036

organischer Stoffe Substratcharakterisierung, V. (2016). *VEREIN DEUTSCHER INGENIEURE Characterisation of the substrate, sampling, collection of material data, fermentation tests VDI 4630 VDI-RICHTLINIEN*. *November*. www.vdi.de/richtlinien

Poggio, D., Walker, M., Nimmo, W., Ma, L., & Pourkashanian, M. (2016). Modelling the anaerobic digestion of solid organic waste - Substrate characterisation method for ADM1 using a combined biochemical and kinetic parameter estimation approach. *Waste Management*, *53*, 40–54. https://doi.org/10.1016/j.wasman.2016.04.024

Rosen, C., & Jeppsson, U. (2006). Benchmark 2 ADM1. *Technical Report*, 1–37.

Rozzi, A., & Remigi, E. (2004). Methods of assessing microbial activity and inhibition under anaerobic conditions: A literature review. *Reviews in Environmental Science and Biotechnology*, *3*(2), 93–115. https://doi.org/10.1007/s11157-004-5762-z

Serna-García, R., Zamorano-López, N., Seco, A., & Bouzas, A. (2020). Co-digestion of harvested microalgae and primary sludge in a mesophilic anaerobic membrane bioreactor (AnMBR): Methane potential and microbial diversity. *Bioresource Technology*, *298*(November 2019), 122521. https://doi.org/10.1016/j.biortech.2019.122521

Sibiya, N. T., Tesfagiorgis, H. B., & Muzenda, E. (2015). *Influence of nutrients addition for enhanced biogas production from energy crops: A Review*. https://doi.org/10.15242/iie.e1115038

Siddique, M. N. I., & Wahid, Z. A. (2018). Achievements and perspectives of anaerobic co-digestion: A review. *Journal of Cleaner Production*, *194*(1), 359–371. https://doi.org/10.1016/j.jclepro.2018.05.155

Solon, K., Flores-Alsina, X., Gernaey, K. V., & Jeppsson, U. (2015). Effects of influent fractionation, kinetics, stoichiometry and mass transfer on CH4, H2and CO2 production for (plant-wide) modeling of anaerobic digesters. *Water Science and Technology*, *71*(6), 870–877. https://doi.org/10.2166/wst.2015.029

Sørensen, A. H., & Ahring, B. K. (1993). Measurements of the specific methanogenic activity of anaerobic digestor biomass. *Applied Microbiology and Biotechnology*, *40*(2–3), 427–431. https://doi.org/10.1007/BF00170405

Soto, M., Mendez, R., & Lema, J. M. (1993). Soto Et Al.Pdf. *Dept de Enxeneria Quimica, Universidade de Santiago de Compostela*.

Wang, B., Strömberg, S., Li, C., Nges, I. A., Nistor, M., Deng, L., & Liu, J. (2015). Effects of substrate concentration on methane potential and degradation kinetics in batch anaerobic digestion. In *Bioresource Technology* (Vol. 194, pp. 240–246). https://doi.org/10.1016/j.biortech.2015.07.034

Ware, A., & Power, N. (2017). Modelling methane production kinetics of complex poultry slaughterhouse wastes using sigmoidal growth functions. *Renewable Energy*, *104*, 50–59. https://doi.org/10.1016/j.renene.2016.11.045

Xie, S., Wickham, R., & Nghiem, L. D. (2017). Synergistic effect from anaerobic co-digestion of sewage sludge and organic wastes. *International Biodeterioration and Biodegradation*, *116*, 191–197. https://doi.org/10.1016/j.ibiod.2016.10.037

Xie, T., Xie, S., Sivakumar, M., & Nghiem, L. D. (2017). Relationship between the

synergistic/antagonistic effect of anaerobic co-digestion and organic loading. *International Biodeterioration and Biodegradation*, *124*, 155–161. https://doi.org/10.1016/j.ibiod.2017.03.025

Zhou, P., Meshref, M. N. A., & Dhar, B. R. (2021). Optimization of thermal hydrolysis process for enhancing anaerobic digestion in a wastewater treatment plant with existing primary sludge fermentation. *Bioresource Technology*, *321*(November 2020), 124498. https://doi.org/10.1016/j.biortech.2020.124498

# APPENDIX A

All the biochemical rate coefficients and the kinetic rate equations for soluble and particulate components of the ADM1 model are shown in the Petersen matrix (Table A.2 and A.3).

Table A.1 summarizes the nomenclatures and units used in the ADM1 and in the current work.

Table A.1 - Nomenclature and units used

| | | |
|---|---|---|
| $C_i$ | carbon content of component *i* | kmoleC·kgCOD$^{-1}$ |
| $i$ | component index | |
| $I$ | inhibition function | |
| $j$ | process index | |
| $k_{A/B,i}$ | acid-base rate constant for component *i* | M$^{-1}$·d$^{-1}$ |
| $k_{dec}$ | first order decay rate for biomass death | d$^{-1}$ |
| $k_La$ | gas–liquid transfer coefficient | d$^{-1}$ |
| $k_m$ | specific Monod maximum uptake rate | kgCOD·m$^{-3}$_S·kgCOD·m$^{-3}$_X·d$^{-1}$ |
| $K_a$ | acid-base equilibrium constant | M (kmole·m$^{-3}$) |
| $K_H$ | Henry's law coefficient | M.bar$^{-1}$ |
| $K_I$ | inhibition constant | nominally kgCOD·m$^{-3}$ |
| $K_S$ | Monod half saturation constant | kgCOD·m$^{-3}$ |
| $N_i$ | nitrogen content of component *I* | kmoleN·kg COD$^{-1}$ |
| $p_{gas}$ | pressure of gas | bar |
| pH | $-\log_{10}[S_{H+}]$ | |
| $pK_a$ | $-\log_{10}[K_a]$ | |
| $q$ | flow | m$^3$ |
| $S_i$ | soluble component *i* (dynamic or algebraic variable) | nominally kgCOD·m$^{-3}$ |
| $S_I$ | inhibitory component | nominally kgCOD·m$^{-3}$ |
| $t$ | time | d |
| $T$ | temperature | K |
| $V$ | volume | m$^3$ |
| $X_i$ | particulate component *i* | kgCOD·m$^{-3}$ |
| $Y_{substrate}$ | yield of biomass on substrate | kgCOD_X·kgCOD_S |
| $v_{i,j}$ | rate coefficients for component *i* on process *j* | nominally kgCOD·m$^{-3}$ |
| $f_{product,substrate}$ | yield (catabolism only) of product on substrate | kgCOD·kgCOD$^{-1}$ |
| $\rho_i$ | rate for process *j* | kgCOD.m$^{-3}$ |

The inhibition functions in the Petersen matrix are as follows:

$$I_{pH} = \begin{cases} exp\left(-3\left(\frac{pH - pH_{UL}}{pH_{UL} - pH_{LL}}\right)^2\right) \; if \; pH < pH_{UL} \\ 1 \; otherwise \end{cases}$$

$$I_{IN,lim} = \frac{1}{1 + {K_{S,IN}}/{S_{IN}}}$$

$$I_{h2} = \frac{1}{1 + {S_{h2}}/{K_I}}$$

$$I_{NH3,Xac} = \frac{1}{1 + {S_{nh3}}/{K_{I,nh3}}}$$

Table A.2 - Biochemical rate coefficients ($\nu_{i,j}$) and the kinetic rate equations ($\rho_j$) for soluble components (i = 1-12)

| | Component → *i* | 1 | 2 | 3 | 4 | 5 | 6 | 7 | 8 | 9 | 10 | 11 | 12 | Rate ($\rho_j$, kg COD.m$^{-3}$.d$^{-1}$) |
|---|---|---|---|---|---|---|---|---|---|---|---|---|---|---|
| *j* | Process ↓ | $S_{su}$ | $S_{aa}$ | $S_{fa}$ | $S_{va}$ | $S_{bu}$ | $S_{pro}$ | $S_{ac}$ | $S_{h2}$ | $S_{ch4}$ | $S_{IC}$ | $S_{IN}$ | $S_I$ | |
| 1 | Disintegration | | | | | | | | | | | | $f_{sI,xc}$ | $k_{dis} X_c$ |
| 2 | Hydrolysis carbohydrates | 1 | | | | | | | | | | | | $k_{hyd,ch} X_{ch}$ |
| 3 | Hydrolysis of proteins | | 1 | | | | | | | | | | | $k_{hyd,pr} X_{pr}$ |
| 4 | Hydrolysis of lipids | $1-f_{fa,li}$ | | $1-f_{fa,li}$ | | | | | | | | | | $k_{hyd,li} X_{li}$ |
| 5 | Uptake of sugars | −1 | | | | $(1-Y_{su})f_{bu,su}$ | $(1-Y_{su})f_{pro,su}$ | $(1-Y_{su})f_{ac,su}$ | $(1-Y_{su})f_{h2,su}$ | | $-\sum_{i=9,11-24} C_i \nu_{i,5}$ | $-(Y_{su})\,N_{bac}$ | | $k_{m,su} \frac{S_{su}}{K_S + S} X_{su} I_1$ |
| 6 | Uptake of amino acids | | −1 | | $(1-Y_{aa})f_{va,aa}$ | $(1-Y_{aa})f_{bu,aa}$ | $(1-Y_{aa})f_{pro,aa}$ | $(1-Y_{aa})f_{ac,aa}$ | $(1-Y_{aa})f_{h2,aa}$ | | $-\sum_{i=1-9,11-24} C_i \nu_{i,6}$ | $N_{aa}-(Y_{aa})\,N_{bac}$ | | $k_{m,aa} \frac{S_{aa}}{K_S + S_{aa}} X_{aa} I_1$ |
| 7 | Uptake of LCFA | | | −1 | | | | $(1-Y_{fa})\,0.7$ | $(1-Y_{fa})\,0.3$ | | | $-(Y_{fa})\,N_{bac}$ | | $k_{m,fa} \frac{S_{fa}}{K_S + S_{fa}} X_{fa} I_2$ |
| 8 | Uptake of valerate | | | | −1 | | $(1-Y_{c4})\,0.54$ | $(1-Y_{c4})\,0.31$ | $(1-Y_{c4})\,0.15$ | | | $-(Y_{c4})\,N_{bac}$ | | $k_{m,c4} \frac{S_{va}}{K_S + S_{va}} X_{c4} \frac{1}{1+S_{bu}/S_{va}} I$ |
| 9 | Uptake of butyrate | | | | | −1 | | $(1-Y_{c4})\,0.8$ | $(1-Y_{c4})\,0.2$ | | | $-(Y_{c4})\,N_{bac}$ | | $k_{m,c4} \frac{S_{bu}}{K_S + S_{bu}} X_{c4} \frac{1}{1+S_{va}/S_{bu}} I$ |
| 10 | Uptake of propionate | | | | | | −1 | $(1-Y_{pro})\,0.57$ | $(1-Y_{pro})\,0.43$ | | $-\sum_{i=1-9,11-24} C_i \nu_{i,10}$ | $-(Y_{pro})\,N_{bac}$ | | $k_{m,pr} \frac{S_{pro}}{K_S + S_{pro}} X_{pro} I_2$ |
| 11 | Uptake of acetate | | | | | | | −1 | | $(1-Y_{ac})$ | $-\sum_{i=1-9,11-24} C_i \nu_{i,11}$ | $-(Y_{ac})\,N_{bac}$ | | $k_{m,ac} \frac{S_{ac}}{K_S + S_{ac}} X_{ac} I_3$ |
| 12 | Uptake of hydrogen | | | | | | | | −1 | $(1-Y_{h2})$ | $-\sum_{i=1-9,11-24} C_i \nu_{i,12}$ | $-(Y_{h2})\,N_{bac}$ | | $k_{m,h2} \frac{S_{h2}}{K_S + S_{h2}} X_{h2} I_1$ |
| 13 | Decay of $X_{su}$ | | | | | | | | | | | | | $k_{dec,Xsu} X_{su}$ |
| 14 | Decay of $X_{aa}$ | | | | | | | | | | | | | $k_{dec,Xaa} X_{aa}$ |
| 15 | Decay of $X_{fa}$ | | | | | | | | | | | | | $k_{dec,Xfa} X_{fa}$ |
| 16 | Decay of $X_{c4}$ | | | | | | | | | | | | | $k_{dec,Xc4} X_{c4}$ |
| 17 | Decay of $X_{pro}$ | | | | | | | | | | | | | $k_{dec,Xpro} X_{pro}$ |
| 18 | Decay of $X_{ac}$ | | | | | | | | | | | | | $k_{dec,Xac} X_{ac}$ |
| 19 | Decay of $X_{h2}$ | | | | | | | | | | | | | $k_{dec,Xh2} X_{h2}$ |
| | | Monosaccharides (kgCOD·m$^{-3}$) | Amino acids (kgCOD·m$^{-3}$) | Long chain fatty acids (kgCOD·m$^{-3}$) | Total valerate (kgCOD·m$^{-3}$) | Total butyrate (kgCOD·m$^{-3}$) | Total propionate (kgCOD·m$^{-3}$) | Total acetate (kgCOD·m$^{-3}$) | Hydrogen gas (kgCOD·m$^{-3}$) | Methane gas (kgCOD·m$^{-3}$) | Inorganic carbon (kmoleC·m$^{-3}$) | Inorganic nitrogen (kmoleN·m$^{-3}$) | Soluble inerts (kgCOD·m$^{-3}$) | Inhibition factors: $I_1 = I_{pH}{}^{I}{}_{IN}{}^{I}{}_{lim}$ $I_2 = I_{pH}{}^{I}{}_{IN}{}^{I}{}_{lim}{}^{I}{}_{h2}$ $I_3 = I_{pH}{}^{I}{}_{IN}{}^{I}{}_{lim}{}^{I}{}_{NH3,Xac}$ |

Table A.3 - Biochemical rate coefficients (vi,j) and the kinetic rate equations (ρj) for particulate components (i = 13-24)

| j | Component → i / Process ↓ | 13 $X_c$ | 14 $X_{ch}$ | 15 $X_{pr}$ | 16 $X_{li}$ | 17 $X_{su}$ | 18 $X_{aa}$ | 19 $X_{fa}$ | 20 $X_{c4}$ | 21 $X_{pro}$ | 22 $X_{ac}$ | 23 $X_{h2}$ | 24 $X_I$ | Rate ($\rho_j$, kg COD.m$^{-3}$.d$^{-1}$) |
|---|---|---|---|---|---|---|---|---|---|---|---|---|---|---|
| 1 | Disintegration | -1 | $f_{ch,xc}$ | $f_{pr,xc}$ | $f_{li,xc}$ | | | | | | | | $f_{xI,xc}$ | $k_{dis}X_c$ |
| 2 | Hydrolysis carbohydrates | | -1 | | | | | | | | | | | $k_{hyd,ch}X_{ch}$ |
| 3 | Hydrolysis of proteins | | | -1 | | | | | | | | | | $k_{hyd,pr}X_{pr}$ |
| 4 | Hydrolysis of lipids | | | | -1 | | | | | | | | | $k_{hyd,li}X_{li}$ |
| 5 | Uptake of sugars | | | | | $Y_{su}$ | | | | | | | | $k_{m,su}\frac{S_{su}}{K_S+S}X_{su}I_1$ |
| 6 | Uptake of amino acids | | | | | | $Y_{aa}$ | | | | | | | $k_{m,aa}\frac{S_{aa}}{K_S+S_{aa}}X_{aa}I_1$ |
| 7 | Uptake of LCFA | | | | | | | $Y_{fa}$ | | | | | | $k_{m,fa}\frac{S_{fa}}{K_S+S_{fa}}X_{fa}I_2$ |
| 8 | Uptake of valerate | | | | | | | | $Y_{c4}$ | | | | | $k_{m,c4}\frac{S_{va}}{K_S+S_{va}}X_{c4}\frac{1}{1+S_{bu}/S_{va}}I$ |
| 9 | Uptake of butyrate | | | | | | | | $Y_{c4}$ | | | | | $k_{m,c4}\frac{S_{bu}}{K_S+S_{bu}}X_{c4}\frac{1}{1+S_{va}/S_{bu}}I$ |
| 10 | Uptake of propionate | | | | | | | | | $Y_{pro}$ | | | | $k_{m,pr}\frac{S_{pro}}{K_S+S_{pro}}X_{pro}I_2$ |
| 11 | Uptake of acetate | | | | | | | | | | $Y_{ac}$ | | | $k_{m,ac}\frac{S_{ac}}{K_S+S_{ac}}X_{ac}I_3$ |
| 12 | Uptake of hydrogen | | | | | | | | | | | $Y_{h2}$ | | $k_{m,h2}\frac{S_{h2}}{K_S+S_{h2}}X_{h2}I_1$ |
| 13 | Decay of $X_{su}$ | 1 | | | | -1 | | | | | | | | $k_{dec,Xsu}X_{su}$ |
| 14 | Decay of $X_{aa}$ | 1 | | | | | -1 | | | | | | | $k_{dec,Xaa}X_{aa}$ |
| 15 | Decay of $X_{fa}$ | 1 | | | | | | -1 | | | | | | $k_{dec,Xfa}X_{fa}$ |
| 16 | Decay of $X_{c4}$ | 1 | | | | | | | -1 | | | | | $k_{dec,Xc4}X_{c4}$ |
| 17 | Decay of $X_{pro}$ | 1 | | | | | | | | -1 | | | | $k_{dec,Xpro}X_{pro}$ |
| 18 | Decay of $X_{ac}$ | 1 | | | | | | | | | -1 | | | $k_{dec,Xac}X_{ac}$ |
| 19 | Decay of $X_{h2}$ | 1 | | | | | | | | | | -1 | | $k_{dec,Xh2}X_{h2}$ |
| | | Composites (kgCOD·m$^{-3}$) | Carbohydrates (kgCOD·m$^{-3}$) | Proteins (kgCOD·m$^{-3}$) | Lipids (kgCOD·m$^{-3}$) | Sugar degraders (kgCOD·m$^{-3}$) | Amino acid degraders (kgCOD·m$^{-3}$) | LCFA degraders (kgCOD·m$^{-3}$) | Valerate and butyrate degraders (kgCOD·m$^{-3}$) | Propionate degraders (kgCOD·m$^{-3}$) | Acetate degraders (kgCOD·m$^{-3}$) | Hydrogen degraders (kgCOD·m$^{-3}$) | Particulate inerts (kgCOD·m$^{-3}$) | Inhibition factors: $I_1 = I_{pH}\cdot I_{IN,lim}$; $I_2 = I_{pH}\cdot I_{IN,lim}\cdot I_{h2}$; $I_3 = I_{pH}\cdot I_{IN,lim}\cdot I_{NH3,Xac}$ |

# APPENDIX B

List of all the parameters that have been assumed as default from Rosen and Jeppsson, 2006.

Table B.4 ADM1 stoichiometric parameter values (on the left of the table) and biochemical parameter values (on the right)

| Parameter | Value | Unit | Parameter | Value | Unit |
|---|---|---|---|---|---|
| **N_Xc** | 0,02 | $kmol_N/kg_{COD}$ | **kdec_h2** | 0,02 | $d^{-1}$ |
| **C_aa** | 0,03 | $kmol_C/kg_{COD}$ | **kdec_Xaa** | 0,02 | $d^{-1}$ |
| **C_ac** | 0,0313 | $kmol_C/kg_{COD}$ | **kdec_Xac** | 0,02 | $d^{-1}$ |
| **C_biom** | 0,0313 | $kmol_C/kg_{COD}$ | **kdec_Xc4** | 0,02 | $d^{-1}$ |
| **C_bu** | 0,025 | $kmol_C/kg_{COD}$ | **kdec_Xfa** | 0,02 | $d^{-1}$ |
| **C_ch** | 0,0313 | $kmol_C/kg_{COD}$ | **kdec_Xpro** | 0,02 | $d^{-1}$ |
| **C_ch4** | 1/64 | $kmol_C/kg_{COD}$ | **kdec_Xsu** | 0,02 | $d^{-1}$ |
| **C_fa** | 0,0217 | $kmol_C/kg_{COD}$ | **kdis** | 0,5 | $d^{-1}$ |
| **C_li** | 0,022 | $kmol_C/kg_{COD}$ | **khyd_ch** | 10 | $d^{-1}$ |
| **C_pr** | 0,03 | $kmol_C/kg_{COD}$ | **khyd_li** | 10 | $d^{-1}$ |
| **C_pro** | 0,0268 | $kmol_C/kg_{COD}$ | **khyd_pr** | 10 | $d^{-1}$ |
| **C_SI** | 0,03 | $kmol_C/kg_{COD}$ | **KI_h2_c4** | 1E-05 | $d^{-1}$ |
| **C_su** | 0,0313 | $kmol_C/kg_{COD}$ | **KI_h2_fa** | 5E-06 | $kgCOD/m^3$ |
| **C_va** | 0,024 | $kmol_C/kg_{COD}$ | **KI_h2_pro** | 3,5E-06 | $kgCOD/m^3$ |
| **C_Xc** | 0,0279 | $kmol_C/kg_{COD}$ | **KI_nh3** | 0,0018 | M |
| **C_XI** | 0,03 | $kmol_C/kg_{COD}$ | **km_aa** | 50 | $d^{-1}$ |
| **f_ac_aa** | 0,4 | - | **km_ac** | 8 | $d^{-1}$ |
| **f_ac_su** | 0,41 | - | **km_c4** | 20 | $d^{-1}$ |

| Parameter | Value | Unit | Parameter | Value | Unit |
|---|---|---|---|---|---|
| **f_bu_aa** | 0,26 | - | **km_fa** | 6 | $d^{-1}$ |
| **f_bu_su** | 0,13 | - | **km_h2** | 35 | $d^{-1}$ |
| **f_fa_li** | 0,95 | - | **km_pro** | 13 | $d^{-1}$ |
| **f_h2_aa** | 0,06 | - | **km_su** | 30 | $d^{-1}$ |
| **f_h2_su** | 0,19 | - | **Ks_aa** | 0,3 | $kgCOD/m^3$ |
| **f_pro_aa** | 0,05 | - | **Ks_ac** | 0,15 | $kgCOD/m^3$ |
| **f_pro_su** | 0,27 | - | **Ks_c4** | 0,2 | M |
| **f_va_aa** | 0,23 | - | **Ks_fa** | 0,4 | $kgCOD/m^3$ |
| **N_aa** | 0,007 | $kmol_N/kg_{COD}$ | **Ks_h2** | 7E-06 | $kgCOD/m^3$ |
| **N_biom** | 0,08/14 | $kmol_N/kg_{COD}$ | **Ks_IN** | 1E-04 | M |
| **N_I** | 0,06/14 | $kmol_N/kg_{COD}$ | **Ks_pro** | 0,1 | $kgCOD/m^3$ |
| **Y_aa** | 0,08 | - | **Ks_su** | 0,5 | $kgCOD/m^3$ |
| **Y_ac** | 0,05 | - | **pH_LL_aa** | 4 | - |
| **Y_c4** | 0,06 | - | **pH_LL_ac** | 6 | - |
| **Y_fa** | 0,06 | - | **pH_LL_h2** | 5 | - |
| **Y_h2** | 0,06 | - | **pH_UL_aa** | 5,5 | - |
| **Y_pro** | 0,04 | - | **pH_UL_ac** | 7 | - |
| **Y_su** | 0,1 | - | **pH_UL_h2** | 6 | - |

Table B.5 ADM1 physiochemical parameter values; Van't Hoff temperature correction has been applied if required

| Parameter | Value | Unit |
|---|---|---|
| **R** | 0,08314 | bar $M^{-1}$ $K^{-1}$ |
| **T** | 308 | K |
| **Ka_ac** | 10^ (-4,76) | M |
| **Ka_bu** | 10^ (-4,82) | M |
| **Ka_co2** | $10^{6,35}\exp\left(\frac{7646}{R*100}\left(\frac{1}{298}-\frac{1}{T}\right)\right)$ | M |
| **Ka_IN** | $10^{9,25}\exp\left(\frac{51965}{R*100}\left(\frac{1}{298}-\frac{1}{T}\right)\right)$ | M |
| **Ka_pro** | 10^ (-4,88) | M |
| **Ka_va** | 10^ (-4,86) | M |
| **kAB_co2** | 1E-14 | $M^{-1}$ $d^{-1}$ |
| **KH_ch4** | $0{,}0014\cdot\exp\left(\frac{-14240}{R*100}\left(\frac{1}{298}-\frac{1}{T}\right)\right)$ | $M_{liq}$ $bar^{-1}$ |
| **KH_co2** | $0{,}035\cdot\exp\left(\frac{-19410}{R*100}\left(\frac{1}{298}-\frac{1}{T}\right)\right)$ | $M_{liq}$ $bar^{-1}$ |
| **KH_h2** | $7{,}8e-4\cdot\exp\left(\frac{-4180}{R*100}\left(\frac{1}{298}-\frac{1}{T}\right)\right)$ | $M_{liq}$ $bar^{-1}$ |
| **kLa** | 200 | $d^{-1}$ |
| **Kw** | $\exp\left(\frac{55900}{R*100}\left(\frac{1}{298}-\frac{1}{T}\right)\right)$ | M |
| **P_atm** | 1,0313 | bar |
| **p_h2o** | $0{,}0313\cdot\exp\left(5290\left(\frac{1}{298}-\frac{1}{T}\right)\right)$ | bar |

# APPENDIX C

The following tables show the analyses results for the characterization of sludge, yogurt, digestate and degassed digestate.

Table C.1 - Analyses results for sludge characterization

| PARAMETER | UNIT | VALUE | | | | | | | | | | Average | Standard deviation |
|---|---|---|---|---|---|---|---|---|---|---|---|---|---|
| | | 08/10/2020 | 22/10/2020 | 05/11/2020 | 19/11/2020 | 03/12/2020 | 30/12/2020 | 03/02/2021 | 24/02/2021 | 18/03/2021 | 22/04/2021 | | |
| **TOTAL FRACTION** | | | | | | | | | | | | | |
| pH | - | 6.61 | 6.06 | 6.33 | 5.90 | 6.15 | 5.95 | 5.81 | 6 | 6.57 | 5.46 | 6.08 | 0.35 |
| Alkalinity | mg$CaCO_3$/L | 1238 | 1789 | 1933 | 1823 | 1898 | 2078 | 1407 | 1376 | 1870 | 1234 | 1665 | 316 |
| TS | gTS/kgFM | 18.3 | 30.8 | 34.4 | 30.8 | 32.8 | 31.4 | 24.7 | 28.5 | 27.9 | 29.6 | 28.9 | 4.6 |
| VS | gVS/kgFM | 14.1 | 24.2 | 26.7 | 24.4 | 26.1 | 25.1 | 19.2 | 22.2 | 21.8 | 22.8 | 22.7 | 3.7 |
| Total COD | gCOD/kg | 21.8 | 35.7 | 39.0 | 37.0 | 41.2 | 32.6 | 30.6 | 31.3 | 33.1 | | 33.6 | 5.7 |
| Total TKN | gN/kg | 1.03 | | 1.51 | | | 2.04 | | | | | 1.53 | 0.51 |
| Total Carbohydrates | gGlu/L | 5.68 | 10.9 | 11.6 | 8.63 | 8.60 | 8.44 | 6.42 | 8.29 | 13.1 | 8.17 | 8.98 | 2.27 |
| Total Proteins | gBSA/L | 4.03 | 9.35 | 9.53 | 9.57 | 10.69 | 9.93 | 7.54 | 9.12 | 8.02 | 7.76 | 8.55 | 1.88 |
| BMP Total | NmLCH4/gVS | 354 | 380 | 366 | 380 | 358 | 398 | 381 | 440 | 410 | 410 | 388 | 27 |
| **PARTICULATE FRACTION - ANALYSIS PERFORMED ON THE SOLID SEPARATED AFTER CENTRUFUGATION** | | | | | | | | | | | | | |
| BMP Particulate | NmLCH4/gVS,p | 337 | 401 | 383 | 398 | 410 | 392 | 362 | 403 | 382 | 382 | 385 | 22 |
| Particulate Lipids | g/kgVS,p | 132 | 159 | 148 | 131 | 132 | 130 | 119 | 124 | 115 | 127 | 132 | 13 |
| Particulate Lipids | g/kgVS | 127 | 154 | 142 | 128 | 127 | 124 | 113 | 120 | 112 | 121 | 127 | 13 |
| TS - particulate fraction | gTS,p/kgFM,p | 110 | 114 | 117 | 115 | 106 | 108 | 114 | 116 | 117 | 110 | 113 | 4 |
| VS - particulate fraction | gVS,p/kgFM,p | 84 | 91 | 92 | 93 | 85 | 88 | 91 | 92 | 92 | 85 | 89 | 3 |
| **SOLUBLE FRACTION - ANALYSIS PERFORMED ON THE LIQUID SEPARATED AFTER CENTRUFUGATION** | | | | | | | | | | | | | |
| VFA: acetic acid | mg/L | 393 | 747 | 581 | 929 | 809 | 829 | 761 | 923 | 514 | 999 | 748 | 196 |
| VFA: propionic acid | mg/L | 100 | 209 | 211 | 318 | 244 | 310 | 263 | 351 | 165 | 319 | 249 | 79 |
| VFA: iso-butyric acid | mg/L | 24 | 35 | 38 | 42 | 28 | 35 | 22 | 64 | 38 | 44 | 37 | 12 |
| VFA: butyric acid | mg/L | 25 | 76 | 88 | 151 | 102 | 108 | 136 | 138 | 49 | 132 | 101 | 41 |
| VFA: iso-valeric acid | mg/L | 23 | 0 | 37 | 42 | 22 | 34 | 16 | 41 | 25 | 14 | 26 | 13 |
| VFA: valeric acid | mg/L | 0 | 17 | 30 | 51 | 34 | 44 | 0 | 44 | 19 | 35 | 27 | 18 |
| TS - soluble fraction | gTS,s/kgFM,s | 1.3 | 1.9 | 2.8 | 1.8 | 3.0 | 2.8 | 2.2 | 1.9 | 1.6 | 2.3 | 2.2 | 0.5 |
| VS - soluble fraction | gVS,s/kgFM,s | 0.6 | 0.9 | 1.6 | 0.8 | 1.9 | 1.7 | 1.2 | 1.0 | 0.8 | 1.3 | 1.2 | 0.4 |
| Soluble Carbohydrates | mgGlu/L | 46.1 | 54.3 | 193 | 171 | 206 | 103 | 59 | 66 | 60 | 61 | 102 | 63 |
| Soluble Proteins | mgBSA/L | 148 | 121 | 545 | 699 | 720 | 630 | 152 | 225 | 201 | 234 | 367 | 248 |
| Soluble Lipids | g/kgVS,s | 60 | 49 | 44 | 57 | 40 | 42 | 46 | 47 | 52 | 43 | 48 | 7 |
| Soluble Lipids | g/kgVS | 2.28 | 1.34 | 1.86 | 1.36 | 2.05 | 2.02 | 2.28 | 1.65 | 1.45 | 1.88 | 1.82 | 0.35 |
| Soluble TKN | mgN/L | 105 | 110 | 191 | 210 | 193 | 185 | | | | | 166 | 46 |
| Soluble COD | gCOD/L | 1.35 | 1.80 | 3.22 | 3.91 | 1.80 | 4.06 | 2.55 | 2.11 | 1.62 | 2.02 | 2.44 | 0.96 |
| Ammoniacal Nitrogen | mgN/L | 8.9 | 49.2 | 42.4 | 126 | 93.2 | 104 | 88.2 | 116 | 96.6 | 62.5 | 79 | 37 |

Table C.2 - Data analysis of sludge analytical measurements

| PARAMETER | UNIT | VALUE | | | | | | | | | | Average | Standard deviation |
|---|---|---|---|---|---|---|---|---|---|---|---|---|---|
| | | 08/10/2020 | 22/10/2020 | 05/11/2020 | 19/11/2020 | 03/12/2020 | 30/12/2020 | 03/02/2021 | 24/02/2021 | 18/03/2021 | 22/04/2021 | | |
| Total Carbohydrates | gCOD/L | 6.07 | 11.70 | 12.40 | 9.23 | 9.20 | 9.03 | 6.87 | 8.87 | 13.97 | 8.74 | 9.61 | 2.43 |
| Total Proteins | gCOD/L | 6.34 | 14.7 | 15.0 | 15.1 | 16.8 | 15.6 | 11.9 | 14.3 | 12.6 | 12.2 | 13.4 | 3.0 |
| Total Lipids | gCOD/L | 5.31 | 11.00 | 11.17 | 9.22 | 9.79 | 9.25 | 6.49 | 7.88 | 7.19 | 8.18 | 8.55 | 1.90 |
| Carbohydrates/CODtot | - | 33% | 30% | 31% | 26% | 25% | 25% | 26% | 27% | 40% | 28% | 29% | 5% |
| Proteins/CODtot | - | 34% | 38% | 37% | 42% | 45% | 44% | 44% | 43% | 36% | 39% | 40% | 4% |
| Lipids/CODtot | - | 29% | 28% | 28% | 26% | 26% | 26% | 24% | 24% | 21% | 26% | 26% | 2% |
| TVFA | gCOD/L | 0.71 | 1.35 | 1.31 | 2.01 | 1.58 | 1.46 | 1.53 | 2.06 | 1.05 | 1.97 | 1.50 | 0.43 |
| COD total calculated | gCOD/L | 18.5 | 38.8 | 39.9 | 35.6 | 37.5 | 35.4 | 26.8 | 33.2 | 34.9 | 31.2 | 33.2 | 6.4 |
| COD/VS | gCOD/gVS | 1.54 | 1.47 | 1.46 | 1.52 | 1.58 | 1.30 | 1.59 | 1.41 | 1.44 | | 1.48 | 0.09 |
| VS/TS | gVS/gTS | 0.77 | 0.79 | 0.78 | 0.79 | 0.79 | 0.80 | 0.78 | 0.78 | 0.78 | 0.77 | 0.78 | 0.01 |
| N/COD | gN/gCOD | 0.0004 | 0.0014 | 0.0011 | 0.0034 | 0.0023 | 0.0032 | 0.0029 | 0.0037 | 0.0029 | | 0.00 | 0.00 |
| CODsol/COD | - | 0.06 | 0.05 | 0.08 | 0.11 | 0.04 | 0.12 | 0.08 | 0.07 | 0.05 | | 0.07 | 0.03 |
| VFA/CODsol | - | 0.52 | 0.75 | 0.41 | 0.51 | 0.88 | 0.36 | 0.60 | 0.97 | 0.64 | 0.98 | 0.66 | 0.22 |

Table C.3 - ADM1 sludge characterization

| PARAMETER | UNIT | VALUE | | | | | | | | | | Media | Std deviation |
|---|---|---|---|---|---|---|---|---|---|---|---|---|---|
| | | 08/10/2020 | 22/10/2020 | 05/11/2020 | 19/11/2020 | 03/12/2020 | 30/12/2020 | 03/02/2021 | 24/02/2021 | 18/03/2021 | 22/04/2021 | | |
| S_su_in | gCOD/L | 0.05 | 0.06 | 0.21 | 0.18 | 0.22 | 0.11 | 0.06 | 0.07 | 0.06 | 0.07 | 0.11 | 0.07 |
| S_aa_in | gCOD/L | 0.23 | 0.19 | 0.86 | 1.22 | 1.25 | 1.00 | 0.24 | 0.36 | 0.32 | 0.37 | 0.60 | 0.43 |
| S_fa_in | gCOD/L | 0.09 | 0.09 | 0.15 | 0.09 | 0.09 | 0.15 | 0.13 | 0.11 | 0.09 | 0.12 | 0.11 | 0.02 |
| S_va_in | gCOD/L | 0.05 | 0.03 | 0.14 | 0.19 | 0.11 | 0.16 | 0.03 | 0.17 | 0.09 | 0.10 | 0.11 | 0.06 |
| S_bu_in | gCOD/L | 0.09 | 0.20 | 0.23 | 0.35 | 0.24 | 0.26 | 0.29 | 0.37 | 0.16 | 0.32 | 0.25 | 0.09 |
| S_pro_in | gCOD/L | 0.15 | 0.32 | 0.32 | 0.48 | 0.37 | 0.47 | 0.40 | 0.53 | 0.25 | 0.48 | 0.38 | 0.12 |
| S_ac_in | gCOD/L | 0.42 | 0.80 | 0.62 | 0.99 | 0.86 | 0.88 | 0.81 | 0.98 | 0.55 | 1.07 | 0.80 | 0.21 |
| S_h2_in | gCOD/L | 1.00E-08 | 1.00E-08 | 1.00E-08 | 1.00E-08 | 1.00E-08 | 1.00E-08 | 1.00E-08 | 1.00E-08 | 1.00E-08 | 1.00E-08 | 0.00 | 0.00 |
| S_ch4_in | gCOD/L | 1.00E-05 | 1.00E-05 | 1.00E-05 | 1.00E-05 | 1.00E-05 | 1.00E-05 | 1.00E-05 | 1.00E-05 | 1.00E-05 | 1.00E-05 | 0.00 | 0.00 |
| S_ic_in | M | 2.40E-02 | 5.41E-02 | 4.70E-02 | 5.30E-02 | 4.77E-02 | 7.21E-02 | 4.67E-02 | 1.68E-02 | 3.88E-02 | 4.20E-02 | 0.04 | 0.02 |
| S_in_in | M | 6.36E-04 | 3.51E-03 | 3.03E-03 | 9.00E-03 | 6.66E-03 | 7.40E-03 | 6.30E-03 | 8.31E-03 | 6.90E-03 | 4.46E-03 | 0.01 | 0.00 |
| S_i_in | gCOD/L | 4.69 | 2.02 | 2.11 | 3.36 | 4.58 | 0.87 | 0.00 | 0.00 | 0.00 | 0.00 | 1.76 | 1.90 |
| S_cat_in | M | 0.044 | 0.052 | 0.056 | 0.047 | 0.052 | 0.054 | 0.048 | 0.039 | 0.054 | 0.040 | 0.05 | 0.01 |
| S_an_in | M | 0.02 | 0.02 | 0.02 | 0.02 | 0.02 | 0.02 | 0.02 | 0.02 | 0.02 | 0.02 | 0.02 | 0.00 |
| X_c_in | gCOD/L | 2.85 | 3.71 | 3.74 | 3.36 | 3.20 | 3.27 | 2.48 | 3.06 | 3.33 | 2.86 | 3.19 | 0.39 |
| X_ch_in | gCOD/L | 3.74 | 7.85 | 8.43 | 6.33 | 6.68 | 7.00 | 5.15 | 7.04 | 9.70 | 7.12 | 6.90 | 1.65 |
| X_pr_in | gCOD/L | 4.68 | 9.87 | 9.85 | 10.84 | 12.93 | 11.56 | 8.87 | 11.28 | 8.64 | 9.80 | 9.83 | 2.23 |
| X_li_in | gCOD/L | 0.74 | 7.38 | 7.66 | 6.40 | 4.28 | 7.16 | 4.83 | 6.24 | 4.97 | 6.63 | 5.63 | 2.06 |
| X_su_in | gCOD/L | 0.01 | 0.01 | 0.01 | 0.01 | 0.01 | 0.01 | 0.01 | 0.01 | 0.01 | 0.01 | 0.01 | 0.00 |
| X_aa_in | gCOD/L | 0.01 | 0.01 | 0.01 | 0.01 | 0.01 | 0.01 | 0.01 | 0.01 | 0.01 | 0.01 | 0.01 | 0.00 |
| X_fa_in | gCOD/L | 0.01 | 0.01 | 0.01 | 0.01 | 0.01 | 0.01 | 0.01 | 0.01 | 0.01 | 0.01 | 0.01 | 0.00 |
| X_c4_in | gCOD/L | 0.01 | 0.01 | 0.01 | 0.01 | 0.01 | 0.01 | 0.01 | 0.01 | 0.01 | 0.01 | 0.01 | 0.00 |
| X_pro_in | gCOD/L | 0.01 | 0.01 | 0.01 | 0.01 | 0.01 | 0.01 | 0.01 | 0.01 | 0.01 | 0.01 | 0.01 | 0.00 |
| X_ac_in | gCOD/L | 0.01 | 0.01 | 0.01 | 0.01 | 0.01 | 0.01 | 0.01 | 0.01 | 0.01 | 0.01 | 0.01 | 0.00 |
| X_h2_in | gCOD/L | 0.01 | 0.01 | 0.01 | 0.01 | 0.01 | 0.01 | 0.01 | 0.01 | 0.01 | 0.01 | 0.01 | 0.00 |
| X_i_in | gCOD/L | 11.76 | 6.28 | 5.62 | 3.29 | 0.35 | 2.83 | 3.48 | 2.98 | 6.67 | 2.18 | 4.54 | 3.20 |

Table C.4 - Analyses results for yogurt characterization

| PARAMETER | UNIT | VALUE | | | Average | Standard deviation |
|---|---|---|---|---|---|---|
| | | 03/02/2021 | 24/02/2021 | 18/03/2021 | | |
| VS - particulate fraction | $g_{VS,p}/kg_{FM,p}$ | 134 | 140 | 148 | 141 | 7 |
| TS - particulate fraction | $g_{TS,p}/kg_{FM,p}$ | 152 | 152 | 173 | 159 | 12 |
| Lipids from label | g/L | 15.6 | 13.8 | 28.6 | 19.3 | 8.1 |
| Charb measured | g/L | 135 | 160 | 157 | 151 | 13 |
| Proteins measured | g/L | 40.5 | 52.3 | 46.8 | 46.5 | 5.9 |
| $BMP_{part}$ | $NmL_{CH4}/gVSp$ | 718 | 805 | 762 | 762 | 44 |

Table C.5 - Data analysis of yogurt analytical measurements

| PARAMETER | UNIT | VALUE | | | Average | Standard deviation |
|---|---|---|---|---|---|---|
| | | 03/02/2021 | 24/02/2021 | 18/03/2021 | | |
| VS/TS | gVS/gTS | 0.88 | 0.92 | 0.86 | 0.88 | 0.03 |
| Total Carbohydrates | gCOD/L | 145 | 171 | 168 | 161 | 14 |
| Total Proteins | gCOD/L | 63.9 | 82.6 | 73.9 | 73.5 | 9.3 |
| Total Lipids | gCOD/L | 45.2 | 39.9 | 83.0 | 56.0 | 23.5 |
| COD total calculated | gCOD/L | 257 | 296 | 328 | 294 | 36 |
| Carbohydrates/CODtot | - | 56% | 58% | 51% | 0.55 | 0.03 |
| Proteins/CODtot | - | 25% | 28% | 23% | 0.25 | 0.03 |
| Lipids/CODtot | - | 18% | 13% | 25% | 0.19 | 0.06 |
| COD/VS | gCOD/gVS | 1.92 | 2.11 | 2.22 | 2.08 | 0.15 |

Table C.6 - ADM1 yogurt characterization

| PARAMETER | UNIT | VALUE | | | Average | Standard deviation |
|---|---|---|---|---|---|---|
| | | 03/02/2021 | 24/02/2021 | 18/03/2021 | | |
| S_su_in | gCOD/L | 0 | 0 | 0 | 0.00 | 0.00 |
| S_aa_in | gCOD/L | 63.9 | 82.6 | 73.9 | 73.5 | 9.3 |
| S_fa_in | gCOD/L | 0 | 0 | 0 | 0.00 | 0.00 |
| S_va_in | gCOD/L | 0 | 0 | 0 | 0.00 | 0.00 |
| S_bu_in | gCOD/L | 0 | 0 | 0 | 0.00 | 0.00 |
| S_pro_in | gCOD/L | 0 | 0 | 0 | 0.00 | 0.00 |
| S_ac_in | gCOD/L | 0 | 0 | 0 | 0.00 | 0.00 |
| S_h2_in | gCOD/L | 0 | 0 | 0 | 0.00 | 0.00 |
| S_ch4_in | gCOD/L | 0 | 0 | 0 | 0.00 | 0.00 |
| S_ic_in | M | 0 | 0 | 0 | 0.00 | 0.00 |
| S_in_in | M | 0 | 0 | 0 | 0.00 | 0.00 |
| S_i_in | gCOD/L | 0 | 0 | 0 | 0.00 | 0.00 |
| S_cat_in | M | 0.0199 | 0.0199 | 0.0199 | 0.02 | 0.00 |
| S_an_in | M | 0.020 | 0.020 | 0.020 | 0.02 | 0.00 |
| X_c_in | gCOD/L | 0 | 0 | 0 | 0.00 | 0.00 |
| X_ch_in | gCOD/L | 145 | 171 | 168 | 161 | 14 |
| X_pr_in | gCOD/L | 0 | 0 | 0 | 0.00 | 0.00 |
| X_li_in | gCOD/L | 45.2 | 39.9 | 83.0 | 56.0 | 23.5 |
| X_su_in | gCOD/L | 0 | 0 | 0 | 0.00 | 0.00 |
| X_aa_in | gCOD/L | 0 | 0 | 0 | 0.00 | 0.00 |
| X_fa_in | gCOD/L | 0 | 0 | 0 | 0.00 | 0.00 |
| X_c4_in | gCOD/L | 0 | 0 | 0 | 0.00 | 0.00 |
| X_pro_in | gCOD/L | 0 | 0 | 0 | 0.00 | 0.00 |
| X_ac_in | gCOD/L | 0 | 0 | 0 | 0.00 | 0.00 |
| X_h2_in | gCOD/L | 0 | 0 | 0 | 0.00 | 0.00 |
| X_i_in | gCOD/L | 0 | 0 | 0 | 0.00 | 0.00 |

Table C.7 - Analyses results for digestate characterization

| PARAMETER | UNIT | VALUE | | | | | | | | | | Average | Standard deviation |
|---|---|---|---|---|---|---|---|---|---|---|---|---|---|
| | | 08/10/2020 | 22/10/2020 | 05/11/2020 | 19/11/2020 | 03/12/2020 | 30/12/2020 | 03/02/2021 | 24/02/2021 | 18/03/2021 | 22/04/2021 | | |
| **TOTAL FRACTION** | | | | | | | | | | | | | |
| pH | - | 7.13 | 7.11 | 7.09 | 7.29 | 7.3 | 7.24 | 7.44 | 7.49 | 7.7 | 7.3 | 7.31 | 0.19 |
| Alkalinity | $mgCaCO_3/L$ | 3615 | 3162 | 3604 | 4413 | 4802 | 4880 | 4901 | 5323 | 5755 | 4381 | 4484 | 819 |
| TS | gTS/kgFM | 22.1 | 17.7 | 21.3 | 22.1 | 21.1 | 21.7 | 19.1 | 21.1 | 25.2 | 19.1 | 21.1 | 2.1 |
| VS | gVS/kgFM | 13.3 | 10.8 | 13.6 | 14.2 | 13.8 | 14.7 | 12.8 | 14.3 | 15.9 | 12.7 | 13.6 | 1.4 |
| Total COD | gCOD/kg | 6.10 | 9.6 | 17.2 | 11.4 | 15.1 | 15.6 | 14.6 | 16.2 | 16.5 | | 13.6 | 3.7 |
| Total TKN | gN/kg | 1.13 | 1.13 | 1.33 | | 1.63 | | | | | | 1.30 | 0.23 |
| Total Carbohydrates | gGlu/L | 2.00 | 2.51 | 2.52 | 3.75 | 3.88 | 3.97 | 3.17 | 2.79 | 3.69 | 2.94 | 3.12 | 0.68 |
| Total Proteins | gBSA/L | 4.50 | 9.17 | 6.64 | 8.90 | 11.64 | 11.28 | 9.33 | 7.88 | 11.05 | 8.54 | 8.89 | 2.20 |
| Total Lipids | g/L | 0.22 | 0.32 | 0.57 | 0.46 | 0.20 | 0.65 | | | | | 0.40 | 0.19 |
| Residual BMP | NmLCH4/gVS | 71.4 | 96.5 | 96.5 | 96.5 | 60.5 | 86.3 | 67.7 | 74.1 | 71.0 | 71.0 | 79.2 | 13.6 |
| **PARTICULATE FRACTION - ANALYSIS PERFORMED ON THE SOLID SEPARATED AFTER CENTRUFUGATION** | | | | | | | | | | | | | |
| Particulate lipids | g/kgVS,p | 18 | 33 | 47 | 37 | 16 | 53 | | | | | 33.7 | 15.0 |
| Particulate lipids | g/kgVS | 16 | 30 | 42 | 33 | 14 | 44 | | | | | 29.7 | 12.5 |
| TS - particulate fraction | gTS,p/kgFM,p | 104 | 96 | 99 | 92 | 89 | 92 | 85 | 88 | 83 | 96 | 92.4 | 6.6 |
| VS - particulate fraction | gVS,p/kgFM,p | 63 | 59 | 63 | 60 | 59 | 63 | 58 | 60 | 54 | 64 | 60.3 | 3.0 |
| **SOLUBLE FRACTION - ANALYSIS PERFORMED ON THE LIQUID SEPARATED AFTER CENTRUFUGATION** | | | | | | | | | | | | | |
| VFA: acetic acid | mg/L | 106 | 53 | 85 | 56 | 63 | 69 | 42 | 28 | 28 | 55 | 58.4 | 24.2 |
| VFA: propionic acid | mg/L | 0 | 0 | 0 | 0 | 0 | 0 | 0 | 0 | 0 | 0 | 0.00 | 0.00 |
| VFA: iso-butyric acid | mg/L | 12 | 0 | 0 | 0 | 0 | 0 | 0 | 0 | 0 | 10 | 2.20 | 4.65 |
| VFA: butyric acid | mg/L | 0 | 0 | 0 | 0 | 0 | 0 | 0 | 0 | 0 | 0 | 0.00 | 0.00 |
| VFA: iso-valeric acid | mg/L | 0 | 0 | 0 | 0 | 0 | 0 | 0 | 0 | 0 | 0 | 0.00 | 0.00 |
| VFA: valeric acid | mg/L | 0 | 0 | 0 | 0 | 0 | 0 | 0 | 0 | 0 | 0 | 0.00 | 0.00 |
| TS - soluble fraction | gTS,s/kgFM,s | 2.9 | 2.4 | 3.4 | 3.6 | 3.0 | 4.9 | 3.8 | 3.8 | 3.5 | 3.1 | 3.44 | 0.68 |
| VS - soluble fraction | gVS,s/kgFM,s | 1.5 | 1.2 | 1.9 | 2.0 | 1.6 | 3.0 | 2.1 | 2.1 | 1.9 | 1.7 | 1.91 | 0.47 |
| Soluble Carbohydrates | mgGlu/L | 143 | 127 | 154 | 228 | 183 | 327 | 235 | 241 | 228 | 228 | 209 | 59 |
| Soluble Proteins | mgBSA/L | 858 | 556 | 902 | 1085 | 794 | 2066 | 1315 | 1565 | 1190 | 1190 | 1152 | 431 |
| Soluble TKN | mgN/L | 568 | 570 | 620 | 750 | 829 | 975 | | | | | 719 | 163 |
| Soluble COD | gCOD/L | 2.46 | 2.08 | 2.51 | 3.22 | 2.08 | 4.11 | 3.58 | 3.10 | 3.52 | 2.27 | 2.89 | 0.71 |
| Ammonium | mgN/L | 451 | 398 | 452 | 600 | 743 | 774 | 856 | 960 | 1008 | 670 | 691 | 216 |

Table C.8 - Data analysis of digestate analytical measurements

| PARAMETER | UNIT | VALUE | | | | | | | | | | Average | Std deviation |
|---|---|---|---|---|---|---|---|---|---|---|---|---|---|
| | | 08/10/2020 | 22/10/2020 | 05/11/2020 | 19/11/2020 | 03/12/2020 | 30/12/2020 | 03/02/2021 | 24/02/2021 | 18/03/2021 | 22/04/2021 | | |
| Total Carbohydrates | gCOD/L | 2.14 | 2.68 | 2.70 | 4.01 | 4.15 | 4.24 | 3.39 | 2.99 | 3.95 | 3.14 | 3.34 | 0.73 |
| Total Proteins | gCOD/L | 7.1 | 14.5 | 10.5 | 14.1 | 18.4 | 17.8 | 14.7 | 12.4 | 17.5 | 13.5 | 14.1 | 3.5 |
| Total Lipids | gCOD/L | 0.63 | 0.94 | 1.64 | 1.35 | 0.57 | 1.90 | | | | | 1.17 | 0.55 |
| Carbohydrates/CODtot | - | 0.22 | 0.15 | 0.18 | 0.21 | 0.18 | 0.18 | | | | | 0.18 | 0.02 |
| Proteins/CODtot | - | 0.72 | 0.80 | 0.71 | 0.72 | 0.80 | 0.74 | | | | | 0.75 | 0.04 |
| Lipids/CODtot | - | 0.06 | 0.05 | 0.11 | 0.07 | 0.02 | 0.08 | | | | | 0.07 | 0.03 |
| VS/TS | gVS/gTS | 0.60 | 0.61 | 0.63 | 0.64 | 0.66 | 0.68 | 0.67 | 0.67 | 0.63 | 0.66 | 0.65 | 0.03 |
| TVFA | mgCOD/L | 134 | 57 | 90 | 60 | 67 | 73 | 45 | 29 | 29 | 78 | 66.27 | 30.96 |
| COD total as pr,ch,li,VFA | gCOD/L | 10.0 | 18.2 | 14.9 | 19.5 | 23.2 | 24.0 | | | | | 18.30 | 5.26 |
| COD/VS | gCOD/gVS | 0.46 | 0.89 | 1.27 | 0.80 | 1.09 | 1.06 | 1.14 | 1.14 | 1.04 | | 0.99 | 0.24 |
| COD calculated/VS | gCOD/gVS | 0.74 | 1.68 | 1.09 | 1.37 | 1.67 | 1.63 | | | | | 1.36 | 0.38 |
| N/COD | gN/gCOD | 0.05 | 0.02 | 0.03 | 0.03 | 0.03 | 0.03 | | | | | 0.03 | 0.01 |
| CODsol/COD | - | 0.21 | 0.11 | 0.17 | 0.16 | 0.09 | 0.17 | | | | | 0.15 | 0.04 |
| VFA/CODsol | - | 0.06 | 0.03 | 0.04 | 0.02 | 0.03 | 0.02 | 0.01 | 0.01 | 0.01 | 0.03 | 0.03 | 0.02 |

Table C.9 - Analyses results for degassed digestate characterization

| PARAMETER | UNIT | VALUE | | | | | | | | | | Average | Standard deviation |
|---|---|---|---|---|---|---|---|---|---|---|---|---|---|
| | | 08/10/2020 | 22/10/2020 | 05/11/2020 | 19/11/2020 | 03/12/2020 | 30/12/2020 | 03/02/2021 | 24/02/2021 | 18/03/2021 | 22/04/2021 | | |
| **TOTAL FRACTION** | | | | | | | | | | | | | |
| pH | - | 7.58 | 7.58 | 7.59 | 7.3 | 7.36 | 8.02 | 7.97 | 7.96 | 8.04 | 8.15 | 7.76 | 0.31 |
| TS | gTS/kgFM | 21.8 | 17.1 | 18.3 | 20.4 | 18.9 | 19.5 | 18.8 | 17.7 | 25.2 | 20.2 | 19.8 | 2.3 |
| VS | gVS/kgFM | 12.8 | 10.0 | 11.1 | 12.4 | 11.4 | 11.8 | 11.6 | 11.0 | 15.9 | 12.9 | 12.1 | 1.6 |
| Total Carbohydrates | gGlu/L | 1.58 | 1.95 | 1.65 | 2.56 | 2.74 | 1.48 | 1.19 | 2.65 | | 3.07 | 2.10 | 0.67 |
| Total Proteins | gBSA/L | 4.00 | 6.87 | 4.12 | 8.62 | 10.75 | 3.23 | 3.98 | 9.53 | | 9.97 | 6.79 | 3.00 |
| Total Lipids | g/L | 0.15 | 0.25 | 0.40 | 0.58 | 0.40 | 0.38 | | | | | 0.36 | 0.15 |
| **PARTICULATE FRACTION - ANALYSIS PERFORMED ON THE SOLID SEPARATED AFTER CENTRUFUGATION** | | | | | | | | | | | | | |
| Particulate lipids | g/kgVS,p | 23 | 26 | 38 | 49 | 37 | 34 | | | | | 34 | 9 |
| Particulate lipids | g/kgVS | 12 | 25 | 36 | 47 | 35 | 32 | | | | | 31 | 12 |
| TS - particulate fraction | gTS,p/kgFM,p | 96 | 93 | 93 | 91 | 86 | 84 | 86 | 75 | 83 | 83 | 87 | 6 |
| VS - particulate fraction | gVS,p/kgFM,p | 57 | 56 | 57 | 56 | 53 | 52 | 54 | 47 | 54 | 53 | 54 | 3 |
| **SOLUBLE FRACTION - ANALYSIS PERFORMED ON THE LIQUID SEPARATED AFTER CENTRUFUGATION** | | | | | | | | | | | | | |
| TS - soluble fraction | gTS,s/kgFM,s | 1.6 | 1.8 | 1.7 | 1.5 | 1.5 | 1.5 | 1.5 | 2.0 | 3.5 | 2.8 | 1.95 | 0.68 |
| VS - soluble fraction | gVS,s/kgFM,s | 0.8 | 0.6 | 0.7 | 0.7 | 0.7 | 0.8 | 0.9 | 1.1 | 1.9 | 1.7 | 0.99 | 0.45 |
| Soluble lipids | g/kgVS,s | 6.6 | | | | | | | | | | 6.6 | |
| Soluble lipids | g/kgVS | 3.2 | | | | | | | | | | 3.2 | |
| Ammonium | mgN/L | 474 | 497 | 452 | 526 | 600 | 510 | 595 | 680 | 896 | 705 | 593 | 136 |

# APPENDIX D

The graphs of the BMP tests carried out are shown in this appendix. For some tests, problems were found with one of the duplicates therefore for these graphs the standard deviation is not reported but only the value of the corrected test.

*Blank*

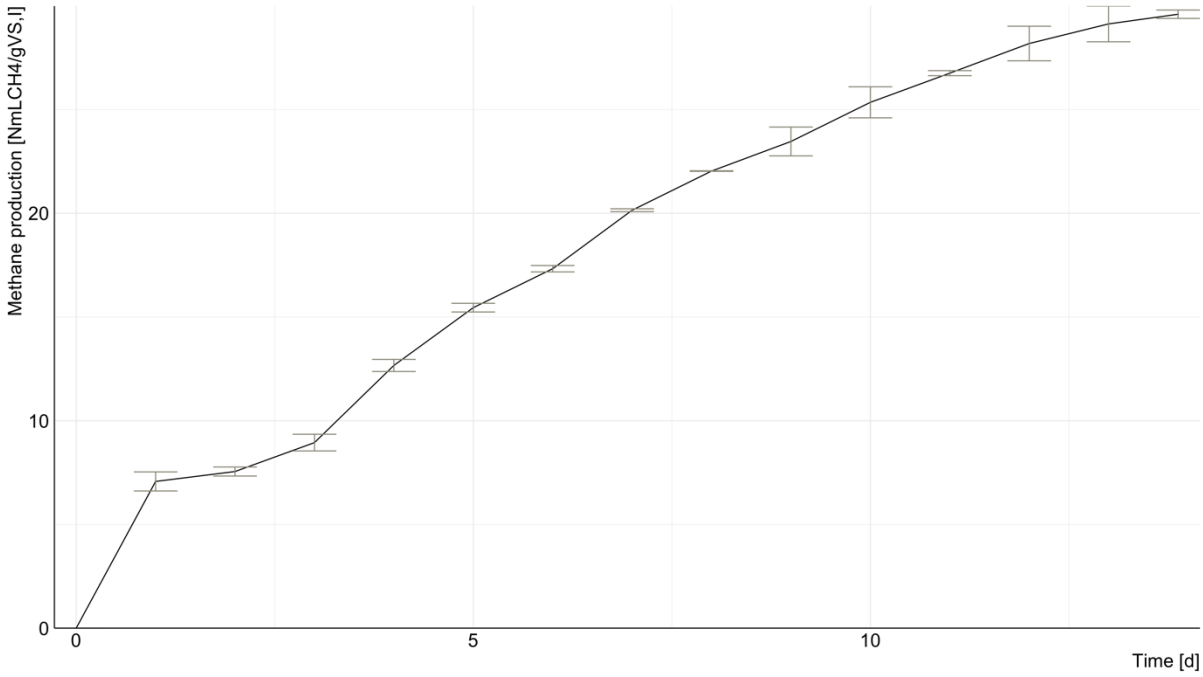


Figure D.1 - Methane production of blank BMP test (22/10/2020).

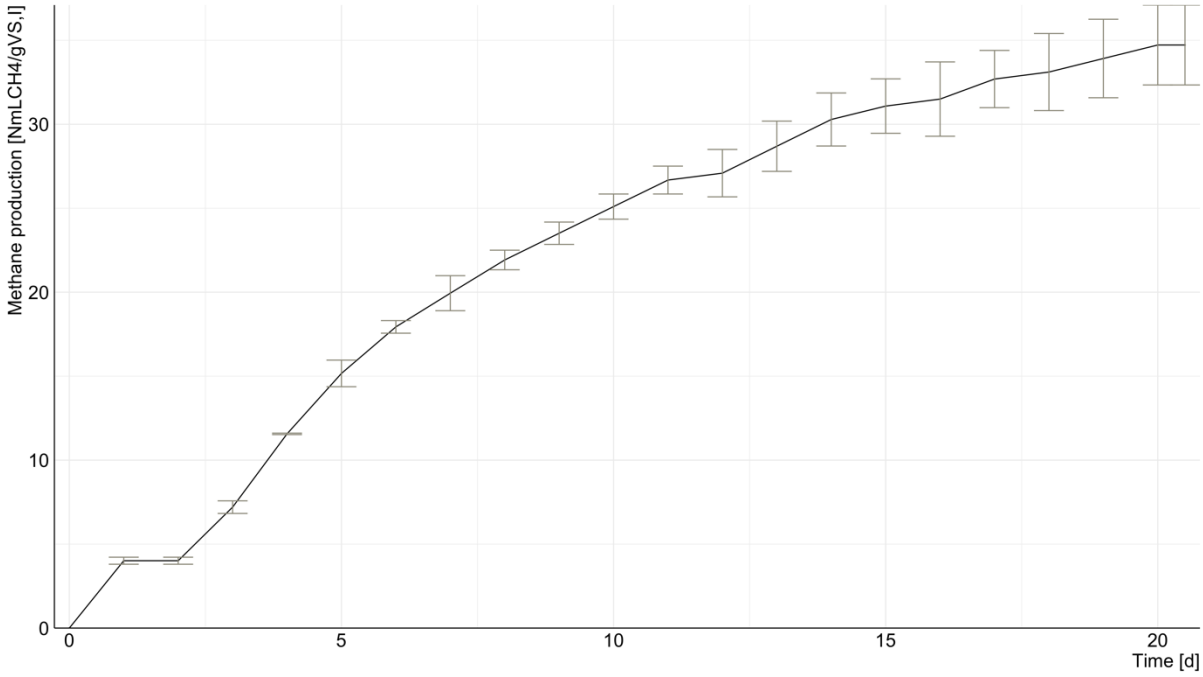

Figure D.2 - Methane production of blank BMP test (05/11/2020).

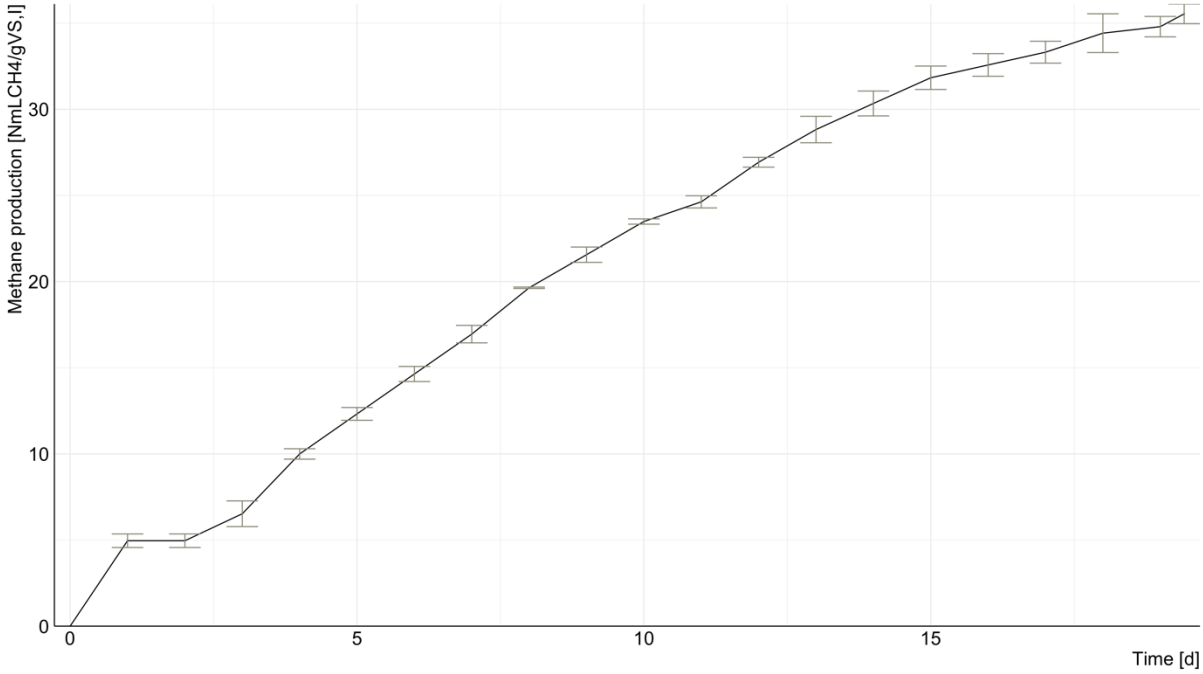


Figure D.3 - Methane production of blank BMP test (19/11/2020).

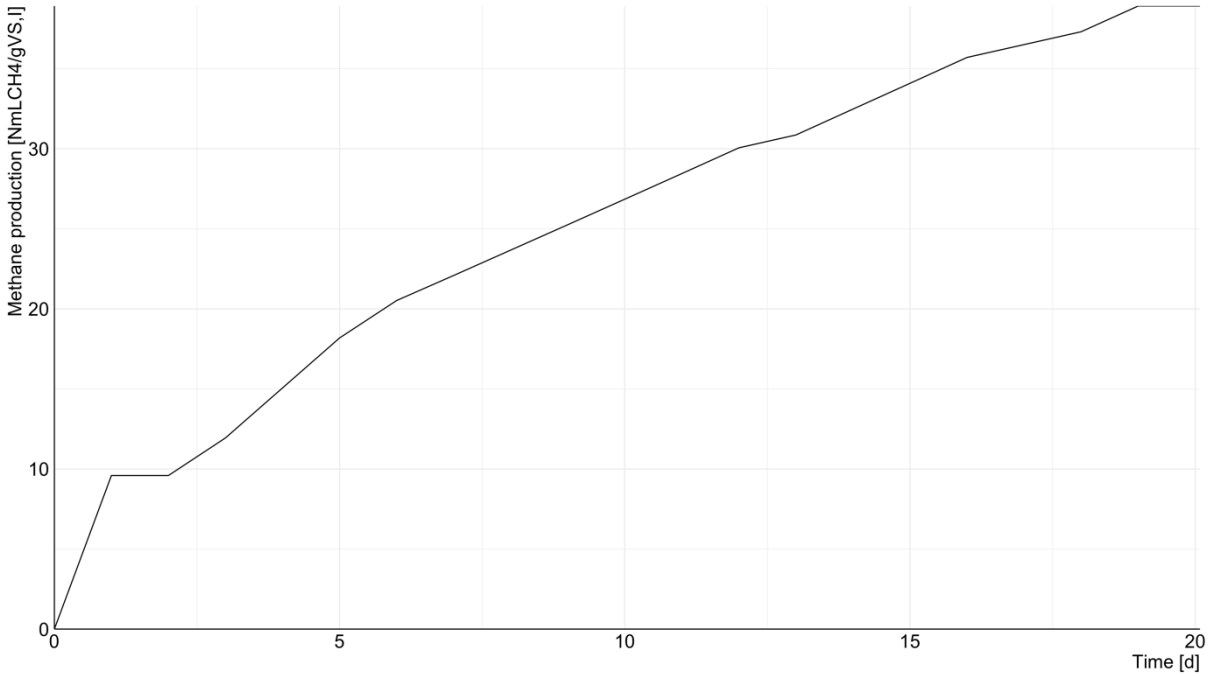


Figure D.4 - Methane production of blank BMP test (03/12/2020).

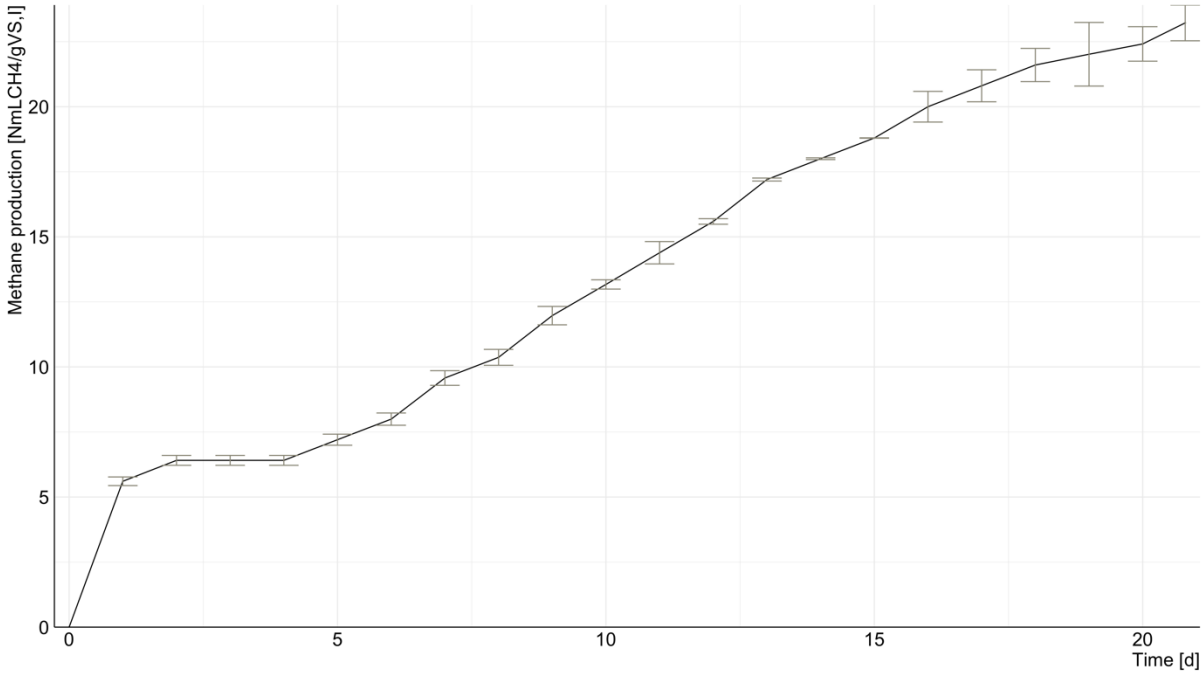


Figure D.5 - Methane production of blank BMP test (30/12/2020).

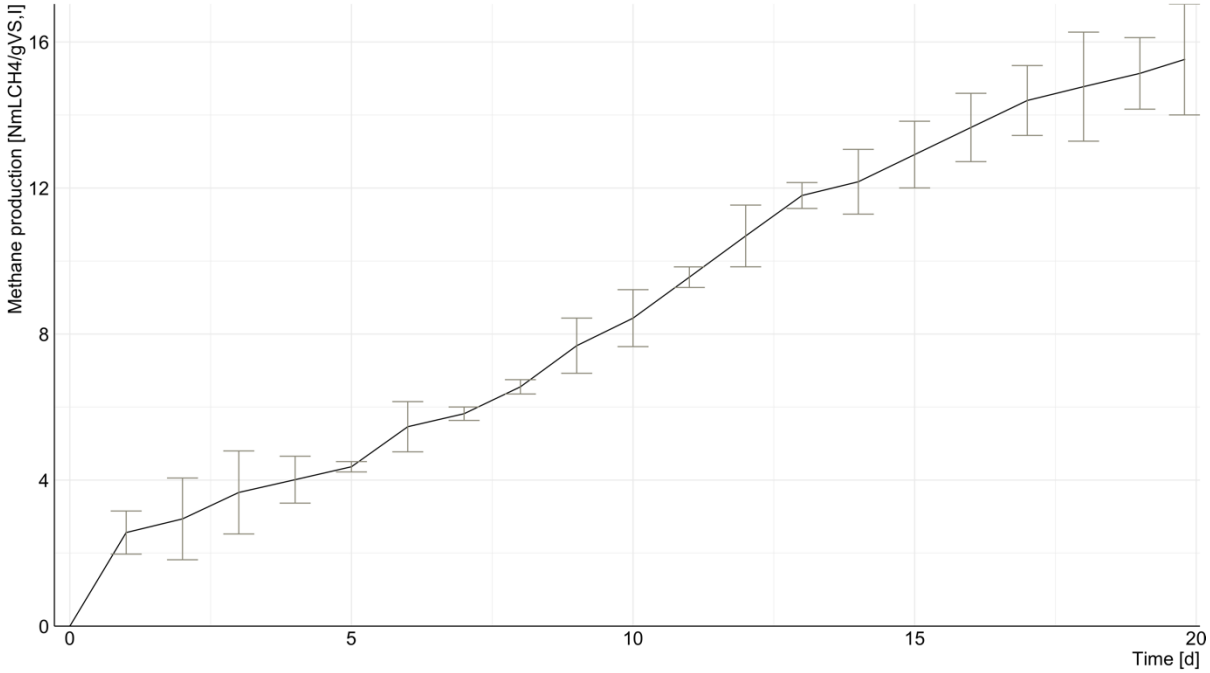


Figure D.6 - Methane production of blank BMP test (04/02/2021).

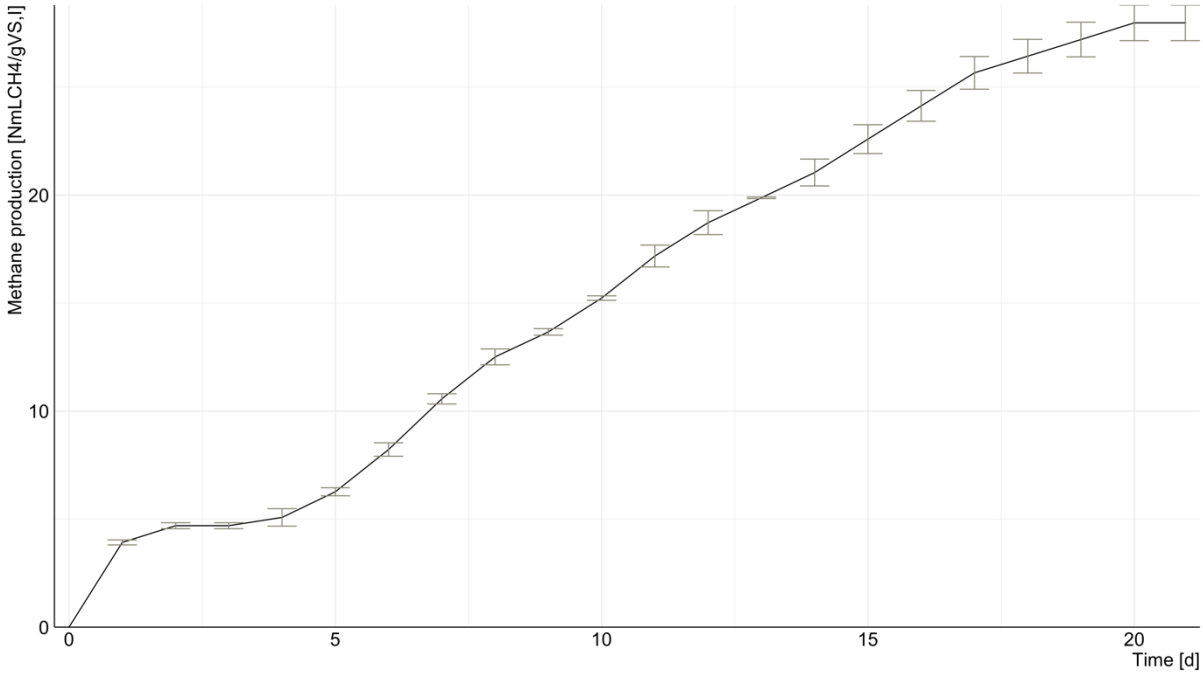


Figure D.7 - Methane production of blank BMP test (25/02/2021).

*Sludge*

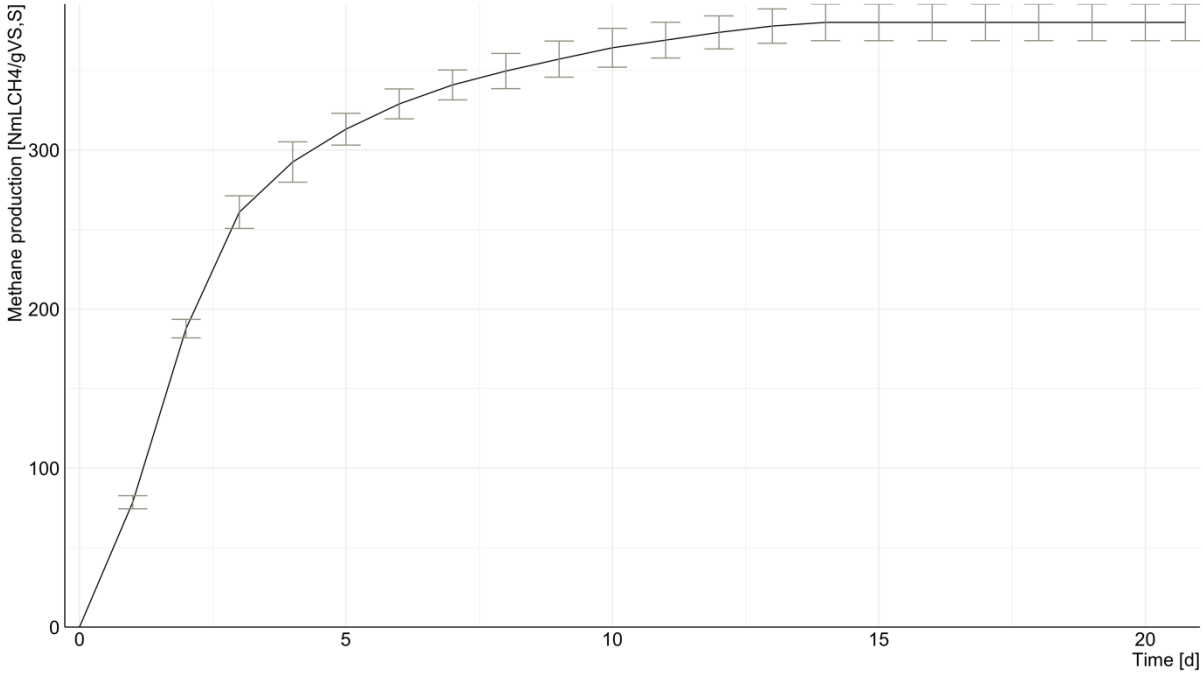


Figure D.8 - Methane production of sludge BMP test (22/10/2020).

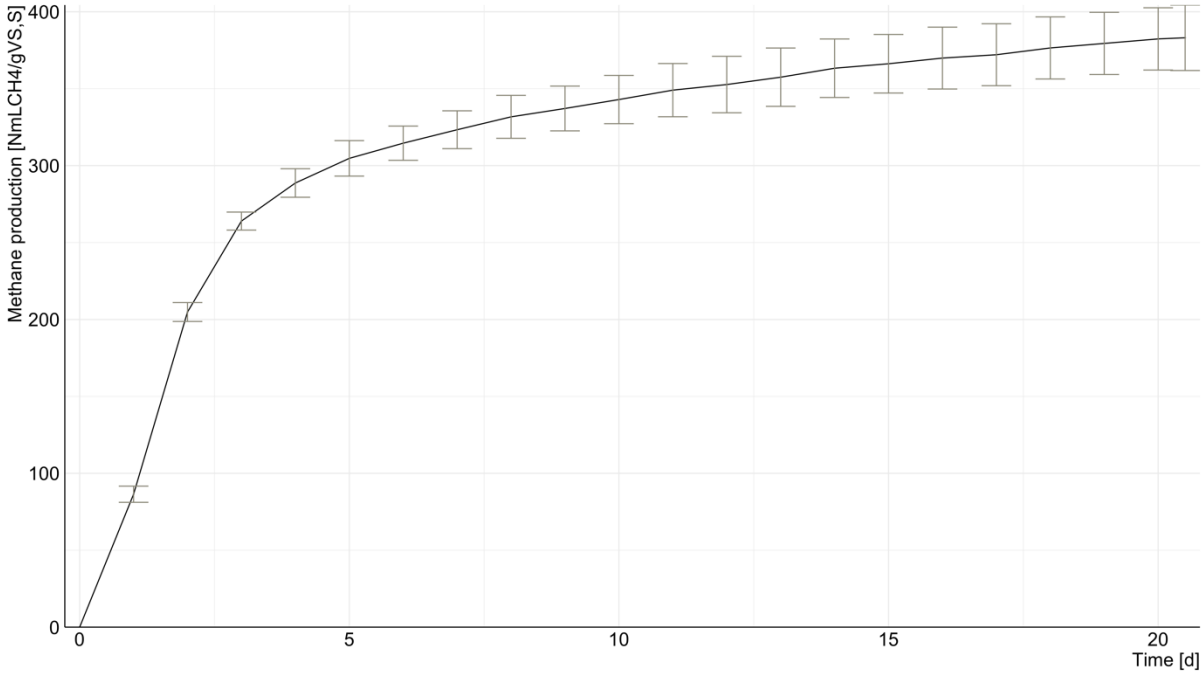


Figure D.9 - Methane production of sludge BMP test (05/11/2020).

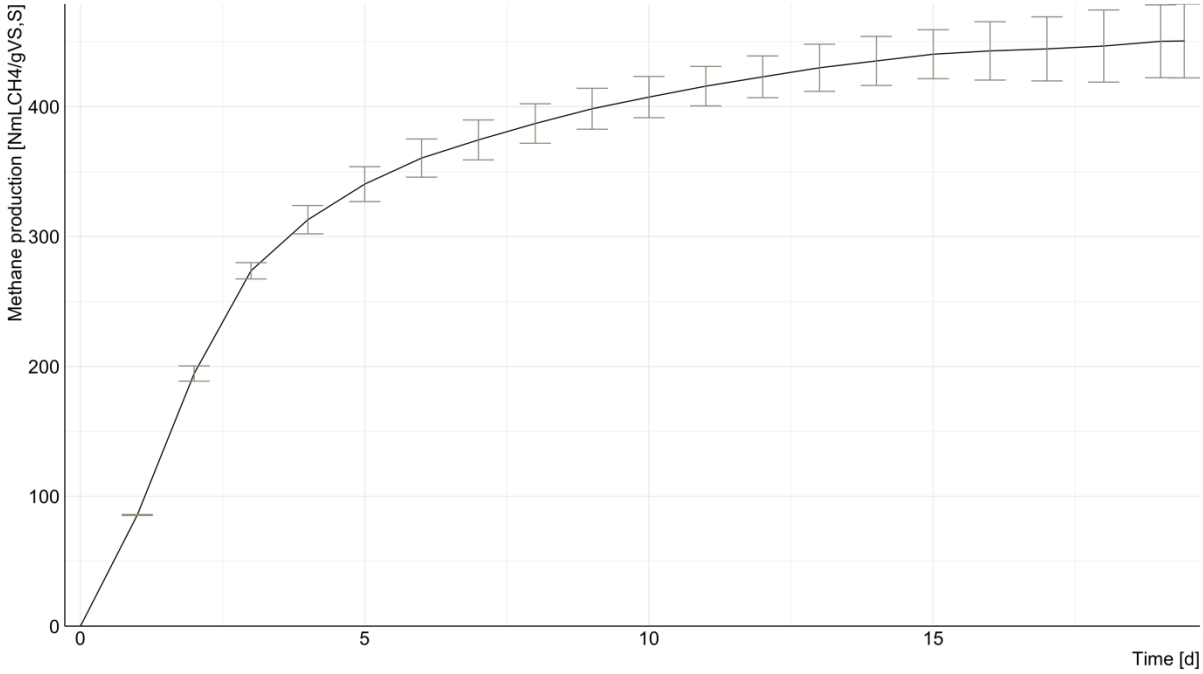


Figure D.10 - Methane production of sludge BMP test (19/11/2020).

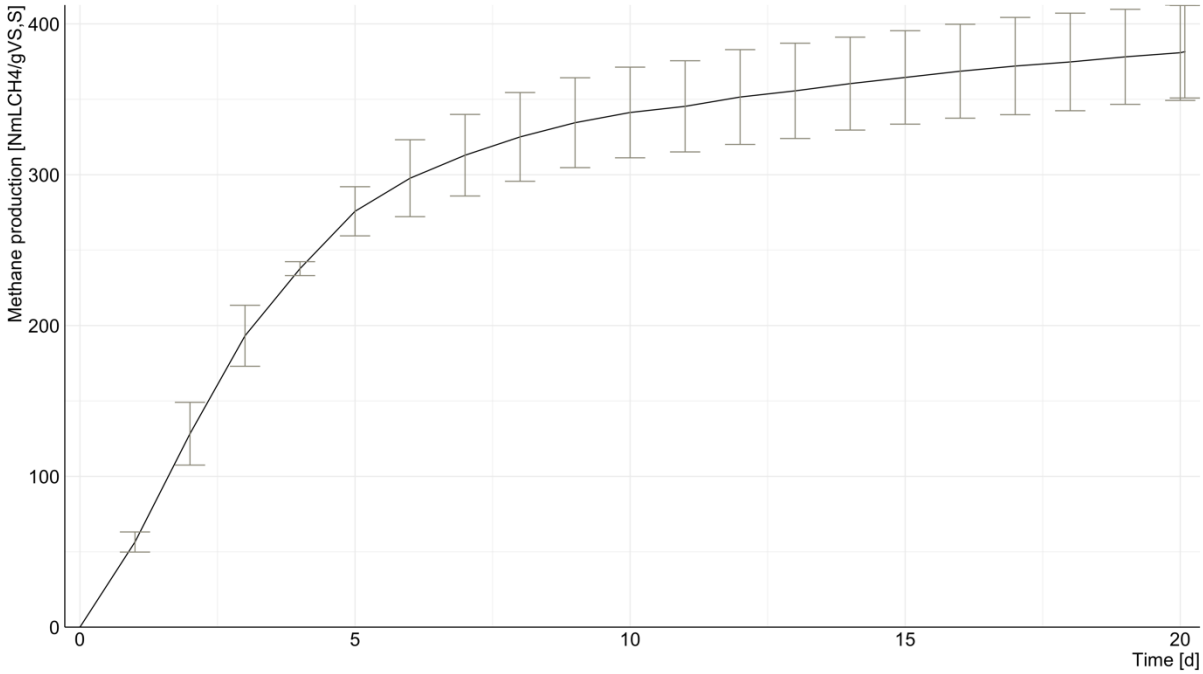


Figure D.11 - Methane production of sludge BMP test (03/12/2020).

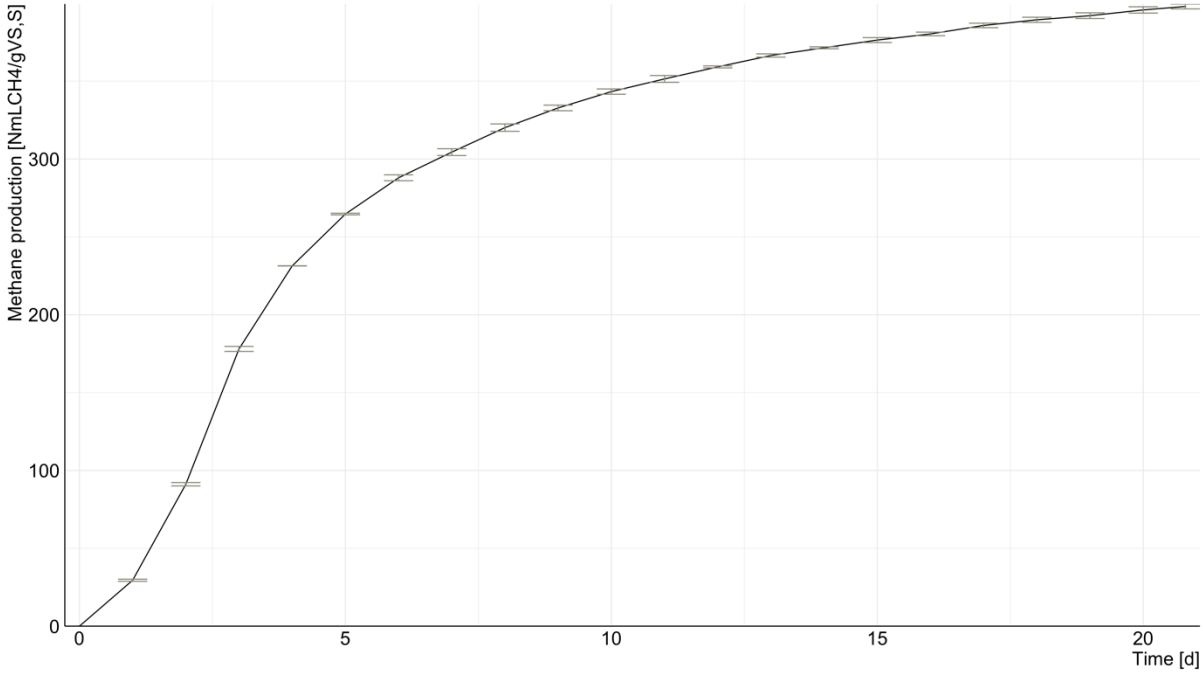


Figure D.12 - Methane production of sludge BMP test (30/12/2020).

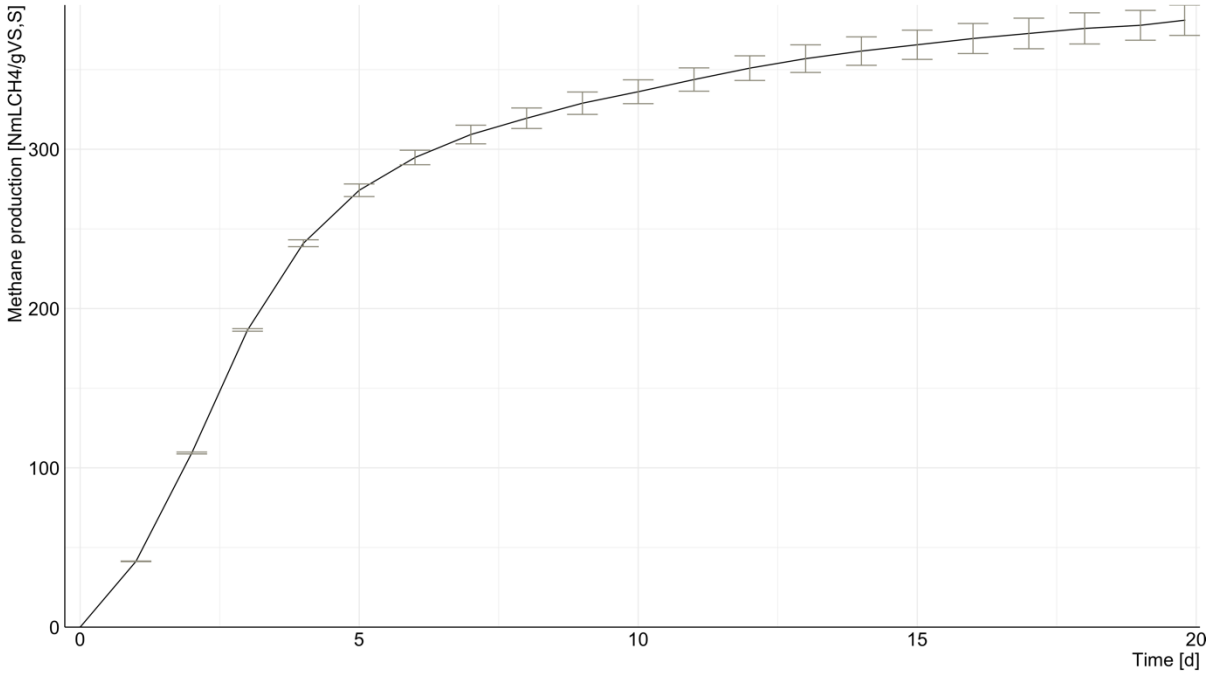


Figure D.13 - Methane production of sludge BMP test (04/02/2021).

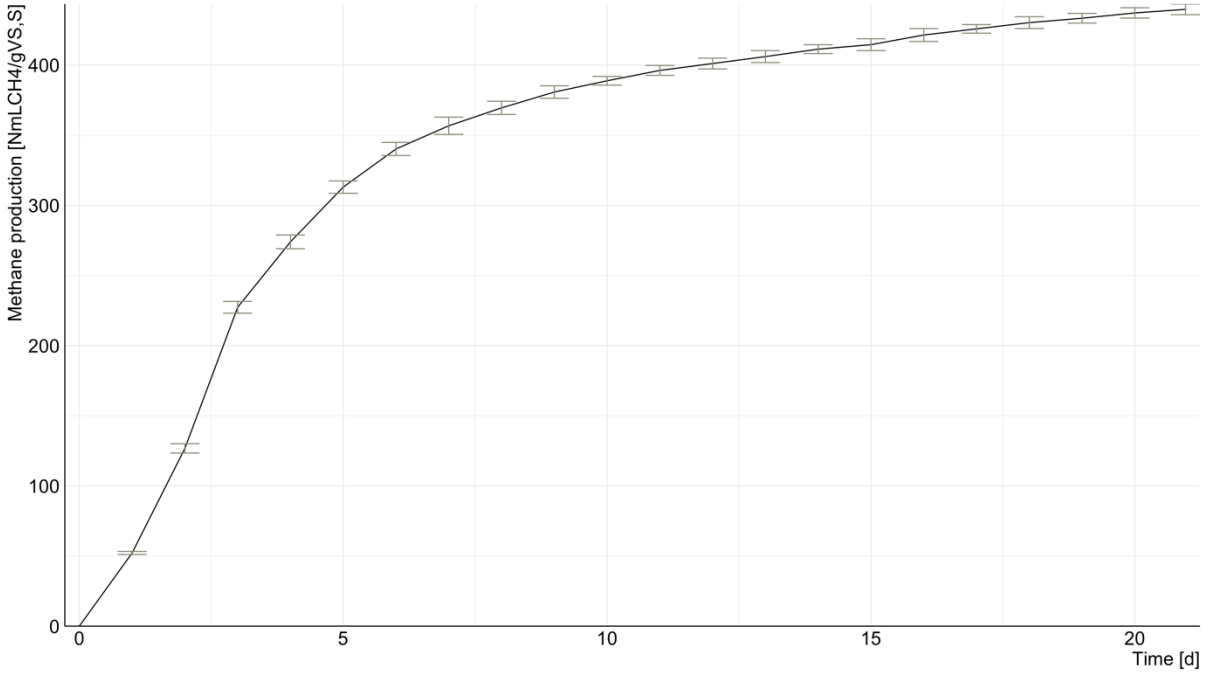


Figure D.14 - Methane production of sludge BMP test (25/02/2021).

*Particulate sludge*

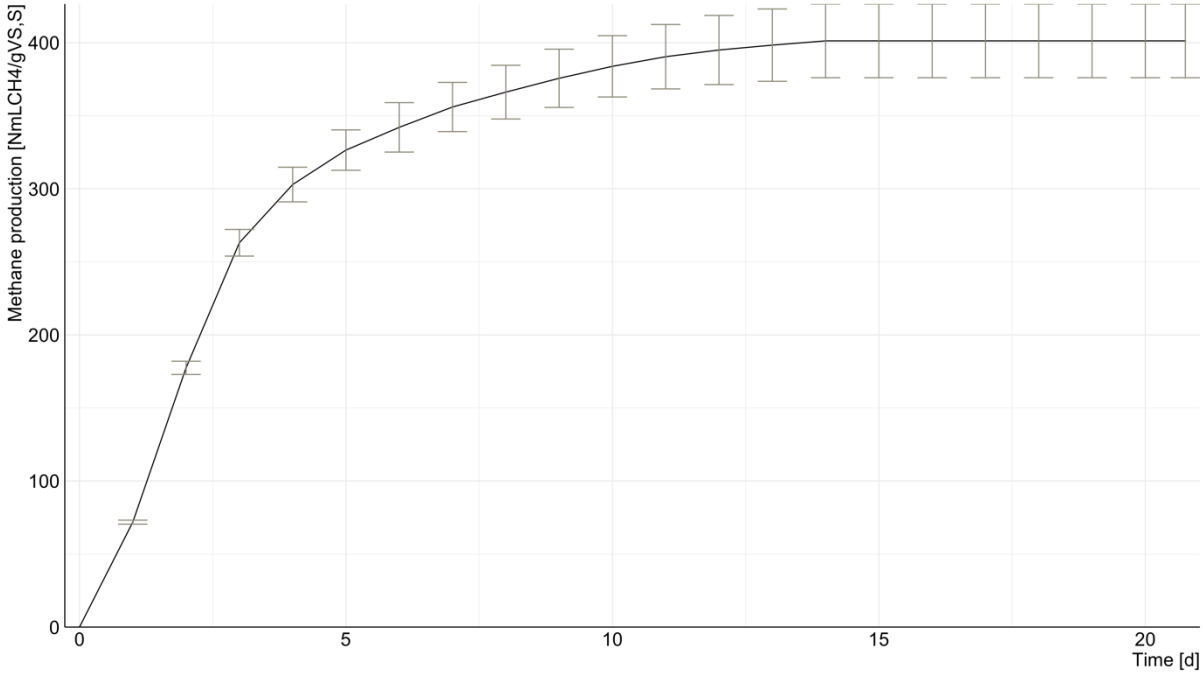


Figure D.15 - Methane production of particulate sludge BMP test (22/10/2020).

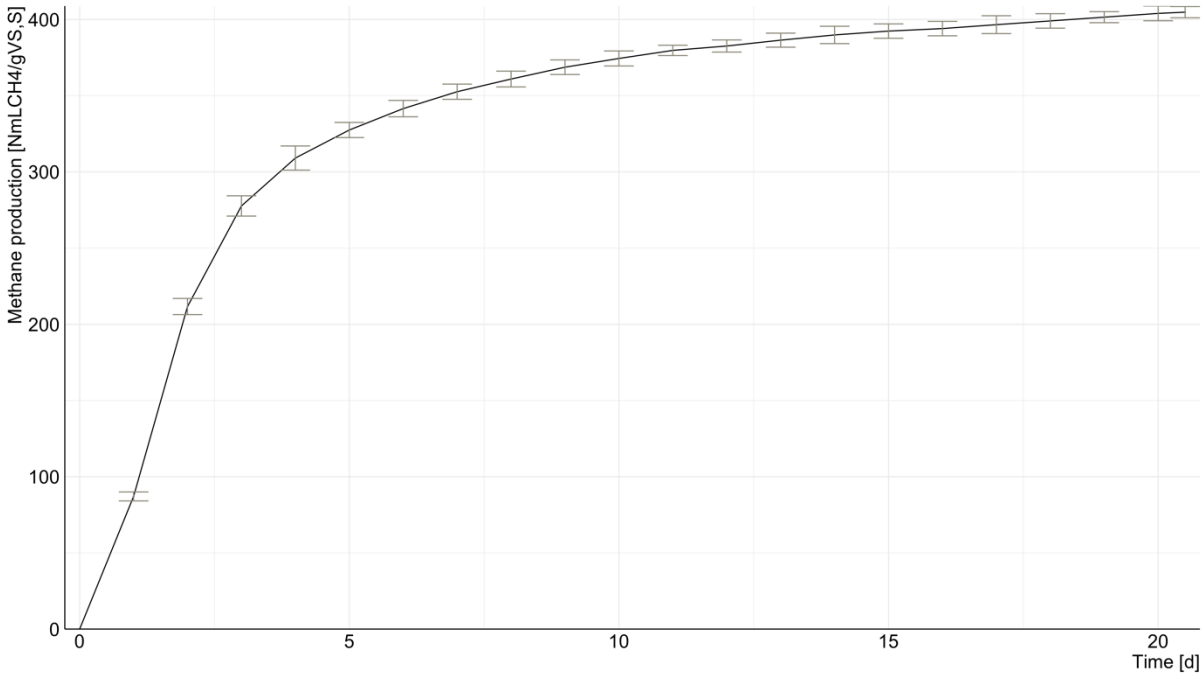


Figure D.16 - Methane production of particulate sludge BMP test (05/11/2020).

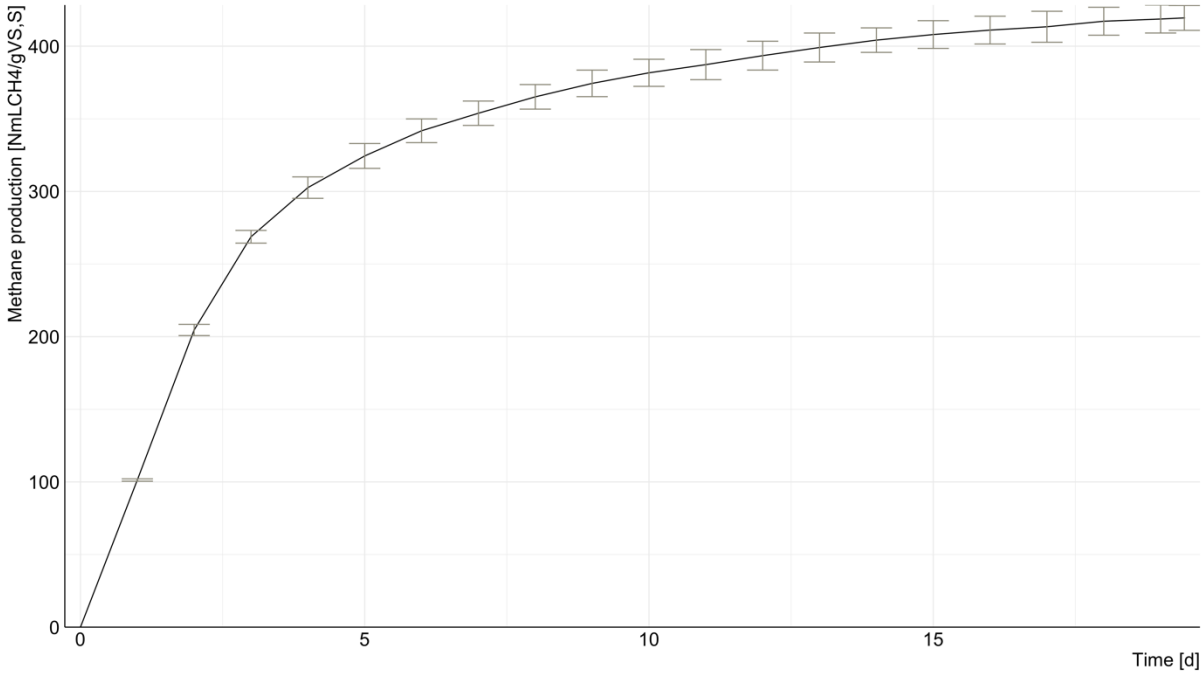


Figure D.17 - Methane production of particulate sludge BMP test (19/11/2020).

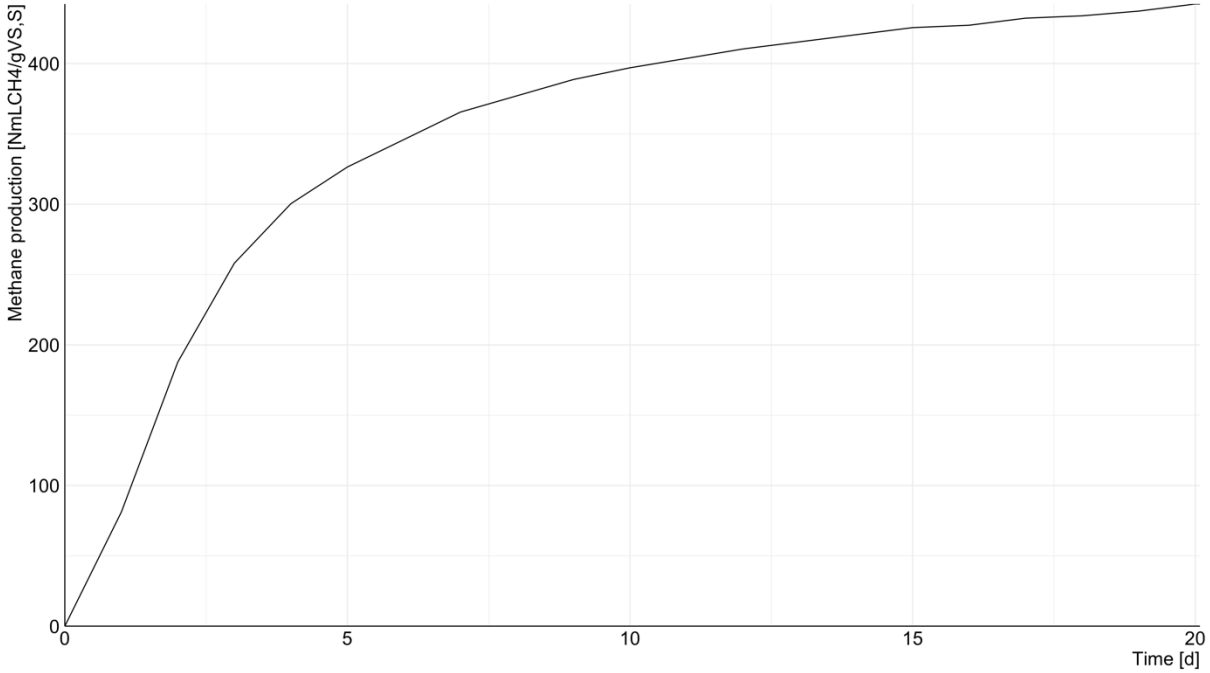


Figure D.18 - Methane production of particulate sludge BMP test (03/12/2020).

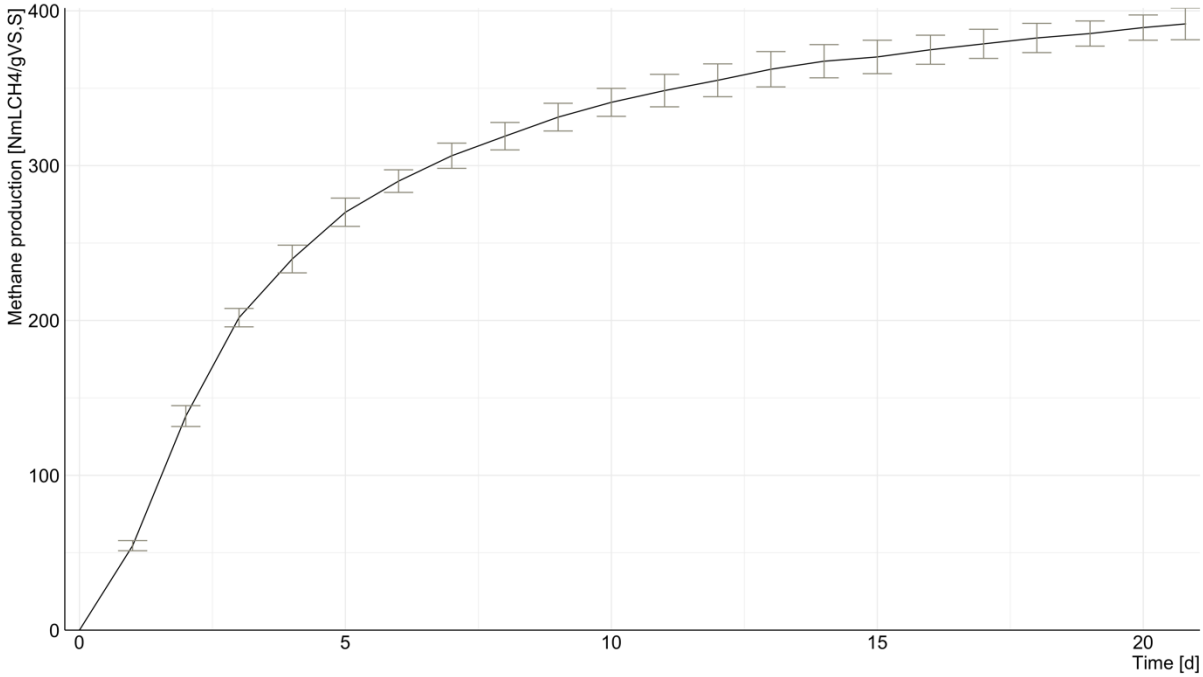


Figure D.19 - Methane production of particulate sludge BMP test (30/12/2020).

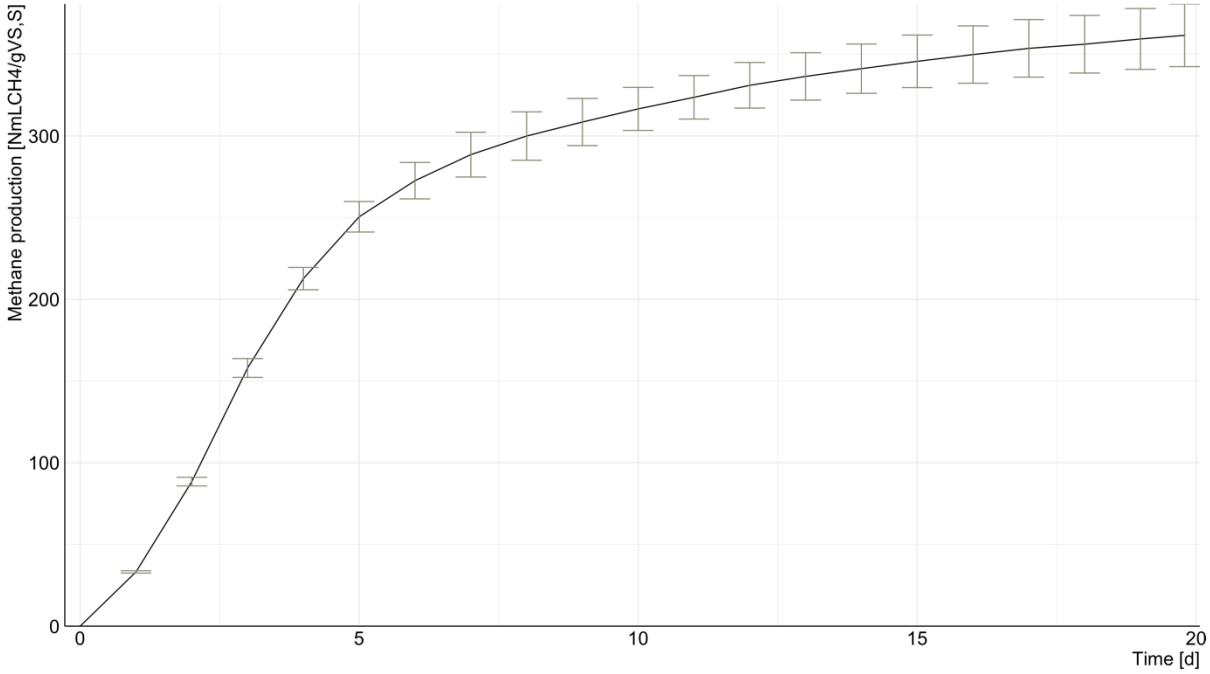


Figure D.20 - Methane production of particulate sludge BMP test (04/02/2021).

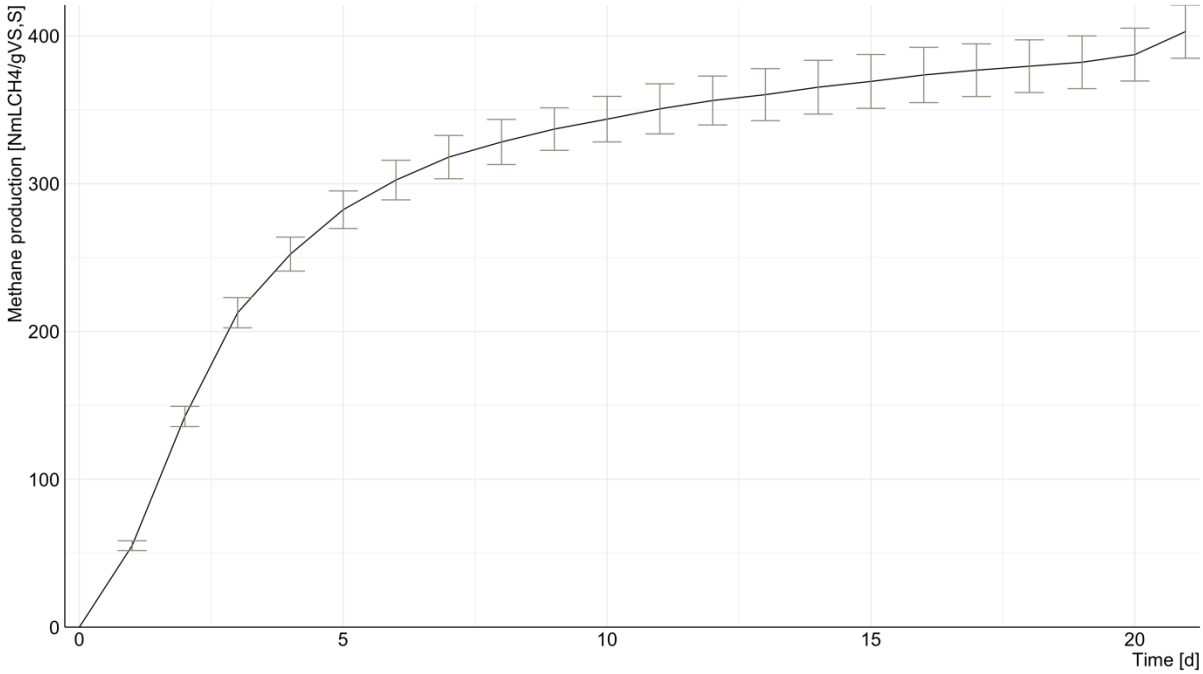


Figure D.21 - Methane production of particulate sludge BMP test (25/02/2021).

*Yogurt*

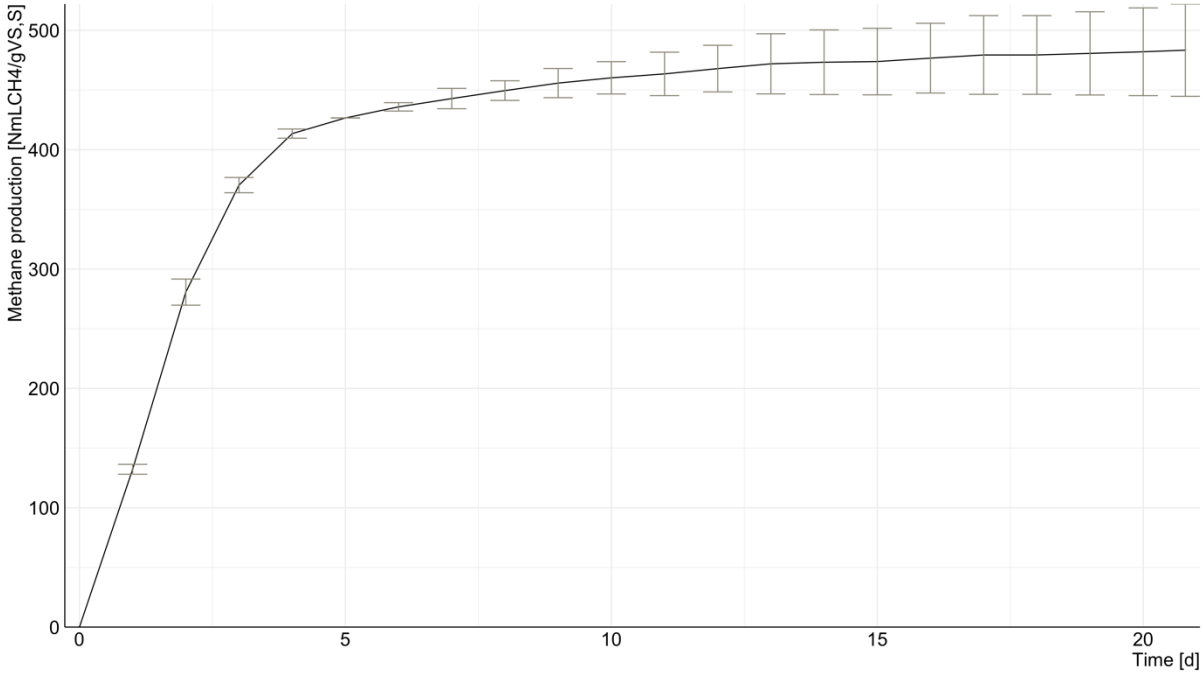


Figure D.22 - Methane production of yogurt BMP test (30/12/2020).

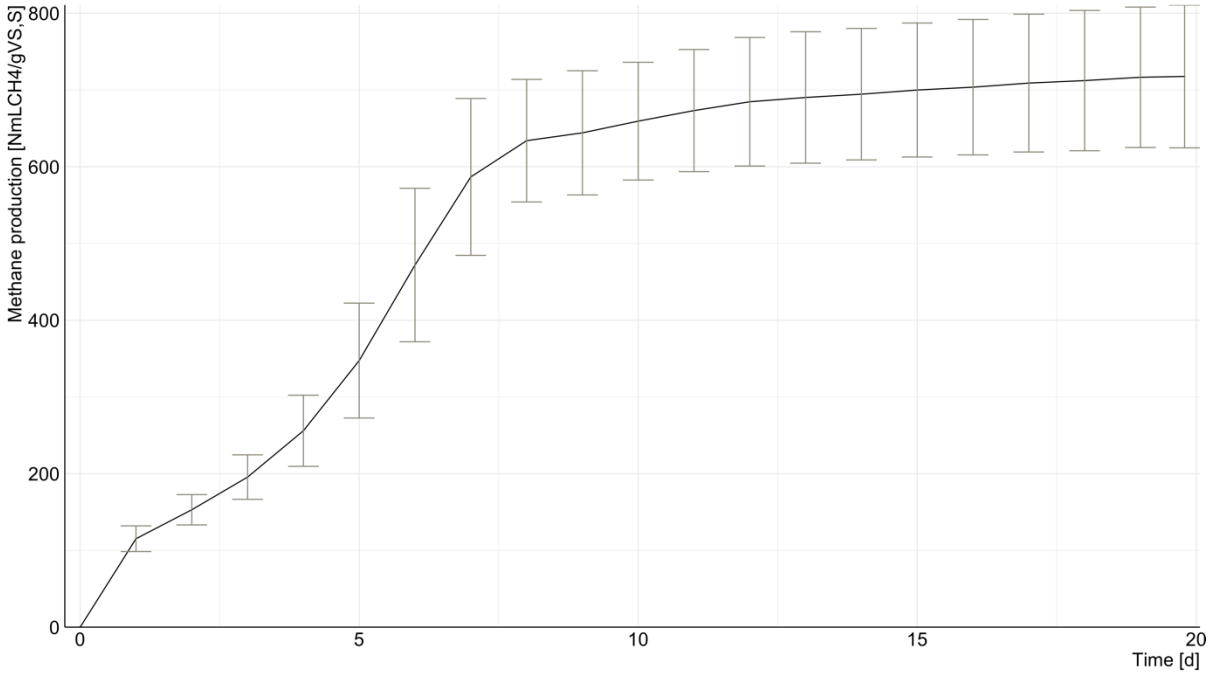


Figure D.23 - Methane production of yogurt BMP test (04/02/2021).

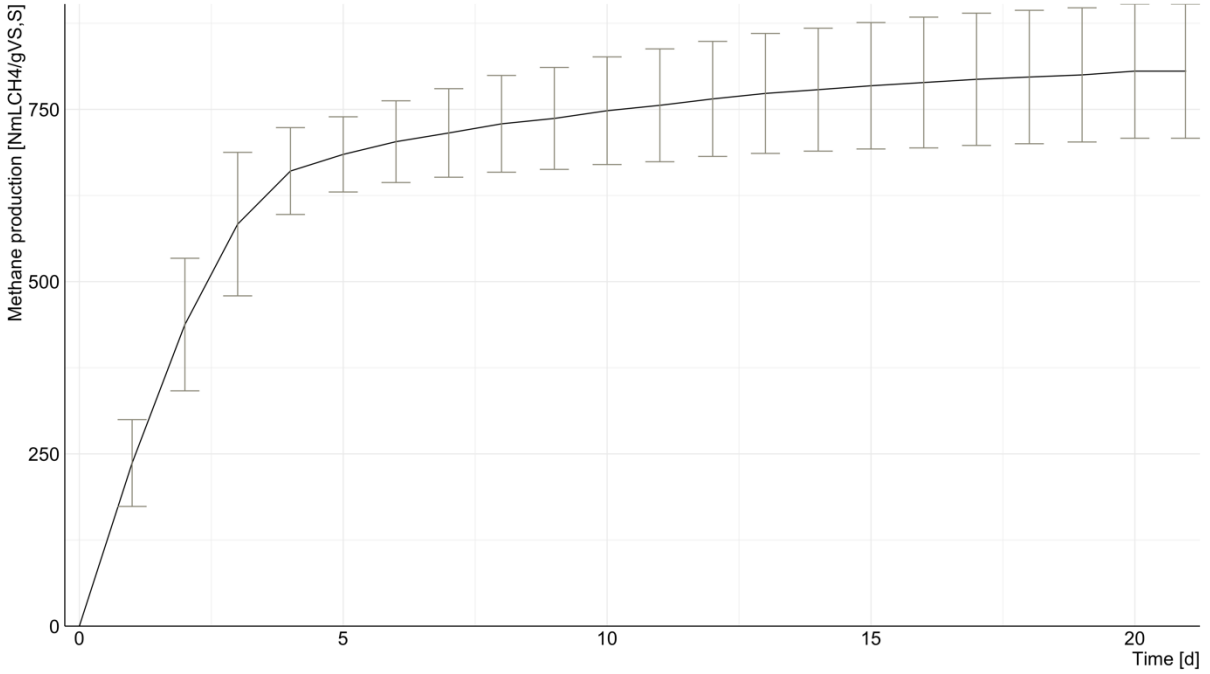


Figure D.24 - Methane production of yogurt BMP test (25/02/2021).

*Co-digestion*

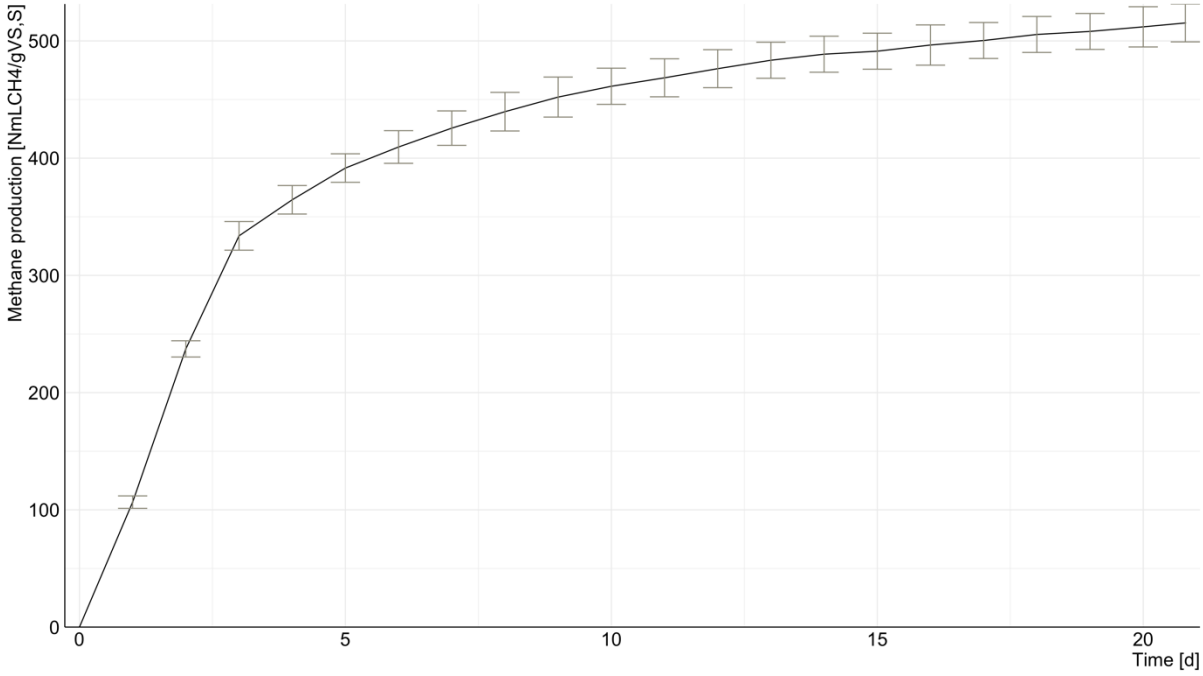


Figure D.25 - Methane production of co-digestion BMP test (30/12/2020).

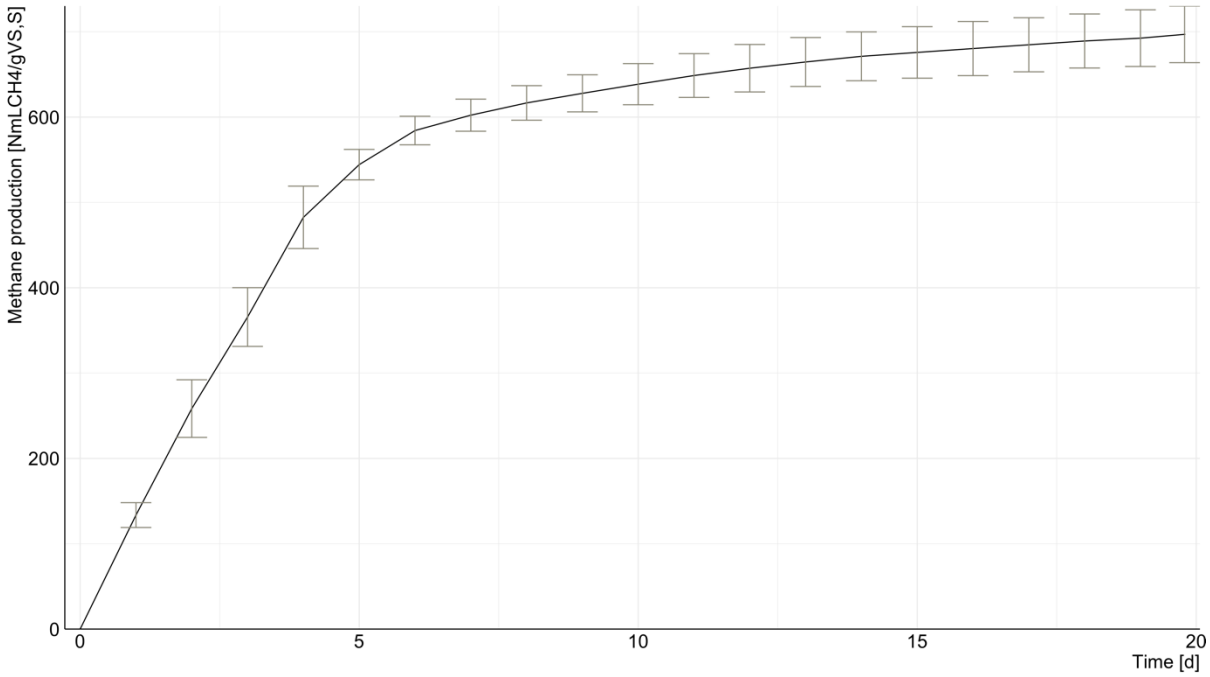


Figure D.26 - Methane production of co-digestion BMP test (04/02/2021).

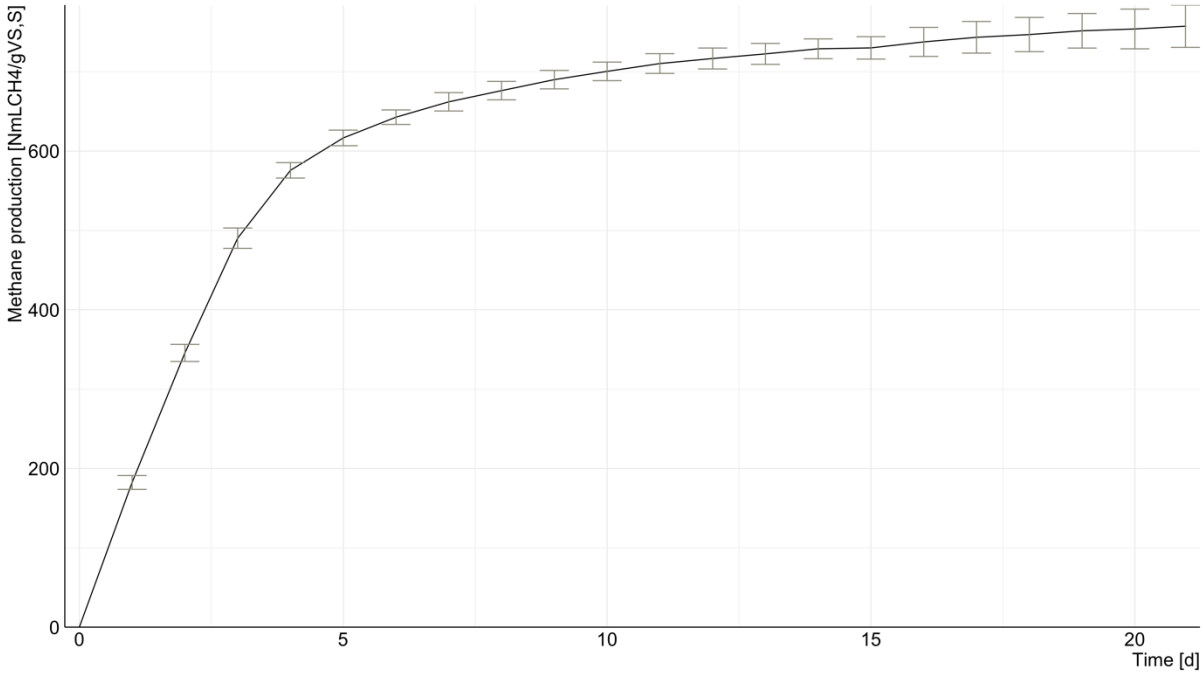


Figure D.27 - Methane production of co-digestion BMP test (25/02/2021).

*Residual*

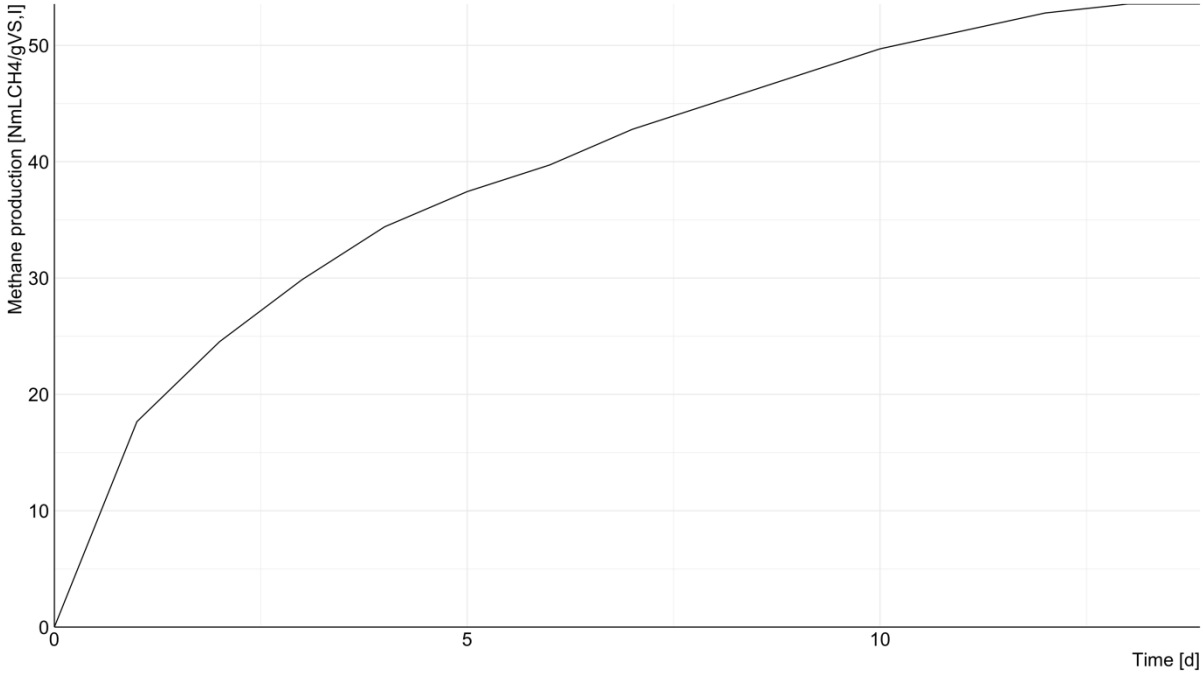


Figure D.28 - Methane production of residual BMP test (22/10/2020).

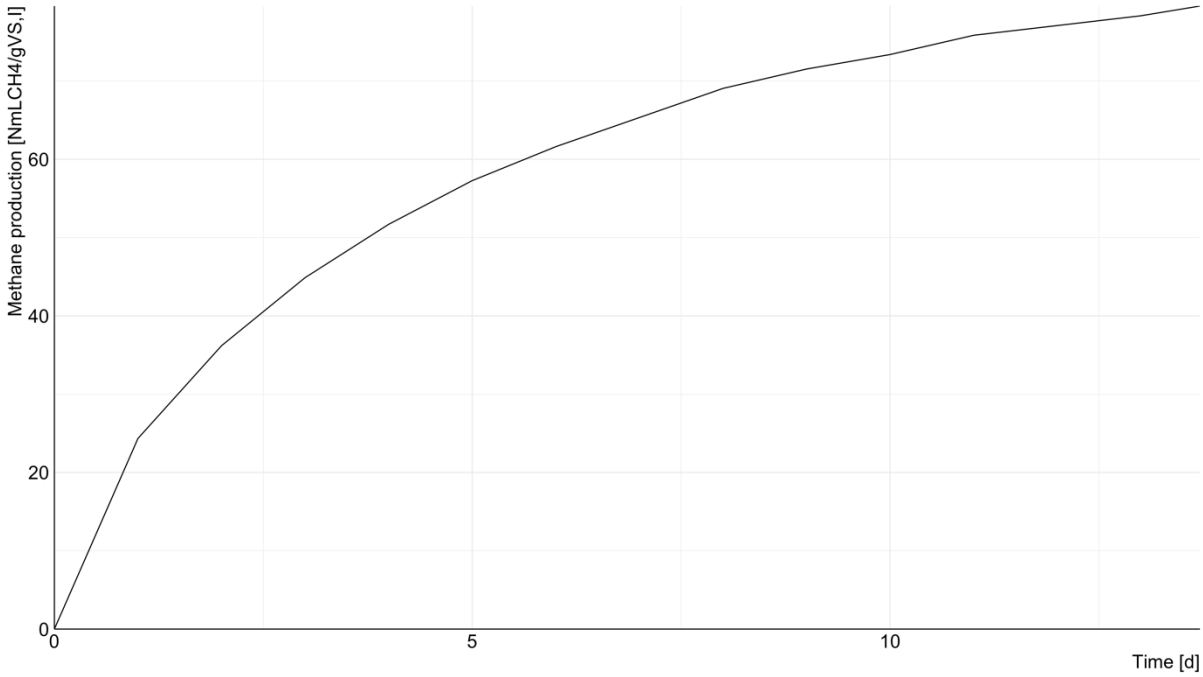


Figure D.0.29 - Methane production of residual BMP test (05/11/2020).

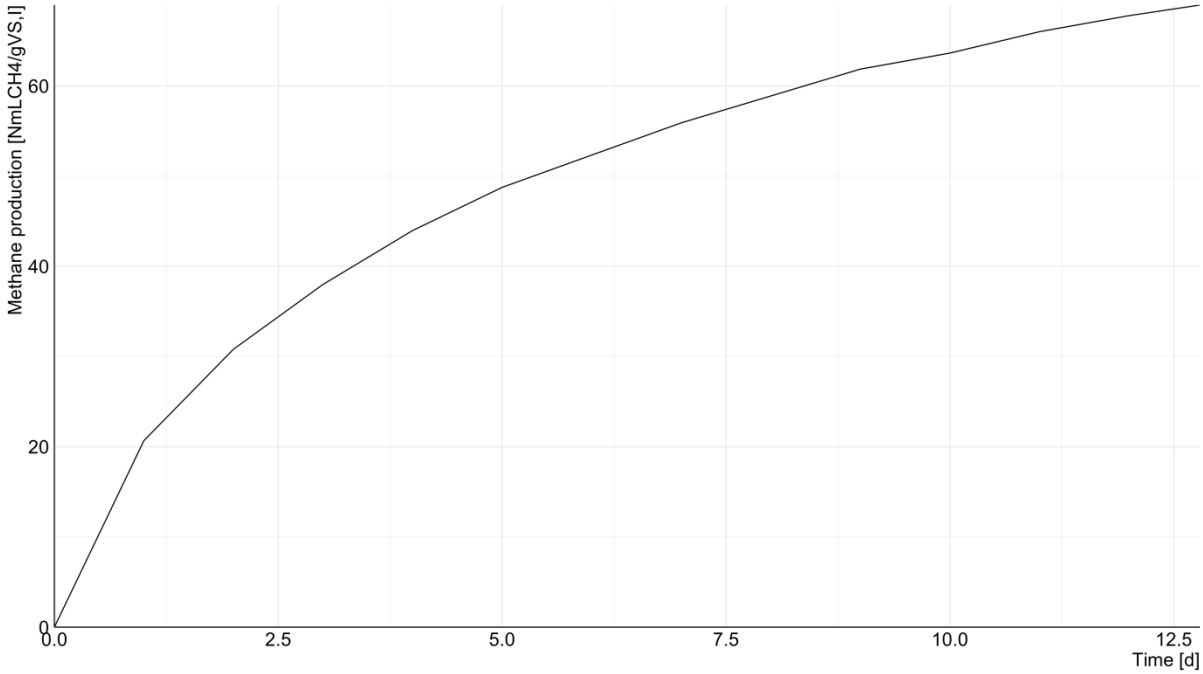


Figure D.30 - Methane production of residual BMP test (19/11/2020).

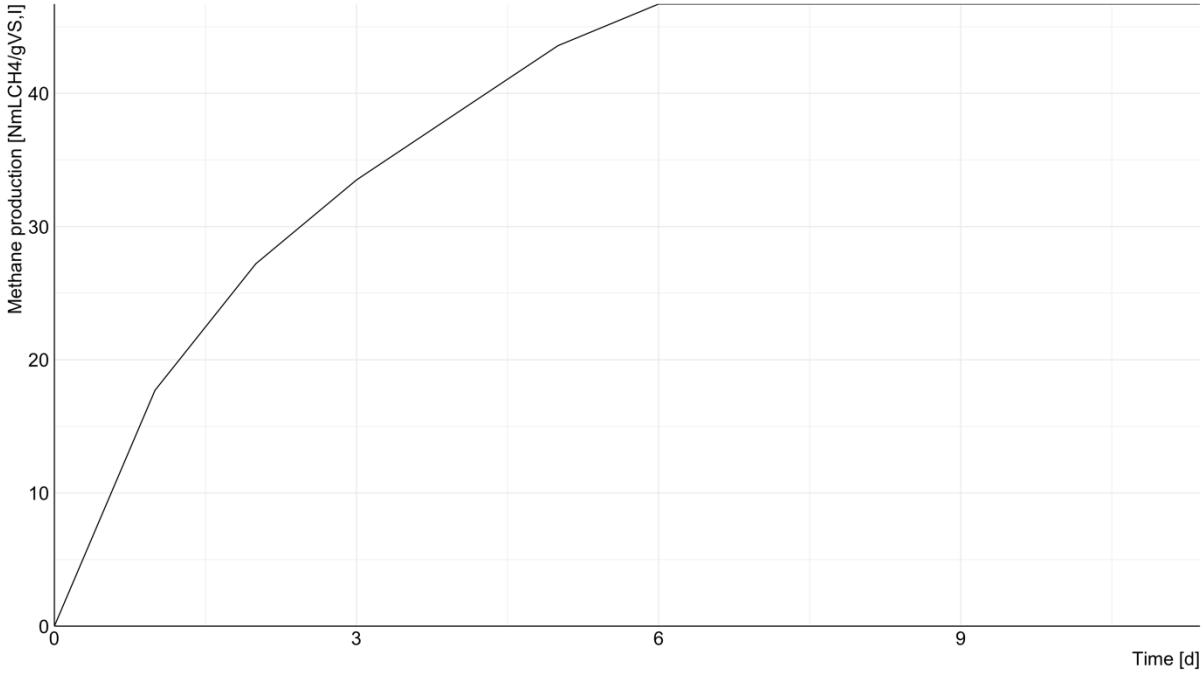


Figure D.31 - Methane production of residual BMP test (26/11/2020).

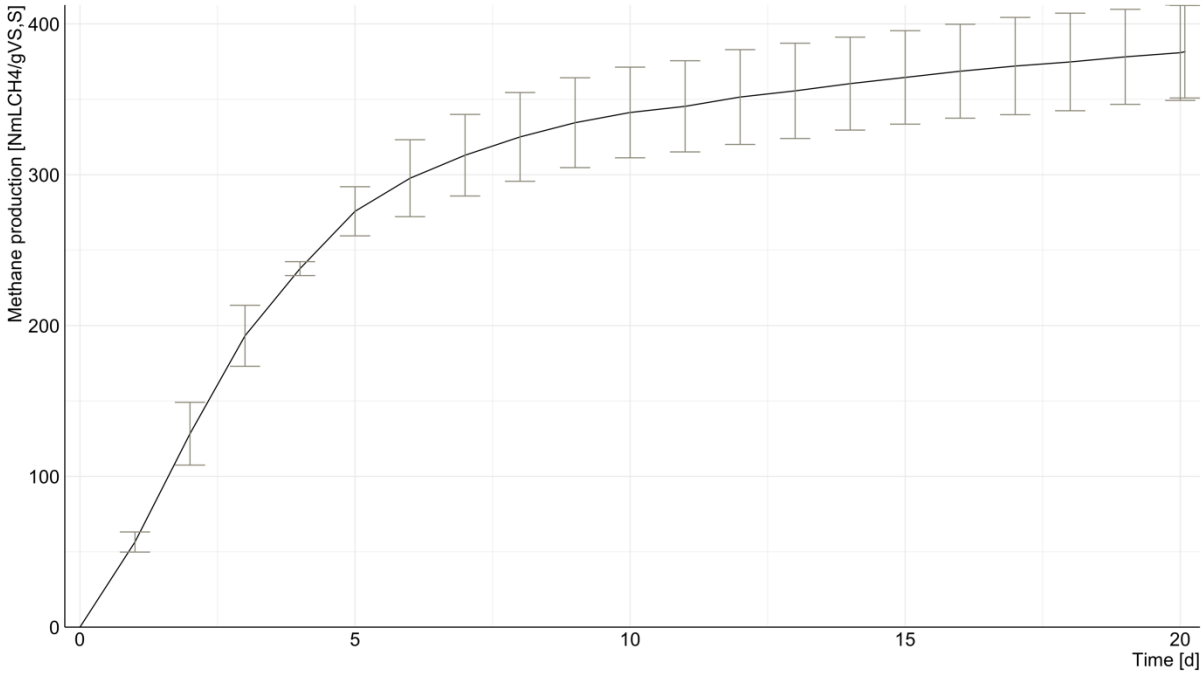


Figure D.32 - Methane production of residual BMP test (03/12/2020).

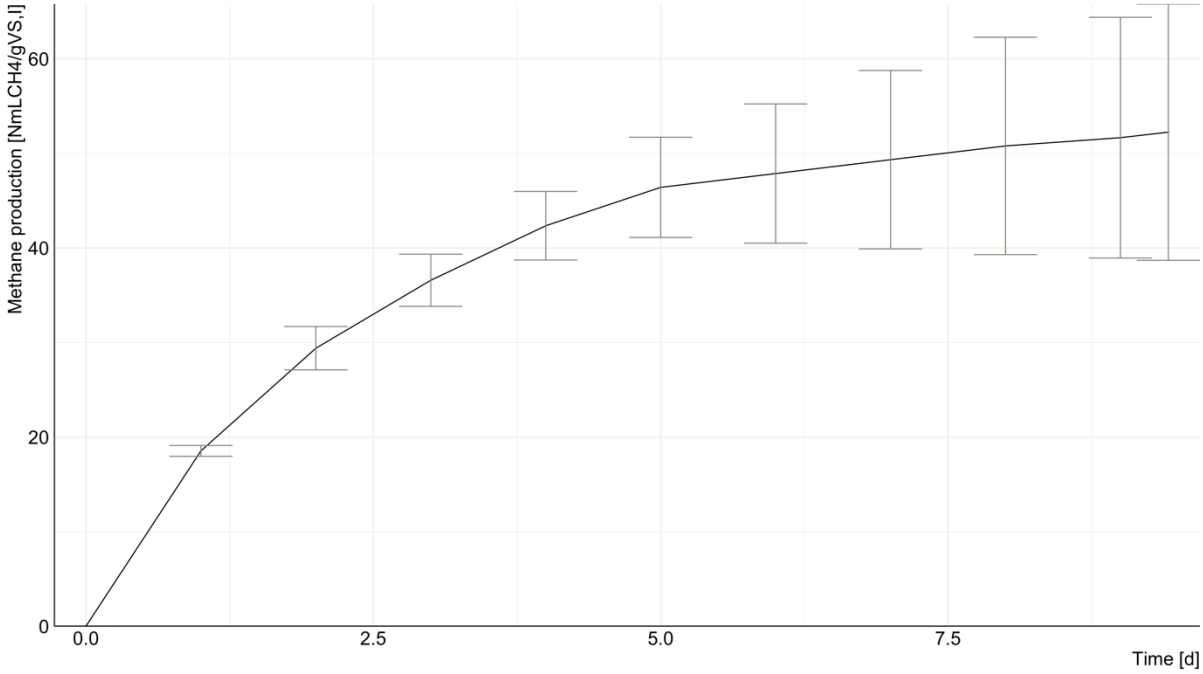


Figure D.33 - Methane production of residual BMP test (10/12/2020).

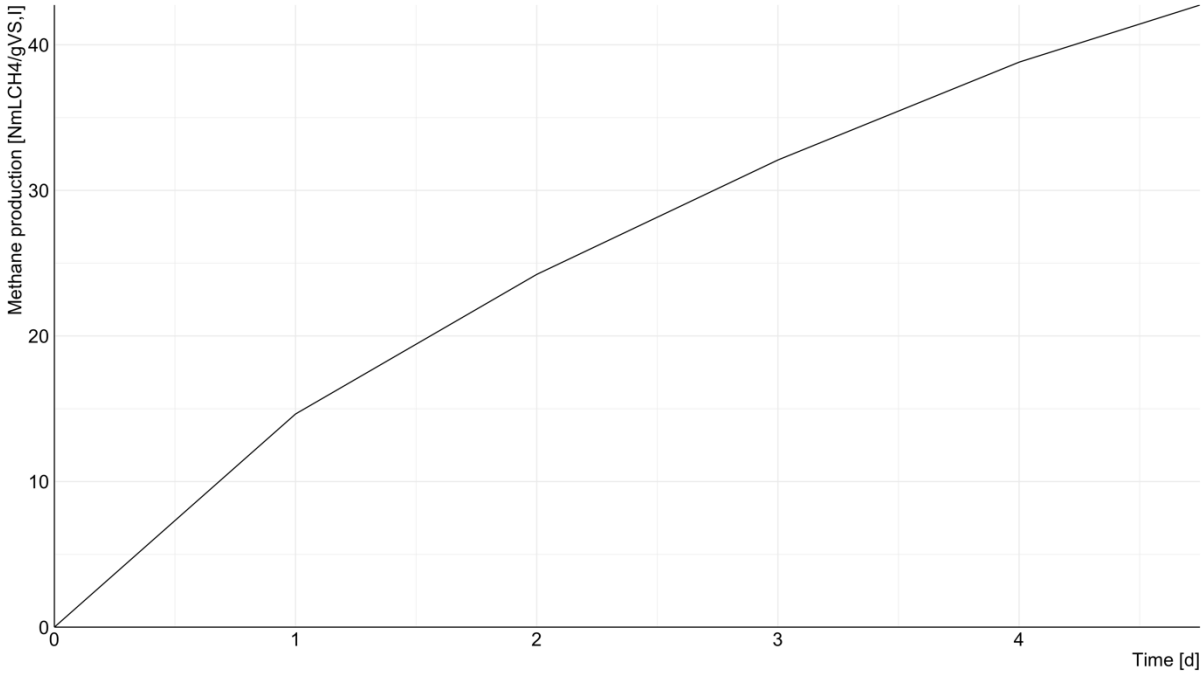


Figure D.34 - Methane production of residual BMP test (17/12/2020).

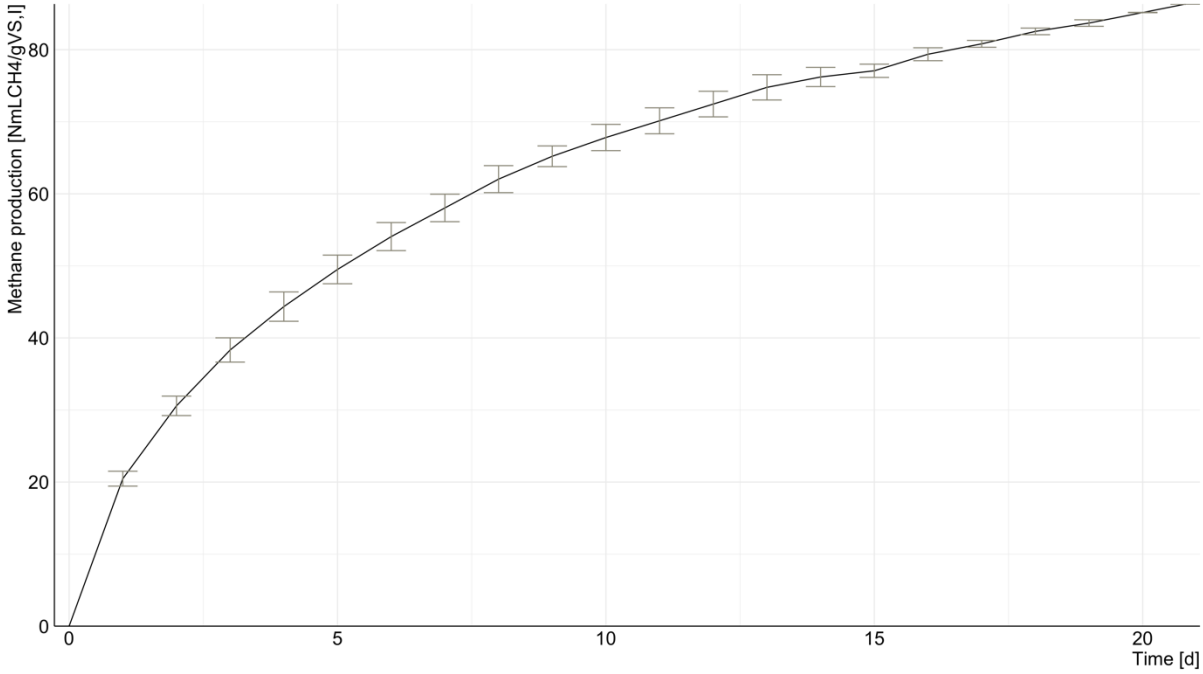


Figure D.35 - Methane production of residual BMP test (30/12/2020).

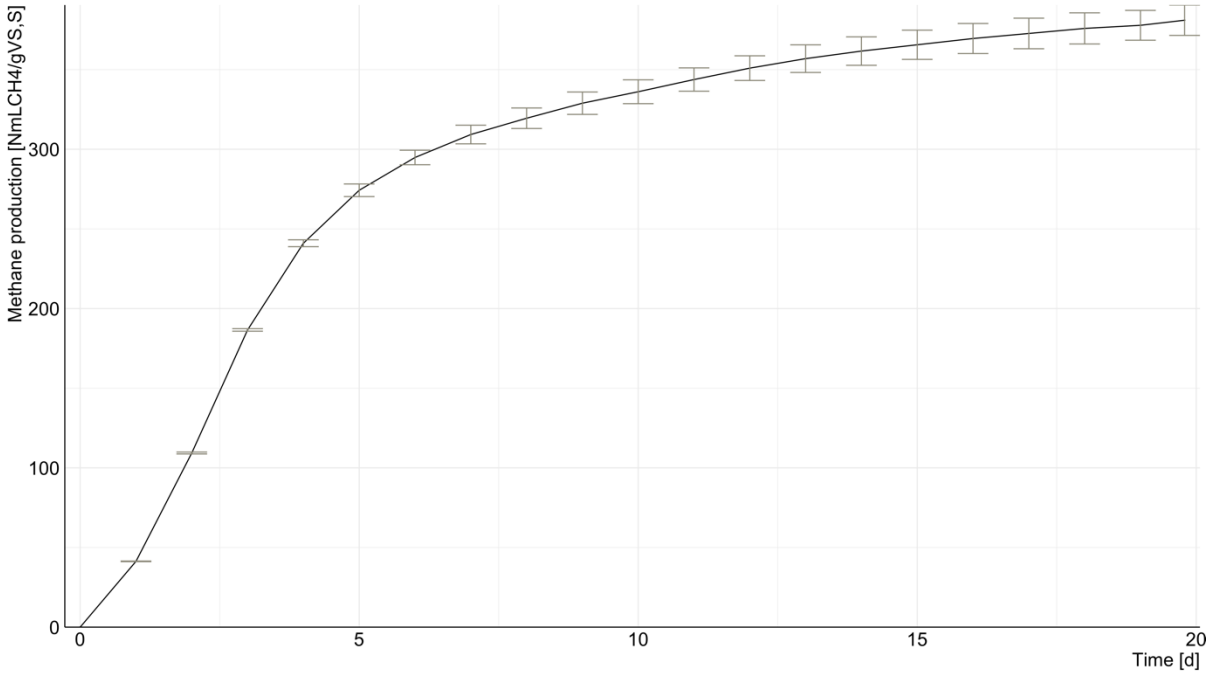


Figure D.36 - Methane production of residual BMP test (04/02/2021).

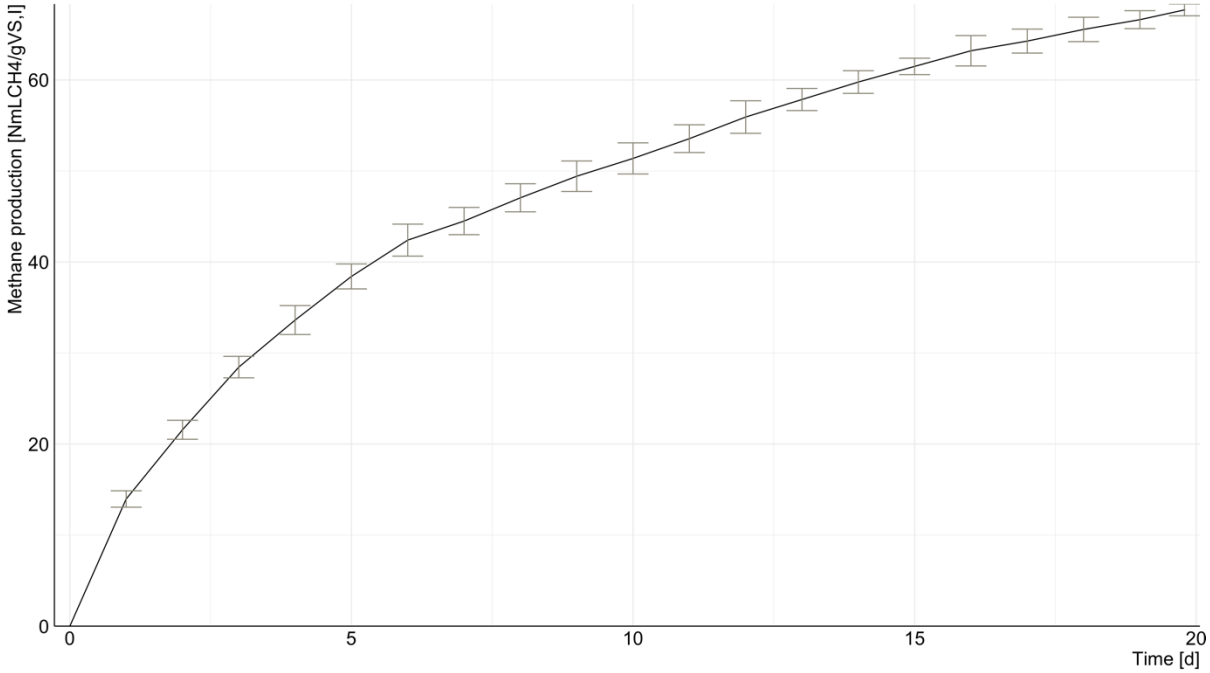


Figure D.37 - Methane production of residual BMP test (25/02/2021).

# APPENDIX E

This appendix shows the graphs of the specific production of methane by mass of COD for each of the biomass activity test carried out during the experimentation.

## *Acetate activity tests*

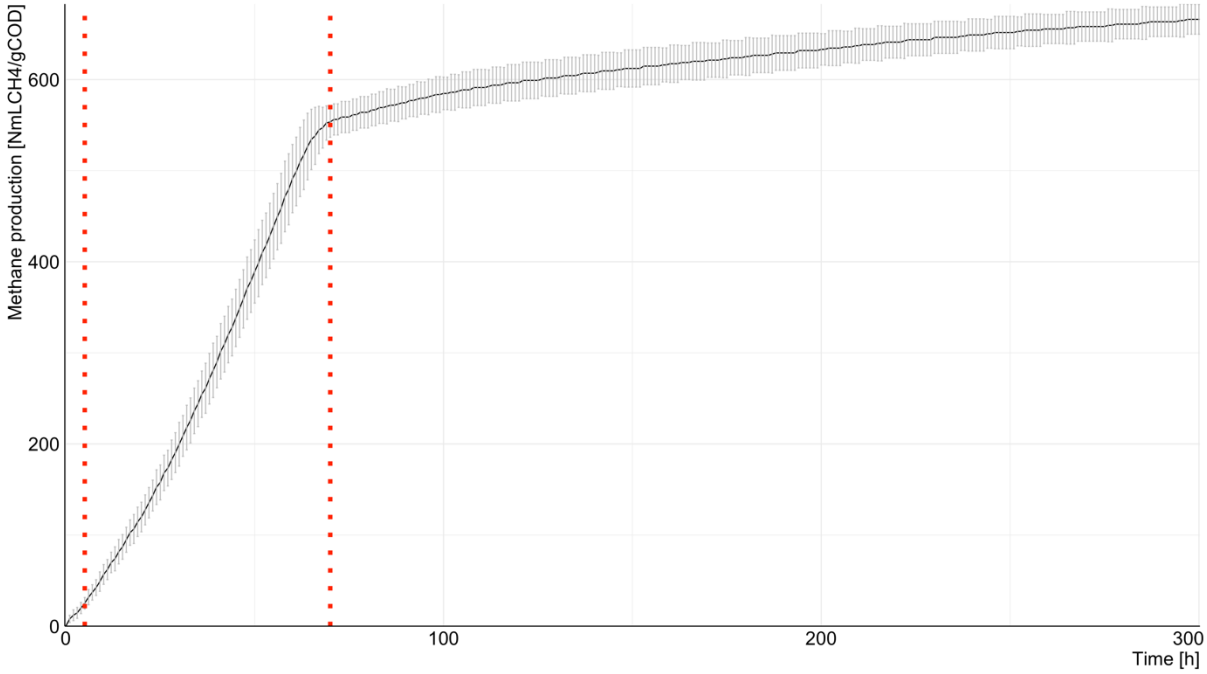


Figure E.1 - Methane production of acetate activity test (22/10/2020).

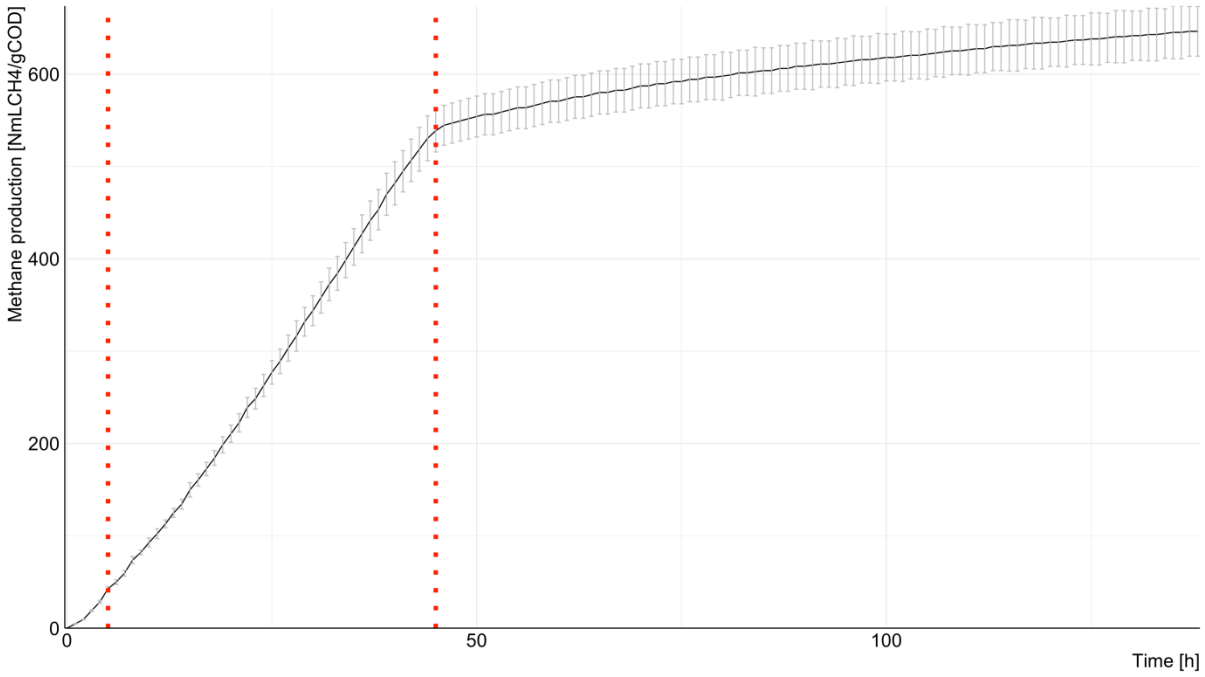


Figure E.2 - Methane production of acetate activity test (26/11/2020).

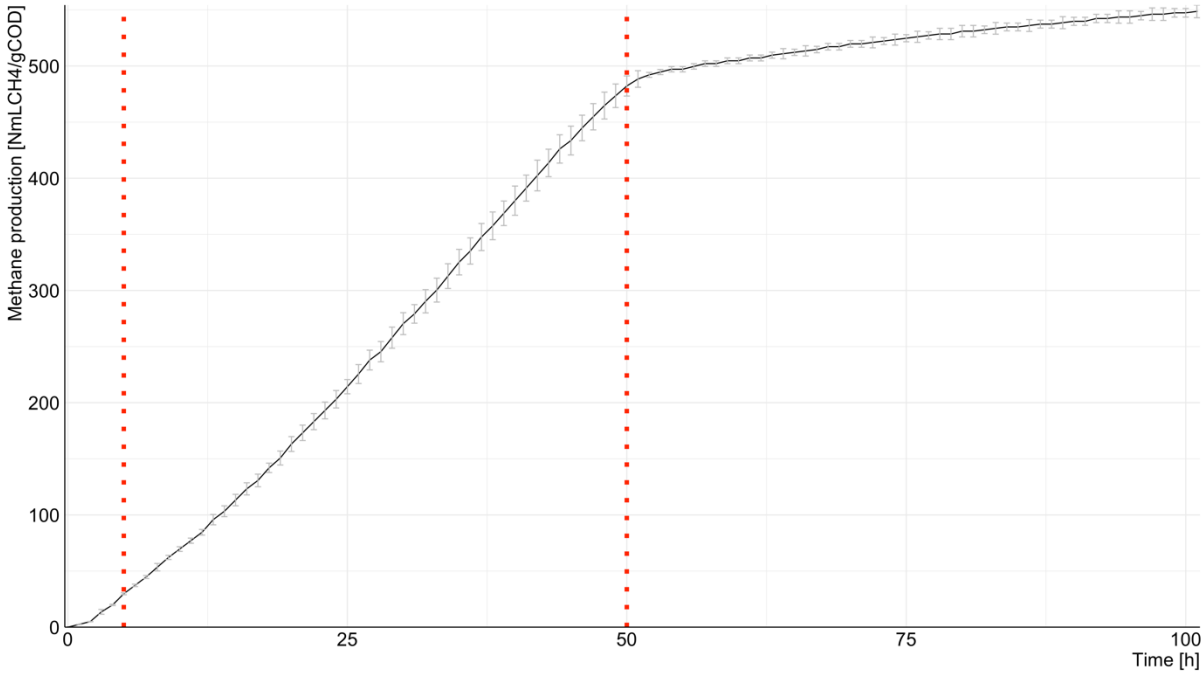


Figure E.3 - Methane production of acetate activity test (10/12/2020).

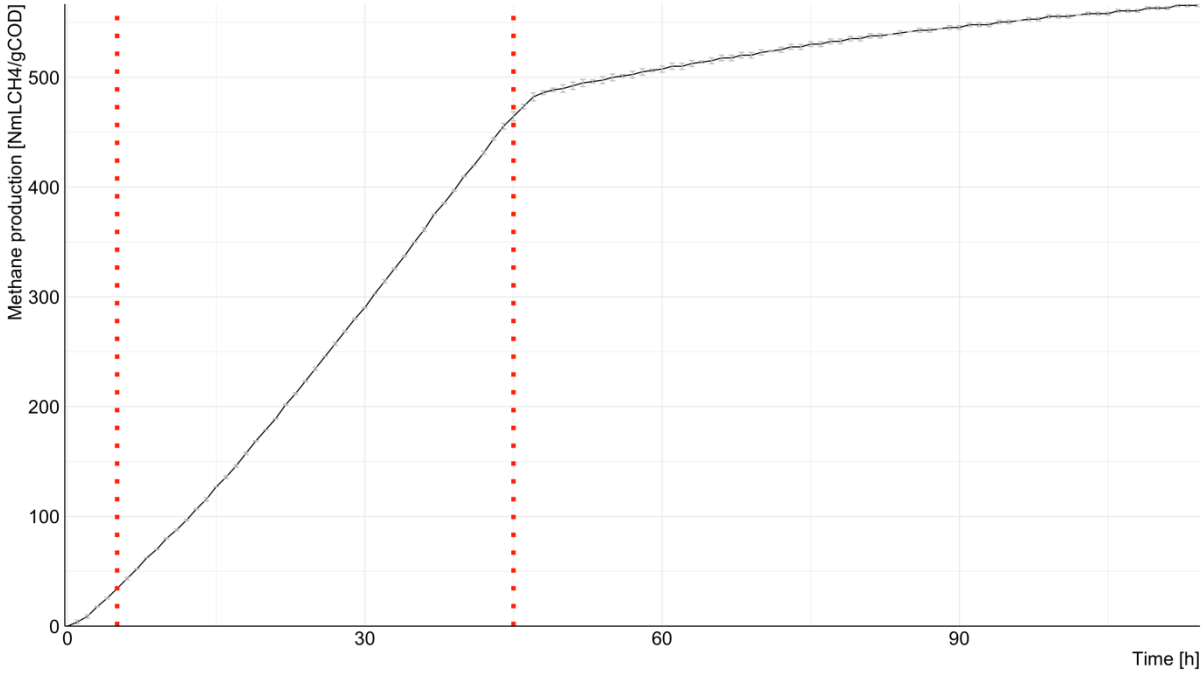


Figure E.4 - Methane production of acetate activity test (17/12/2020).

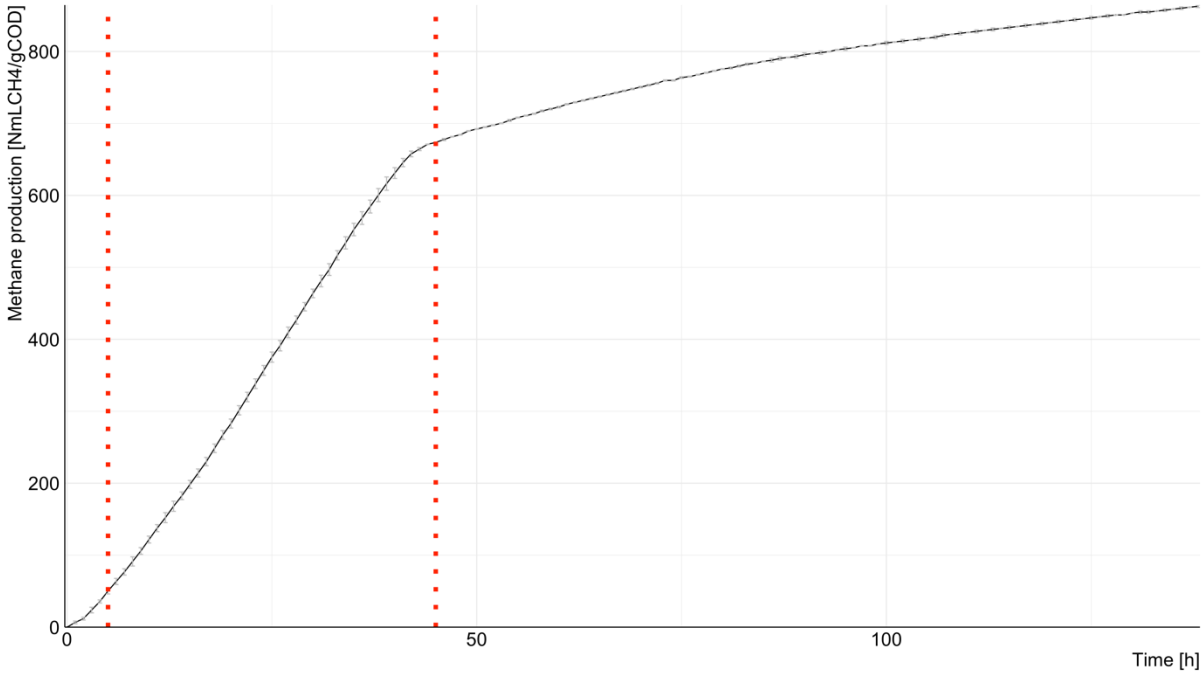


Figure E.5 - Methane production of acetate activity test (14/01/2021).

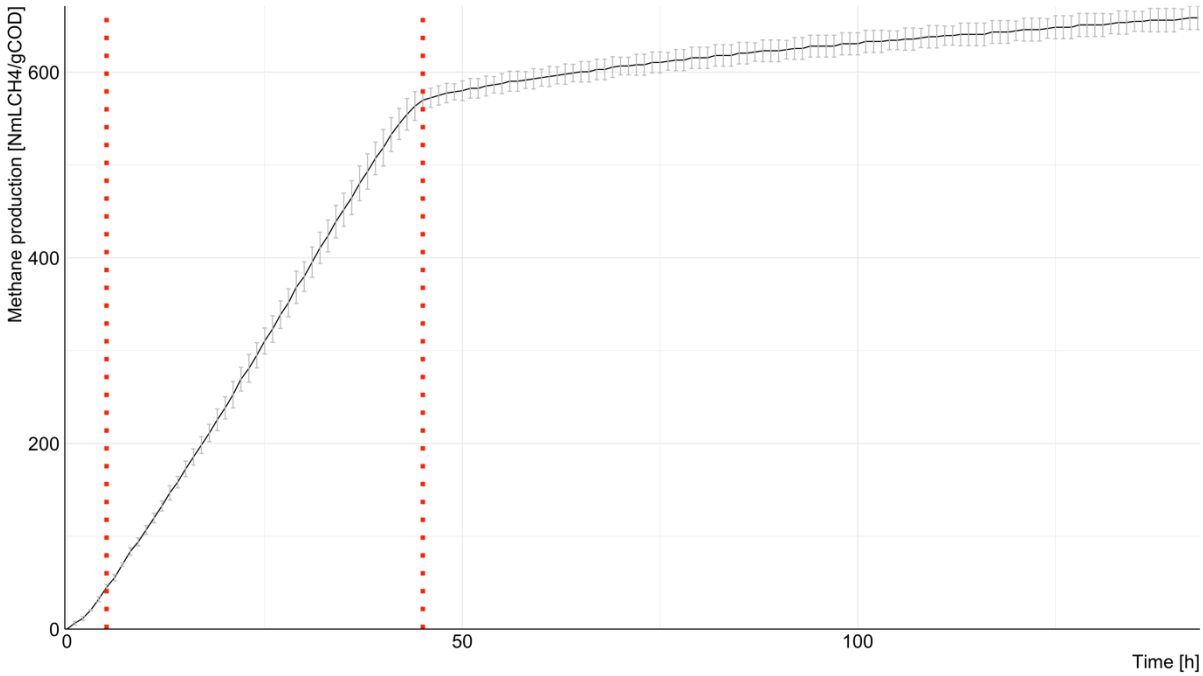


Figure E.6 - Methane production of acetate activity test (04/02/2021).

*Glucose activity tests*

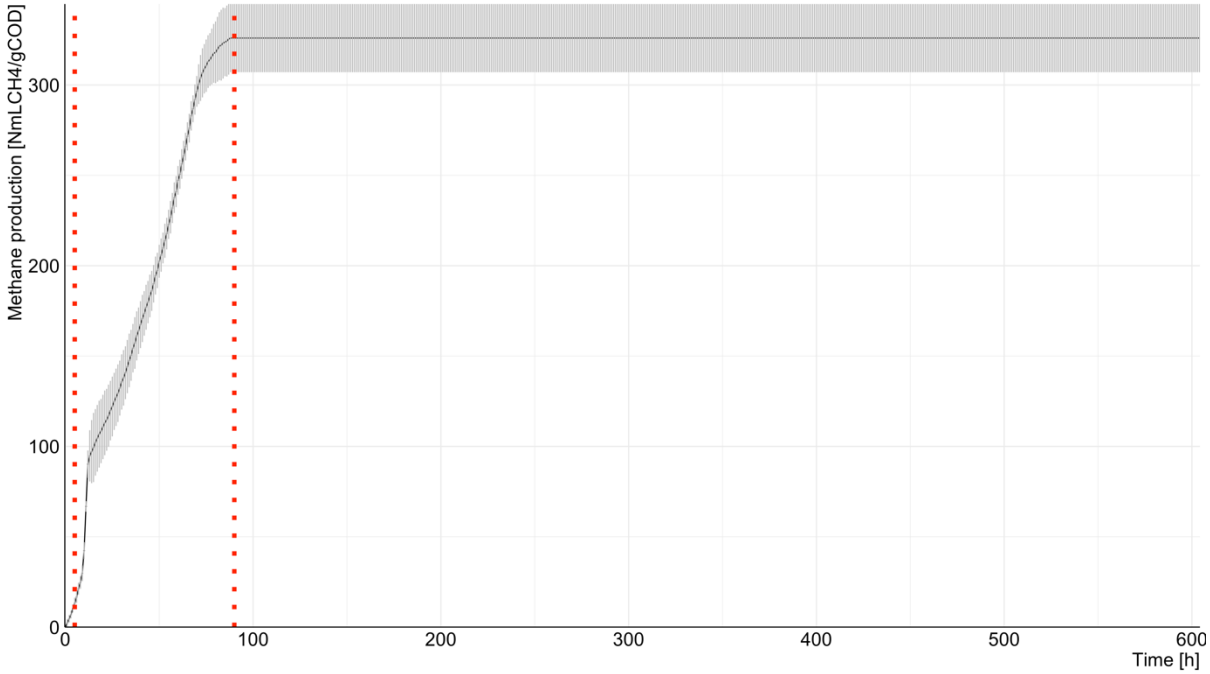


Figure E.7 - Methane production of glucose activity test carried out with a concentration of 5 $g_{COD,glu}$ / L (22/10/2020).

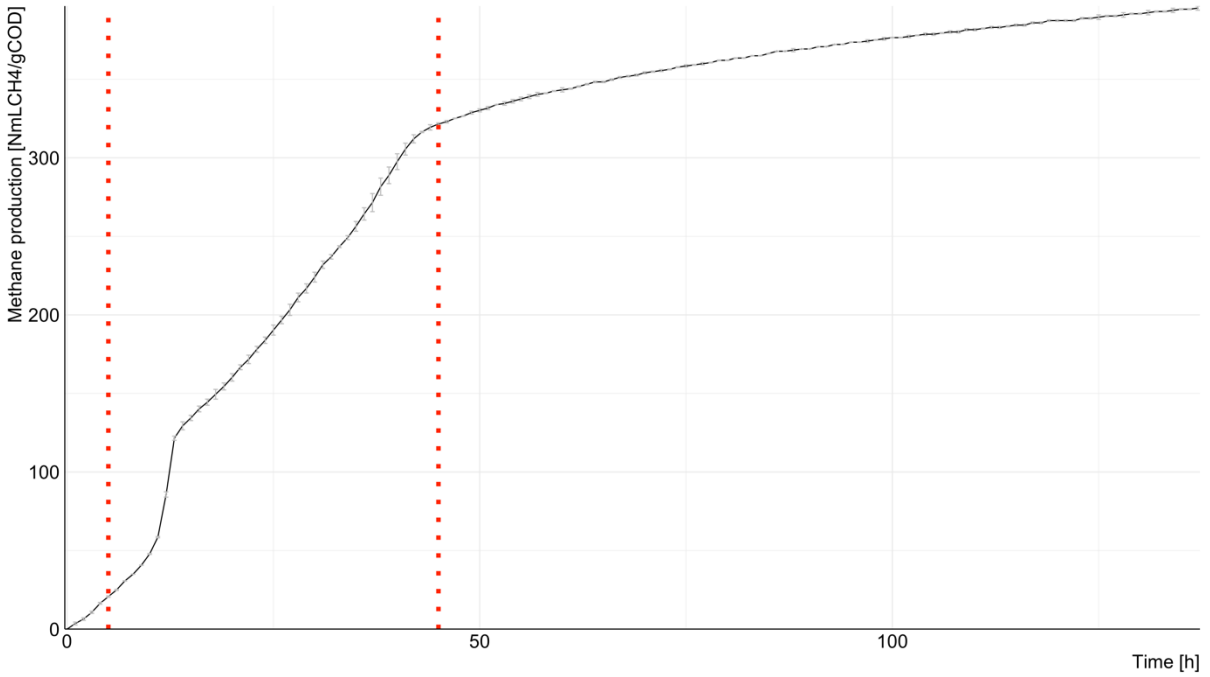


Figure E.8 - Methane production of glucose activity test carried out with a concentration of 4 $g_{COD,glu}$ / L (19/11/2020).

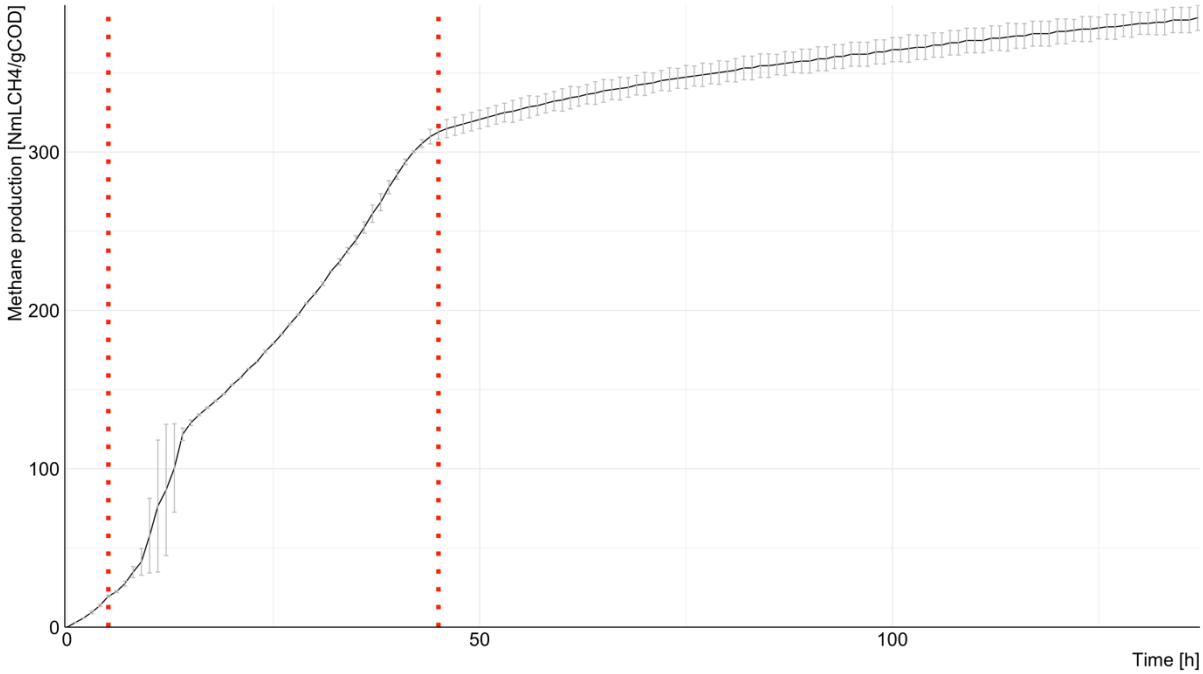


Figure E.9 - Methane production of glucose activity test carried out with a concentration of 4 $g_{COD,glu}$ / L (26/11/2020).

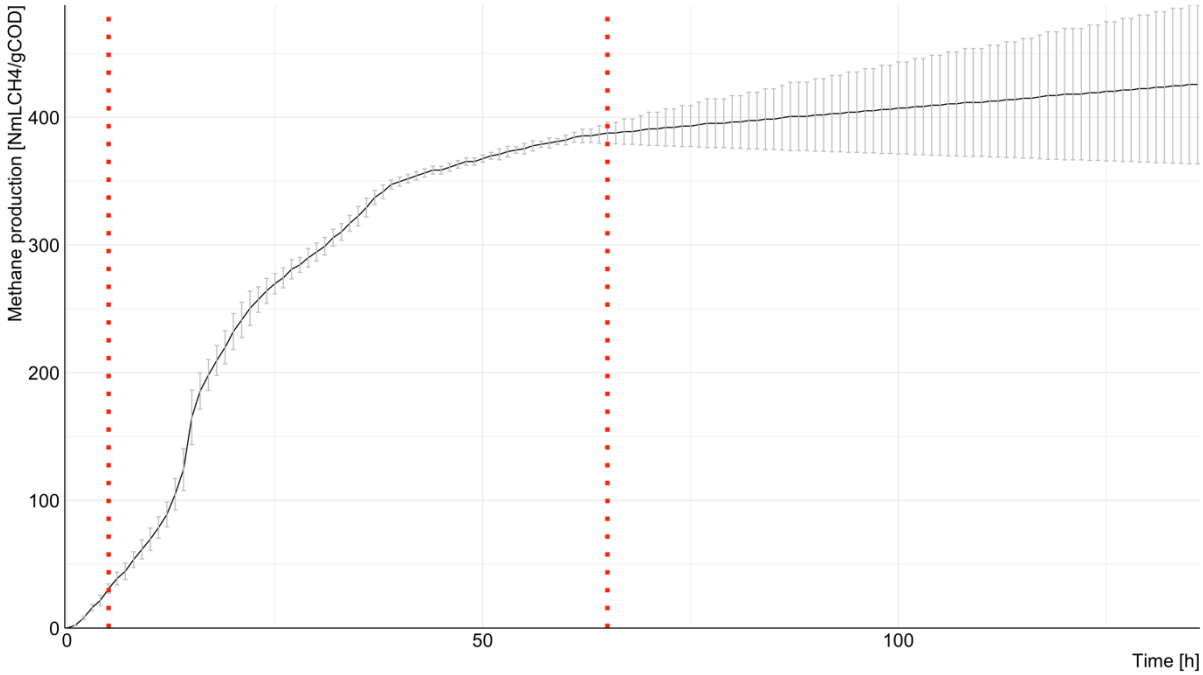


Figure E.10 - Methane production of glucose activity test carried out with a concentration of 2.5 $g_{COD,glu}$ / L (03/12/2020).

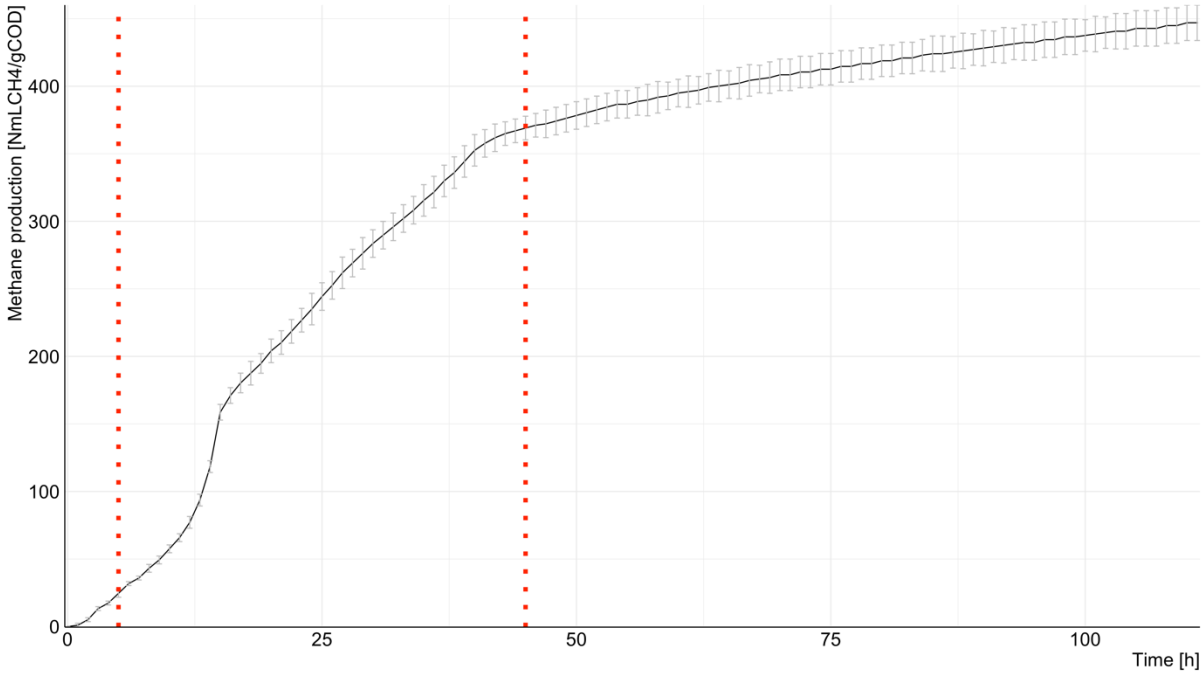


Figure E.11 - Methane production of glucose activity test carried out with a concentration of 3 $g_{COD,glu}$ / L (10/12/2020).

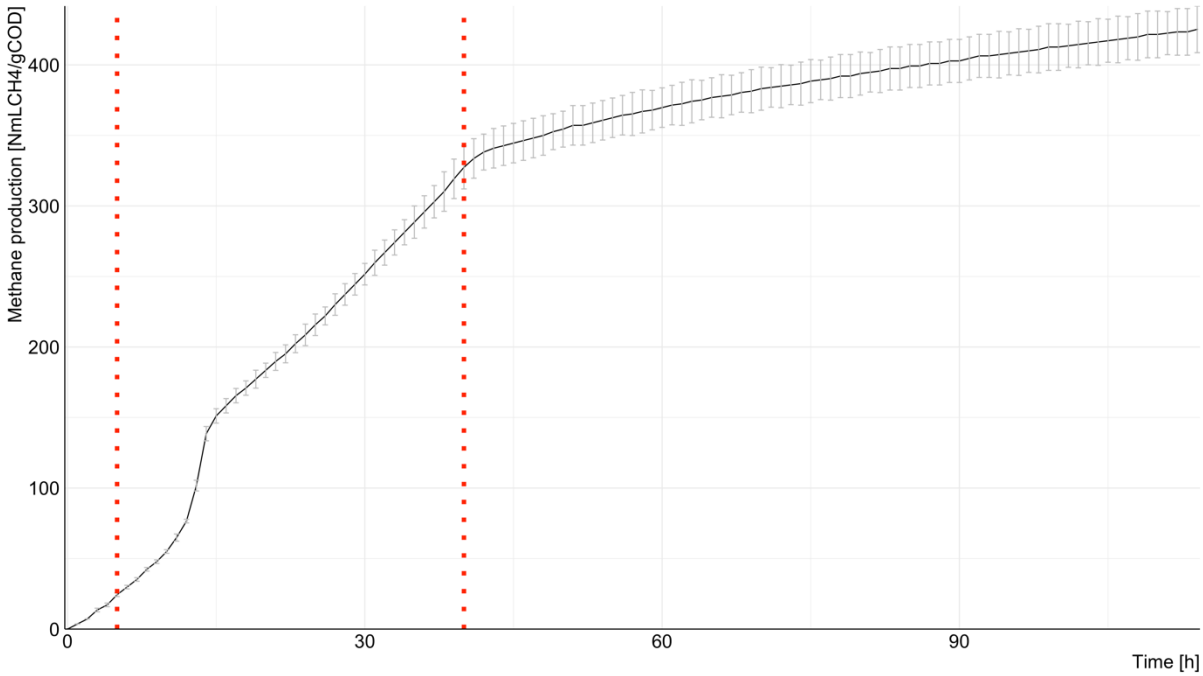


Figure E.12 - Methane production of glucose activity test carried out with a concentration of 3.5 $g_{COD,glu}$ / L (17/12/2020).

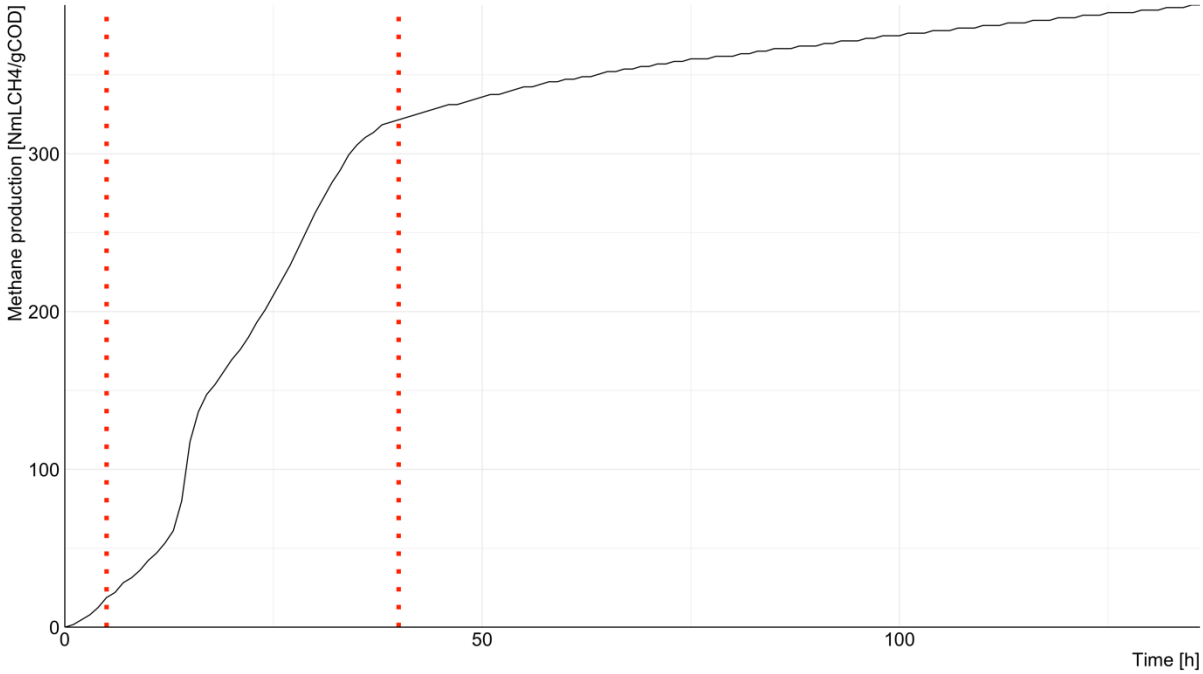


Figure E.13 - Methane production of glucose activity test carried out with a concentration of 3.5 $g_{COD,glu}$ / L (10/02/2021).

## *BSA activity tests*

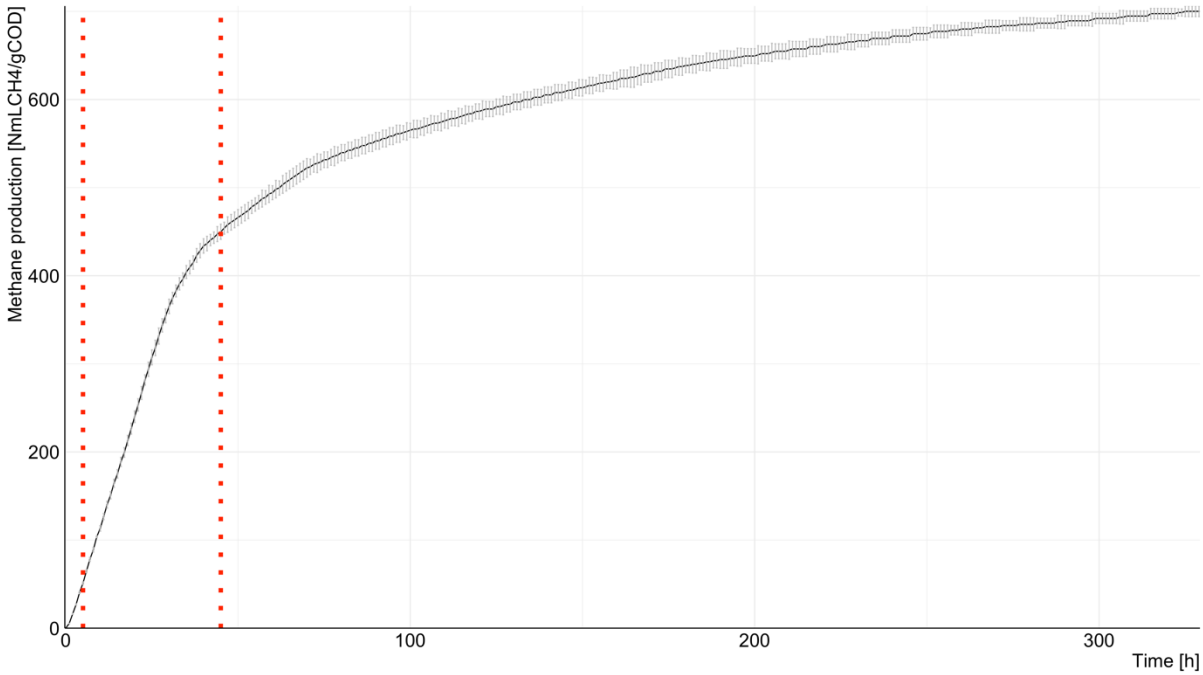


Figure E.14 - Methane production of BSA activity test carried out with a concentration of 3 $g_{COD,BSA}$ / L. (05/11/2020).

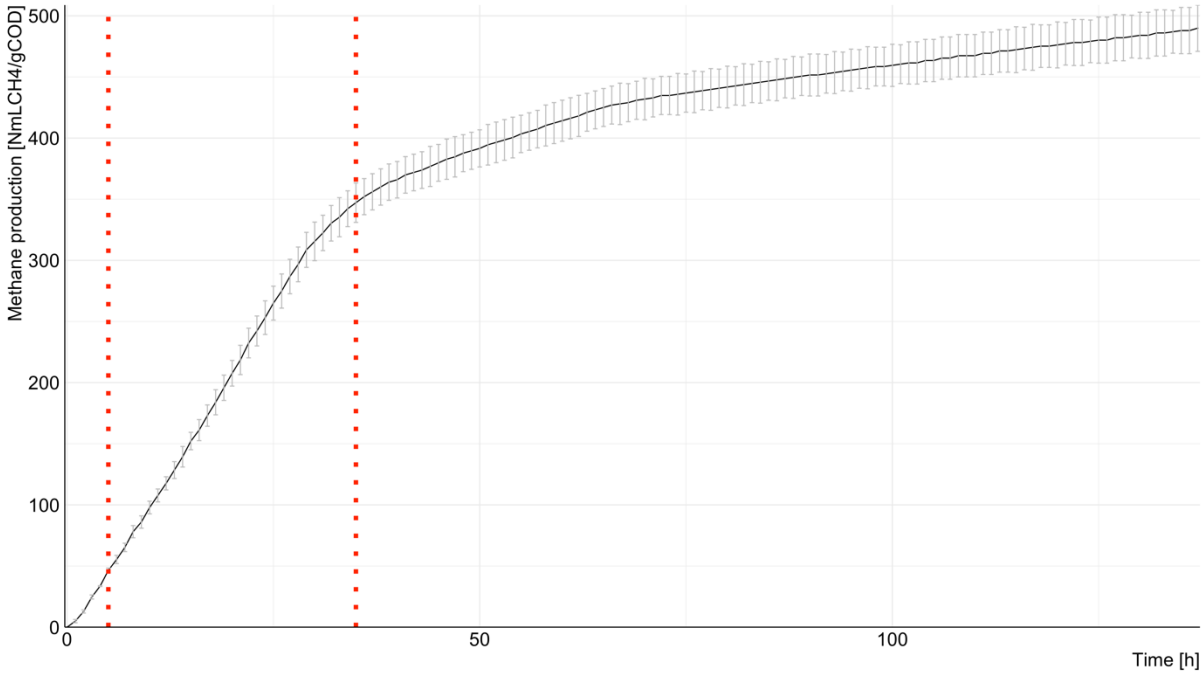


Figure E.15 - Methane production of BSA activity test carried out with a concentration of 3 $g_{COD,BSA}$ / L (26/11/2020).

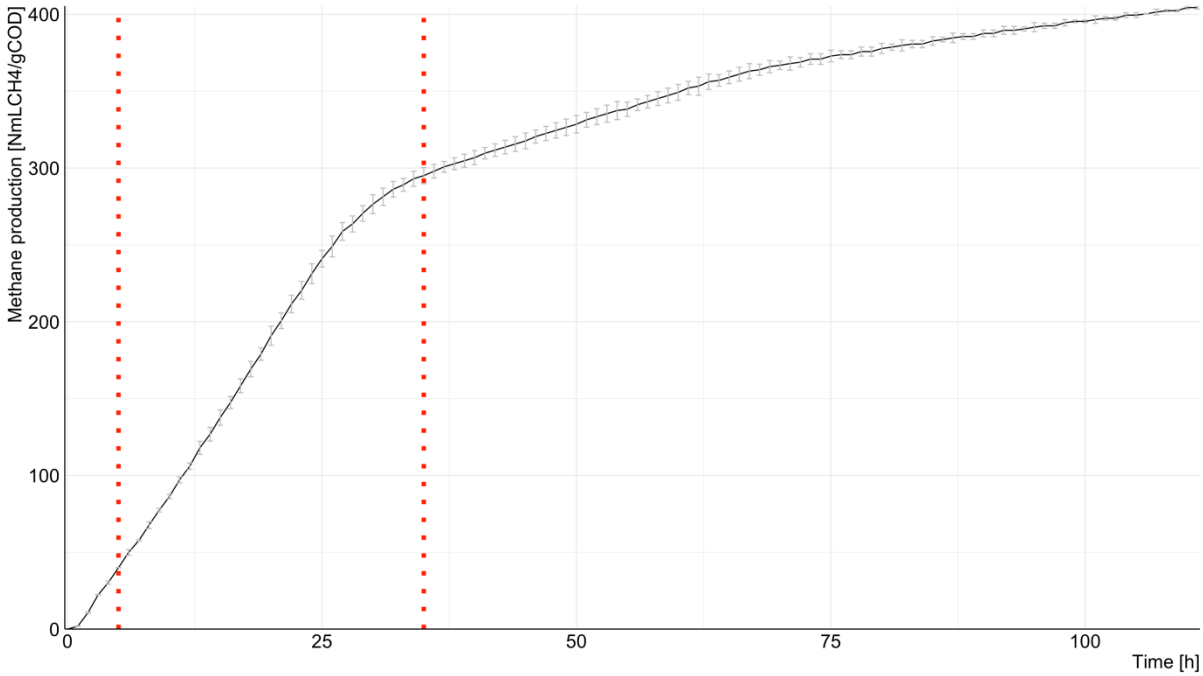


Figure E.16 - Methane production of BSA activity test carried out with a concentration of 3 $g_{COD,BSA}$ / L (10/12/2020).

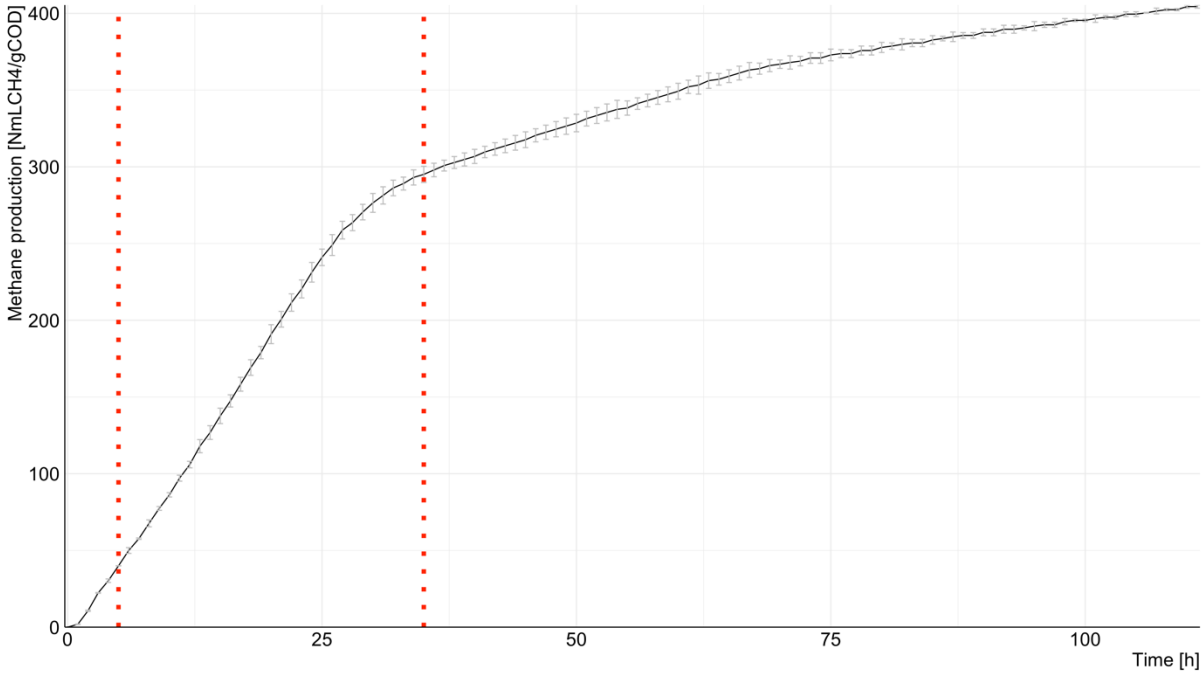


Figure E.17 - Methane production of BSA activity test carried out with a concentration of 3.5 gCOD,BSA / L. (17/12/2020).

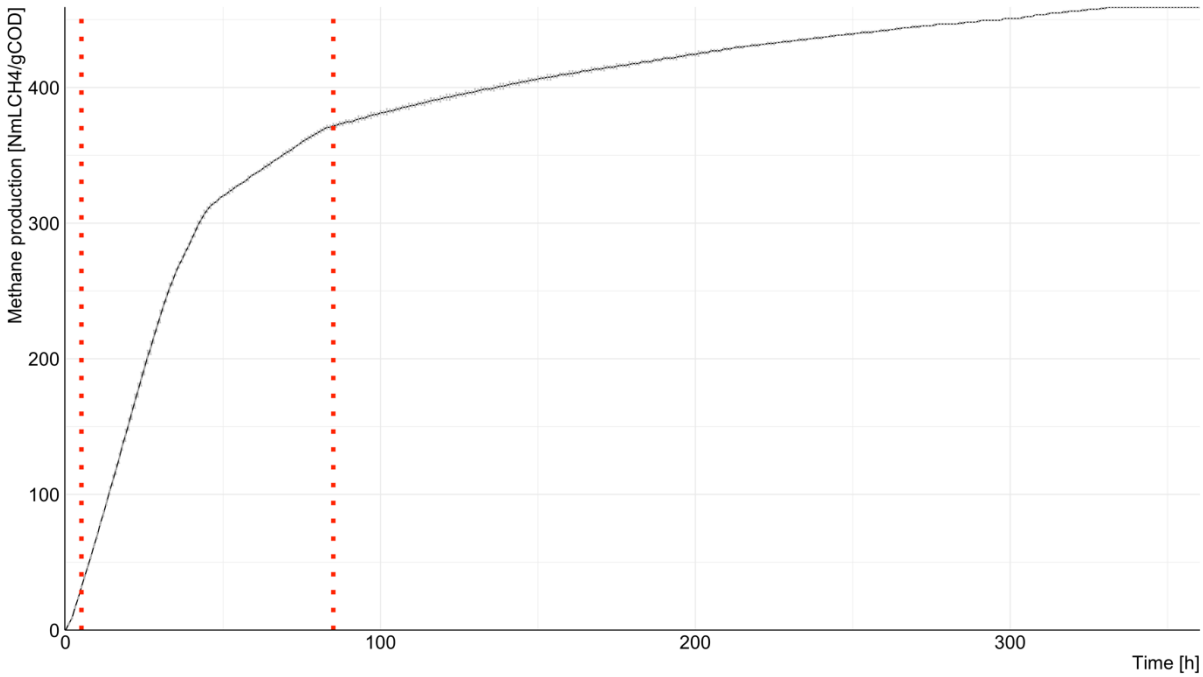


Figure E.18 - Methane production of BSA activity test carried out with a concentration of 4.5 gCOD,BSA / L (29/12/2020).

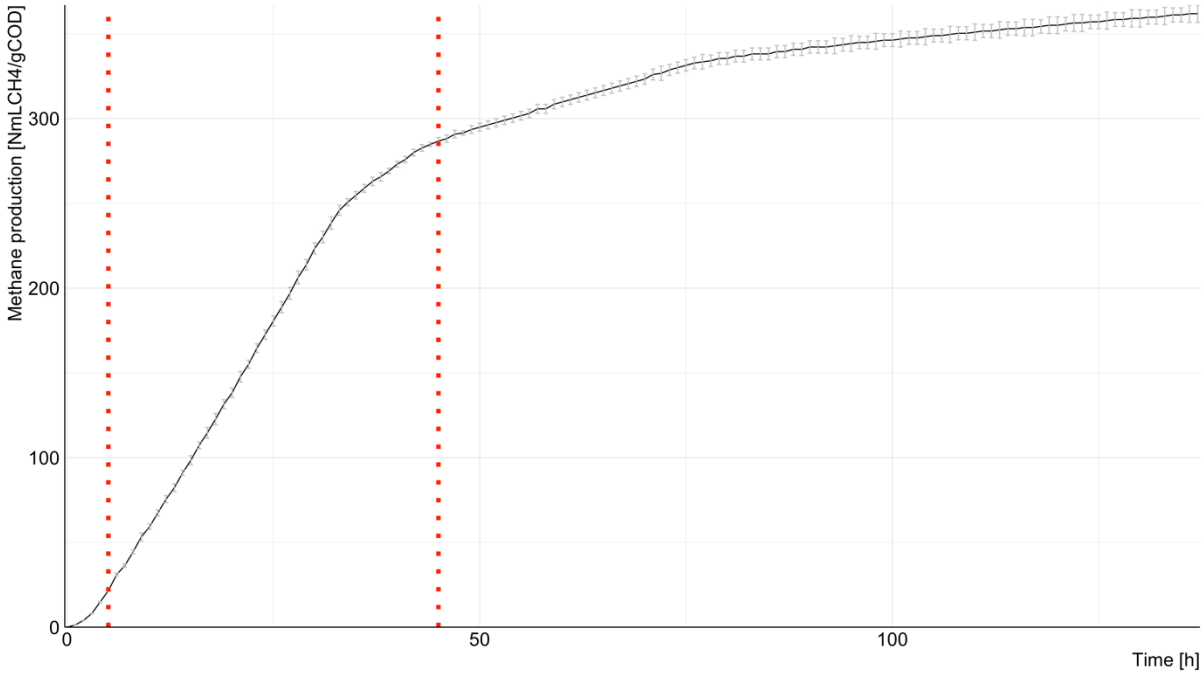


Figure E.19 - Methane production of BSA activity test carried out with a concentration of 4.5 gCOD,BSA / L (17/02/2021).

# APPENDIX F

This appendix presents the graphs of all the simulations of the batch tests carried out during the experimentation.

*Blank BMP tests*

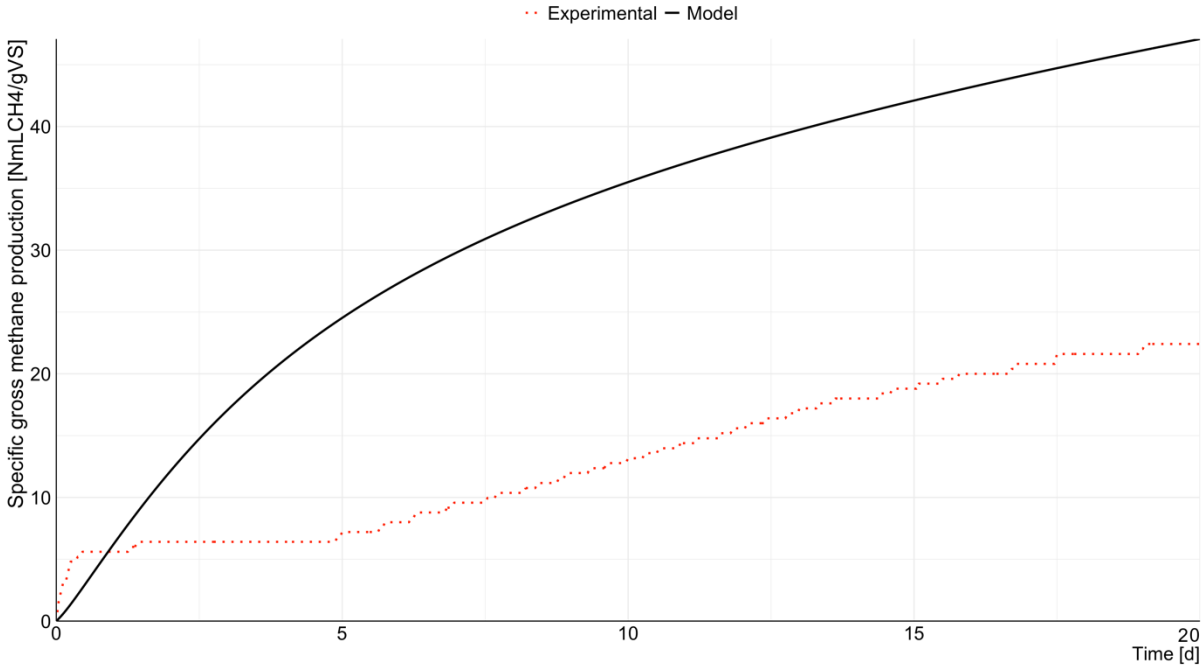


Figure F.1 - Blank BMP test simulation (19/11/2020).

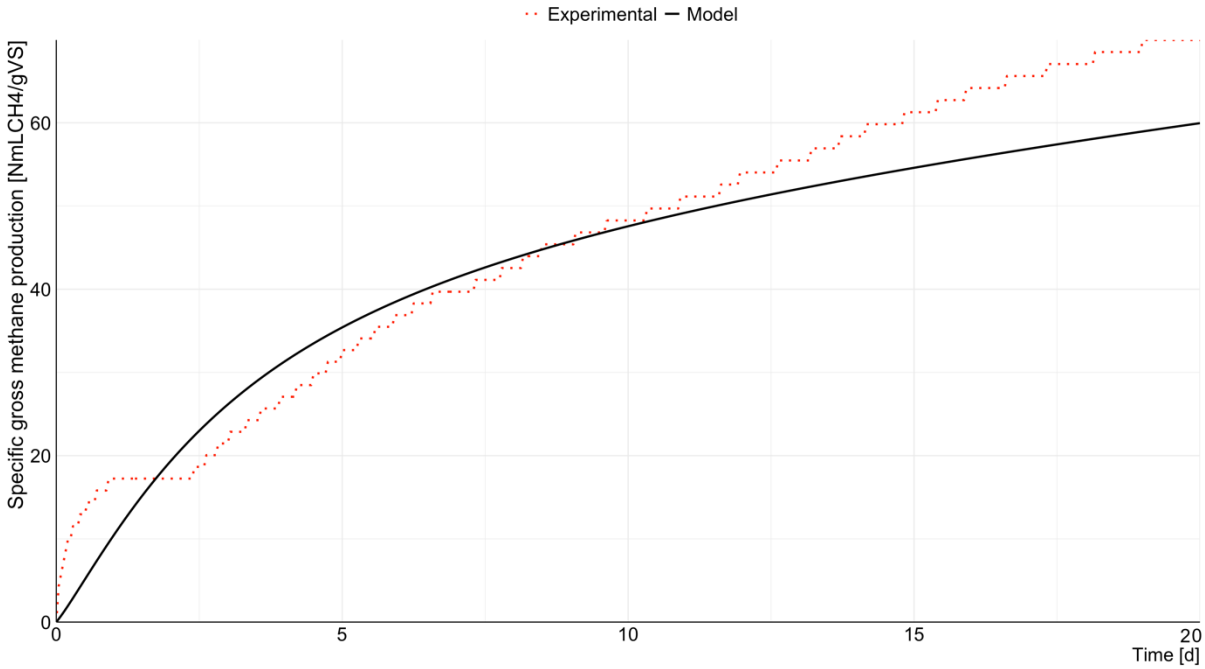


Figure F.2 - Blank BMP test simulation (3/12/2020).

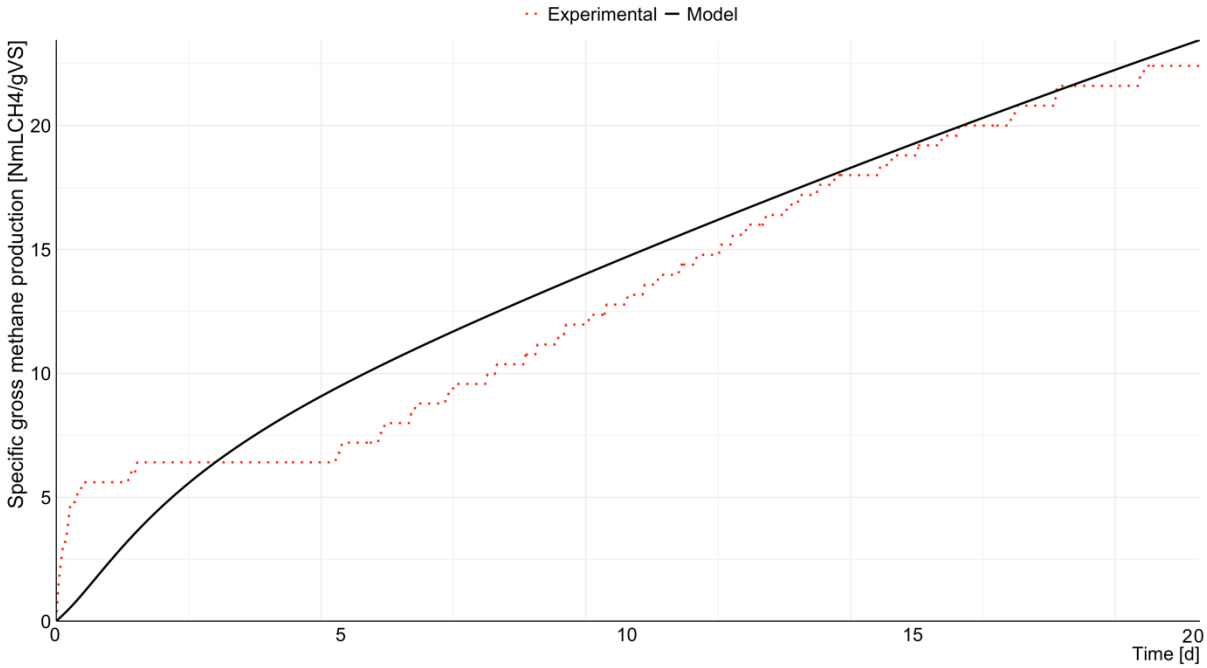


Figure F.3 - Blank BMP test simulation (30/12/2020).

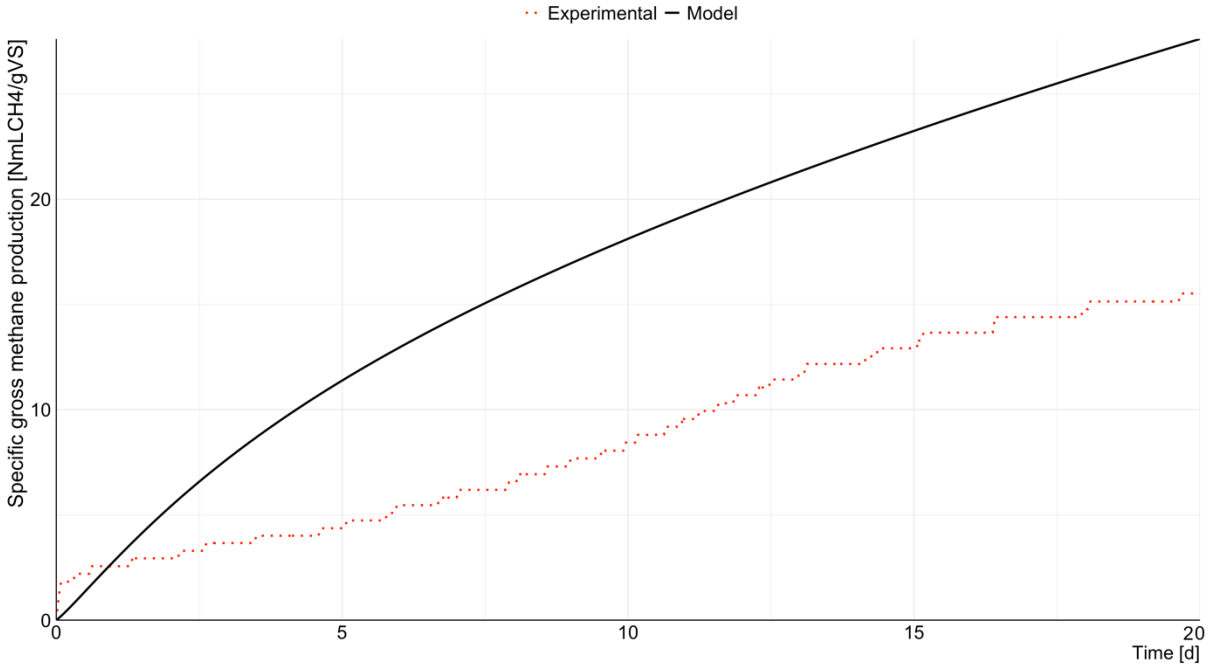


Figure F.4 - Blank BMP test simulation (04/02/2021).

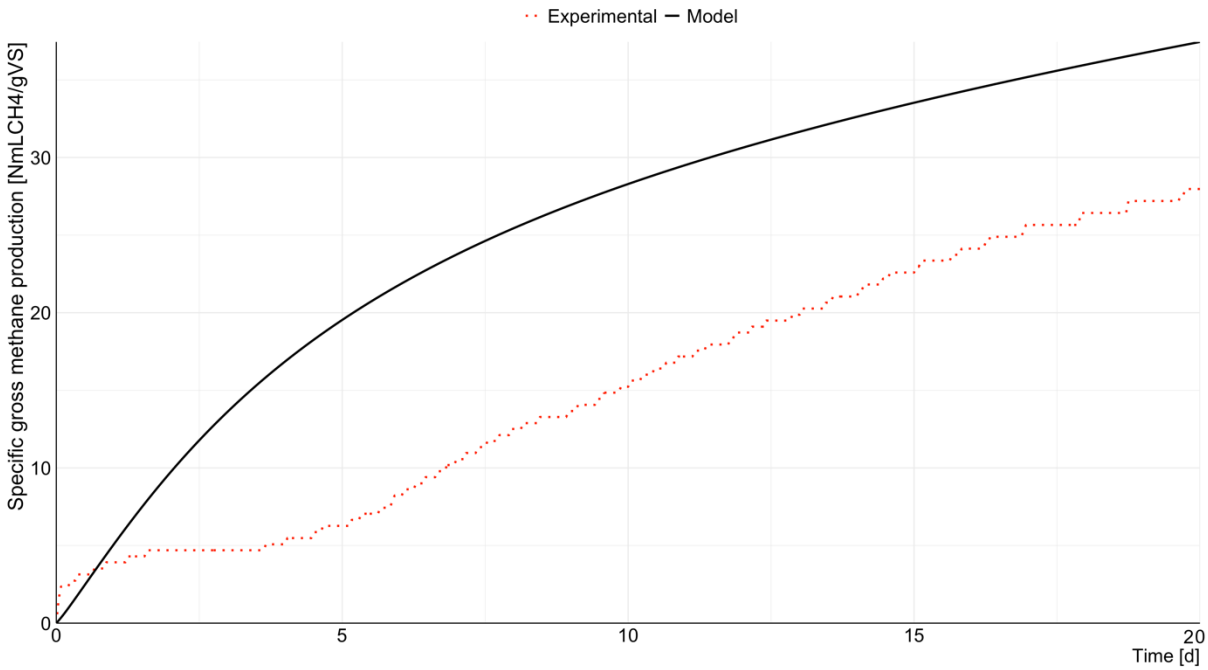


Figure F.5 - Blank BMP test simulation (25/02/2021).

## *Sludge BMP tests*

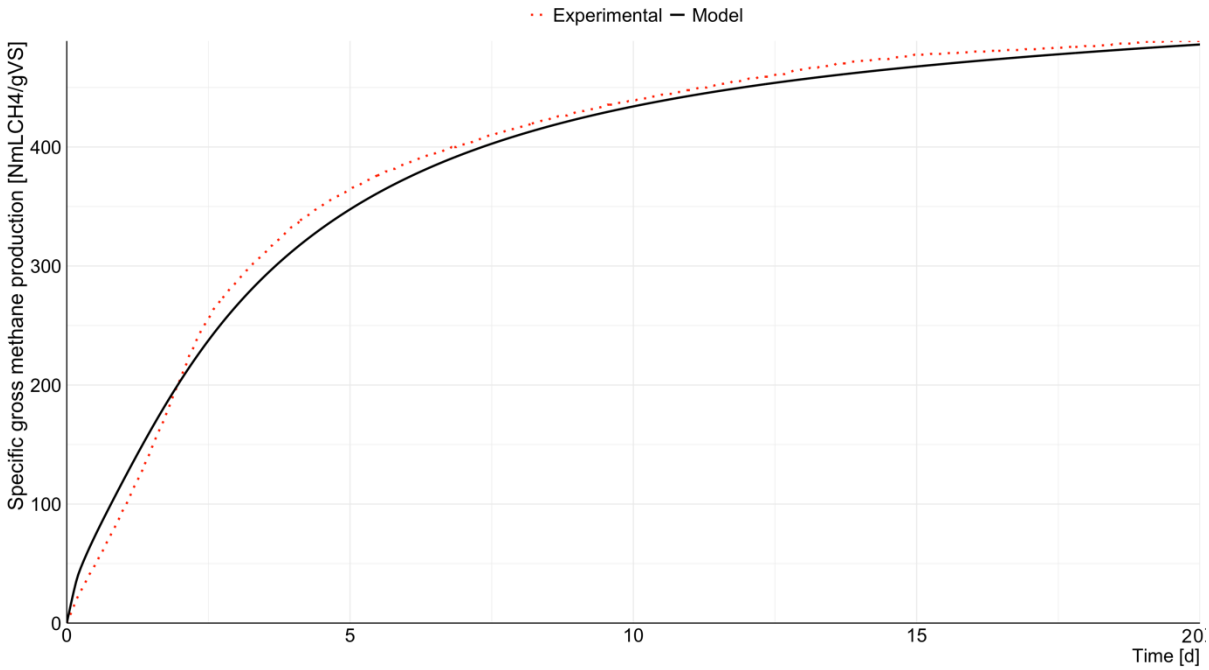


Figure F.6 - Sludge BMP test simulation (19/11/2020).

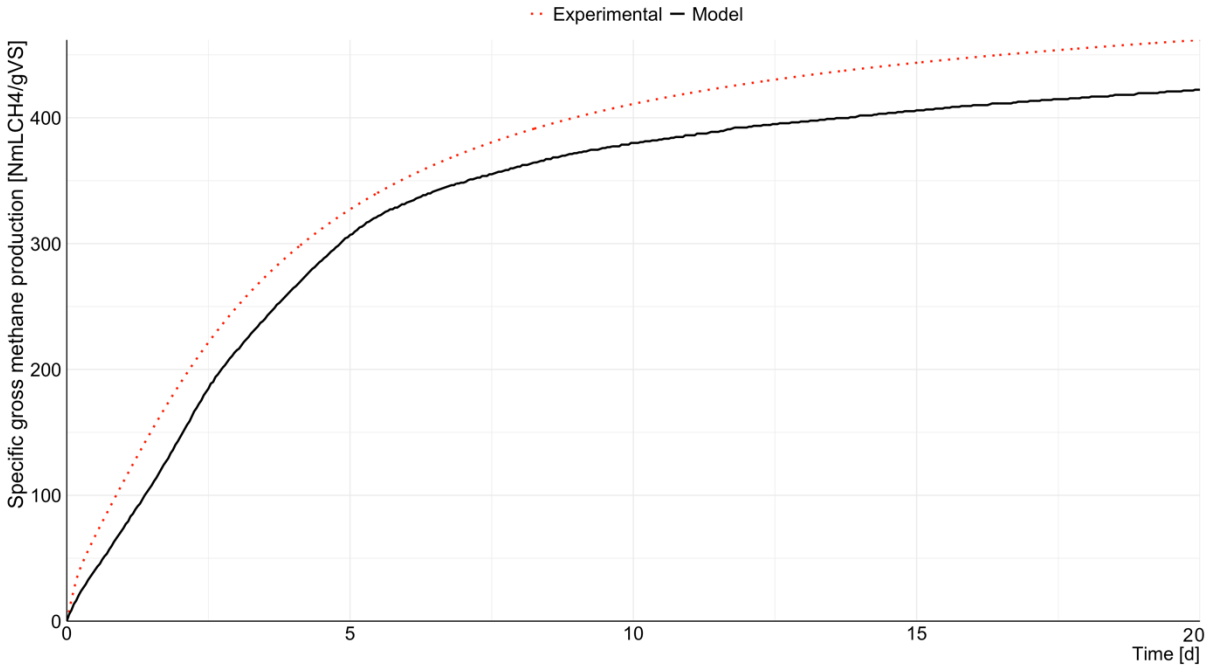


Figure F.7 - Sludge BMP test simulation (3/12/2020).

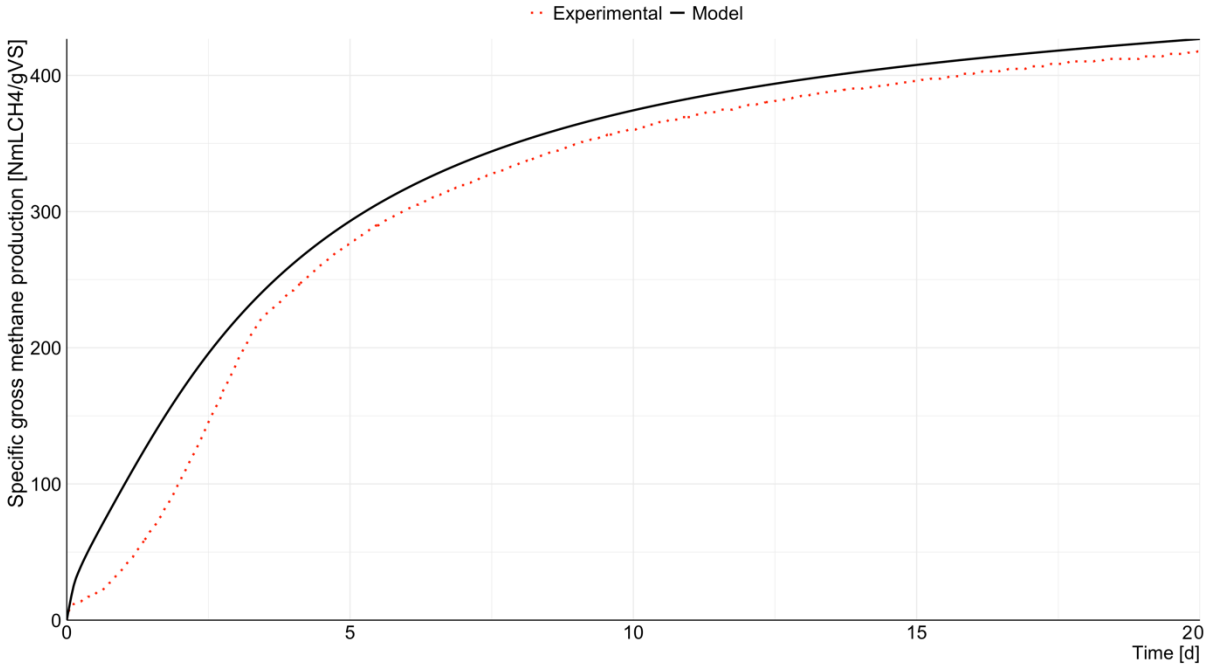


Figure F.8 - Sludge BMP test simulation (30/12/2020).

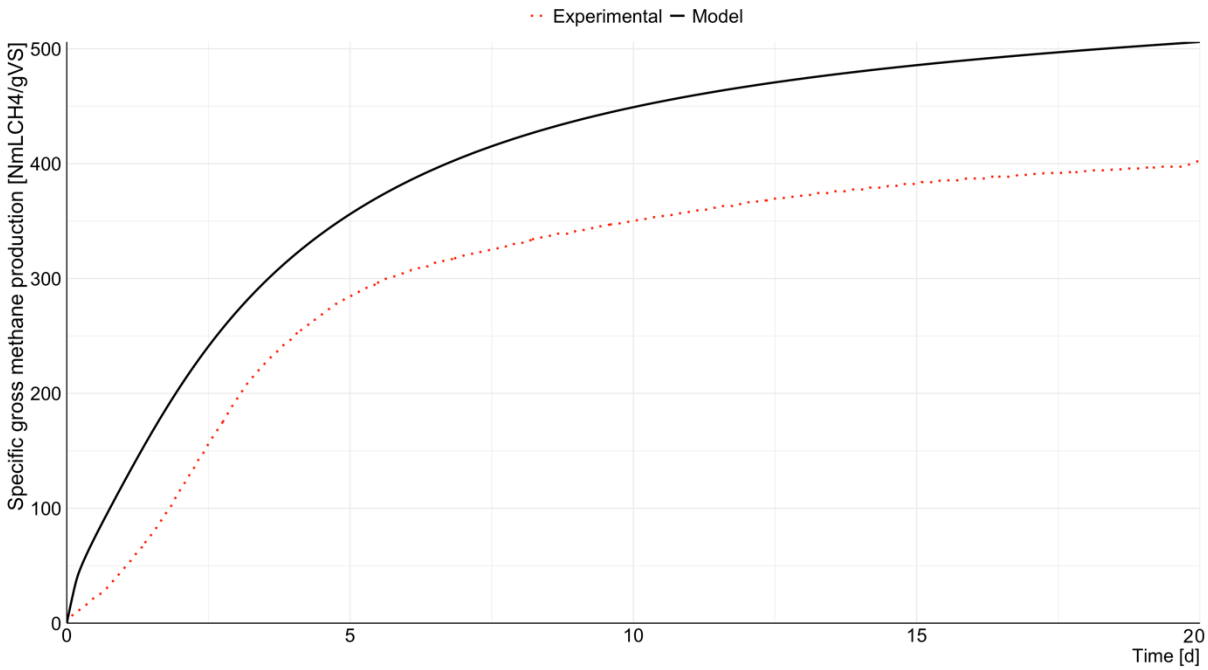


Figure F.9 - Sludge BMP test simulation (04/02/2021).

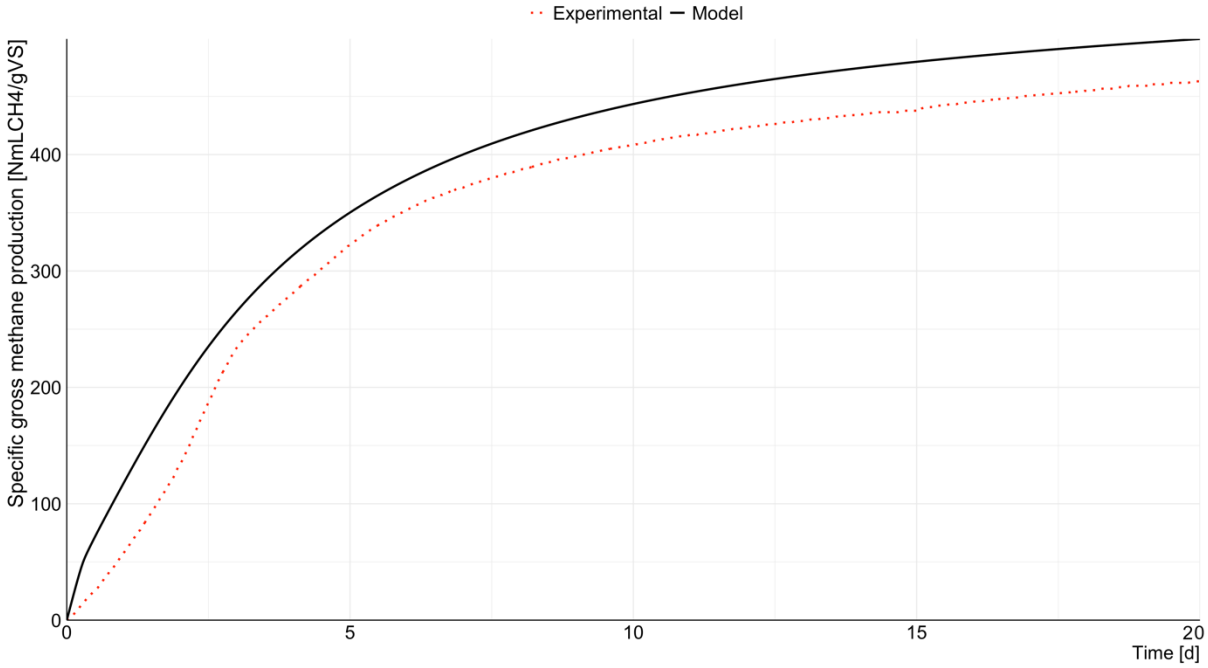


Figure F.10 - Sludge BMP test simulation (25/02/2021).

*Yogurt BMP tests*

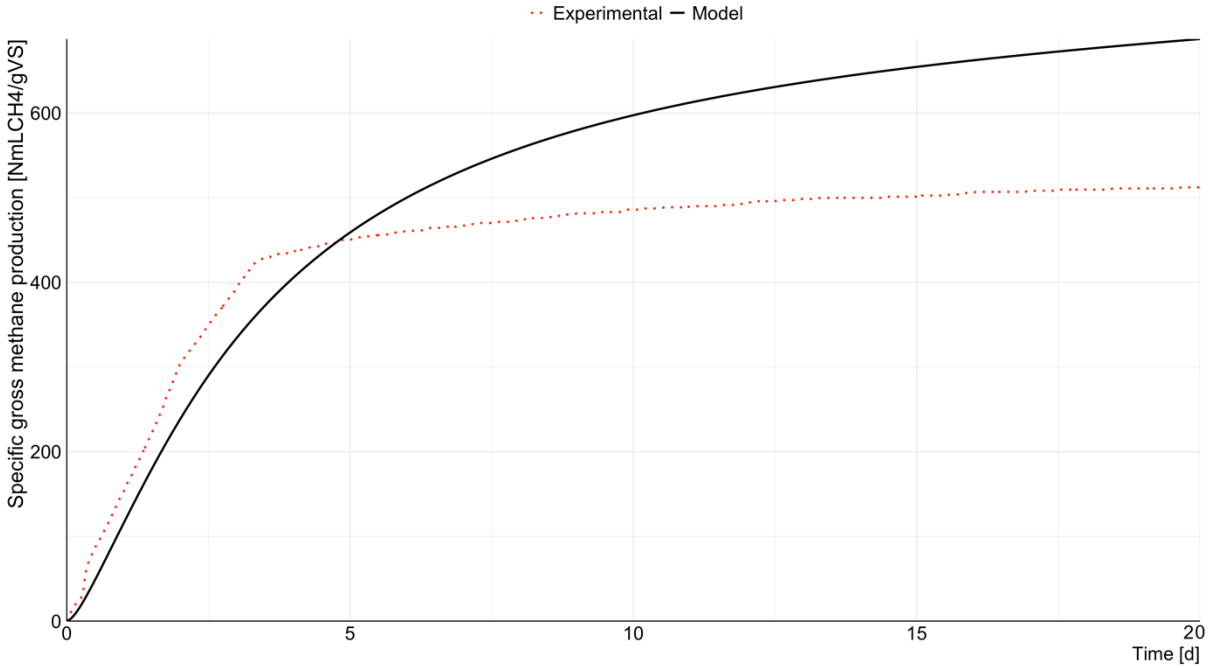


Figure F.11 - Yogurt BMP test simulation with k_hyd_pr = 0.2 (30/12/2020).

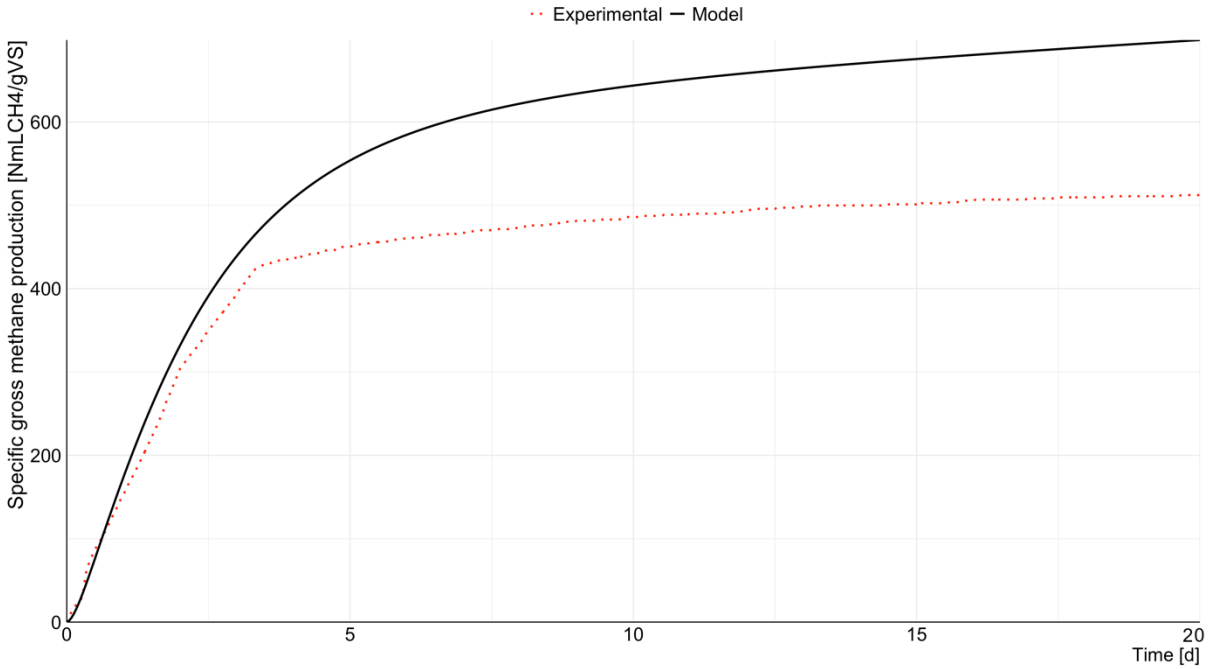


Figure F.12 - Yogurt BMP test simulation with k_hyd_pr = 0.5 (30/12/2020).

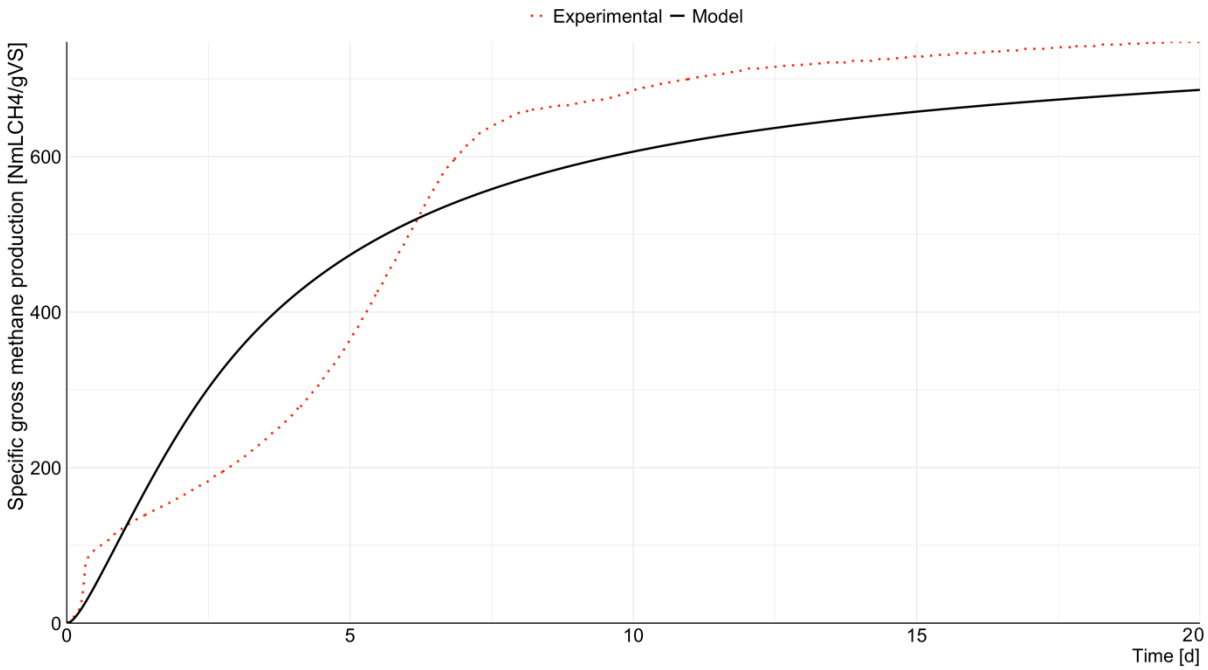


Figure F.13 - Yogurt BMP test simulation k_hyd_pr = 0.2 (04/02/2021).

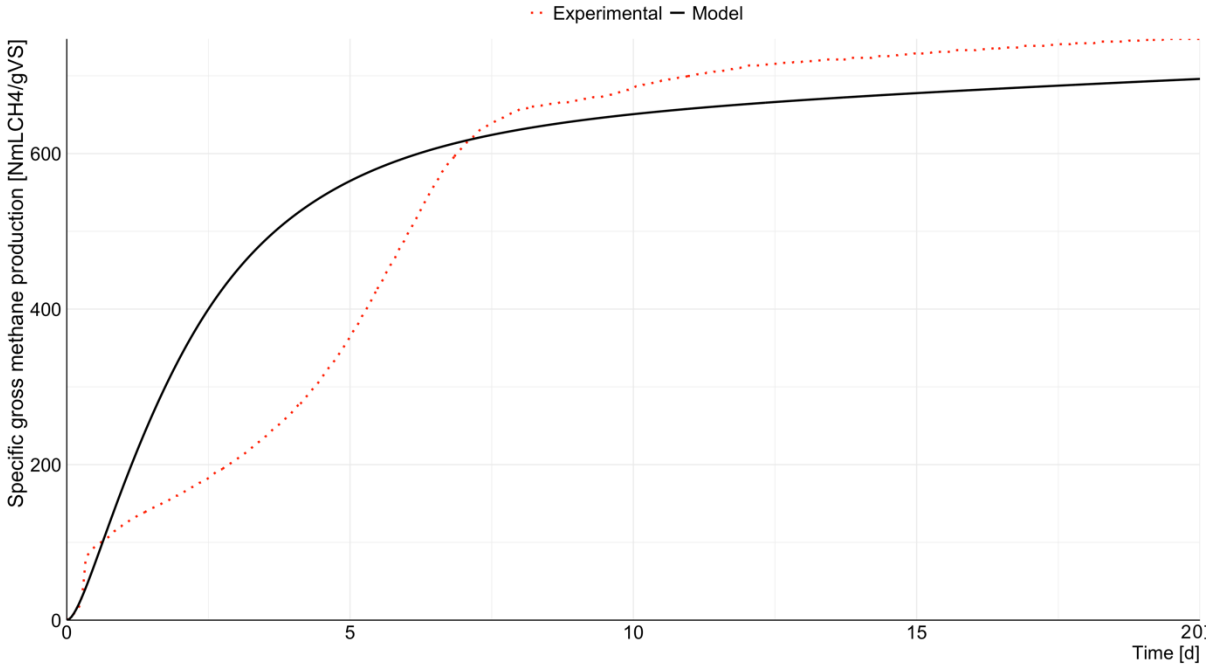


Figure F.14 - Yogurt BMP test simulation k_hyd_pr = 0.5 (04/02/2021).

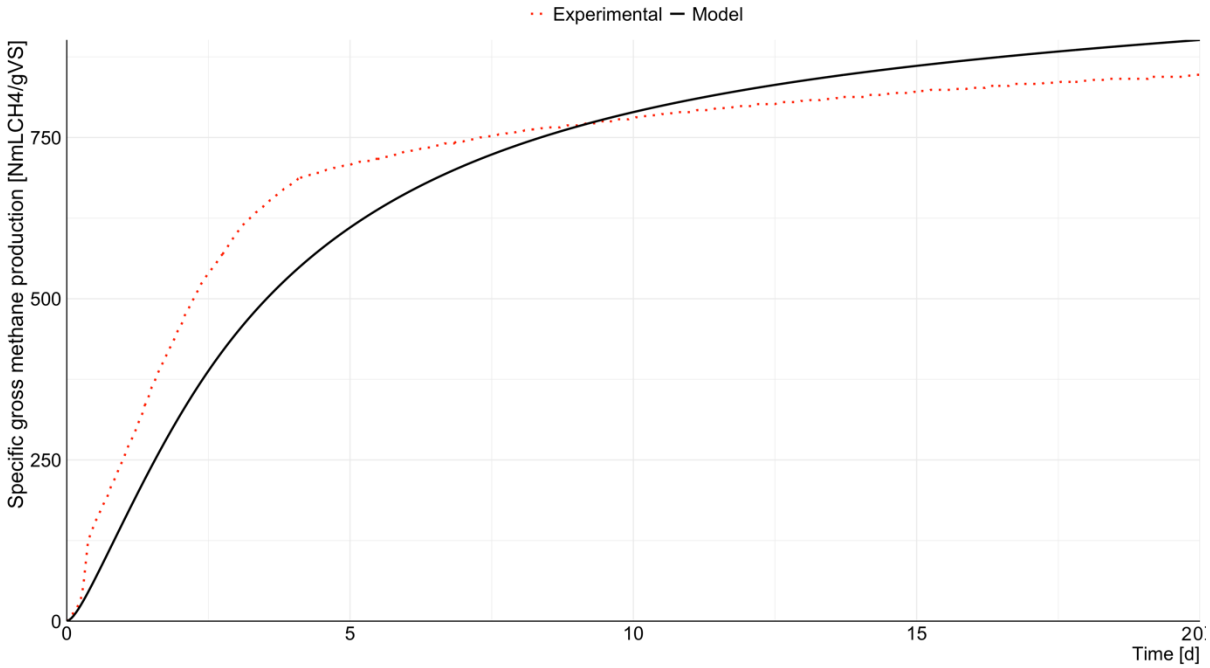


Figure F.15 - Yogurt BMP test simulation k_hyd_pr = 0.2 (25/02/2021).

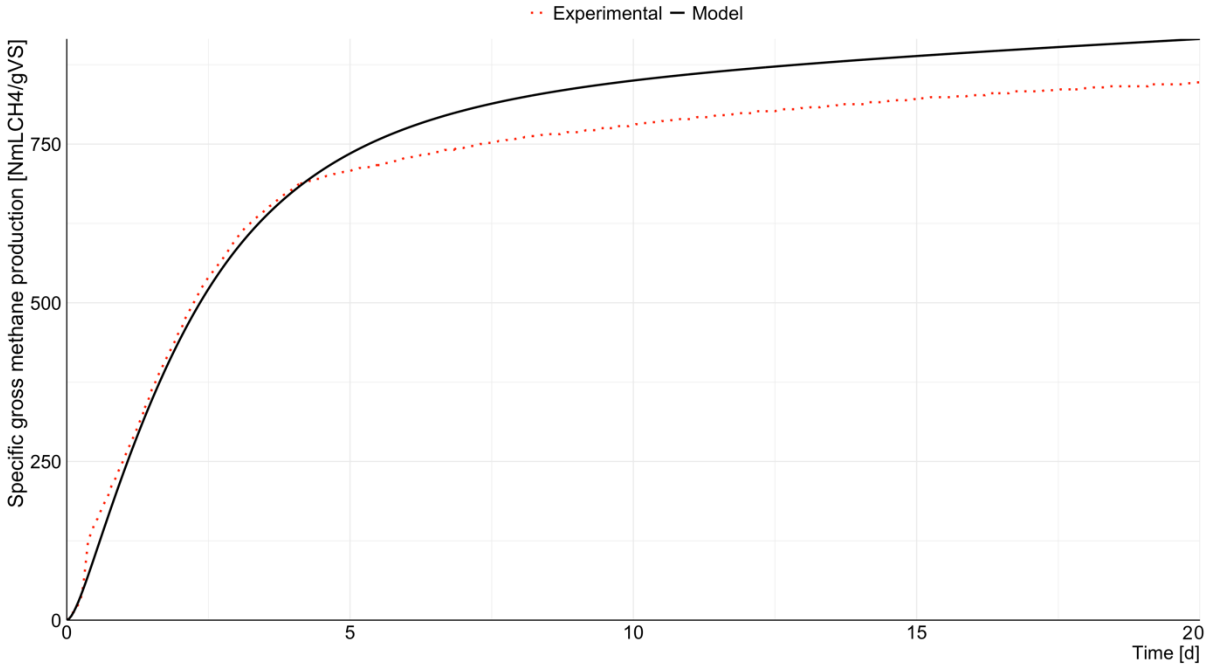


Figure F.16 - Yogurt BMP test simulation k_hyd_pr = 0.5 (25/02/2021).

## *Co-digestion BMP tests*

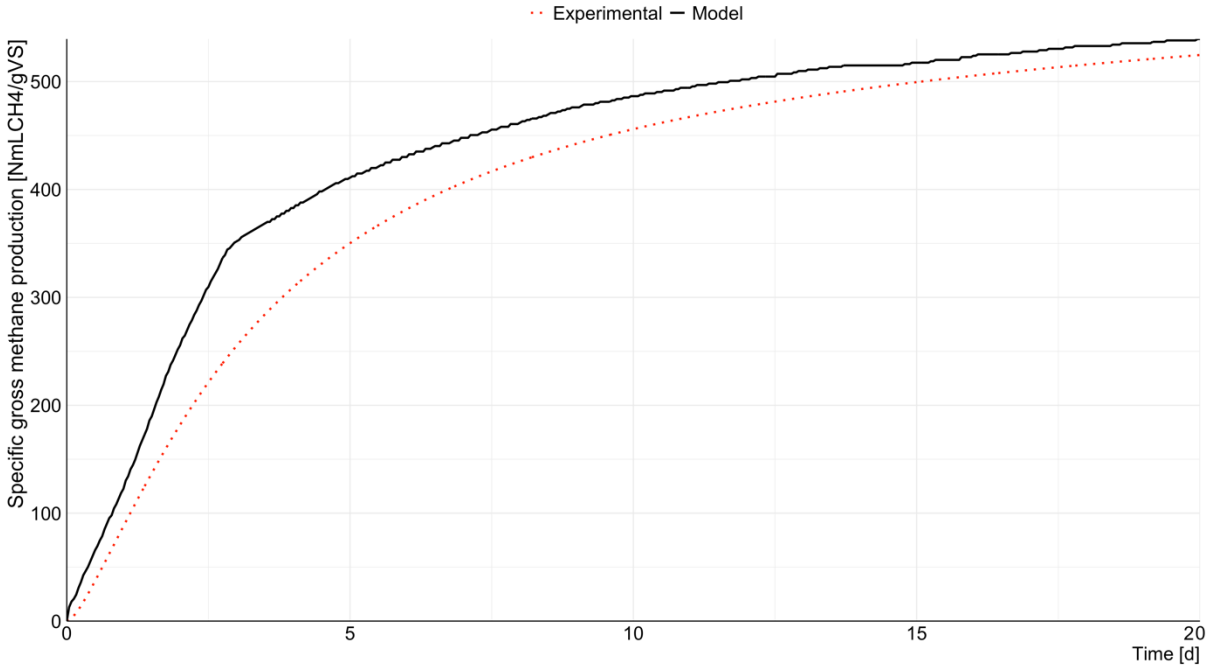


Figure F.17 - Co-digestion BMP test simulation k_hyd_pr = 0.2 (30/12/2020).

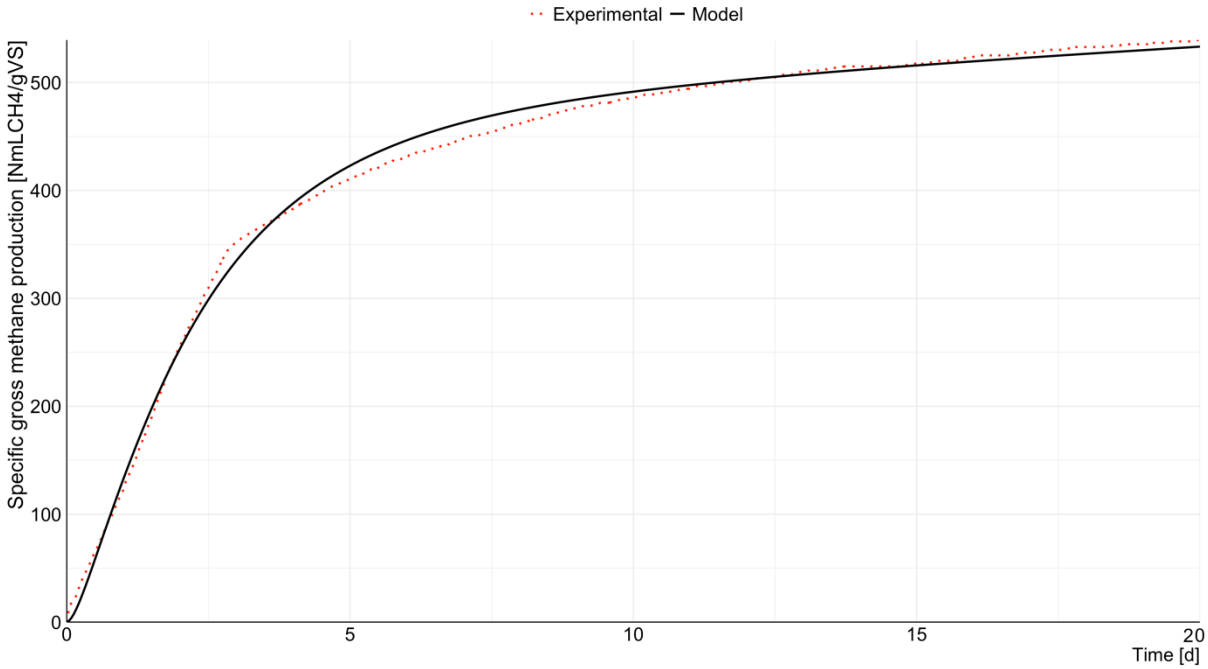


Figure F.18 - Co-digestion BMP test simulation k_hyd_pr = 0.5 (30/12/2020).

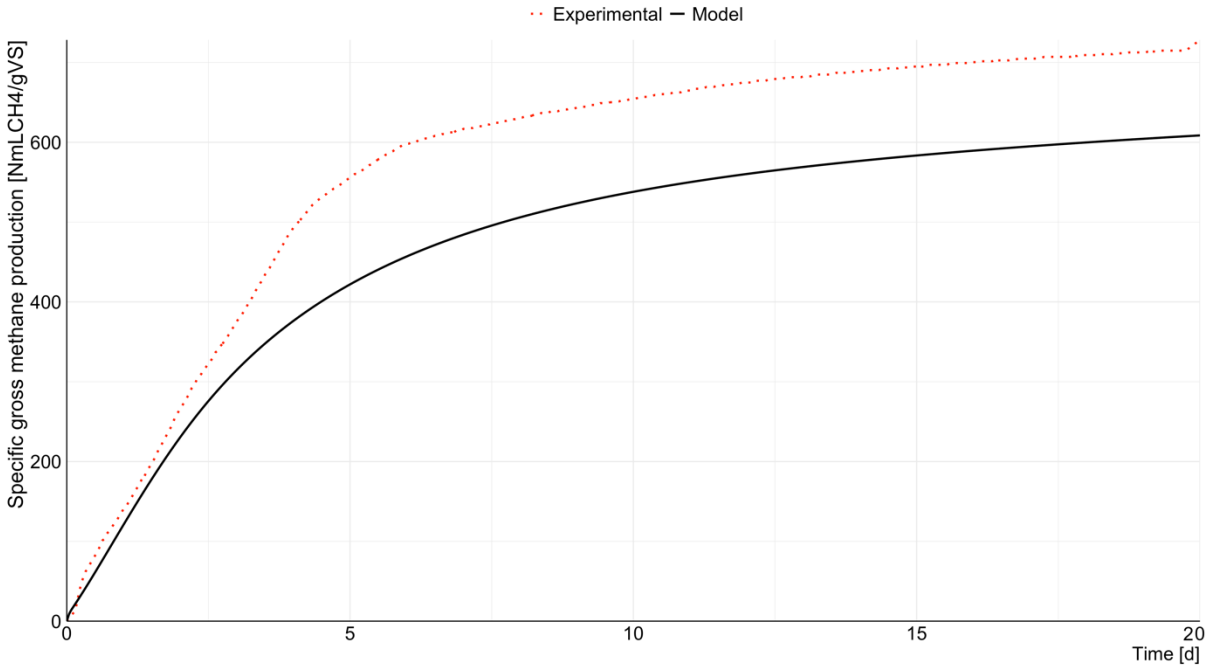


Figure F.19 - Co-digestion BMP test simulation k_hyd_pr = 0.2 (04/02/2021).

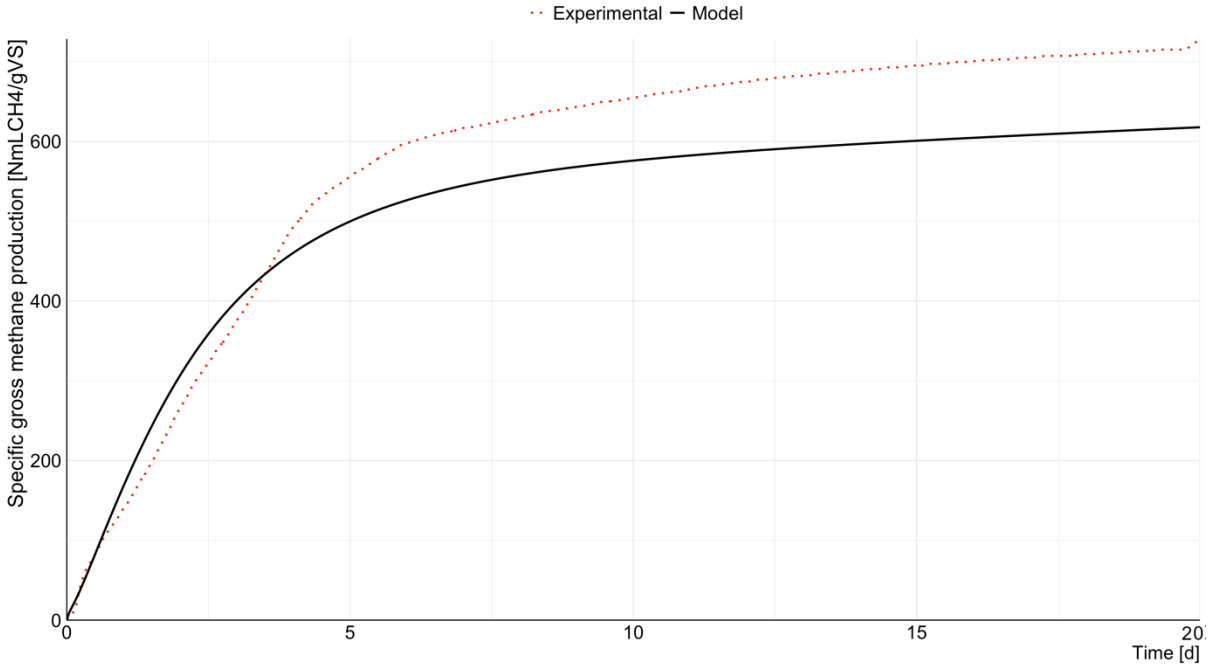


Figure F.20 - Co-digestion BMP test simulation k_hyd_pr = 0.5 (04/02/2021).

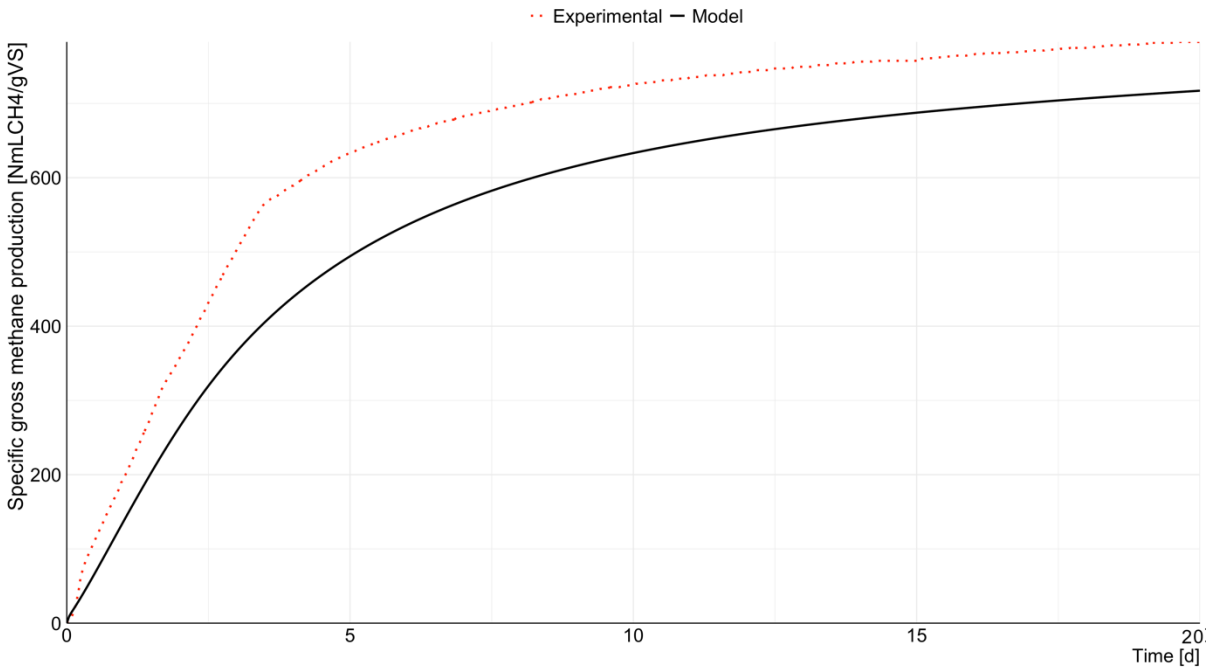


Figure F.21 - Co-digestion BMP test simulation k_hyd_pr = 0.2 (25/02/2021).

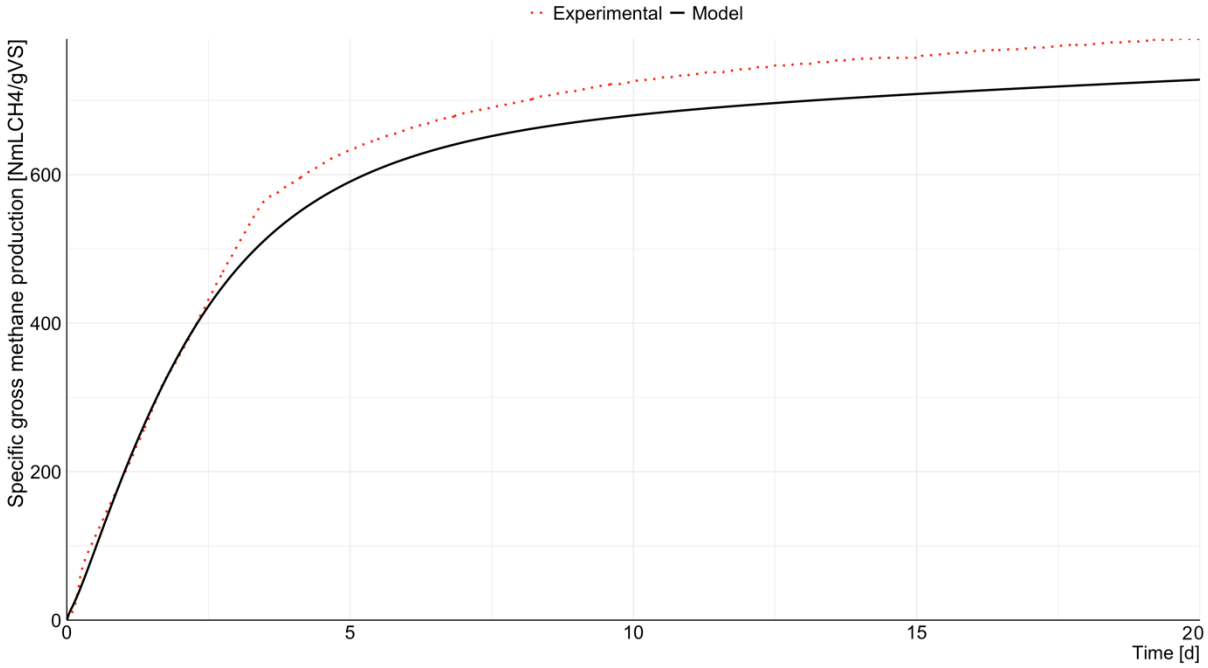


Figure F.22 - Co-digestion BMP test simulation k_hyd_pr = 0.5 (25/02/2021).

*Acetate activity tests*

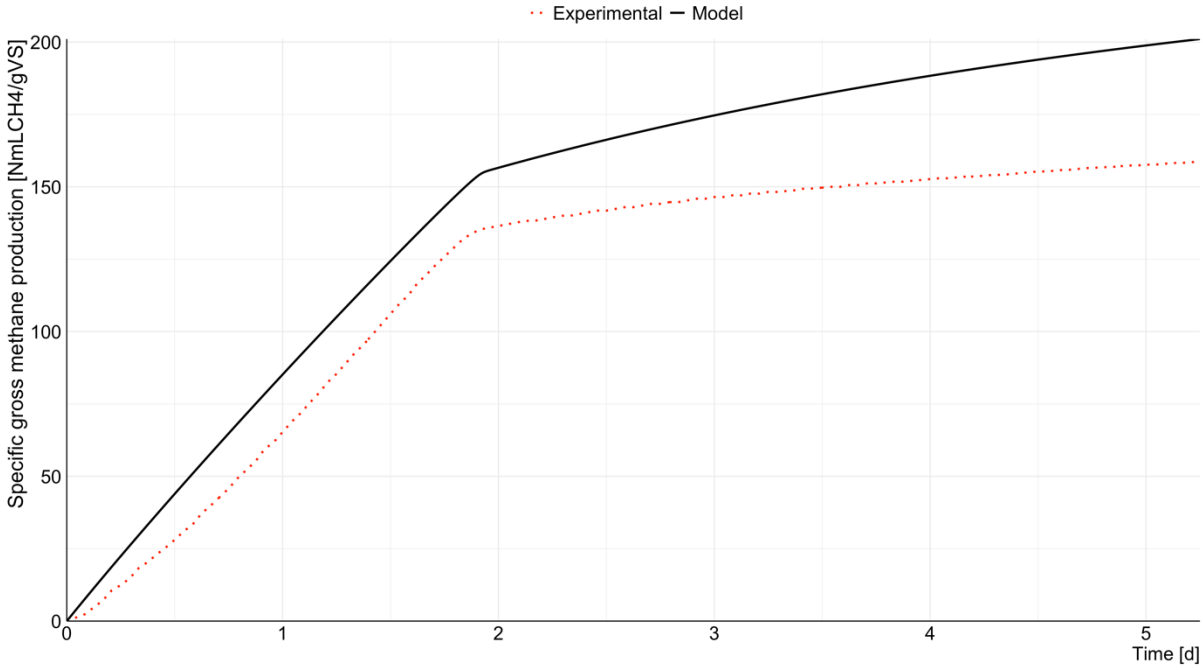


Figure F.23 Acetate activity test simulation (26/11/2020).

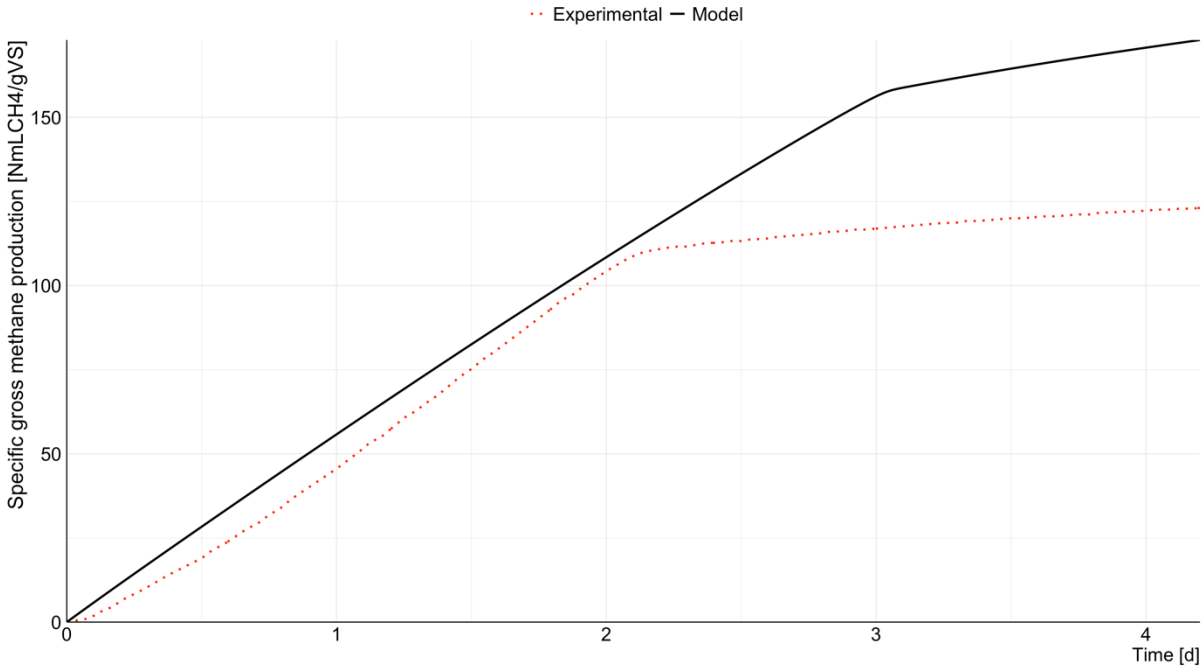


Figure F.24 Acetate activity test simulation (10/12/2020).

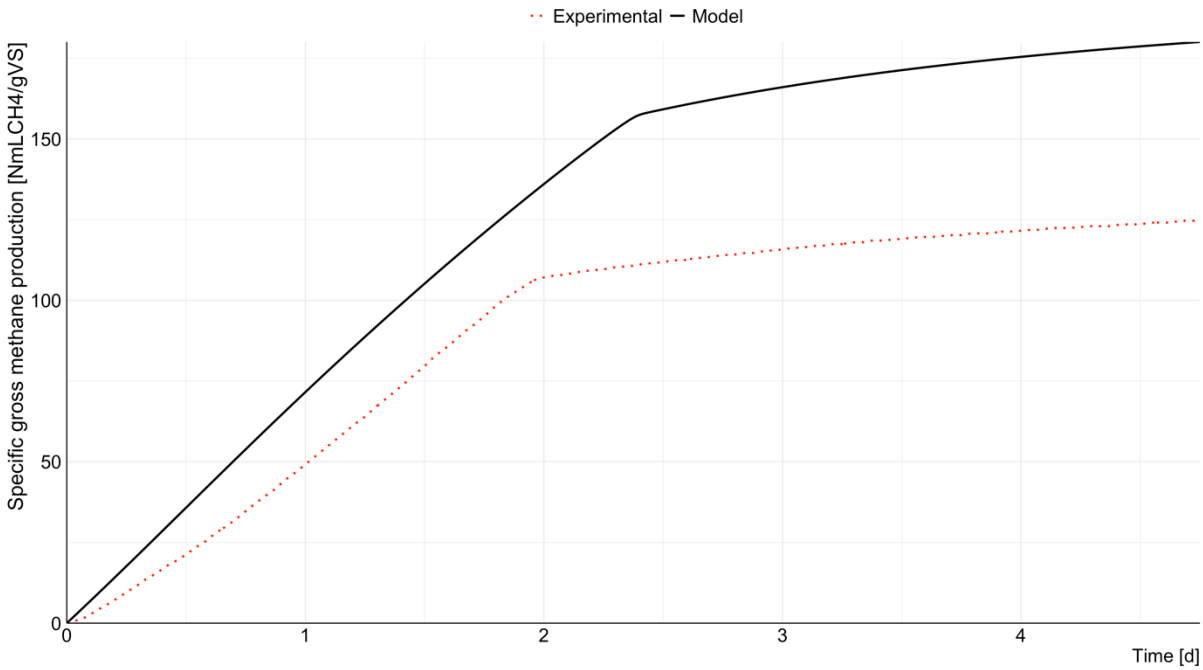


Figure F.25 Acetate activity test simulation (17/12/2020).

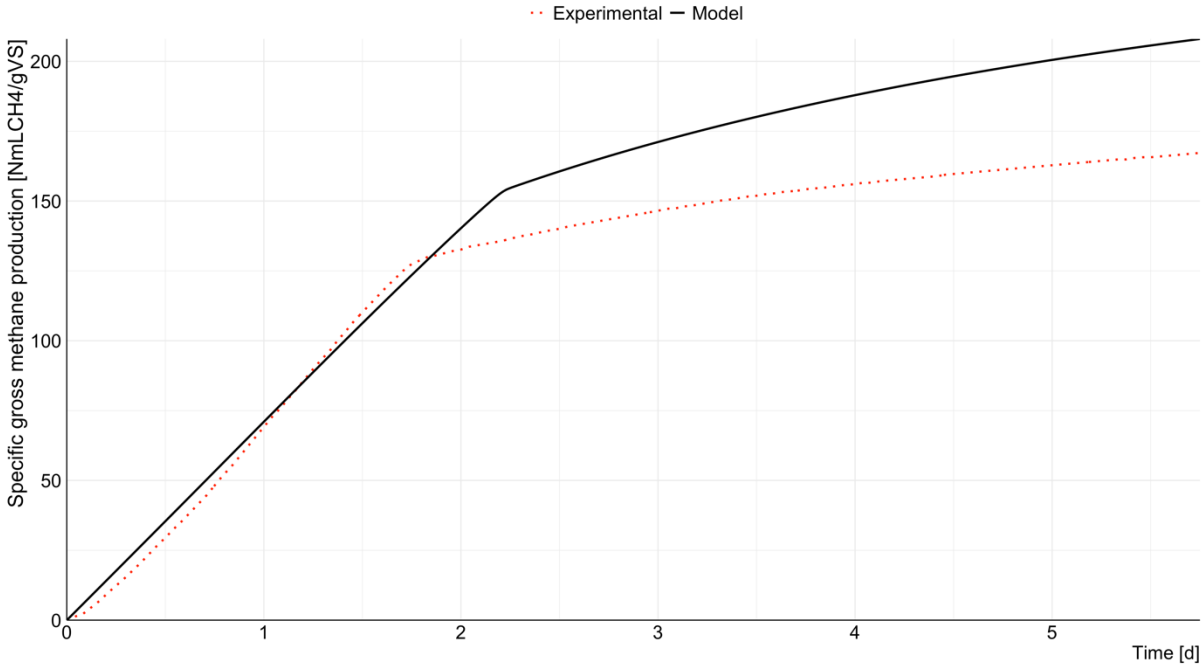


Figure F.26 Acetate activity test simulation (14/01/2021).

*Glucose activity tests*

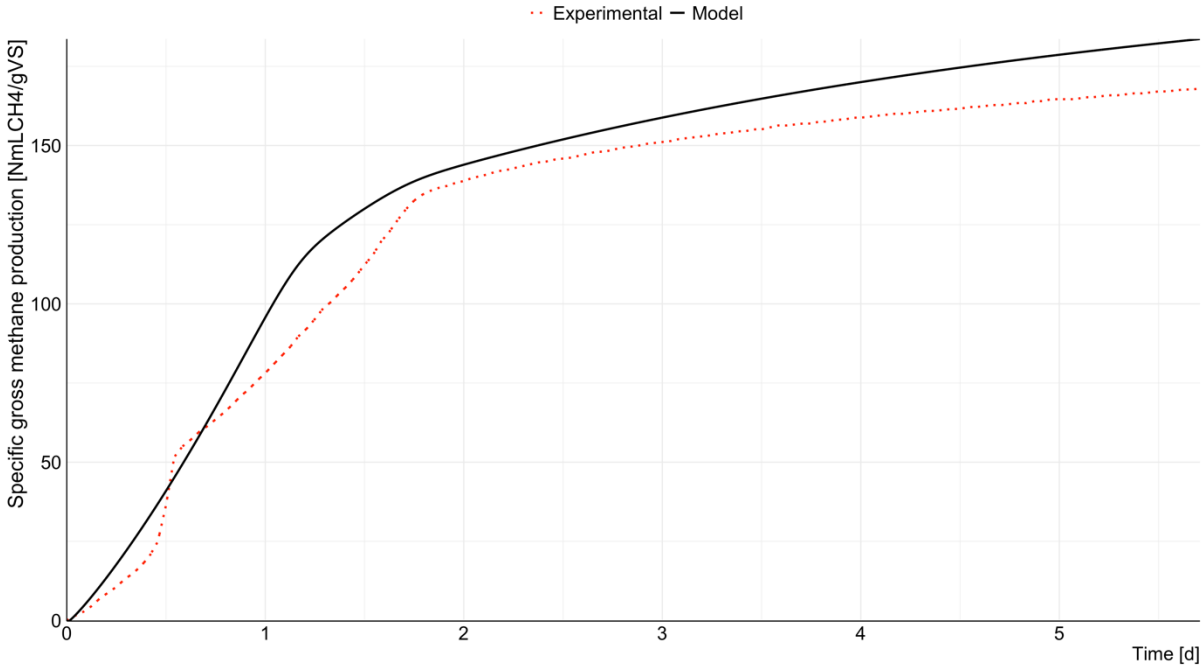


Figure F.27 Glucose activity test simulation (19/11/2020).

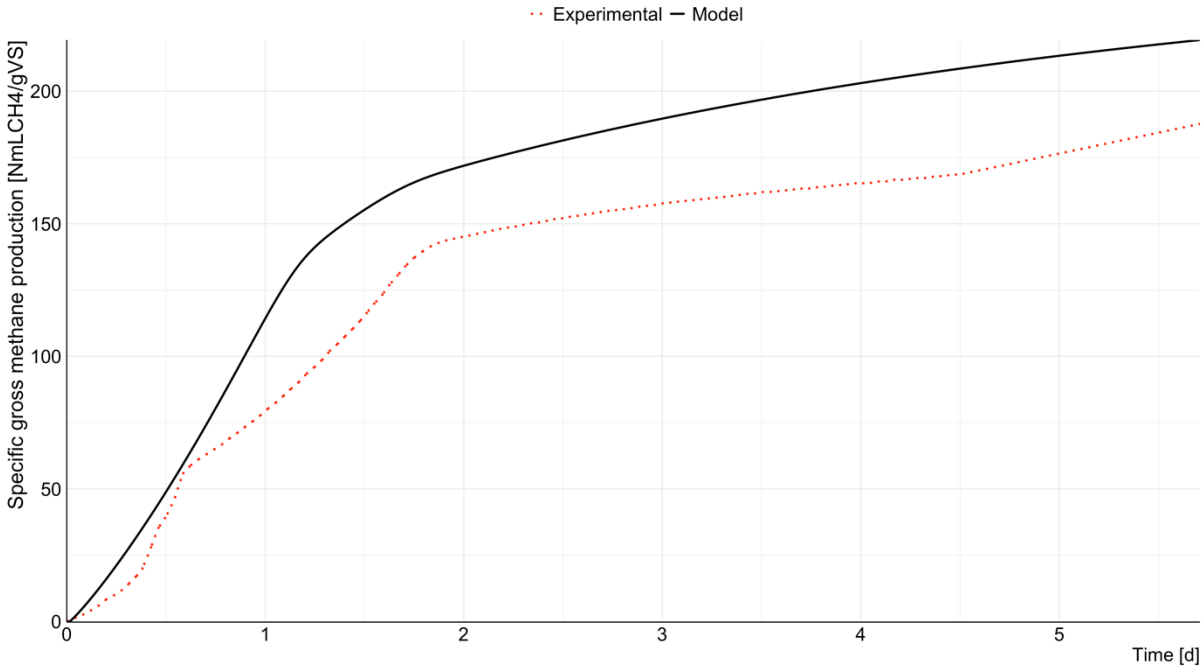


Figure F.28 Glucose activity test simulation (26/11/2020).

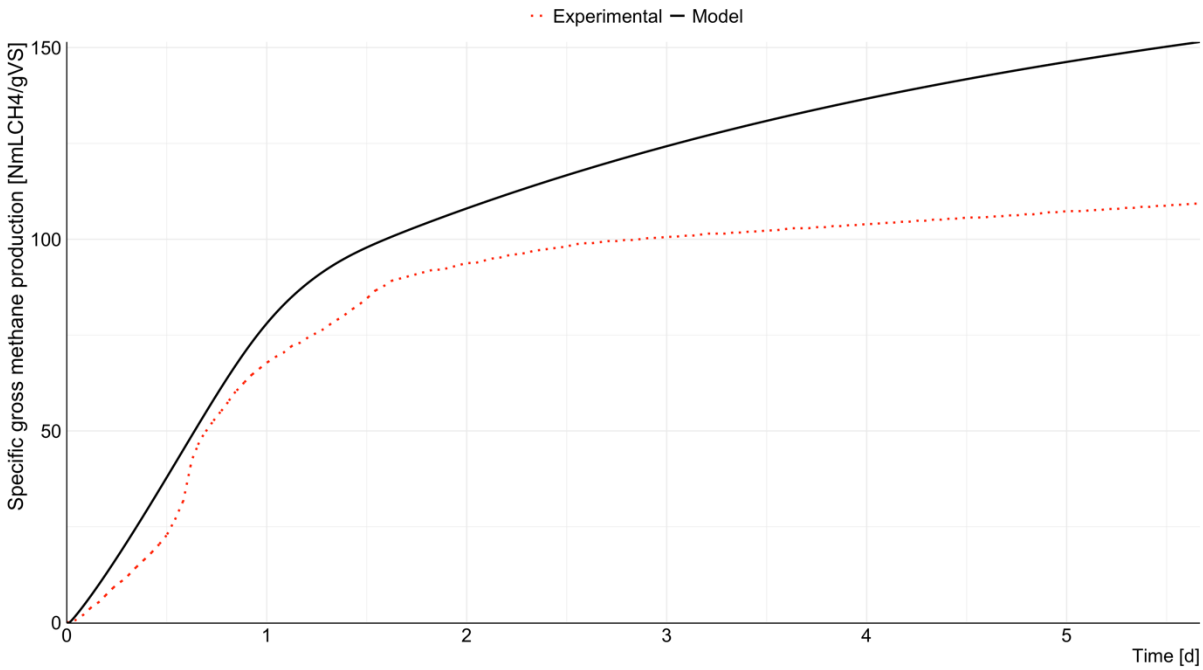


Figure F.29 Glucose activity test simulation (03/12/2020).

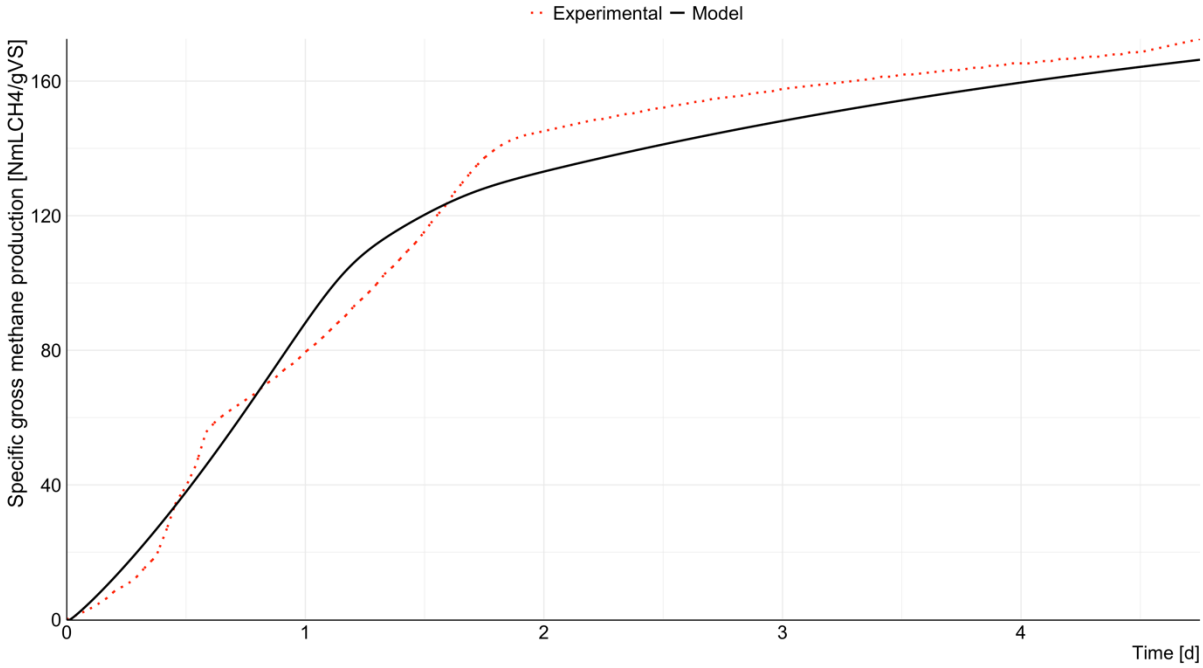


Figure F.30 Glucose activity test simulation (17/12/2020).

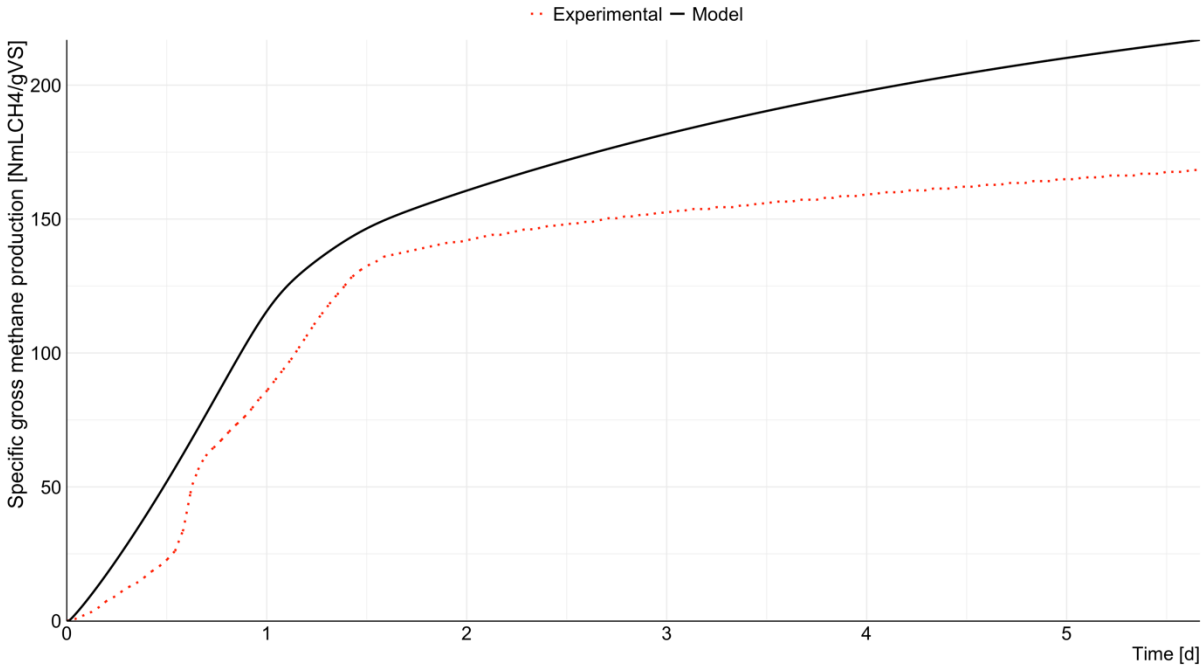


Figure F.31 Glucose activity test simulation (10/02/2021).

## *BSA activity tests*

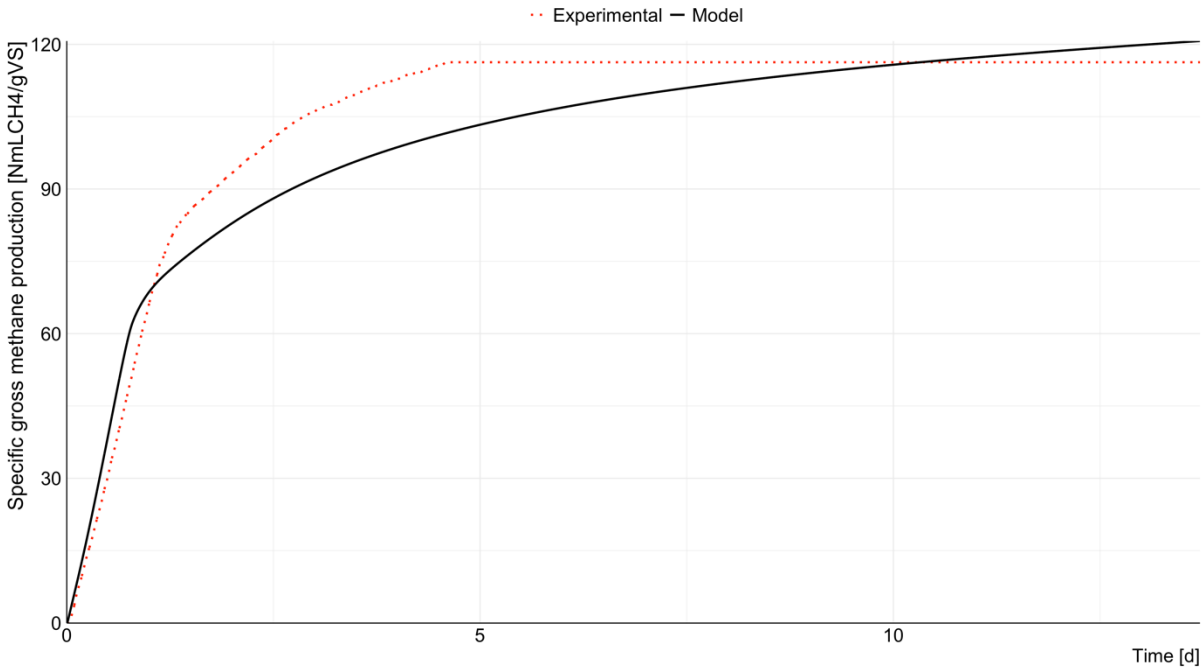


Figure F.32 BSA activity test simulation (05/11/2020).

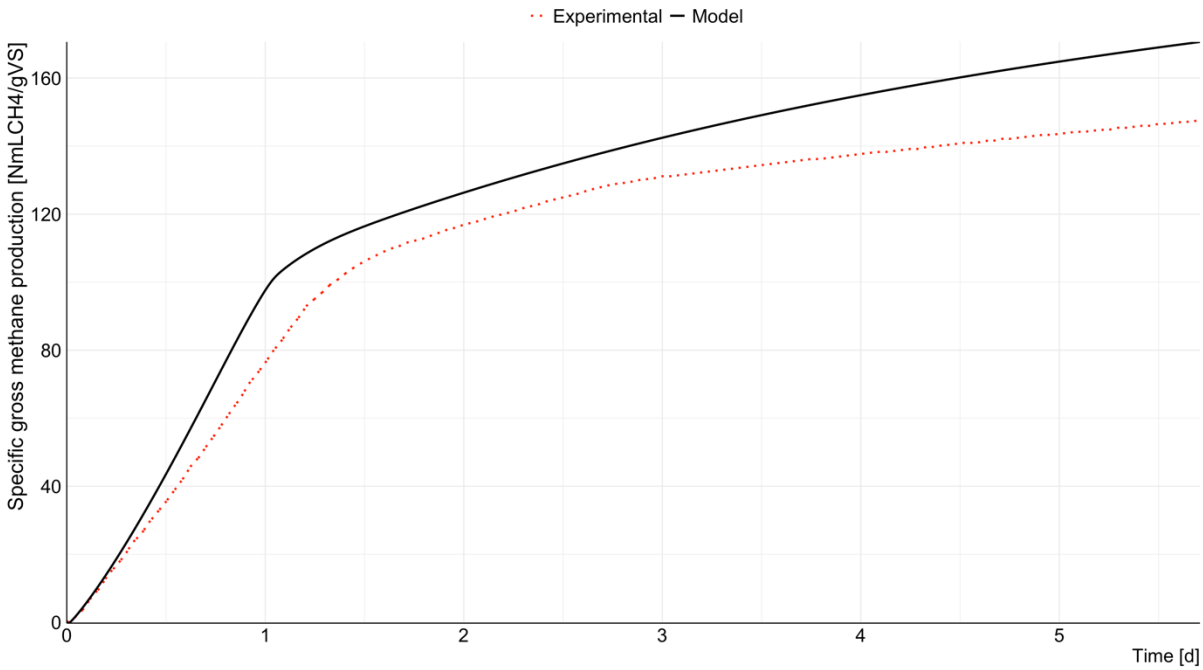


Figure F.33 BSA activity test simulation (26/11/2020).

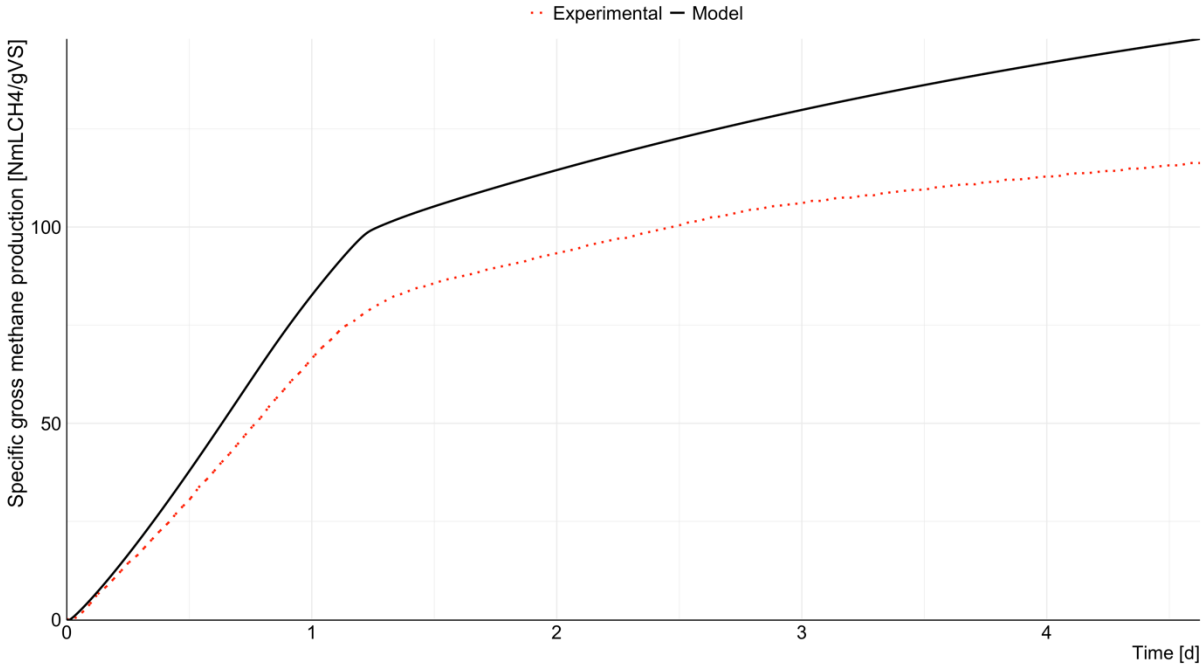


Figure F.34 BSA activity test simulation (10/12/2020).

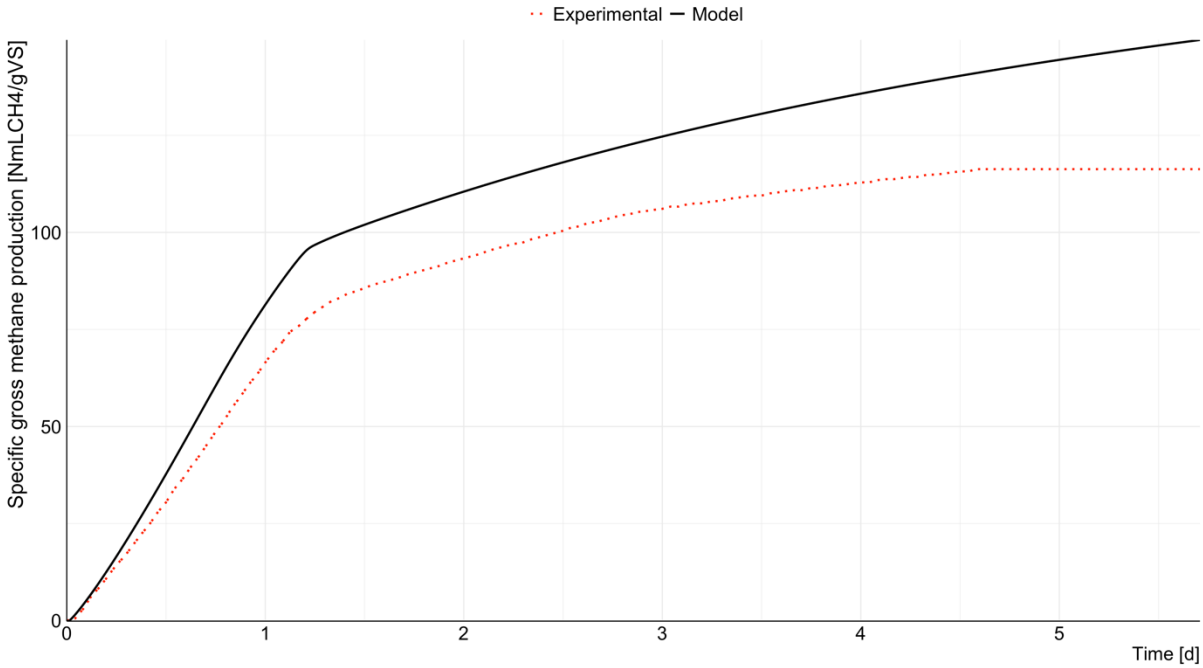


Figure F.35 BSA activity test simulation (17/12/2020).

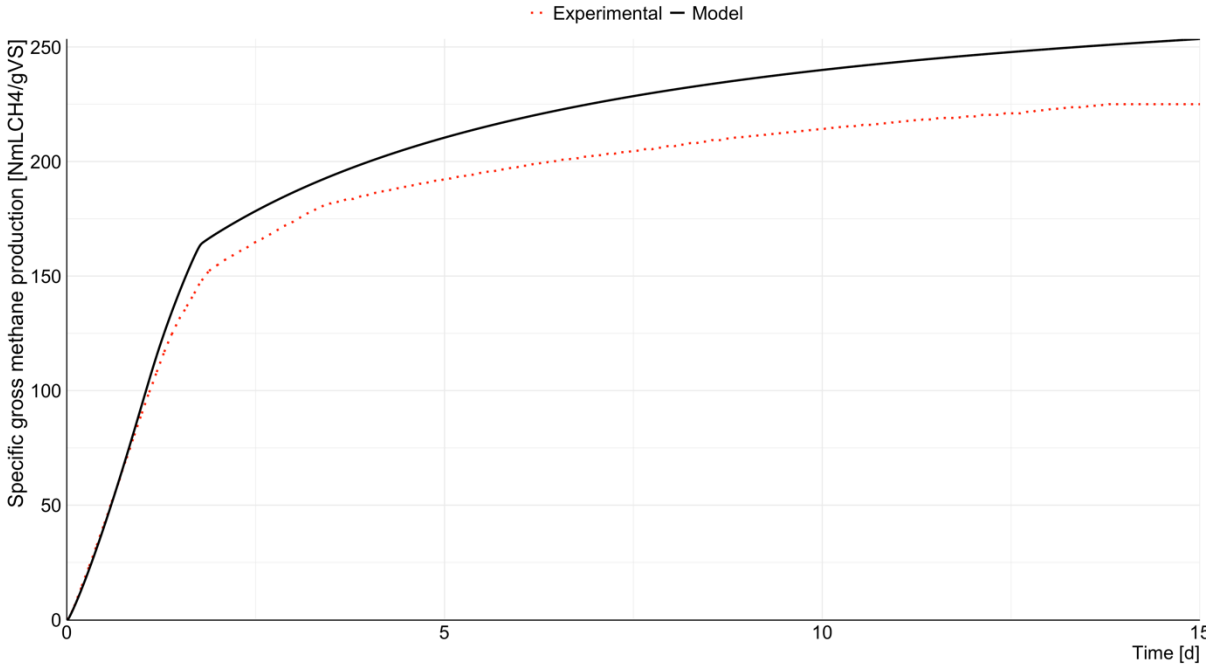


Figure F.36 BSA activity test simulation (29/12/2020).

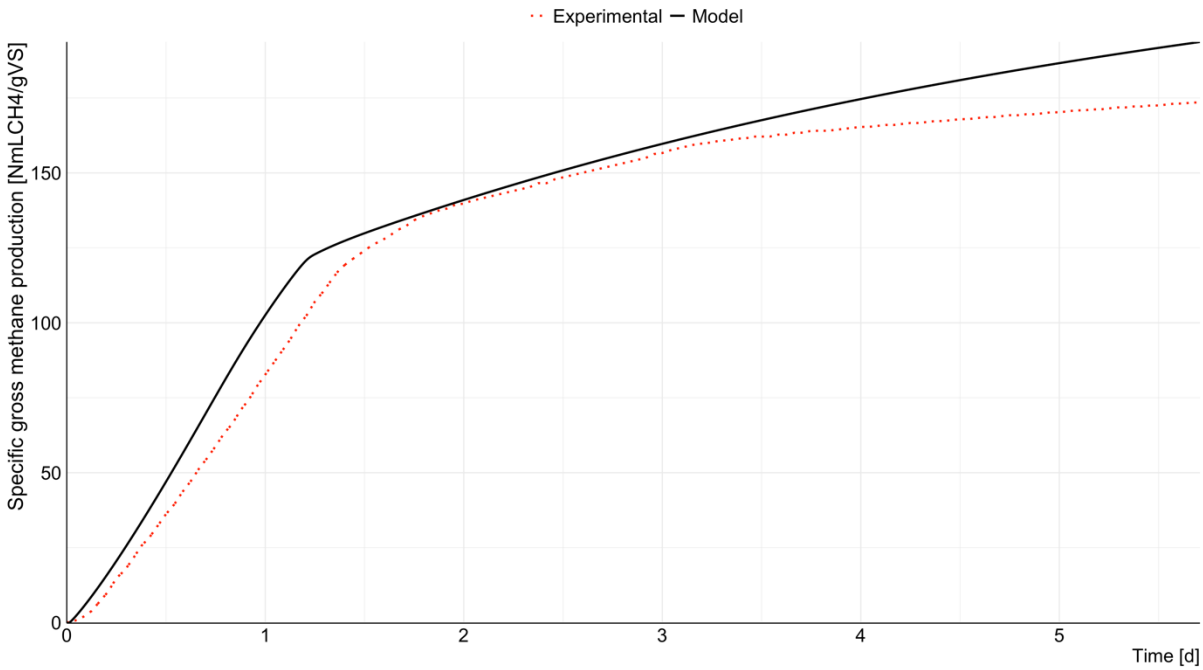


Figure F.37 BSA activity test simulation (17/02/2021).

# APPENDIX G

The following tables show the ingredients used in the preparation of the nutrient solutions used for the BMP tests.

Table G.1 Ingredients of mother solution A

| *Substance* | *Reagentary code* | *Mass (g)* | *Package number* |
|---|---|---|---|
| **$KH_2PO_4$** | AR35 | 2.7 | AR35 |
| **$Na_2HPO_4{*}12H_2O$** | AR40 | 11.2 | AR40 |
| **$NH_4Cl$** | AR23 | 5.3 | AR23 |

Table G.2 Ingredients of mother solution B

| *Substance* | *Reagentary code* | *Mass (g)* | *Package number* |
|---|---|---|---|
| **$CaCl_2{*}2H_2O$** | AR24 | 0.75 | AR24 |

| | | | |
|---|---|---|---|
| **$MgCl_2*6H_2O$** | AR28 | 1.0 | AR28 |
| **$FeCl_2*4H_2O$** | AR26 | 0.2 | AR26 |

Table G.3 Ingredients of mother solution C

| ***Substance*** | ***Mass (g)*** |
|---|---|
| **$MnCl_2*4H_2O$** | 0.05 |
| **$H_3BO_3$** | 0.005 |
| **$ZnCl_2$** | 0.005 |
| **$CuCl_2$** | 0.003 |
| **$Na_2MoO_4*2H_2O$** | 0.001 |
| **$CoCl_2*6H_2O$** | 0.1 |
| **$NiCl_2*6H_2O$** | 0.01 |
| **$Na_2SeO_3$** | 0.005 |

In a flask for each mixture, add distilled water to the mother solution A, B and C in order to obtain final volume of 0.5 L, 0.5 L and 1 L, respectively.

In the bottles with the samples for the test, solution A and B must be added due to 5% of the final test volume; solution C must be added due to 1% of the final test volume.

# APPENDIX H

This appendix contains a pilot plant maintenance diary that describes the accidents encountered during the experimentation:

- A leak of the external hydraulic seal was detected between 11 and 16 September.

- Between 1 and 3 October, there was a level alarm that prevented the reactor from feeding.

- between 9 and 17 November, the pump broke and was repaired in the following days and definitively replaced in mid-January.

- The biogas meter never worked properly, as being a laboratory instrument, it was only able to record the flow partially. With the frost, between December 27 and January 4, the apparatus broke definitively. On March 18, a new biogas meter was installed. However, it only came into operation at the end of the current work.

- Between December 27 and January 4, the winter frost caused the pipes to freeze, making feeding impossible.

- At the beginning of March, the refrigerator containing the pre-storage tank broke. Co-digestion was interrupted due to this. The refrigerator was then replaced at the end of the current work.